# Protein-ligand interactions of Arylamine *N*-acetyltransferase from *Mycobacterium smegmatis*

**Edward W. Brooke**

Department of Pharmacology
and Magdalen College
University of Oxford

**A thesis submitted for the Degree of Doctor of Philosophy at the University of Oxford**

Supervised by Professor E. Sim

Trinity Term 2003

# Protein-ligand interactions of arylamine *N*-acetyltransferase from *Mycobacterium smegmatis*

Edward W. Brooke

**Department of Pharmacology and Magdalen College, University of Oxford**
**Submitted for the degree of Doctor of Philosophy**
**Trinity Term 2003**

## Abstract

Tuberculosis is the world's largest cause of death from an infectious agent. Treatment is by an extended period of combination chemotherapy. Drug resistance is an increasing problem in tuberculosis therapy, particularly to the frontline anti-tubercular drug isoniazid (INH). Recombinant arylamine *N*-acetyltransferase (NAT) of *Mycobacterium tuberculosis* *N*-acetylates INH using the cofactor Acetyl Coenzyme A. NAT from *M. tuberculosis* is a polymorphic enzyme and also acetylates INH *in vivo*. Acetylated INH is inactive therapeutically against *M. tuberculosis* both *in vivo* and *in vitro*. The acetylation of isoniazid in the mycobacterial cell may compete with the activation of INH by the catalase-peroxidase, katG, and hence contribute to INH resistance in clinical isolates. Inhibition of NAT in *M. tuberculosis* may thus increase the efficacy of INH therapy.

A novel assay based around the detection of free Coenzyme A released during the acetylation reaction was used to determine the substrate specificity of recombinant NAT from the related Mycobacterium *M. smegmatis* (MSNAT). A relationship was observed between the lipophilicity of simple arylamine substrates and the rate of acetylation by MSNAT. Several MSNAT substrates possess antibacterial activity. The assay could also be used to screen compound libraries for MSNAT inhibitors.

Synthesis of seventeen thiazolidinedione sultams in collaboration with Dr.Vickers (Dyson Perrins), identified as weak inhibitors of MSNAT, gave a minimum competitive inhibitory constant of 14μM. Screening a library of 5,074 drug-like compounds for inhibition of MSNAT identified thirteen compounds with semi-maximal inhibition constants ($IC_{50}$) of below 10μM. Based on this, fifteen maleimides were synthesised and were irreversible inhibitors of MSNAT with submicromolar potency. Similarly, ninety-six aminothiazoles were synthesised by Dr. Vickers and were uncompetitive inhibitors of MSNAT with a minimum $IC_{50}$ of 1.5μM. The most potent aminothiazole showed no effect on the growth of *M. smegmatis* or *M. bovis* BCG or the sensitivity of the bacteria to isoniazid. However the aminothiazoles were shown not to penetrate the cells.

# Contents

# Contents of Figures

## Chapter 1 - Introduction



## Chapter 2 – Materials, Methods and Syntheses



## Chapter 3 – A novel assay for NAT activity

## Chapter 4 – Inhibitors of MSNAT

## Chapter 5 – Effect of MSNAT inhibitors on Mycobacteria



## Chapter 6 – Conclusions

No Figures

# Abbreviations

**5AS** – 5-Aminosalicylate

**$A_{600}$** – Absorbance of 10mm pathlength at 600nm

**AcCoA** – Acetyl Coenzyme A

**ACP** – Acyl Carrier Protein

**ADC** – Albumin dextrose catalase

**APS** – Ammonium persulphate

**BCG** – Bacille Calmette Guerin

**CoA** – Coenzyme A

**CXCoA** – Acyl Coenzyme A with acyl chain X carbon atoms long

**CPK** – Corey, Pauling and Kultun

**DMAB** – *p*-Dimethylaminobenzaldehyde

**DMF** – *N,N*-Dimethylformamide

**DMSO** – Dimethylsulphoxide

**DNA** – Deoxyribonucleic acid

**DTNB** – 5,5'-Dithio-(bis-2-nitrobenzoic acid)

**DTT** – Dithiothreitol

**EDTA** – Ethylenediamine-tetraacetic acid

**FAS** – Fatty acid synthase

**GSH** – Glutathione (reduced form)

**HIV** – Human immunodeficiency virus

**$IC_{50}$** – Concentration giving 50% inhibition

**INH** – Isoniazid (isonicotinic acid hydrazide)

**IR** – Infra Red

**IPTG** – Isopropyl-β-D-thiogalactopyranoside

**LB** – Luria Bertani

**MAC** – *Mycobacterium avium-intracellulare* complex

**MES** – 2-[*N*-Morpholino]ethanesulfonic acid

**MIC** – Minimum inhibitory concentration

**mRNA** – Messenger ribonucleic acid

**MS** – Mass spectrometry

**MSNAT** – Arylamine *N*-acetyltransferase from *Mycobacterium smegmatis*

**NADH** – Nicotinamide adenine dinucleotide (reduced form)

**NAT** – Arylamine *N*-acetyltransferase

**NMR** – Nuclear magnetic resonance

**NTA** – Nitrilotriacetic acid agarose

**OADC** – Oleic acid, albumin, dextrose, catalase

**pABA** – *p*-Aminobenzoic acid

**pABA-Glu** – Glutamyl-*p*-aminobenzoate

**PBS** – Phosphate-buffered saline

**PDB** – Protein DataBank

**PS** – Polystyrene bound

**RP-HPLC** – Reverse phase-high performance liquid chromatography

**SDS-PAGE** – Sodium dodecyl sulphate - polyacrylamide gel electrophoresis

**SNP** – Single nucleotide polymorphism

**STNAT** – Arylamine *N*-acetyltransferase from *Salmonella typhiumurium*

**TB** – Tuberculosis

**TBNAT** – Arylamine *N*-acetyltransferase from *Mycobacterium tuberculosis*

**TCA** – Trichloroacetic acid

**TEMED** – *N,N,N',N'*-Tetramethylethylenediamine

**TLC** – Thin layer chromatography

**TNB** – 5-Mercapto-2-nitrobenzoic acid

**Tris** - Triethanolamine

**TZD** – Thiazolidine-2,4-dione

**UV** – Ultraviolet

**WHO** – World Health Organisation

**ZN** – Ziehl Neelsen

# Acknowledgements

*The collaborative nature of this project is such that it would not have been possible without assistance from many people. But first and foremost I am eternally indebted to my supervisor, Professor Edith Sim. She has provided a rich seam of ideas throughout this project, given me the opportunities to fulfil the goals that I desired, taught me tirelessly about scientific writing and provided a steadying hand and watchful eye at all times. This project is a product of her energy and enthusiasm.*

*None of the chemistry described herein would have been possible without the collaboration between this laboratory and Professor Steve Davies in the Dyson Perrins laboratory. I am grateful for the space and resources that he has provided. Dr. Andy Mulvaney has been instrumental in the progression of the chemical side of this work. He is an excellent medicinal chemist and careful mentor. I am so thankful for the patience and advice of Dr. Richard Vickers, with whom I worked on much of the chemistry. One day I may repay the glassware bill…*

*The collaboration with Dr. Martin Noble in the Laboratory of Molecular Biophysics has allowed me to set down many crystal trials. James Sandy has been ever-present with technical assistance in Biophysics and in Pharmacology.*

*Two other members of the SimLab deserve a special mention. Firstly, Dr. Anna Upton taught me so much about tuberculosis and biochemistry in general and for that I am very appreciative. Secondly, I am very grateful to Dr. Adeel Mushtaq for setting up the UNIX programs for the docking side of this work.*

*I must also thank all my other co-workers in the SimLab for constant scientific assistance and for making my DPhil a thoroughly enjoyable experience. In no particular order (and apologies if I miss anyone out) thanks to Akane, Isaac, Matt, Fred, Katalin, Valerie, Nikki, Giannoulis and Rea, Clarissa, Sanjib, Carolyn and many others. The same goes to the chemists for some fun times.*

*It wouldn't be right not to thank all those people from outside the scientific arena who have been there for me. I won't name and shame you all but you know who you are. I love you all very dearly. Thanks also to the Fives and Frisbee teams.*

*And a final word must go to my family, who have always been and always will be there. This is for them and for the Lord God.*

*For ARK*

*'For my eyes have seen your salvation'*

*Luke 2:30*

# Chapter 1

# Introduction

## 1.1 Tuberculosis

### 1.1.1 Recent Tuberculosis History

In the mid to late twentieth century, tuberculosis became a forgotten disease in the West. With effective treatments and vaccines widely available in the developed world, improved quality of living and advances in detection technology, interest in tuberculosis research faded. The success of tuberculosis control led Waksman to state that:

'the ancient foe of man, known as consumption, the great white plague, tuberculosis, or by whatever other name, is on the way to being reduced to a minor ailment of man. The future appears bright indeed, and the complete eradication of the disease is in sight.' (Waksman 1964)

However, in the developing world the situation was vastly different. In 1993 the World Health Organisation classed tuberculosis as a 'Global Health Emergency', the first disease ever to be given this title. Now, ten years on, the WHO along with the Global Stop TB Partnership have produced sustainable, effective and, above all, affordable guidelines for the detection and treatment of tuberculosis in every country. However, the current Global Tuberculosis Control, WHO Report 2003 (www.who.org), provides sobering reading; it is currently

estimated that one third of the world's population is infected with the tuberculosis bacteria, of which ten percent will develop an active infection. Current death rates are estimated at 2-4 million deaths a year, the greatest cause of death from an infectious agent.

In the next few sections, the causes behind this disease will be investigated, with particular reference to current treatment strategies, drug resistance and the characterisation of the bacteria responsible, *Mycobacterium tuberculosis*. The fully sequenced genome of *M. tuberculosis* has lead to the identification of new genes with possible roles in drug resistance and as drug targets (Section 1.1). This thesis is directed to the characterisation of one such gene, arylamine *N*-acetyltransferase (Section 1.2). The direct aims of this project will then be discussed (Section 1.4).

### 1.1.2 *Mycobacterium tuberculosis*

The aetiological agent of tuberculosis is *Mycobacterium tuberculosis*, as discovered by Koch in 1882 (Koch 1932). This rod-shaped gram-positive slow-growing aerobic bacterium is a member of the wider Mycobacterium genus, in the bacterial family *Actinomycetales* (Parish *et al.* 1998). There are over seventy members of the mycobacteria family and they possess a broad range of features. They are all linked by the presence of unique cell wall fatty acids termed mycolic acids. Because of the unique cell wall, mycobacteria can be detected using the acid-fast test (Heifets *et al.* 1994). Pathogenic members of the mycobacteria family include other members of the *M. tuberculosis* complex (*e.g. Mycobacterium kansasii*, *Mycobacterium bovis*), members of the *Mycobacterium avium-intracellulare* complex (MAC) and the causative agent for leprosy,

*Mycobacterium leprae*. The MAC causes a major class of opportunistic infections in patients positive for any member of the Human Immunodeficiency Virus group (HIV+) (Cohn 1997). Non-pathogenic members of the mycobacterial family are generally saprophytic (*e.g. Mycobacterium smegmatis*) and mycobacteria are found widely in soil environments. *M. smegmatis* is a fast-growing mycobacterium often used as a model for *M. tuberculosis* research (Reyrat *et al.* 2001).

The evolution of the mycobacterial family has been an area of particular interest recently with the completion of the GC-rich genome sequences for *M. tuberculosis* (Cole *et al.* 1998), *M. bovis* BCG (Garnier *et al.* 2003), *M. leprae* (Cole *et al.* 2001) along with ongoing genomic projects studying other members of the complex (Brosch *et al.* 2001) (http://genolist.pasteur.fr/Tuberculist). The mycobacteria can be separated phylogenetically between slow-growing and fast-growing species (Springer *et al.* 1996) and it has been suggested that the progenitor of the *M. tuberculosis* complex originally developed from a soil bacterium (Brosch *et al.* 2001). It is thought that *M. tuberculosis* in its current form is only 10,000 years old and contains a remarkably low rate of single-nucleotide polymorphisms (Sreevatsan *et al.* 1997a). Even under pressure from a range of anti-tuberculosis drugs, the genome of *M. tuberculosis* is notably stable (Victor *et al.* 1997). A number of insertion and deletion events have taken place across the complex and this appears to be the major route of phenotypic variation both between strains of *M. tuberculosis* and between different members of the *M. tuberculosis* complex (Brosch *et al.* 2001). This is exemplified by *M. leprae* which has deletion and decay of approximately one quarter of its genome compared to other mycobacterial genomes (Cole *et al.* 2001).

The success of *M. tuberculosis* as a pathogen lies within the cell wall of the bacterium. The cell wall contains a unique outer layer that is visible at the electron microscopic level. The inner wall is formed from a common peptidoglycan base, but the muramic acid in the peptidoglycan is *N*-glycolylated rather than *N*-acetylated (Brennan *et al.* 1995). A complex polysaccharide, arabinogalactan, is attached to 10-12% of the *N*-glycolyl muramic acid units by a phosphodiester bond and it is to the arabinan sidechains of this polysaccharide that the mycolic acids are covalently bound. These mycolic acids are $C_{60}$-$C_{90}$ fatty acids containing a 'meromycolate' branch and an alpha branch (Figure 1.1) (Besra *et al.* 1997).

**Meromycolate Branch** **α-branch**

**R-X-$(CH_2)_{13,15}$-Y-$(CH_2)_{16,18}$-CHOH-CH(COOH)-$(CH_2)_{21,23}$-$CH_3$**

| Mycolate | R | X |
|---|---|---|
| α-mycolate | - | $CH_3CH_2$ |
| α'-mycolate | $CH_3$-$(CH_2)_{15\text{-}19}$ | *cis-* 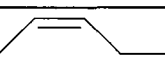 |
| Epoxymycolate | $CH_3$-$(CH_2)_{15\text{-}17}$ | *trans-* 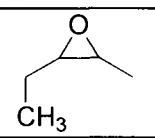 |
| Ketomycolate | $CH_3$-$(CH_2)_{15\text{-}17}$ | 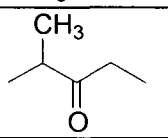 |
| Methoxymycolate | $CH_3$-$(CH_2)_{15\text{-}17}$ | 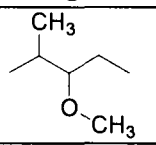 |
| Wax ester | $CH_3$-$(CH_2)_{15\text{-}17}$ | 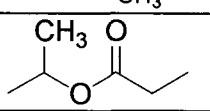 |

**Figure 1.1 – Mycolic acids found in the mycobacteria**
α and α' mycolates contain only double bonds at Y; others can contain any of the units at Y. Adapted from (Brennan *et al.* 1995)

**Y=** 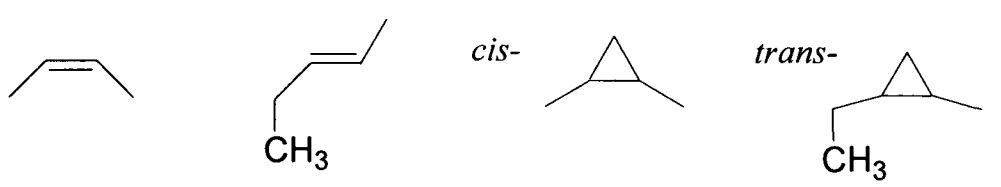


The meromycolate branch possesses, in its most basic form, a fatty acid chain approximately forty carbon atoms long containing two or three double-bonds that

can be *cis* or *trans* and can thus kink the chain. Mycolic acids purified from *M. tuberculosis* can also contain at these positions *cis* or *trans* cyclopropane rings, ketone groups, methoxy groups and ester functionalities (Barry *et al.* 1998; Watanabe *et al.* 2002). The hydrophobic mycolic acid sidechains form a lipid bilayer with a range of glycolipids on the exterior of the cell, particularly lipooligosaccharides, glycopeptidolipids and phenolic glycolipids (Watanabe *et al.* 1997) (Figure 1.2). The cell envelope also includes lipoarabinomannan molecules (Maeda *et al.*, 2003), as well as protein components. A porin from *M. tuberculosis* of diameter 1.4-1.8Å has been described (Senaratne *et al.* 1998) and the bacterium is sensitive to small hydrophilic molecules such as hydroxylamine and *p*-nitrobenzoic acid. The very low fluidity of the mycolic acid bilayer provides a significant permeation barrier and it has been shown that more lipophilic antibiotics are more effective against *M. tuberculosis* (Haemers *et al.* 1990). When the bacterium is phagocytosed, the bacteria are still able to multiply within the phagosome. The waxy cell wall protects the bacterium from attack from oxygen radicals and digestive hydrolases produced in active macrophages as a result of the immune defence (Rojas-Espinosa et al. 2002). The engulfed mycobacteria are also specifically resistant to the acidic phagocytic compartment (Manabe *et al.* 2000). Another key to the pathogenic success of the organism is the ability of the cell to enter a dormant or persistent state. The mycobacterial cell can enter a non-multiplying state and can adjust its carbon metabolism depending on available carbon sources (Wayne *et al.* 1982; McKinney *et al.* 2000).

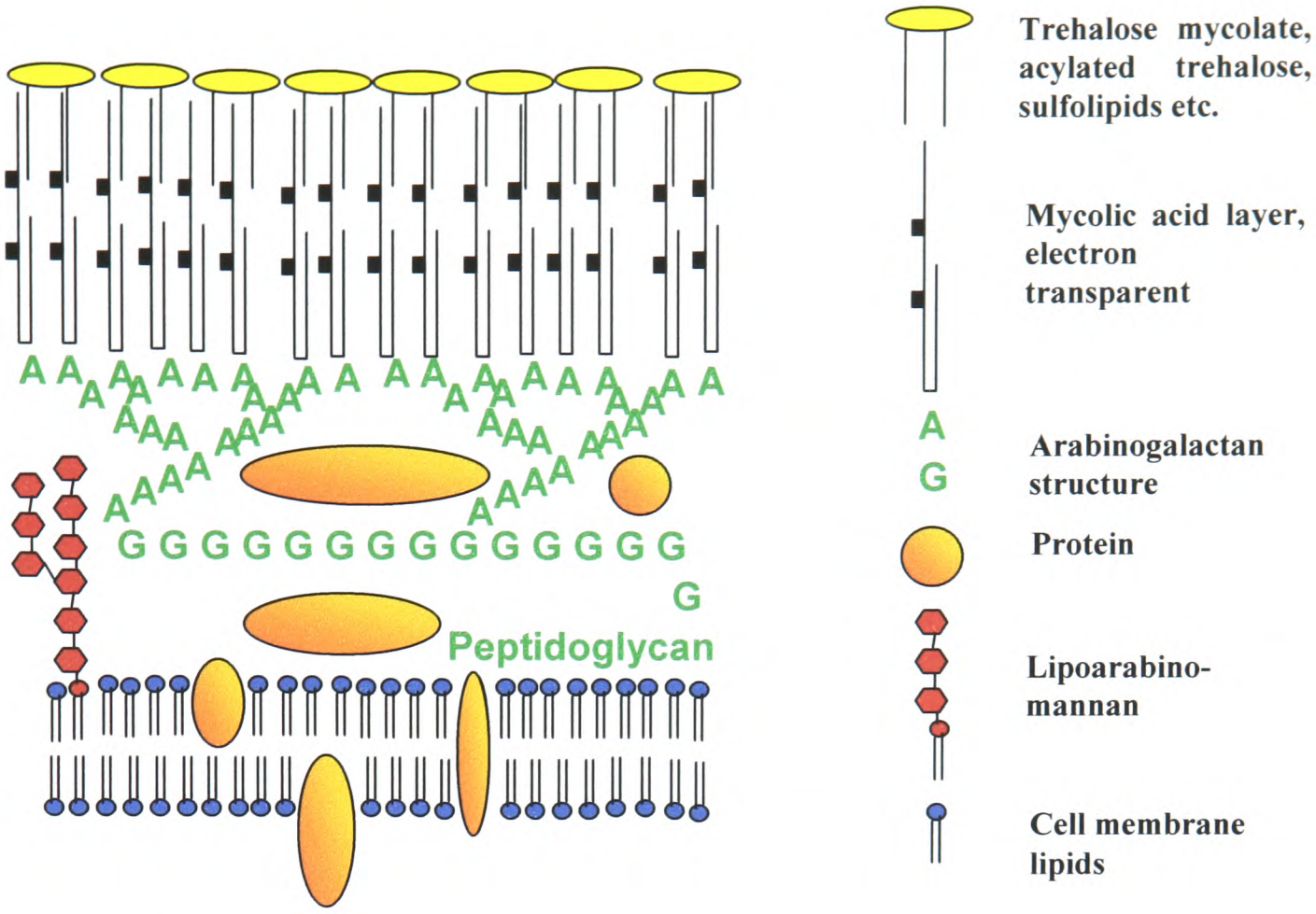


**Figure 1.2 – The cell wall of mycobacteria**
Adapted from (Besra *et al.* 1997)

### 1.1.3 Tuberculosis pathogenicity and treatment

It is currently estimated that one third of the world's population tests positive for present or past exposure to *M. tuberculosis* by skin-testing (Dye *et al.* 1999). Of these, approximately 10% will develop active disease leading to 2 million deaths annually worldwide. Fatality rates are higher in patients with HIV.

Tuberculosis is most commonly transferred by airborne droplets particularly in the presence of prolonged physical contact such as in family groups (Figure 1.3) (Smith 1994). The initial bacteria settle deep in the sterile lung areas and become established in the lung tissue. The bacteria then reduce their rate of replication until a weakening of the immune system occurs (Bishai 2000). Host macrophages attack and internalize the bacteria, but *M. tuberculosis* can survive and replicate within the phagocytic compartment. Increased intracellular growth and further

macrophage recruitment produces a granuloma of active bacteria and necrotic debris surrounded by macrophages, lymphocytes and multi-nucleated giant cells (Manabe *et al.* 2000). Granuloma formation is an effective immune response and halts disease progression. Those that cannot effectively mount this host response progress immediately to full transmissible disease (primary tuberculosis) (Smith 1994). However, bacteria within the granuloma are still viable and can persist in this state for decades (latent infection) (McKinney *et al.* 2000).

**Figure 1.3 – Progress of infection by *M. tuberculosis* leading to tuberculosis**
Adapted from (Bishai 2000)

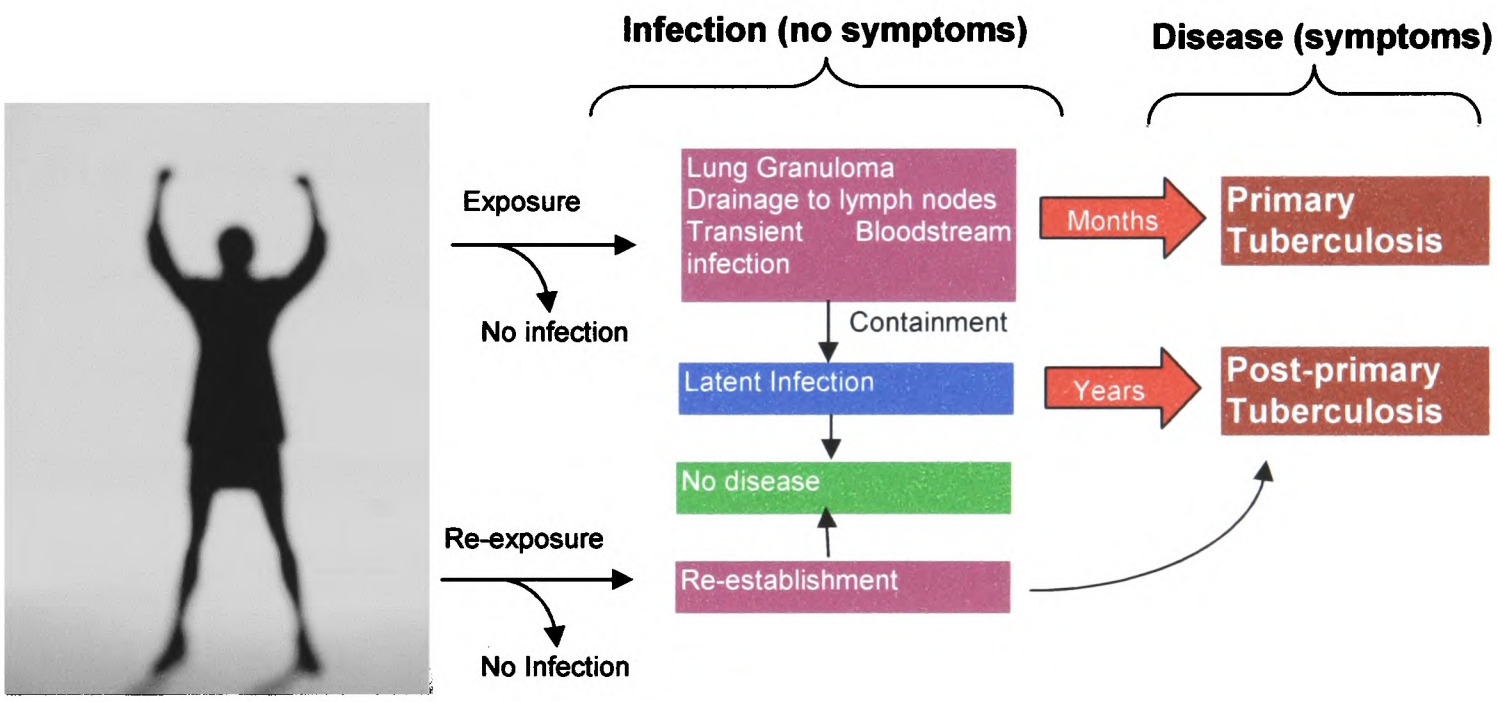


Reactivation of the bacteria within the granuloma occurs with 5-10% of individuals to develop post-primary tuberculosis. This reactivation can occur after many years and is often as a result of the individual becoming immunocompromised, e.g. as a result of old age, malnutrition or HIV infection (Hopewell 1994).

During reactivation, the granulomas undergo caseous necrosis to form pulmonary cavities and the bacteria spread throughout the lungs. Damage to the blood-vessels in the lungs and accumulation of bacteria in the draining lymph-nodes can allow the spread of the bacteria to other organs and extra-pulmonary disease occurs in

15% of non-HIV patients. In extreme cases of dissemination, generalised miliary tuberculosis results particularly with HIV+ patients (Corbett *et al.* 1996).

The first effective antibiotic treatment developed for tuberculosis was streptomycin in 1945 (Hinshaw *et al.* 1945). However, almost immediately, streptomycin resistant strains developed under monotherapy (Medical Research Council 1948). Screening of compounds against replicating *M. tuberculosis* cultures gave a range of antibiotics that are now used in combination therapy (Table 1.1). Many of the drugs specifically target the cell-wall synthetic processes and show how vital the cell wall is for the survival of *M. tuberculosis*.

### 1.1.4 Isoniazid action and resistance

Isoniazid functions by the inhibition of mycolic acid synthesis in the cell wall (Takayama *et al.* 1972).

Isoniazid enters the cell by passive diffusion (Bardou *et al.* 1998). Once in the cell isoniazid is activated by a catalase-peroxidase enzyme, KatG (Zhang *et al.* 1992). KatG activates the pro-drug isoniazid by two sequential electron transfers to oxidise isoniazid which then undergoes nitrogen loss to form a range of reactive forms (Johnsson *et al.* 1994). A series of mutations in KatG have been discovered in drug-resistant strains of *M. tuberculosis* (Pretorius *et al.* 1995; Musser *et al.* 1996) and a loss of catalase-peroxidase activity was observed in the earliest isoniazid-resistant strains (Middlebrook 1954). The S315T mutation

| Drug | Structure | Target and gene | Drug | Structure | Target and gene |
|---|---|---|---|---|---|
| Isoniazid | 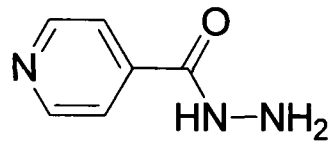 | Cell wall mycolic acid synthesis: *InhA* and possibly *KasA* | Ethambutol | 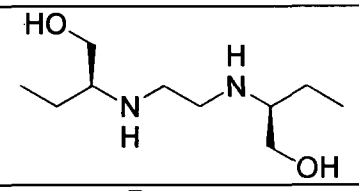 | Cell wall arabinogalactan synthesis: *EmbAB* |
| Ethionamide | 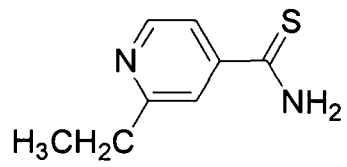 | Cell wall mycolic acid synthesis: *InhA* | Fluoroquinolones | 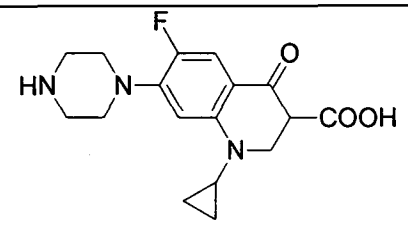 | DNA synthesis: *GyrAB* |
| Pyrazinamide | 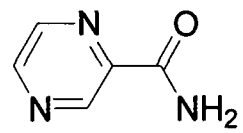 | Cell wall fatty acid synthesis: *Fas* | *p*-aminosalicylic acid | 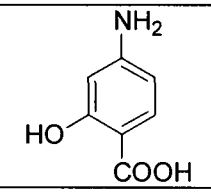 | Folic acid synthesis: *FolP* |
| Rifampin | 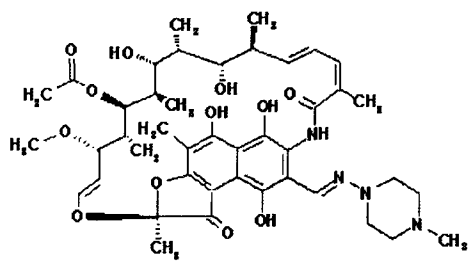 | RNA Synthesis (RNA polymerase beta subunit): *RpoB* | Streptomycin | 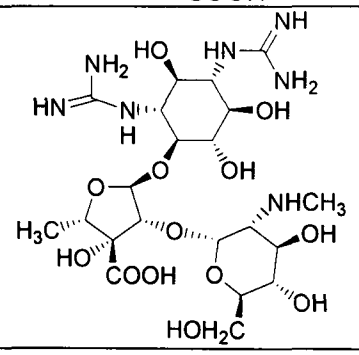 | Polypeptide synthesis (16S rRNA and S12 ribosomal protein): *Rrs* and *RpsL* |
| Cycloserine | 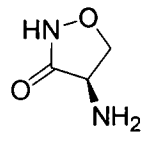 | Cell wall peptidoglycan synthesis: *DdlA* and *Alr* | | | |

**Table 1.1 – Drugs for treatment of TB and their molecular targets (derived from McKinney *et al* 2000)**

in KatG has been shown to reduce the activity of the enzyme on isoniazid (Wengenack *et al.* 1997). However, mutations in the KatG gene are not always linked to an increase in isoniazid resistance (Haas *et al.* 1997; Victor *et al.* 1997). KatG is part of a set of enzymes involved in the oxidative stress response that is controlled in many bacteria by the transcriptional regulator, *oxyR*, (Storz *et al.* 1990) but this is deleted in *M. tuberculosis* (Deretic *et al.* 1997). This allows constant oxidation of INH and explains the specificity of isoniazid for *M. tuberculosis* but not all mycobacteria. In some strains of *M. tuberculosis katG* has been completely deleted, but this is generally accompanied by an increase in expression of a gene, *ahpC*, a subunit of alkyl hydroperoxide reductase (Sreevatsan *et al.* 1997b). Both KatG and AhpC are detoxifying enzymes that can protect the cell from peroxide mediated damage. Mutations have been determined in *AhpC* but have not been correlated directly with INH resistance (Kelley *et al.* 1997).

Because of the number and simplicity of the reactive species formed, there is potential for activated INH to attack a range of molecular targets (Slayden *et al.* 2000). A build-up of $C_{24}$-$C_{26}$ fatty acids on INH-treated cells indicates a block in the elongation of long-chain fatty acids to very long-chain fatty acids. Two enzymes that are the subject of intense discussion are InhA and KasA, both parts of the fatty acid synthase system, FASII.

InhA is an enoyl-acyl carrier protein (ACP) reductase that was shown to confer isoniazid resistance on *M. smegmatis* when overexpressed (Banerjee *et al.* 1994). Characterisation of InhA mutants found in INH-resistant clinical isolates *in vitro* showed a decreased affinity for the cofactor nicotine adenine dinucleotide (NADH) ((Basso *et al.* 1998). Originally it was thought that the activated INH attacked the

InhA-$NAD^+$ complex but it has been shown that the activated INH forms an adduct with NADH in solution (Wilming 1999). Hence the decreased affinity for NADH could be represented as a decreased affinity for the INH-NAD adduct. The binding of this adduct to InhA has been determined by X-ray crystallography (Dessen *et al.* 1995; Rozwarski *et al.* 1998). However, studies in *M. tuberculosis* produced conflicting evidence in comparison to the studies in *M. smegmatis* (Mdluli *et al.* 1996).

Another member of the FASII system was discovered to have links with the mode of action of isoniazid. KasA is a ketoacylsynthase that forms a complex with a small acyl carrier protein, AcpM (Mdluli *et al.* 1998). This complex binds to isoniazid and INH treatment seemed to provide the fatty acid composition expected from the inhibition of KasA. Mutations are found in the KasA sequence in INH-resistant strains of *M. tuberculosis* and some of these have an effect on isoniazid binding. Further work described in more detail the role of KasA and KasB in mycolic acid synthesis and their use as drug targets (Kremer *et al.* 2000; Schaeffer *et al.* 2001; Slayden *et al.* 2002). However, recently, reports have suggested that some of the phenomena associated with the link between KasA and INH are as a result of the InhA inhibition by INH, not as a direct result of KasA inhibition, and confirmed InhA as the specific target (Larsen *et al.* 2002; Kremer *et al.* 2003).

It is clear that the mode of action of INH is a complex one and that it may simultaneously affect several pathways involved in cell wall fatty acid synthesis. This is also reflected in the isoniazid resistance profile of tuberculosis. Mutations or frame-shifts in the activating pathway, KatG, can account for approximately 50% of resistant strains (Ramaswamy *et al.* 1998). Similarly, mutations in InhA

and KasA can account for some resistant strains. However, in no report have all INH-resistant strains been accounted for by known molecular targets.

### 1.1.5 New Drug Targets

Because of the rapid rise in drug-resistant strains of tuberculosis, a great effort is currently underway to develop new drugs to treat this disease. A particular area of interest at present is characterising the persistent stage of the bacteria. Specifically targeting the persistent bacteria could result in a decrease of the treatment time required, thus increasing patient compliance and reducing the risk of future drug-resistance (Global Alliance for TB Drug Development, http://www.tballiance.org). At a meeting to discuss "Current Developments in Drug Discovery for Tuberculosis" (Bangalore, India, February 2002) a range of new targets and molecules active against TB were presented (Brooke *et al.* 2002).

The fluoroquinolones, proven antibiotics with other infections, also have activity against *M. tuberculosis* by inhibiting a DNA gyrase and blocking DNA polymerisation (Zhao *et al.* 1999). The most successful fluoroquinolones tested are levofloxacin, gatifloxacin, moxifloxacin and ofloxacin and these have shown sterilizing activity as well as activity against multiplying bacteria (Rodriguez *et al.* 2002; Hu *et al.* 2003). The nitroimidazopyran PA-824 has shown excellent activity against *M. tuberculosis* in *in vitro* and *in vivo* studies (Stover *et al.* 2000; Duncan 2003) and the Global Alliance for TB Drug Development has recently obtained the worldwide license for this drug. Isoxyl was used as a clinical treatment of tuberculosis in the 1960s and substituted derivatives have shown improved anti-tubercular action (Phetsuksiri, Baulard *et al.* 1999). Thiolactomycin also possesses antimycobacterial activity by inhibiting KasA and KasB and

derivatives have shown more potent action against these enzymes and the mycobacteria (Kremer, Douglas *et al.* 2000). A library of 63,238 ethambutol analogues have been synthesised and have shown a rise in activity against *M. tuberculosis* of over an order of magnitude over ethambutol itself (Lee *et al.* 2003). Recent interest has been sparked in the processes involved in the persistent phase of the bacteria. It has been shown that the glyoxylate shunt pathway of carbon metabolism is activated in the persistent form of *M. tuberculosis* (McKinney *et al.* 2000). Studies have now determined the structures of malate synthase (Smith *et al.* 2003) and isocitrate lyase (Sharma *et al.* 2000), two enzymes of the glyoxylate shunt pathway and these are potential drug targets for latent TB.

## 1.2 Arylamine *N*-acetyltransferase

### 1.2.1 History of Arylamine *N*-acetyltransferase

Arylamine *N*-acetyltransferases (NATs) are a family of Phase II xenobiotic-metabolizing enzymes that have been found in a wide range of prokaryotes and eukaryotes (Upton *et al.* 2001a). The enzyme was first characterized in humans as the factor responsible for the polymorphic inactivation of the anti-tubercular drug isoniazid (Evans *et al.* 1960). The two human isoenzymes are 30-34kDa cytosolic proteins found in a range of human tissues and have both distinct and overlapping substrates (Grant *et al.* 1989; Hickman *et al.* 1998). The acetyl transfer reaction involves the use of acetyl Coenzyme A (AcCoA) as a cofactor (Riddle *et al.* 1971). NATs can generally acetylate a wide range of arylamines, arylhydroxylamines and aryl hydrazines including environmental toxins (Hein *et al.* 1993) and drugs (Weber *et al.* 1985). Subsequent work on NATs has focused on a wide variety of

fields including, in particular, carcinogenesis (Hein *et al.* 1993), developmental studies (Smelt *et al.* 2000) and pharmacogenetics (Weber *et al.* 1985).

NAT activity was first described in bacteria in one of the Ames mutagenicity tester strains that had a high susceptibility to food-based carcinogens (Saito *et al.* 1983). Advances in recombinant protein technology and genomics has allowed the in depth analysis of NAT structure and function and the discovery of many more bacterial NATs. Current investigations in this area are focussed around the role of NATs in different bacterial families and the effect that bacterial NATs may have on human diseases such as tuberculosis and inflammatory bowel disease.

### 1.2.2 Catalytic action and structure of NAT

The early studies on NAT showed that it worked by a 'ping-pong' bi-bi mechanism (Riddle *et al.* 1971), involving the binding of acetyl CoA to the enzyme, acetyl transfer to the enzyme, followed by binding of the arylamine and the final acetyl transfer. The inhibition of NAT activity by iodoacetic acid and subsequent amino acid analysis showed that the active residue in NATs was a cysteine (Andres *et al.* 1988). Sequencing of the NAT from *Salmonella typhimurium* (STNAT) showed that it was $Cys^{69}$ that was involved in the acetyl transfer (Watanabe *et al.* 1992).

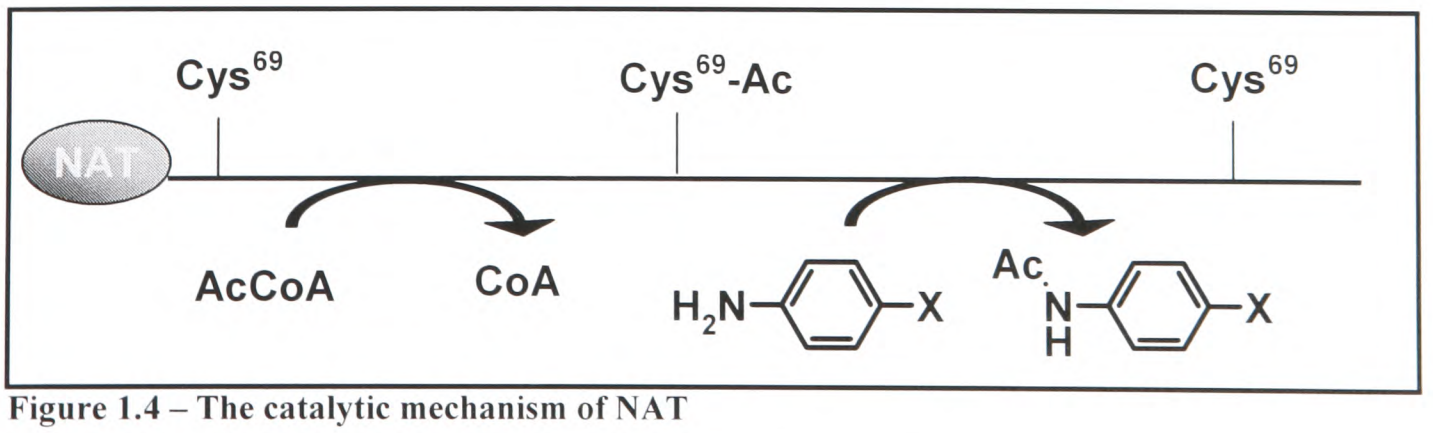


**Figure 1.4 – The catalytic mechanism of NAT**

The figure shows the transfer of an acetyl group from acetyl Coenzyme A to an arylamine via a ping-pong mechanism utilizing $Cys^{69}$ (STNAT nomenclature).

The first three-dimensional structure of NAT was determined by X-ray diffraction of recombinant STNAT crystals (Sinclair *et al.* 2000). The structure, at 2.8Å resolution, was sufficiently detailed to elucidate the catalytic residues involved in the acetyl transfer reaction. A catalytic triad of $Cys^{69}$-$His^{107}$-$Asp^{122}$ was observed that provided the general-base catalysis required for the reaction to occur. Previously, a highly conserved arginine residue, $Arg^{65}$, was thought to play a catalytic role (Watanabe *et al.* 1992). However, correlation with known human NAT polymorphisms suggest that the conserved arginine may well be key to the stability of the NAT structure (Rodrigues-Lima *et al.* 2001). The unique fold showed that the protein fell into three clear domains: an α-helical bundle of 84 residues, a β-sheet barrel of 95 residues and an α/β lid of 98 residues. The catalytic residues are found in the first two domains, and these residues are conserved throughout the NAT family. The triad provides for a charge transfer system, with the aspartate pulling a proton from the histidine and the histidine either partially or fully deprotonating the cysteine residue thiol. The thiolate would thus be sufficiently active to attack the AcCoA thioester and allow the acetyl transfer to occur (Sandy *et al.* 2002).

The structure of STNAT showed a strong similarity to the structures of several members of the cysteine protease superfamily, including the papain family. Cysteine proteases have been the target of several drugs to treat diseases as diverse as malaria (Rosenthal *et al.* 2002) and Alzheimer's disease (Hook *et al.* 2002). NAT and the cysteine proteases are likely to have evolved from a common precursor and it is thus possible that NAT may have a role in the cell other than the acetyltransferase reaction assayed *in vitro*, at least in some organisms.

A further 1.7Å structure of NAT from *M. smegmatis* showed a near identical fold (Figure 1.5) and suggested the presence of an oxy-anion hole that would stabilise the transition state of acetyl transfer (Sandy *et al.* 2002). Alignment of eukaryotic and prokaryotic NATs has identified several conserved regions in many members of the NAT family including a FENL region around amino acid 40 particularly in eukaryotic NATs (Figure 1.6a) and an RGGX sequence immediately prior to the active-site cysteine (Figure 1.6). The alignment also shows an extra 16 amino acid section in eukaryotes towards the end of the second domain (Figure 1.6). This is predicted to form a random loop on the exterior of the protein, and this may explain the difficulties observed in crystallizing eukaryotic NATs (Sticha, Sieg *et al.* 1997). A partial model of the first two domains of human NAT2 predicted that the eukaryotic NATs would maintain the same fold (Rodrigues-Lima *et al.* 2001); Mushtaq, 2002).

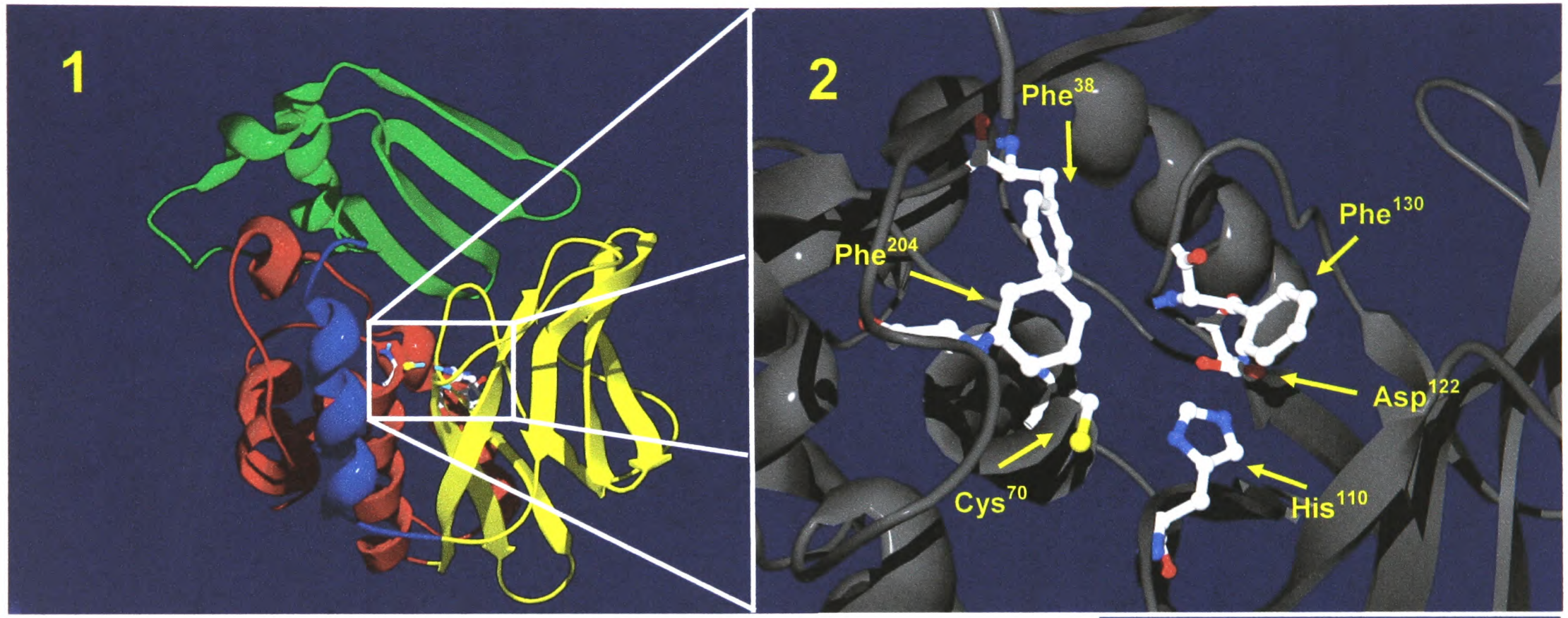


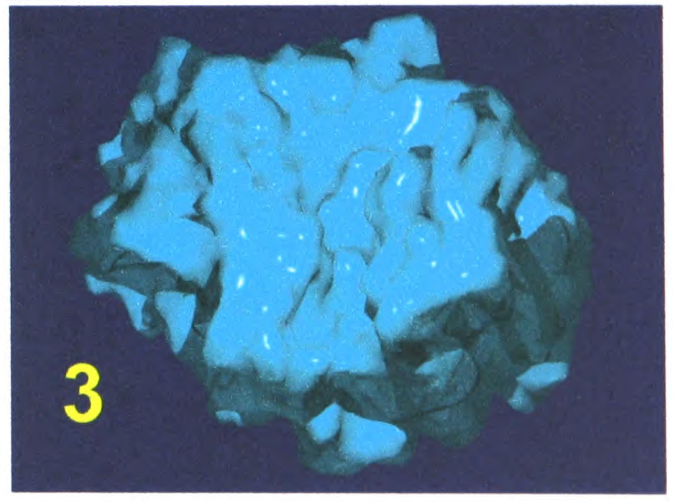


**Figure 1.5 – The structure of arylamine *N*-acetyltransferase from *Mycobacterium smegmatis***

The structure of MSNAT was downloaded from The Protein Data Bank (http://www.rcsb.org, accession number 1GX3) and viewed in Swiss PDB Viewer. Plate 1 shows the three domains in ribbon format – domain 1 (*N*-terminal) in red, domain 2 in yellow, the interdomain region in blue and domain 3 (*C*-terminal) in green. Plate 2 shows the active site in CPK colouring, including the catalytic triad and three closely positioned phenylalanine residues (Brooke, Davies *et al.* 2003b). Plate 3 shows the molecular surface of MSNAT. All MSNAT structures in this thesis are drawn using the same orientation.

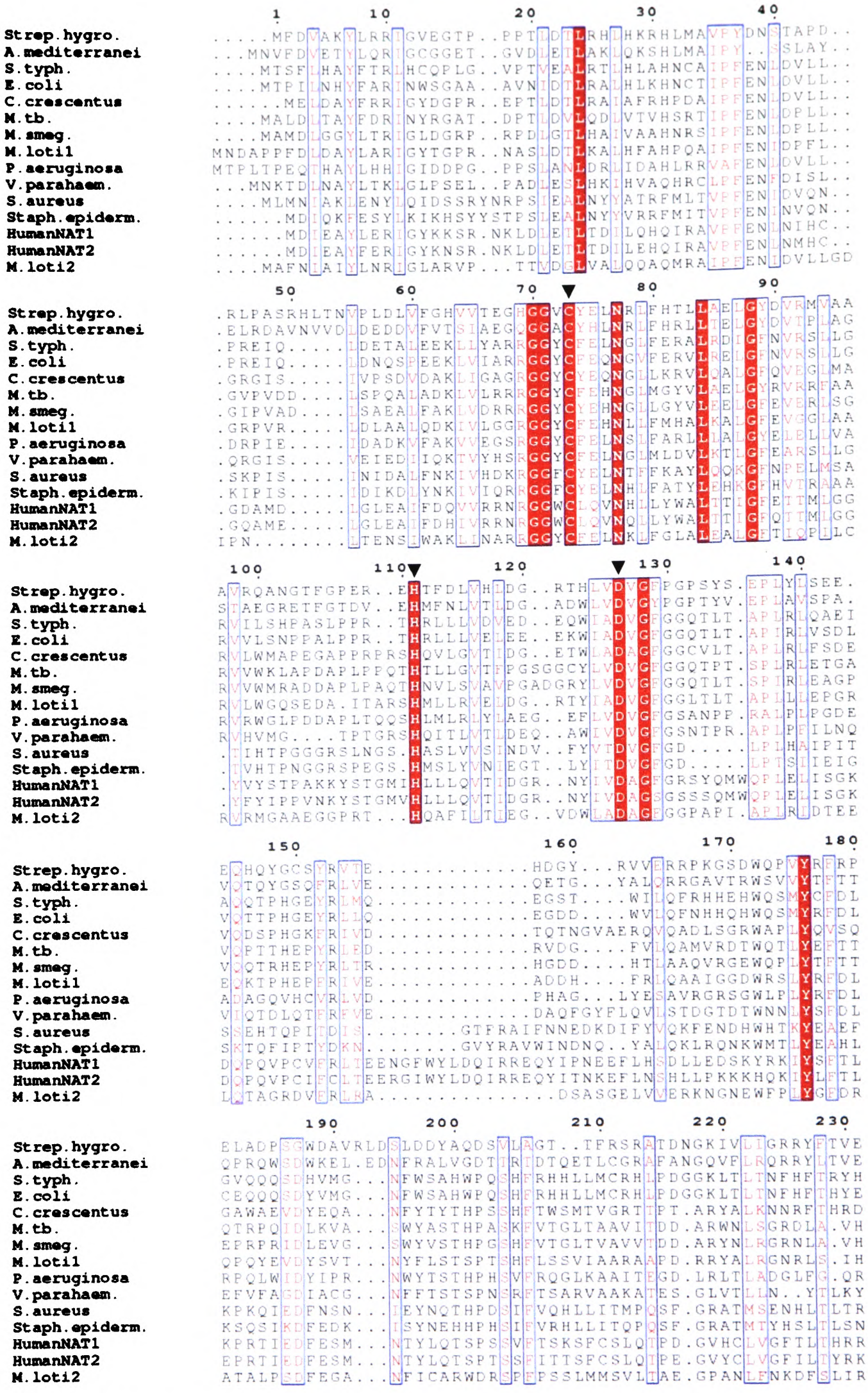


**Figure 1.6b: Sequence alignment of a selection of bacterial and human NATs**

Sequence alignment was performed on ClustalW on http://www.ebi.ac.uk and picture generated with ESPript on http://www.expasy.ch. The first two domains are shown. Abbreviations are: Strep.hygro. – *Streptomyces hygroscopicus*; A. – *Amycolatopsis*; C. – *Caulobacter*; S.typh. – *Salmonella typhimurium*; M.tb. – *Mycobacterium tuberculosis*; M.smeg. – *M. smegmatis*; M.loti1 & M.loti2 – *Mesorhizobium loti*; P. – Pseudomonas; V.parahaem. – *Vibrio parahaemolyticus*; S.aureus – *Staphylococcus aureus*; Staph.epiderm. – *Staphylococcus epidermidis*. The catalytic triad is marked with arrows.

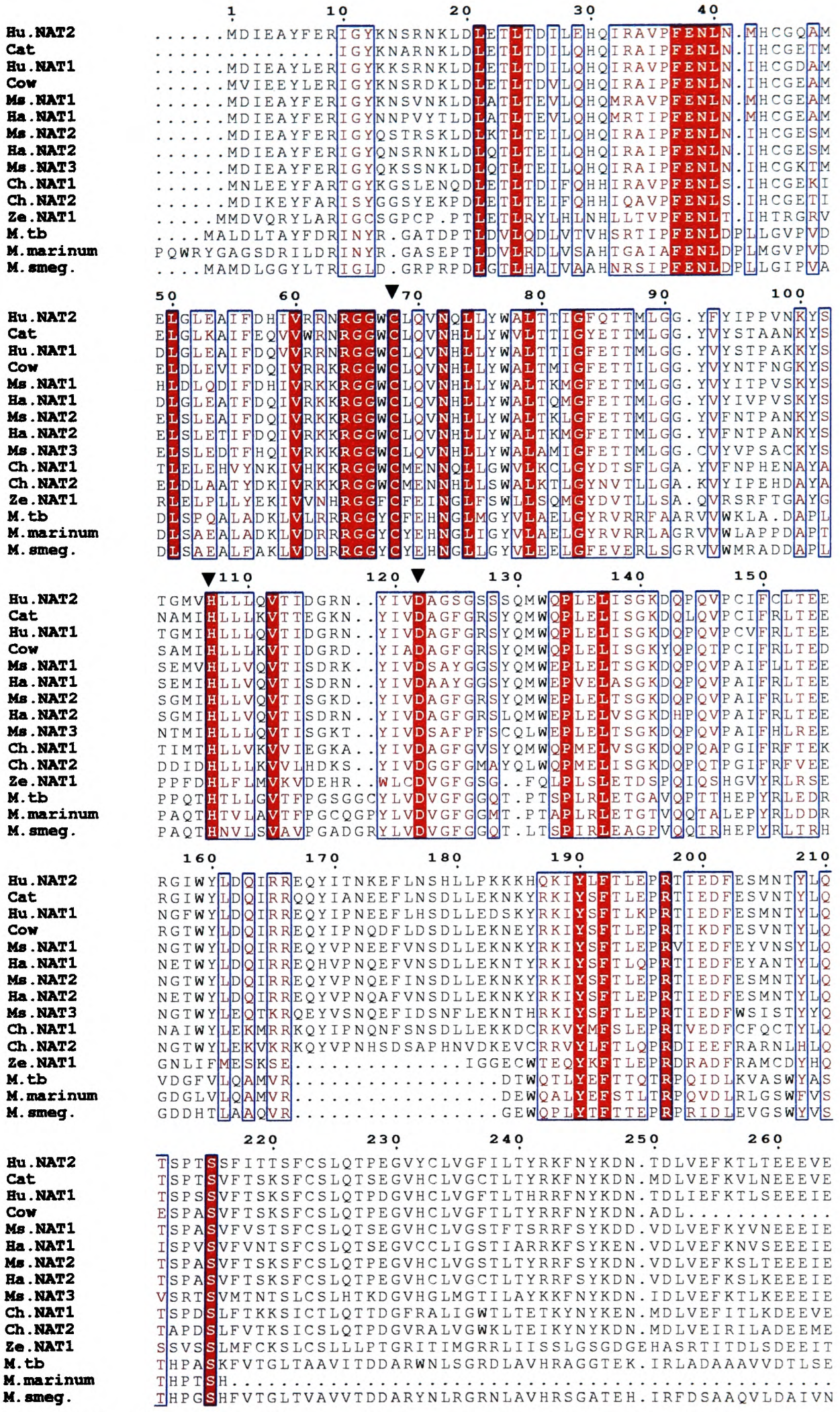


**Figure 1.6a: Sequence alignment of a selection of eukaryotic and mycobacterial NATs**

Sequence alignment was performed on ClustalW on http://www.ebi.ac.uk and picture generated with ESPript on http://www.expasy.ch. The first two domains are shown. Abbreviations are: Hu. – *Homo sapiens*; Cat – *Felis silvestris catus*; Cow – *Bovis bovis*; Ha. – Syrian Hamster *Mesocricetus auratus*; Ms. – *Mus musculus*; M.tb. – *Mycobacterium tuberculosis*; M.smeg. – *M. smegmatis*; Ze. – *Danio rerio*. The catalytic triad is marked with arrows.

### 1.2.3 NAT in bacteria

*1.2.3.1 The Ames Test*

Many environmental arylamines are mutagenic in humans and their mutagenic effects have been related to NAT acetylation status and polymorphism (Fretland *et al.* 2002). The relationship between NAT activity and mutagen susceptibility is complex and depends on the tumour type and location in the body (Agundez *et al.* 1995; Varzim *et al.* 2002). It is generally accepted that *N*-acetylation of arylamines leads to the deactivation of the mutagenic properties and the excretion of these compounds. However, if the arylamine is first oxidised by cytochrome P450 (e.g. CYP1A2)(Brockmoller *et al.* 1996) the *N*-hydroxy product formed can be *O*-acetylated and leads to the formation of highly reactive arylnitrenes that can form DNA adducts (Hein *et al.* 1993).

The Ames tester strains of *S. typhimurium* have been used for many years as a diagnostic test of the mutagenicity of chemical and biological samples (Mortelmans *et al.* 2000). The strains possess a mutation in the gene controlling histidine production that greatly inhibits growth without a histidine source. Incubation of the bacteria with a mutagenic compound can lead to a reverse mutation in the mutant *his* gene, allowing the bacteria to grow again without added histidine. The frequency of growing bacteria indicates the mutagenicity of the compound (Ames *et al.* 1973). One particular strain, TA98/1,8-DNP, was resistant to the toxic and mutagenic effects of arylamines (Saito *et al.* 1983). Another strain, YG1024, was more susceptible to these effects (Watanabe *et al.* 1993). Subsequent studies showed that strain TA98/1,8-DNP was deficient in NAT activity, and YG1024 overexpressed the *nat* gene. Hence, the increased rate of *O*-acetylation by NAT lead to an increased toxicity of these compounds.

*1.2.3.2 NAT in S. typhimurium*

Recombinant NAT from *S. typhimurium* (STNAT) was produced and showed 25-33% similarity over the 170 amino acids at the N-terminus to the eukaryotic NAT enzymes that had been previously sequenced (Watanabe *et al.* 1992). A key cysteine residue was found ($Cys^{69}$) that was conserved in all NAT sequences and a mechanism was suggested involving an acetylated cysteine intermediate. This correlated with the inhibition of NAT activity by iodoacetamide and *N*-ethylmaleimide. The C-terminus shows much weaker homology to the eukaryotic proteins. A deletion mutant of the eleven C-terminal amino acids of STNAT possessed poor acetyl transfer activity but could hydrolyse AcCoA in the absence of an arylamine substrate (Mushtaq *et al.* 2002). When the entire third domain is missing, STNAT has no acetyl transfer activity, as had been observed with a truncated human NAT isozyme (Sinclair *et al.* 1997). Again the truncated STNAT hydrolysed AcCoA, suggesting a role for the C-terminus in substrate binding and protection of the acetylated enzyme intermediate from hydrolysis (Mushtaq *et al.* 2002).

*1.2.3.3 The distribution of NATs in bacteria*

The rapid production of bacterial genomes has been an invaluable resource in many areas of microbiology and bacteriology (Fitzgerald *et al.* 2001; Raczniak *et al.* 2001; Schoolnik 2002). In the NAT field, the availability of bacterial genomes has shown the diversity of *nat* genes in bacteria and pinpointed key conserved residues found in many NAT sequences. Genes which are *nat* homologues have not been found in all bacterial phyla, but have been identified extensively in three of the eubacterial phyla: proteobacteria, gram-positive bacteria (firmicutes) and actinobacteria. Genome searches have shown *nat*-like genes in over twenty

eubacteria (Payton *et al.* 2001b; Rodrigues-Lima *et al.* 2002). The NAT sequences show 30-80% amino acid similarity over the first two domains (Figure 1.6) and active recombinant proteins of many of these genes have been created (Payton *et al.* 2001b). Similarly, in an activity based study, NAT activity was detected in lysates from fifteen strains of bacteria from the gut flora (Delomenie *et al.* 2001). Many of the bacteria that possess NAT activity live in the soil or the gut where high concentrations of potentially toxic organic material are present, reinforcing the suggestion of NAT playing a general role as a protective enzyme for the breakdown of exogenous arylamine toxins (Delomenie *et al.* 2001; Payton *et al.* 2001b; Brooke *et al.* 2003). This is compatible with the presence of several genes in the region of the *nat* gene that show homology to enzymes used for the degradation of aromatic compounds such as biphenyl-2,3-diol-1,2-dioxygenase (Payton *et al.* 2001b). In *M. smegmatis*, the *nat* gene is transcribed as part of a larger message suggesting that NAT forms part of an operon in this organism (Payton *et al.* 2001a).

NATs have been found extensively throughout the eubacterial and the vertebrate kingdoms (Rodrigues-Lima *et al.* 2002). However, no NAT sequences have so far been discovered in any members of the Archaea (Payton *et al.* 2001b) or in non-vertebrates, apart from the urochordate *Ciona intestinalis* (Rodrigues-Lima *et al.* 2002) which possesses considerable similarities to vertebrates in development. In other lower organisms and plants, NATs may not be required due to other arylamine metabolising pathways. Alternatively the organisms may synthesize arylamines themselves making NAT activity detrimental (Deguchi 1992). Studies of the distribution of NATs throughout eukaryotes and prokaryotes have suggested that NATs have spread from a common ancestor (Rodrigues-Lima *et al.*

2002). NAT had been placed as part of a set of 41 genes thought to have passed laterally from bacteria to vertebrates (horizontal gene transfer) (Salzberg *et al.* 2001) but the existence of this phenomenon is not convincingly supported (Stanhope *et al.* 2001).

Interestingly, the two NAT paralogs in *Mesorhizobium loti* are the first example of NAT paralogs in bacteria (Rodrigues-Lima *et al.* 2002). Although the sequence identity between the paralogs is very low (31%, Figure 1.7), it has been suggested that the paralogs are a result of ancestral gene duplication rather than horizontal gene transfer. Bacteria within the same bacterial class (e.g. γ-Proteobacteria) can have both similar (e.g. *Eschirichia coli* and *S. typhimurium*) and diverse (e.g. *Pseudomonas aeruginosa*) NAT sequences, but differing rates of evolution can account for the differences observed. Those bacteria that do not possess a NAT sequence have probably undergone gene loss, as observed in the *M. leprae* genome compared to the *M. tuberculosis* genome (Cole *et al.* 2001).

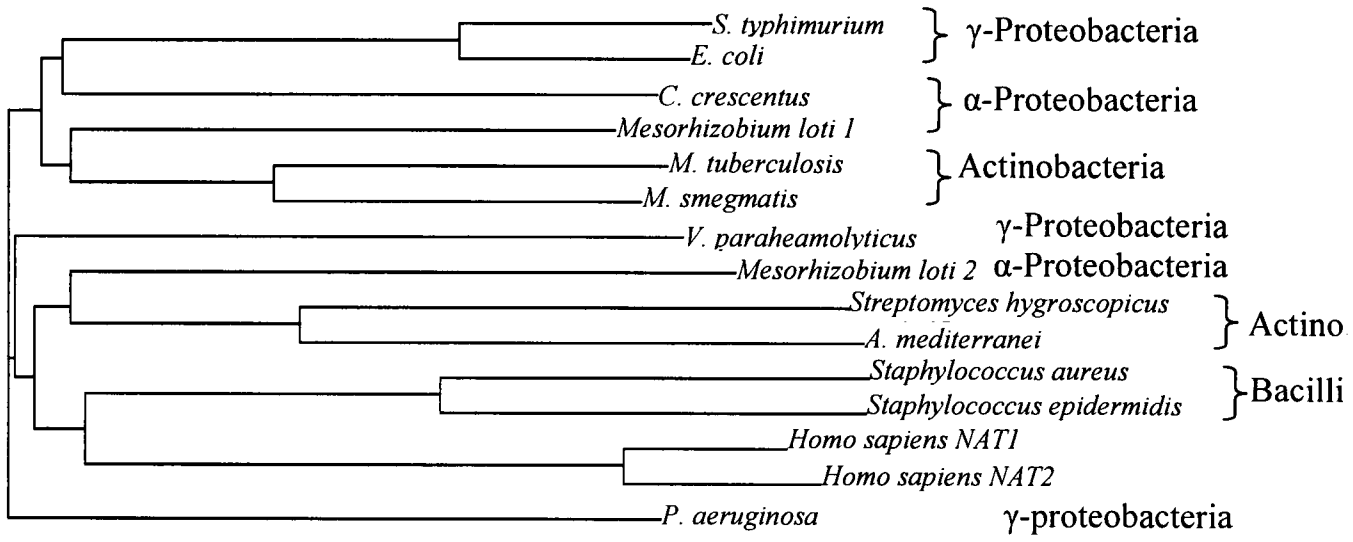


**Figure 1.7 – Phylogenetic tree of a selection of bacterial and human NATs**
A phylogram of the NAT sequences aligned in Figure 1.6b was created using ClustalW (http://www.ebi.ac.uk).

### *1.2.3.4 NAT-like enzymes in antibiotic biosynthesis*

Several NAT homologues do appear to be encoded in an operon and to have very specific endogenous functions. Genome searches showed that there was a NAT homologue in *Amycolatopsis mediterranei* (Payton *et al.* 2001b), an actinomycete that produces the antibiotic Rifamycin B. The NAT homologue was shown to be the final enzyme, RifF, in the rifamycin synthetic pathway. Rifamycin B is formed from an aromatic precursor that is then extended by the polyketide synthase genes *rifA-rifE* (Yu *et al.* 1999). This produces an aromatic amine base with a long polyketide chain, attached to the polyketide synthase by a thioester bond. RifF catalyses the amide bond formation via an intra-molecular acyl transfer reaction. The protein is 40% similar to STNAT and contains the three key catalytic residues ($Cys^{69}$-$His^{107}$-$Asp^{122}$ STNAT numbering, Figure 1.6) but does not possess the FENL region around position 40 (Figure 1.6b). This protein has been expressed and purified and does not show any acetyltransfer activity (Pompeo *et al.* 2002b). The catalytic site of RifF has been modelled and shows a more open structure, as would be expected to be required to accommodate the

large polyketide substrate. The NAT-like sequences in *Actinosynnema pretiosum* and *Streptomyces achromogenes* play similar roles in the synthesis of ansamitocin and rubranosol (Payton *et al.* 2001b). The genes *shnN* and *gdmF* (in strain NRRL 3602) from *S. hygroscopicus*, (Rascher *et al.* 2003) are NAT-like and found in the gene-clusters for ansamycin and geldamycin antibiotic biosynthesis. This subfamily are examples of NAT-like proteins with an intra-molecular acyltransfer activity and comparisons between these enzymes and the other members of the NAT family could give key insights to the function and mechanism of NATs.

*1.2.3.5 The endogenous role of NATs in eukaryotes and prokaryotes*

In humans, there are two NAT enzymes, NAT1 and NAT2 (Grant *et al.* 1989); (Blum *et al.* 1990). These two enzymes exhibit differing yet overlapping substrate specificities (Minchin *et al.* 1992; Minchin 1995) and tissue distributions (Jenne 1965; Hickman *et al.* 1998; Smelt *et al.* 2000). This evidence has suggested differing roles for the two isoenzymes: NAT1 can acetylate *p*-aminobenzoic acid (pABA) and *p*-aminobenzoylglutamate (pABA-Glu), a folate catabolite, suggesting a role for NAT1 in the folate cycle. NAT1 may hence play a key role early in development and has been linked with neural tube defects (Mills *et al.* 1996; Sim *et al.* 2000). NAT2 acetylates a broad range of substrates and its tissue distribution suggests that it plays a role in xenobiotic metabolism (Pompeo *et al.* 2002a). Recently, mice have been generated with a *Nat2* (thought to be equivalent to human NAT1) knockout (Cornish *et al.* 2003) and *Nat1/Nat2* double knockout (Sugamori *et al.* 2003). Both of these organisms were viable and showed no obvious phenotype under laboratory conditions. However, the double knockout had greater area-under-curve plasma concentrations when treated with the drugs

*p*-aminosalicylate and sulfamethazine. In prokaryotes, a genetic knockout approach can be used to elucidate the roles of NATs in different bacteria (Payton *et al.* 2001a). Similarly, a "chemical knockout" approach could also be used for the same purpose (Schreiber 1998) (Section 1.3.1).

The one eukaryotic NAT substrate that is rarely acetylated by bacterial NATs is *p*-aminobenzoic acid (pABA) (Delomenie *et al.* 2001; Brooke *et al.* 2003). In bacteria, pABA plays an essential role as a folate precursor (Herrington 1994) so acetylation of pABA by bacterial NATs would be expected to be highly destructive to the organism. However, *Pseudomonas aeruginosa* has shown weak pABA acetylating activity in cell lysates (Delomenie *et al.* 2001) as does NAT from *P. aeruginosa* when expressed as a recombinant protein (Isaac Westwood, personal communication). This discovery raises several questions as to folate production in this bacterium. *P. aeruginosa* can live in many toxic environments and can grow on organic pollutants (Prescott *et al.* 1999). In line with NAT playing a protective role against aromatic toxins, NAT from *P. aeruginosa* exhibited the highest NAT activities of a series of bacterial cell lysates tested (Delomenie *et al.* 2001). A partial NAT sequence has been found in *Sphingomonas aromaticivorans* (Rodrigues-Lima *et al.* 2002), a bacterium noted for its aromatic compound metabolizing capabilities (Shi *et al.* 2001) suggesting a detoxifying role for NAT in *S. aromaticivorans* also. Further investigation of the enzymes in these bacteria and their expression could prove useful in defining and exploiting NAT activity for detoxification.

### 1.2.4 NAT in mycobacteria

The discovery of NAT with isoniazid-acetylating activity in *M. tuberculosis* suggests that NAT may play a role in isoniazid resistance in TB (Payton *et al.* 1999). *N*-Acetyl-INH is therapeutically inactive both *in vitro* and *in vivo* (Bernstein *et al.* 1952). It has been shown that heterologous expression of *M. tuberculosis* NAT (TBNAT) in *M. smegmatis* results in a three-fold increase in resistance to INH (Payton *et al.* 1999) and a *M. smegmatis nat* knockout mutant gave a slight increase in INH sensitivity (Payton *et al.* 2001a). It can thus be suggested that TBNAT could also be involved in INH resistance (Upton *et al.* 2001b). In some clinical isolates of *M. tuberculosis*, a G619A single nucleotide polymorphism (SNP) of the *nat* open reading frame was identified. This SNP results in G to R change at amino acid 207 of the enzyme (Upton *et al.* 2001b). This substitution results in a lower structural stability or solubility and a 10 times lower affinity of the enzyme for INH. The modelled structures of *M. tuberculosis* 207G NAT and 207R NAT suggest that this mutation causes a Phe residue involved in substrate-binding to be moved, and hence alters the isoniazid acetylation activity (Upton *et al.* 2001b);(Kawamura *et al.* 2003).

NAT may not only play a role in isoniazid metabolism in mycobacteria but may also possess an endogenous function separate to the acetylation of exogenous arylamines. The growth of a genetically modified *M. smegmatis* strain in which the *nat* gene is knocked out is considerably delayed when compared with the $mc^2155$ parental strain, due to an extended lag phase. This suggests that the presence of NAT is required during early growth (Payton *et al.* 2001a). A *M. bovis* BCG strain with the *nat* gene knocked out is currently being characterised in these laboratories (Sanjib Bhakta, personal communication). Further investigation

of mycobacterial *nat* knockout strains may elucidate what function this enzyme plays within the mycobacterial cell itself.

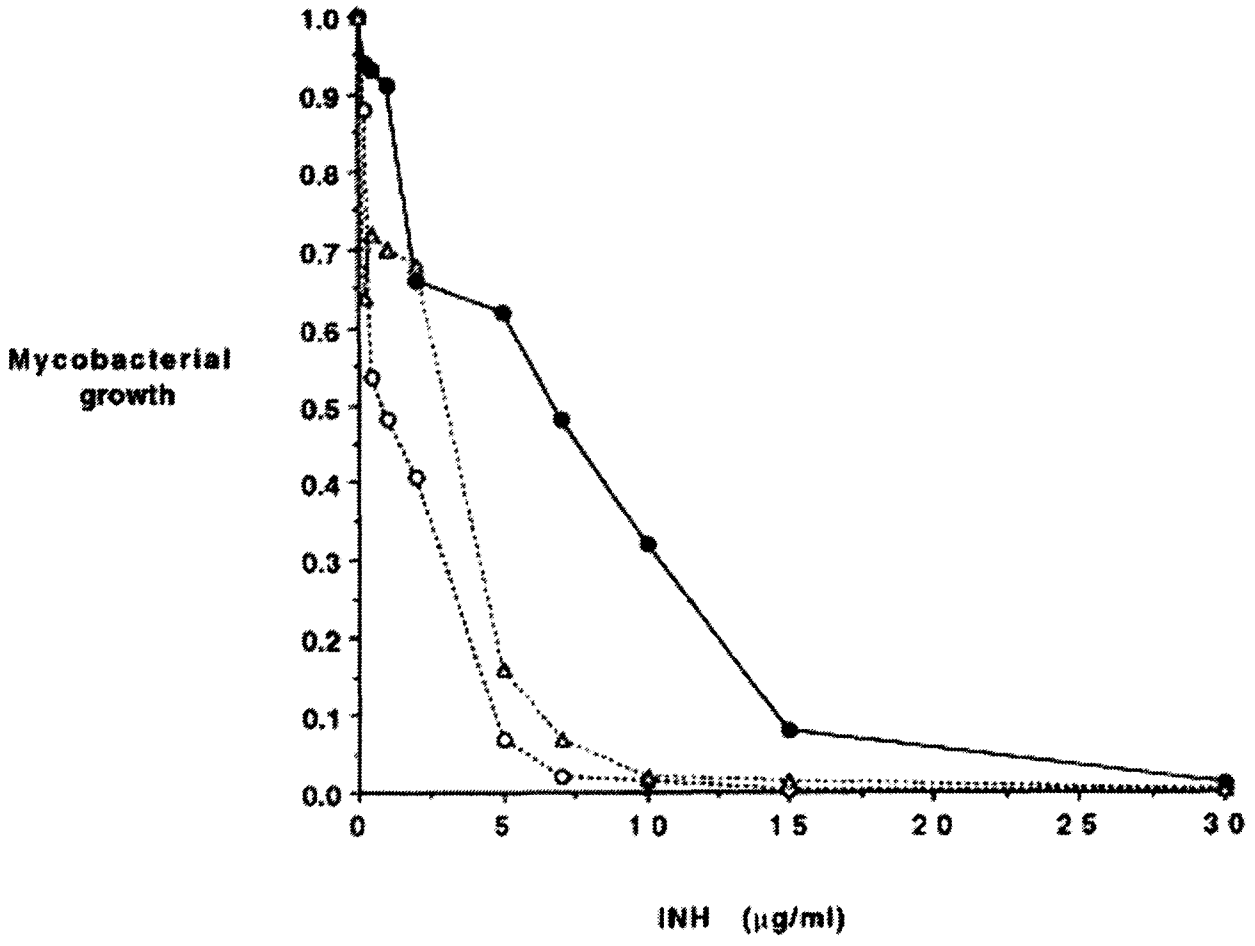


**Figure 1.8 – The effect of NAT overexpression on the sensitivity of *M. smegmatis* to isoniazid (from Payton *et. al.*, 1999)**
NAT from *M. tuberculosis* was overexpressed in *M. smegmatis* and grown on acetamide in varying concentrations of isoniazid (filled circles). Growth was compared to wild-type *M. smegmatis* containing the empty vector grown on acetamide (open circles) and glucose (triangles).

## 1.3 Drug Discovery

### 1.3.1 Drug Target Identification

Over the last decade, great advances in genomics, proteomics, high throughput screening and combinatorial chemistry have revolutionised the modern-day drug discovery programme (Figure 1.9, Sehgal 2002).

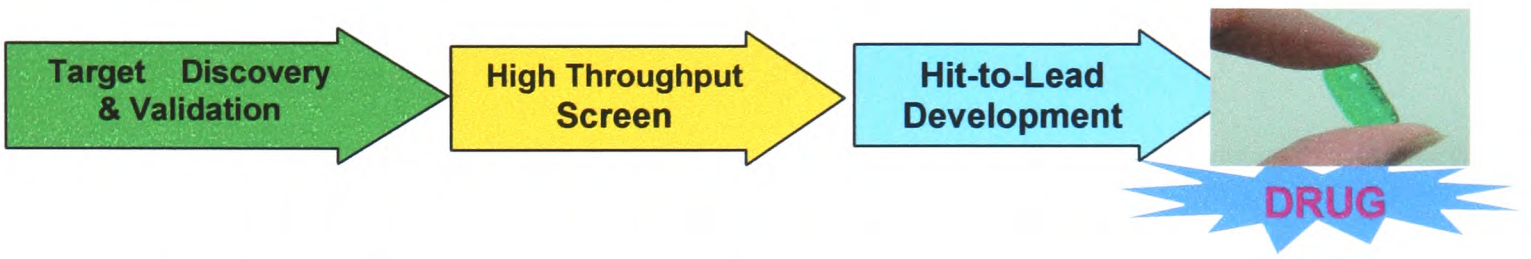


**Figure 1.9 – Twenty-first century drug discovery**

Analysis of current chemotherapies and their molecular targets shows that 45% of all therapeutic targets are cell membrane receptors and 28% are enzymes (Drews 2000). For antibiotic drug discovery, it is common to search for a biochemical pathway not present in the host but unique and vital to the organism. On deletion of the activity of an enzyme in this pathway, the organism should no longer be viable. Validation of a target can be performed genetically by creating a knockout of the gene in question and investigating the viability of the resultant organism *in vitro* and *in vivo*. Proteomics can allow the discovery of those proteins that are upregulated in a disease state as a route to target identification (Mullner *et al.* 1998). Alternatively, if a protein has been characterised and has known inhibitors, a 'chemical genetic' approach can be used to validate the protein as a target (Schreiber 1998). Finally, the target should be 'druggable' in that it should have a clearly defined binding site that a small molecule could bind to with enough strength to block the action of the target (Hopkins *et al.* 2002). With the increasingly rapid completion of whole genomes, especially bacterial genomes, *in*

*silico* bioinformatics can rapidly suggest roles for unknown genes by sequence homology and identify novel drug targets.

### 1.3.2 Hit-to-Lead

Once an enzyme target has been identified, small molecule ligands of the target must be discovered that block the enzyme's action. Firstly, an assay is required that can be used to determine the enzymic activity and to quantify the effect that small molecules have on the target. Secondly, a large library of compounds is tested against the target and those compounds with the highest activity are denoted as 'hits'. The more 'high-throughput' an assay system is, the more compounds can be tested and hence increases the likelihood of discovering successful hit molecules (Landro *et al.* 2000). High-throughput systems commonly use 96-well plate formats, although advances in robotics and liquid handling have allowed screens to be performed using 384- and 1536-well plates (Berg *et al.* 2000). Assays can be colorimetric, fluorescent, luminescent or radiometric and must be performed under acceptable conditions for the target involved, such as being performed around the $K_m$ value of a substrate for an enzymic target (Landro *et al.* 2000). After a hit molecule has been discovered, analogues of the molecule are synthesised under medicinal chemistry guidelines such as Lipinski's Rule-of-Five (Lipinski *et al.* 2001) to develop both the activity and the pharmacokinetic properties of the molecule. A drug-like molecule with sub-micromolar potency is termed a 'lead' molecule and can progress to more in-depth *in vivo* studies (Alanine *et al.* 2003).

As well as a suitable assay system, it is also necessary to acquire a library of small molecules to be tested. Advances in combinatorial chemistry and parallel

synthesis have greatly increased the possible output of chemical entities. This is particularly useful in the hit-to-lead stage of drug discovery, whereby large numbers of analogues of the hit molecule can be synthesised. Proper integration of chemical and biological research can greatly accelerate the drug discovery process (Floyd *et al.* 1999). In tuberculosis research (Section 1.1.5), Barry and co-workers synthesised a library of 63,238 ethambutol analogues in a 96-well format and tested them in a split-pool method, resulting in a maximal increase in potency of over an order of magnitude (Lee *et al.* 2003).

The combination of genomics, enzymology, structural biology and combinatorial chemistry can thus create a powerful tool in the development of novel antibacterial compounds.

## 1.4 Aims of this project

It has been demonstrated that NAT is potentially involved in INH resistance in *M. smegmatis* and *M. tuberculosis* (Upton *et al.* 2001b) (Section 1.2.4). The hypotheses to be tested by this project are that:

- NAT has an endogenous role in mycobacteria that is important to normal bacterial growth and development.
- Inhibition of NAT in *M. tuberculosis* will affect the normal growth of the cells and increase the sensitivity of the bacteria to isoniazid.

The aims of this study are thus:

i. To develop a rapid and efficient assay for the detection of NAT substrates and inhibitors.

ii. To screen a range of possible substrates to gain information about NAT substrate specificity and endogenous role.

iii. To search a large chemical library for novel inhibitors of NAT.

iv. To perform iterative syntheses and testing to improve inhibitor efficacy.

v. To determine the effect NAT inhibitors have on the growth of mycobacteria and the sensitivity of mycobacteria to isoniazid.

# Chapter 2

# Materials, Methods and Syntheses

## 2.1 Materials

### 2.1.1 Chemicals and other Reagents

All biochemicals were purchased from Sigma-Aldrich (Poole, Dorset) unless otherwise stated. Reagents for chemical syntheses were purchased from Sigma-Aldrich and Lancaster (Morecambe, Lancs.) except where indicated.

### 2.1.2 Bacterial strains

*M. smegmatis* strain $mc^2155$ was kindly provided by Dr. M. A. Payton. *M. bovis* BCG Pasteur was provided by Dr. T. Victor (University of Stellenbosch, South Africa). *E. coli* BL21(DE3)pLysS transformed with the pET28b expression containing either the *stnat* (Sinclair *et al.* 1998) or *msnat* (Sandy *et al.* 2002) genes were kindly provided by Mr. J. Sandy.

## 2.2 Methods

### 2.2.1 Bacterial Growth Conditions

Preparation of all bacterial cultures was performed under sterile conditions in a laminar flow hood. Growth of liquid cultures was monitored by measuring the

absorbance at 600nm of a 1mL aliquot using a Cecil 5500 spectrometer and a 10mm pathlength cuvette.

*a) E. coli*

*E. coli* was grown at 37°C either on solid Luria-Bertani medium-agar (LB-Agar) or in liquid cultures in LB medium with shaking (180rpm). LB medium in sterile glass conical flasks or sterile plastic tubes was inoculated with either single colonies from agar plates or with liquid cultures in late-log phase ($A_{600}$ greater than 1.5) diluted to an $A_{600}$ of 0.02. Cells were harvested at late-log phase at an $A_{600}$ of over 1.5. Cultures for MSNAT expression also contained 1M sorbitol and 2.5mM betaine and were grown at 27°C after induction of expression with isopropyl-β-D-thiogalactopyranoside (IPTG, 0.25mM). Glycerol stocks were made with aliquots of cultures at mid-log phase ($A_{600}$=0.6) added to sterile glycerol (10% v/v) and frozen at -70°C.

*b) M. smegmatis* (Parish *et al.* 1998a)

*M. smegmatis* was grown in Middlebrook 7H9 medium (Difco) containing 0.5% w/v Tween-80 and 1% v/v glycerol with 10% v/v albumin-dextrose-catalase enrichment (ADC, Becton Dickinson, Sparks, MD). Liquid cultures were grown at 37°C with shaking, 180rpm in sterile glass conical flasks or sterile plastic tubes until late log-phase ($A_{600}$=1.0, approximately 36 hours). *M. smegmatis* was also grown on solid 7H11 medium containing 10% v/v oleic acid-ADC enrichment (OADC, Becton Dickinson) at 37°C until colonies formed (approximately 3 days).

*c) M. bovis* BCG

*M. bovis* BCG was grown in Middlebrook 7H9 medium (Difco) containing 0.5% w/v Tween-80 and 1% v/v glycerol with 10% v/v albumin-dextrose-catalase (ADC) enrichment (Becton and Beckinson). Liquid cultures were grown at 37°C

in 450mL sterile plastic containers on a rolling incubator, 60rpm until late log-phase ($A_{600}$=1.0, approximately 7 days). Cultures at late log-phase were diluted 1/100 into fresh medium for a maximum of 7 passages. *M. bovis* BCG was also grown on solid 7H10 medium containing 10% v/v oleic acid-ADC enrichment (OADC, Becton and Beckinson) at 37°C until colonies formed (approximately 30 days).

*d)* Growth of mycobacteria was also carried out in the presence of isoniazid or NAT inhibitors. Compounds soluble in water were sterile filtered and diluted to 20 times the required concentration in sterile water. Samples were added to the bacterial culture at $A_{600}$=0.05 which was then incubated at 37°C (Sections 2.2.1b and 2.2.1c). Compounds that were insoluble in watter were dissolved in dimethylsulphoxide (DMSO) and added to the bacterial culture without sterilization to give a final concentration of DMSO of between 1% and 5% and compared with control cultures containing DMSO but no compound. Purity of the cultures was checked with Ziehl Neelsen staining (Section 2.2.2).

### 2.2.2 Ziehl Neelsen (ZN) Staining of Mycobacteria

Mycobacterial cultures were checked for contamination by ZN staining (Parish *et al.* 1998a). A drop of liquid culture at late-log phase was placed on the centre of a microscope slide and dried in a laminar flow hood. Carbol fuchsin stain (1mL, 1% w/v fuchsin in 85:10:5 water:ethanol:phenol) was added to the slide which was heated gently over a flame without boiling for 2 minutes. Slides were rinsed gently with water then decolourised with acid-alcohol solution (3% v/v conc. HCl in EtOH) and rinsed again. Counterstaining was performed with methylene blue solution (0.2% w/v in 3:1 water:ethanol containing 0.0075% w/v KOH) for 30

seconds before further rinsing and inspection under a light microscope (Olympus NH-2) at 1000x magnification with oil immersion.

### 2.2.3 AlamarBlue™ Cell Viability Assay

Bacteria were tested for active cell respiration by the reagent alamarBlue™ (Resazurin, BDH, Poole (Yajko *et al.* 1995; Palomino *et al.* 2002)). One tablet of Resazurin was dissolved in 50mL sterile water and the solution was added to growing cultures at 10% v/v. Cultures were allowed to grow until there was a clear colour difference between control samples with and without the relevant antibiotic present (isoniazid, 20μg/mL for mycobacteria; chloramphenicol, 34μg/mL for *E. coli*). Actively respiring cells cause the solution to turn pink while non-respiring cells remain blue. Test samples were compared with the controls to determine the Minimum Inhibitory Concentration (MIC) of a compound.

### 2.2.4 Fractionation of mycobacteria (Parish *et al.* 1998b)

Mycobacteria in the late-log phase were harvested by centrifugation (3,000x*g*, Sorvall RT 6000D, 15 mins, 4°C) before removal of the supernatant and resuspension in 10mL phosphate-buffered saline (PBS, 137mM NaCl, 10mM phosphate, 2.7mM KCl, pH 7.4) containing 1% w/v Tween-80. Samples were centrifuged under the same conditions, the wash solution removed and the pellet re-washed with fresh PBS-Tween solution for a total of three washes. The pellet was then resuspended in 1.5mL fractionation buffer (20mM triethanolamine (Tris).HCl, 2mM DTT, 1x EDTA-free Protease Inhibitor Cocktail (Roche), 10mM EDTA, pH 8.0) and ribolysed (2x 50sec at maximum rate) in a Mini Bead-Beater (Biospec) with an equal volume of 0.1mm glass beads. The supernatant was

removed and ultracentrifuged (27,000x*g*, 1hr, Optima TLX Ultracentrifuge with Beckman TLA rotor) resulting in the cell wall fraction being in the pellet. Subsequent ultracentrifugation of the supernatant (100,000x*g*, 1hr) gave the cell membrane fraction in the pellet and the cytosolic fraction in the remaining supernatant.

### 2.2.5 Expression of MSNAT and STNAT

Recombinant MSNAT (Sandy *et al.* 2002) and STNAT (Sinclair *et al.* 1998) with *N*-terminal hexahistidine tags were prepared as described previously. Expression was induced in the bacterial cultures (Section 2.2.1a) with isopropyl-β-D-thiogalactopyranoside (IPTG) at 1mM (STNAT) or 0.25mM (MSNAT) when the $A_{600}$ reached 0.4. Cells were harvested at 10,000x*g* (GSA rotor, Sorvall RC-5B, 20 minutes, 4°C), resuspended in 20mM Tris-HCl, 300mM NaCl, 1mM Pefabloc (Pentapharm) pH 8.0 and frozen at -70°C for up to one week.

### 2.2.6 Purification of MSNAT and STNAT

The recombinant proteins were purified by immobilized metal ion chromatography. Frozen cell pellets were thawed at 37°C immediately before use and sonicated (Soniprep 150) on wet ice using twenty bursts of 45 secs on, 30 secs off at 10 microns. Lysed cells were centrifuged (12,000x*g*, Sorvall RC-5B centrifuge, SS34 rotor, 20 mins, 4°C) to pellet cell debris. Soluble lysate containing either MSNAT or STNAT was loaded onto 4.0mL washed Ni-NTA agarose (Qiagen) and incubated at 4°C for 1 hour rotating at 15rpm before centrifugation (3,000x*g*, Sorvall RT 6000D, 15 mins, 4°C) and removal of the supernatant. The protein was eluted from the resin by either a column or batch

method. In each instance, the protein was eluted from the resin by washing sequentially (2 x 10 mL each) with wash buffer (20mM Tris.HCl, 300mM NaCl, pH 8.0) containing imidazole (1mM, 10mM, 50mM & 250mM, pH 8.0). MSNAT was eluted in the 50mM and 250mM washes and STNAT was eluted in the 250mM washes as determined by activity assays (Section 2.2.8) and SDS-PAGE (2.2.7). Fractions containing NAT were combined and dialysed against 100 volumes of dialysis buffer (20mM Tris.HCl pH 8.0, 1mM EDTA, 1mM dithiothreitol (DTT)) at 4°C. When required, the *N*-terminal His-tag was cleaved with Thrombin (Calbiochem) (5U.(mg protein)$^{-1}$, 37°C, 4 hours) and dialysed again. Protein was concentrated to approximately 5mg.mL$^{-1}$ using a Centricon-10 concentrator (Millipore). Typically the yield of pure active protein was 20mg (MSNAT) and 7mg (STNAT) per litre of culture.

### 2.2.7 Sodium dodecylsulphate - Polyacrylamide Gel Electrophoresis (SDS-PAGE)

Purification of NATs was followed by SDS-PAGE. Separating gels contained 10% v/v acrylamide:bisacrylamide (29:1) (Anachem), 375mM Tris.HCl pH 8.0, 0.125% w/v SDS, 0.05% w/v ammonium persulphate (APS) and 0.002% v/v *N,N,N',N'*-tetramethyl-ethylenediamine (TEMED). Stacking gels contained 6% v/v acrylamide:bisacrylamide 29:1, 125mM Tris.HCl pH 8.0, 0.125% w/v SDS, 0.05% APS and 0.002% TEMED. Gel sample preparation buffer (6mg.mL$^{-1}$ DTT, 50μg.mL$^{-1}$ bromophenol blue, 20mg.mL$^{-1}$ SDS, 5% w/v β-mercaptoethanol and 5% v/v glycerol) was added to an equal volume of protein sample and heated at 95°C for 10 minutes. Electrophoresis was performed at 25mA in gel running buffer (50mM Tris.HCl pH 8.3, 50mM glycine, 1% w/v SDS) with BioRad low

range molecular weight markers in one track of each gel. Gels were stained for 2 mins with Coomassie Blue R250 (3.75g.$L^{-1}$, 0.5M methanol, 1.87M acetic acid) and destained in 0.5M methanol, 0.75M acetic acid.

### 2.2.8 Arylamine acetylation assay

NAT activity was observed with a colorimetric arylamine acetylation assay (Andres *et al.* 1985). Detection of acetylation of arylamines was performed in a total volume of 100µl. Samples of enzyme (0.1-2µg protein) and arylamine (50-200µM final concentration) in assay buffer (20mM Tris.HCl, 1mM DTT, pH 8.0) were pre-incubated at 37°C for 5 minutes. AcCoA (400µM final concentration) was added to start the reaction and the samples were incubated at 37°C. The reaction was quenched with 100µl of ice-cold aqueous trichloroacetic acid (TCA, 20% w/v). 4-Dimethylaminobenzaldehyde (DMAB, 800µL, 5% w/v in 9:1 acetonitrile:water) was added and the absorbance was measured in a 10mm pathlength cuvette at $\lambda_{max}$=450nm (Cecil CE5502 Spectrophotometer). Reactions in which substrate, AcCoA or NAT were each replaced by assay buffer were used as controls. The amount of remaining arylamine was determined from a standard curve prepared from controls containing no NAT protein or AcCoA.

### 2.2.9 Acetyl CoenzymeA (AcCoA) hydrolysis assay

The rate of hydrolysis of AcCoA by arylamine *N*-acetyltransferase (NAT) in the presence of arylamine substrate was determined in assay buffer (20mM Tris.HCl, pH 8.0) using 5,5'-dithio-bis(2-nitrobenzoic acid) (DTNB) as a colorimetric developing agent (Brooke *et al.* 2003b). The arylamine substrate (500µM) and purified recombinant NAT were mixed and pre-incubated (37°C, 5min) in wells of

a 250µL 96-well plate. AcCoA (400µM) was added to start the reaction in a final volume of 100µl. The reaction was quenched with guanidine hydrochloride solution (6.4M guanidine.HCl, 0.1M Tris.HCl, pH 7.3, 25µL) containing 5mM DTNB and the absorbance at 405nm was measured on a plate-reader (Titertek Multiskan Plus MkII) within 5 minutes. Reactions in which substrate, AcCoA or NAT were replaced by assay buffer were used as controls. The amount of CoA produced was determined from a standard curve prepared from dilutions of CoA in assay buffer.

### 2.2.10 Inhibition assays and High Throughput Screening

Compounds dissolved in 20mM Tris.HCl buffer pH 8.0 or DMSO were preincubated with isoniazid as substrate and NAT for 5mins at 37°C (Brooke *et al.* 2003a). AcCoA was added and the amount of CoA produced was determined (Section 2.2.9). The maximum final concentration of DMSO was 5%.

An assay procedure was required to screen a large number of compounds for NAT inhibition. A variation of the detection of CoA with DTNB was used due to the speed of the assay (Section 2.2.9). The compounds were prepared in 96-well plates with 8 spare wells for controls by addition of a fixed amount of DMSO assuming a molecular weight of 300 for every compound. This gave an approximate concentration of 2mM but the exact concentration was determined for those compounds for which IC50 values were determined.

The procedure used was as follows:

- 5µl compound transferred to flat-bottomed 96-well plate using an 8-channel pippettor (Eppendorf);

- 50µl of a premixed solution of INH (1mM) and MSNAT (1.4µg.ml$^{-1}$) was added to all wells and preincubated at 37°C;
- 50µl AcCoA was added (200µM) and plate incubated (37°C, 30mins);
- absorbance of well mixture was measured at 405nm;
- 25µl DTNB solution (5mM) was added to all wells;
- absorbance of well mixture was measured at 405nm again.

The first absorbance value was subtracted from the second and compared to the positive controls (including 5µL DMSO but no sample) in wells A12, B12, C12 and D12 and negative controls (identical to positive controls but AcCoA added after the DTNB solution) in wells E12 and F12 (Figure 2.1). The initial screening limit was set at 80% inhibition of the control activity (Figure 2.2). Compounds that produced a greater change in colouration than the control after addition of DTNB were assumed to either contain a thiol moiety or to be MSNAT substrates. If the initial absorbance was greater than 0.05 then the compound was classified as too coloured to provide a reliable result by this method and was discarded.

Compounds that produced over 80% inhibition under the initial screen (approximately 96µM) were re-screened at a further four-fold dilution of the stock solution (approximately 24µM) using the same protocol with a cut-off at 50% inhibition. Positive compounds from this second assay were tested at a range of concentrations (1-10µM) under the same procedure and the concentration giving a 50% inhibition of activity ($IC_{50}$) was determined graphically.

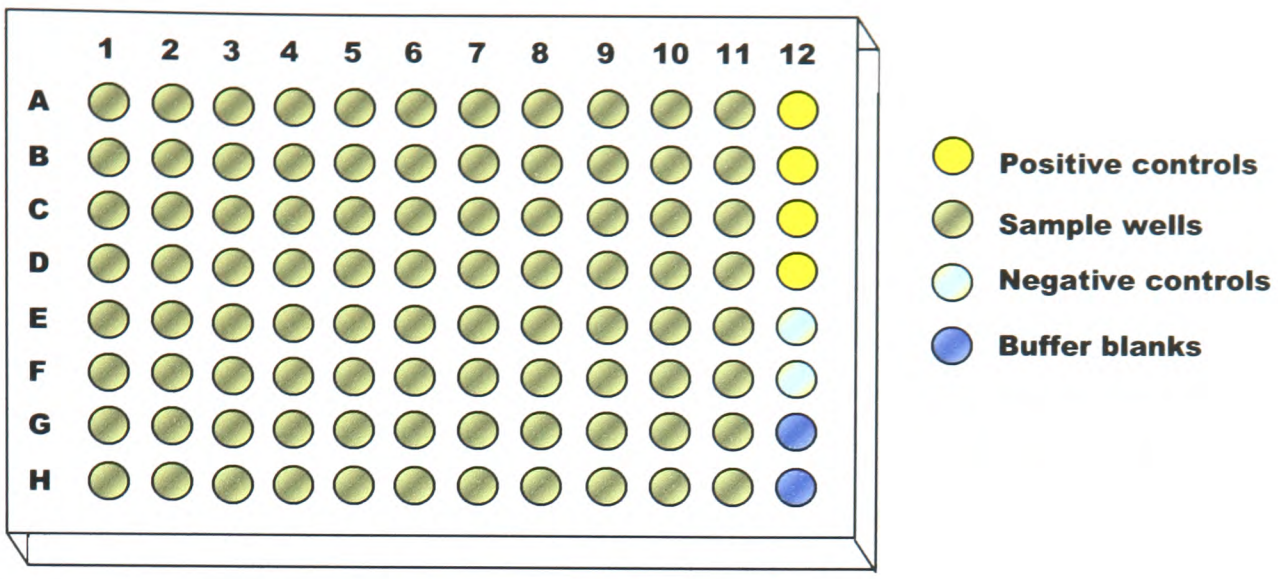


**Figure 2.1 – High Throughput Screening plate format**

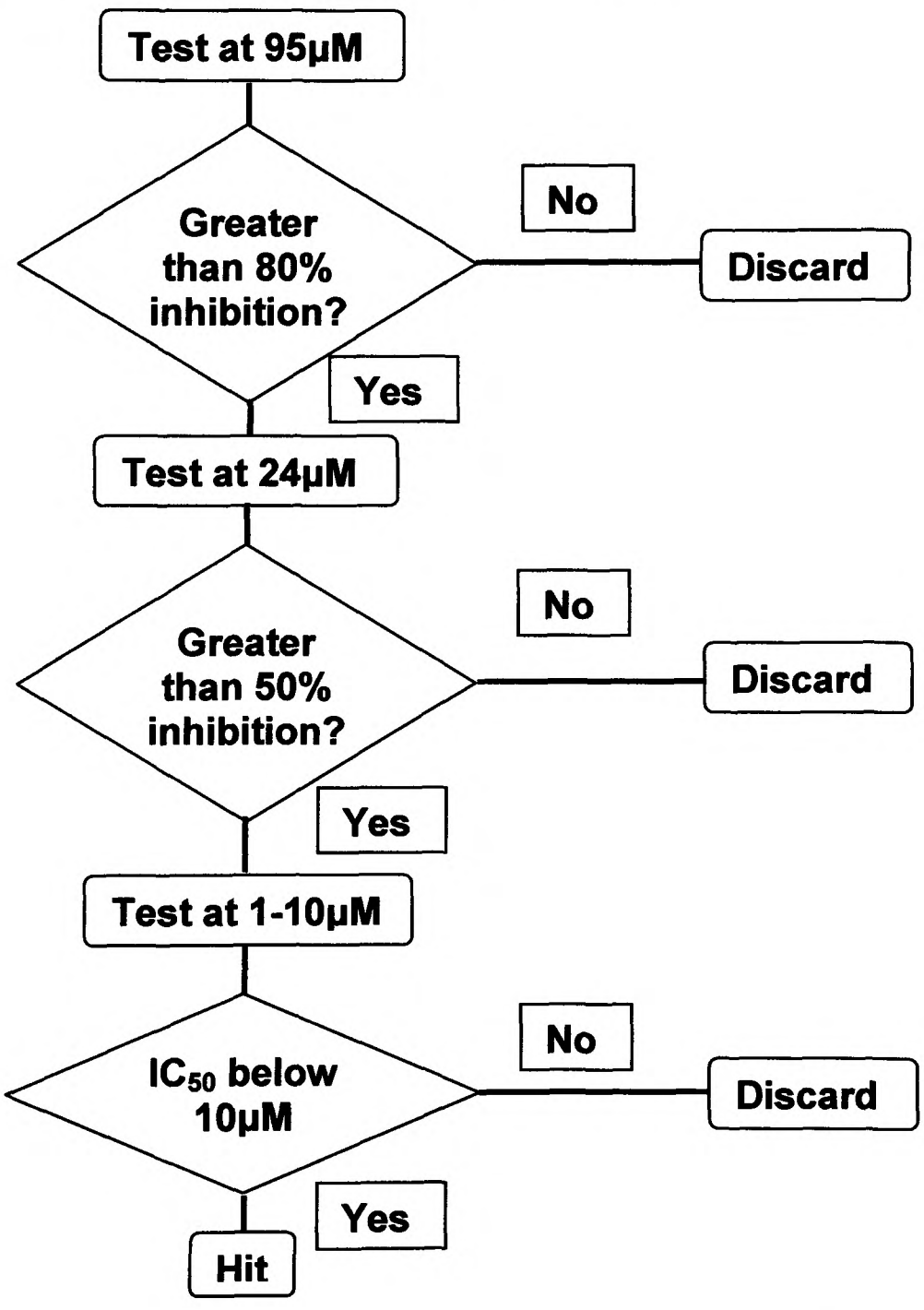


**Figure 2.2 – Flowchart for High Throughput Screening for NAT inhibitors**

Three rounds of testing were performed to screen large libraries for NAT inhibition. Successful compounds from each round were subsequently tested at a lower concentration until final hit compounds with an $IC_{50}$ of below 10µM were determined.

### 2.2.11 Protein Concentration Determination

Protein concentration of pure solutions was approximated by measuring the absorbance of the solution at 280nm assuming that $A_{280}$=1 is equivalent to 1mg.mL$^{-1}$ protein. Protein concentration of impure solutions was determined by a Bradford assay on a 96-well plate (Bradford 1976)) (Sigma Technical Bulletin, product B6916, www.sigmaaldrich.com). Samples of NAT, protein standards (bovine serum albumin) or buffer (5μL) were prepared on the plate and 250μL of Bradford assay solution was added. Protein concentrations were determined from the $A_{595}$ values measured on a plate reader (Titertek Multiskan Plus MkII).

### 2.2.12 Protein crystal trials

Crystallization of MSNAT was performed using the Hampton Research Crystal Screen™ 1 and 2 with the hanging drop method (Mikol *et al.* 1990)) (http://www.hamptonresearch.com/support). A solution of MSNAT of at least 5mg.mL$^{-1}$ was prepared (Section 2.2.6) both with and without removal of the hexahistidine tag. Crystal Screen solutions (500μL) were added to the wells of a greased 24-well plate. MSNAT (2μL) was added to the screening solution (2μL) on a dust-free coverslip and placed over the corresponding well to ensure an airtight seal. Plates were stored at 19°C and inspected daily until crystals had formed (2-14 days). Co-crystallization of MSNAT with substrates or inhibitors was performed by preincubating a solution of the compound and MSNAT (37°C, 5mins), such that the final concentration of compound was at least 5 times the concentration of protein.

### 2.2.13 *In silico* methods

The 3D crystal structure of MSNAT (accession number 1GX3) was downloaded from the Protein Data Bank (http://www.rcsb.org). The Autodock v3.0 suite of programs (Goodsell *et al.* 1996) was used to perform simulated annealing on a Silicon Graphics R12000 mips processor. Partial charges were added to the MSNAT crystal structure, the structure was solvated and saved in the "pdbqs" format using AutoDock Tools (Mushtaq *et al.* 2002). Substrate structures were created using the ChemOffice suite of programs (CambridgeSoft) and energy minimized in Chem3D using the MM2 forcefield. Partial atomic charges, fixed rings and rotatable bonds were added using AutoDock Tools. Ten docking runs were performed and solutions were converted to "pdb" (Brookhaven) format. Docked structures were observed in Swiss PDB Viewer (http://www.expasy.ch) and contact residues determined using LigPlot (Wallace *et al.* 1995).

## 2.3 Chemical Syntheses

### 2.3.1 General features

**a. General.** Reactions described as being performed at 0°C were cooled by means of an ice bath, and those at temperatures over 25°C were heated by means of a silicone oil bath.

**b. Solvents.** $Et_2O$ was distilled from sodium/benzophenone ketyl under nitrogen prior to use. $CH_2Cl_2$ was distilled from calcium hydride under nitrogen prior to use. Toluene was distilled from sodium under nitrogen prior to use. All other solvents were used as supplied unless otherwise stated.

**c. Reagents.** All reagents were used as supplied, without further purification. Unless otherwise stated, all aqueous solutions were saturated and all organic layers were dried over magnesium sulfate.

**d. Chromatography.** Column chromatography was performed on silica gel (Kieselgel 60, Merck). Thin layer chromatography (TLC) was performed on aluminium sheets coated with 0.2mm silica gel 60 $F_{254}$ (Merck). Plates were visualised either by ultraviolet light (UV, 254nm) or by potassium permanganate staining (1.5g $KMnO_4$, 10g $K_2CO_3$, 150mL $H_2O$, 100mg NaOH) followed by gentle heating over a flame.

**e. Infra-red spectroscopy.** Infra-red spectra were recorded as thin films (film) or as KBr discs (disc) using a Perkin-Elmer PARAGON 1000 FT-IR spectrometer. Selected peaks are reported, in $cm^{-1}$.

**f. Nuclear Magnetic Resonance (NMR) spectroscopy.** $^1H$ NMR spectra were recorded on a Bruker DPX-200 (200MHz) or a Bruker DPX-400 (400 MHz). Chemical shifts ($\delta_H$) are reported in parts per million (p.p.m.) and are referenced to the residual solvent peak. Coupling constants (*J*) are measured in Hertz. $^{13}C$ spectra were recorded at 100 MHz on the Bruker DPX-400. Chemical shifts ($\delta_C$) are quoted in p.p.m. and referenced using residual solvent signals.

**g. Mass spectroscopy.** Low resolution mass spectra (*m/z*) were recorded on either a VG Masslab 20-250 instrument ($CI^+$, $NH_3$) or Platform instrument (APCI/ESI). Major peaks are listed with intensities quoted as percentages of the base peak. Accurate mass measurements were recorded on a VG Autospec instrument, and were conducted by Mr. R. Procter and Dr. N. Oldham of the Dyson Perrins Laboratory.

**h. Reverse Phase - High Performance Liquid Chromatography (RP-HPLC).** Analytical RP-HPLC was performed on a Gilson system comprising Gilson 306 pumps, Gilson 811C dynamic mixer, Gilson 806 manometric module with automated sample injection on a Gilson 215C liquid handler, configured with a Gilson 819 valve activator. Separation was performed on a Varian Omnisphere 5CB column (5μm particle size, 150.0mm x 4.6mm). All experiments were performed under gradient elution: Solvent A ($H_2O$, 0.1% trifluoroacetic acid) and Solvent B (acetonitrile), starting from 95% A, 5% B to 5% A, 95% B over 8 minutes then isocratic for 4 minutes at a flow rate of 1.0 $mL.min^{-1}$. Detection was performed at 220, 254 and 290nm wavelength using a Gilson 170 Diode Array Detector.

**i. Melting Points.** Melting points were recorded on a Gallenkamp Hot Stage apparatus and are uncorrected.

**j. Radleys equipment.** Parallel syntheses were performed in either a Radleys Carousel, with twelve 25mL glass tubes under individual reflux and atmospheric control, or a Radleys Greenhouse, with twenty-four 5mL glass tubes under individual reflux and combined atmospheric control.

### 2.3.2 TZD-Sultam synthesis

A series of *N*-substituted thiazolidine-2,4-dione-1,1-dioxo-2,3-dihydrobenzo[1,2]thiazine-4-ylidene (hereafter referred to as TZD-sultam adduct) compounds were synthesized from sodium saccharin as below (Brooke *et al.* 2003a), Scheme 2.1, Section 4.2.2).

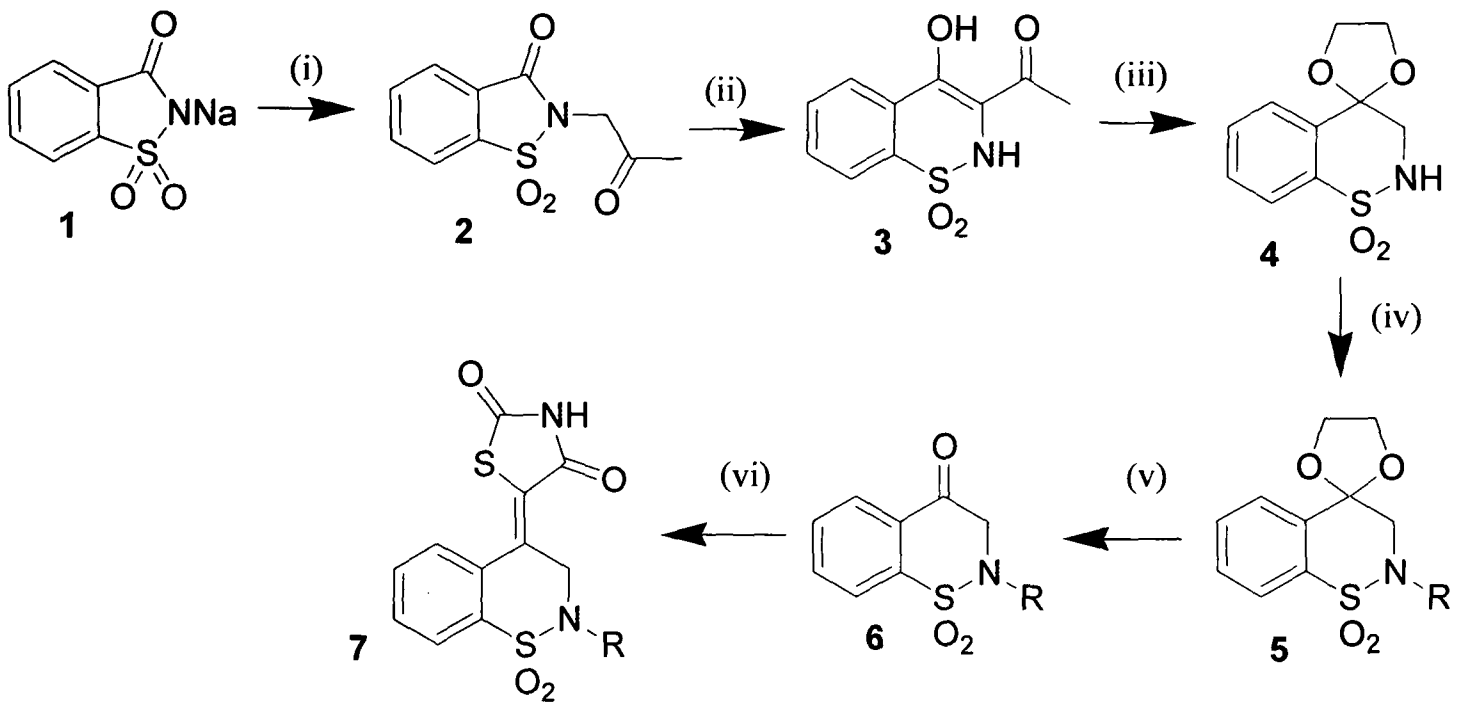


**Scheme 2.1 – The synthesis of *N*-substituted TZD-sultams**

*Reagents and conditions:* (i) $MeCOCH_2Cl$, cetyl trimethylammonium bromide, PhMe, Δ; (ii) NaOEt, EtOH, 55°C then HCl(aq); (iii) ethane-1,2-diol, *p*-TsOH, $C_6H_6$, Δ; (iv) NaH, DMF, RBr, r.t.; (v) HCl, MeOH, Δ; (vi) thiazolidine-2,4-dione, $Et_3N$, $BF_3.OEt_2$, 1,4-dioxane.

Ketal **4** was furnished from sodium saccharin in three steps (Zinnes *et al.* 1965; Zinnes *et al.* 1966). The ketone was furnished by acidic deketalisation before condensation with thiazolidine-2,4-dione, assisted by boron trifluoride and triethylamine.

(i) To a solution of sodium saccharin (**1**, 25g, 1.0 equivalent) in toluene (200mL) was added chloroacetone (16.9g, 1.5 equivalents) and cetyl trimethylammonium bromide (12.2g, 0.25 equivalents) and the mixture was refluxed for four hours. The solid was removed by filtration through Celite and the solution reduced to dryness on a rotary evaporator. The resulting solid was dissolved in ethyl acetate and the solution washed with water before drying over magnesium sulfate and evaporation to give **2**.

(ii) *N*-Alkyl saccharin (**2**, 1.0g, 1.0 equivalent) and freshly made sodium ethoxide (2.0 equivalents of sodium dissolved in dry ethanol to give 0.57g, 2.0 equivalents) were mixed in 10mL dry ethanol and warmed to 50°C for 30mins. The reaction was quenched with HCl (10mL 10% w/v) and the resulting solid was

removed by filtration. The solid **3** was washed with 50% aqueous ethanol and recrystallised from toluene.

(iii) Solid **3** (25.0g, 1.0 equivalent), ethylene glycol (32.3g, 5.0 equivalents) and fresh tosic acid (7.5g, 0.4 equivalents) were refluxed in benzene (270mL **Caution: toxic**) in a Dean-Stark apparatus. The benzene was removed under vacuum and the solid was triturated with 10x25mL diethyl ether. Solid was filtered and washed with ethanol to give white crystals of **4**.

(iv) *N*-Diversification of **4** was performed on a Radleys Carousel using the relevant alkyl bromide. Sodium hydride (180mg, 1.1 equivalents) was added to ketal **4** (1g, 1.0 equivalent) in dimethylformamide (DMF, 20mL) and mixed at room temperature for 30mins under nitrogen. Alkyl bromide was added and the mixture stirred at room temperature for 20 hours. The solution was added to ethyl acetate (100mL) and washed with equal volumes of ammonium chloride solution, water and brine before evaporation. The product **5** was purified by flash silica gel chromatography with 1:1 ethyl acetate:hexane.

(v) Ketal **5** (2mmol) was dissolved in methanolic HCl (9% w/v, 8mL) and heated under reflux for 45 minutes. The cooled solution was reduced under evaporation before dilution with ethyl acetate (50mL). The solution was washed with two equal volumes of water and one volume of brine before evaporation to give ketone **6**.

(vi) Ketone **6** (2mmol, 1.0 equivalent) was dissolved in ice-cold dioxane (10mL) containing thiazolidine-2,4-dione (2mmol, 1.0 equivalent) before addition of boron trifluoride etherate (8mmol, 4.0 equivalents). Triethylamine (4mmol, 2.0 equivalents) was added dropwise and the solution was stirred at room temperature for 48 hours. The solution was diluted in ethyl acetate (50mL) and washed with

equal volumes of water and brine before evaporation. The resulting oil was purified by flash silica gel chromatography (1:1 diethyl ether:hexane) to produce the TZD-sultam **7** in low yield (below 30%). Experimental data is given in Appendix A1.1.

### 2.3.3 Maleimide synthesis

A series of substituted 1-phenylpyrrole-2,5-diones (hereafter referred to as maleimides) were synthesized from arylamines as below (Scheme 2.2, Section 4.3.2).

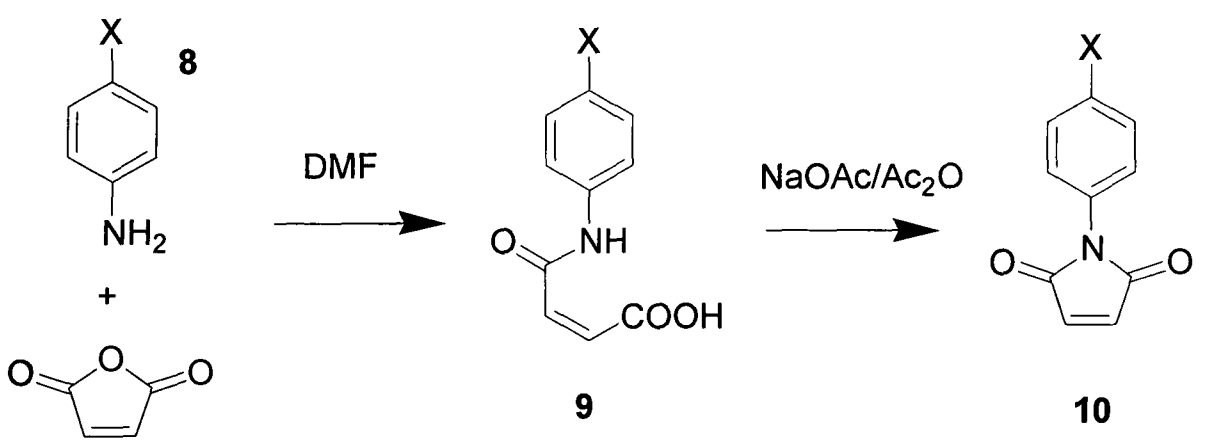


**Scheme 2.2 – The synthesis of the maleimides**

The arylamine (**8**, 4.9mmol, 1.0 equivalents) was dissolved in 5mL DMF in a Radleys Carousel to which was added maleic anhydride (5.1mmol, 1.05 equivalents). Solutions were stirred at room temperature for 17 hours before addition of distilled water (10mL) and vacuum filtration to furnish the crude uncyclised product **9**. Products were recrystallised from methanol. The uncyclised product (2.0mmol, 1.0 equivalent) was dissolved in 3mL acetic anhydride containing sodium acetate (0.2mmol, 0.1 equivalent) and stirred at 65°C for 3hrs. Addition of water (10mL) gave the solid product which was removed by filtration as above and recrystallised from methanol. Cyclisation was confirmed by $^{1}H$

NMR by the collapse of the 2H double doublet from the asymmetric alkene protons into a 2H singlet at 7.15ppm. Succinimides, phthalimides and monomethyl-, dimethyl- and dichloromaleimides were all produced in the same manner using succinic anhydride, phthalic anhydride or the relevant substituted maleic anhydride. Experimental data is given in Appendix A1.2.

### 2.3.4 Aminothiazole synthesis

A series of substituted aminothiazoles were synthesized as below in parallel on a Radleys Greenhouse (Bailey *et al.* 1996; Kearney *et al.* 1998); Scheme 2.3, Section 4.4.1).

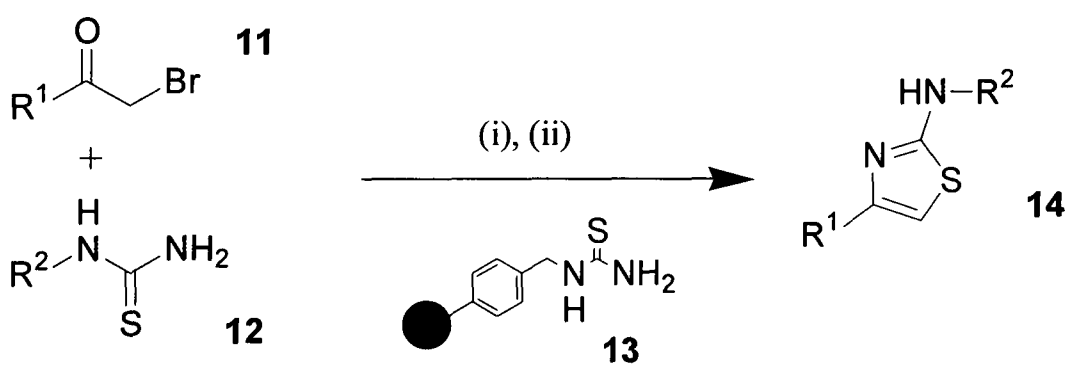


**Scheme 2.3 – The synthesis of aminothiazoles**
(i) DMF, 85°C, 16hrs; (ii) PS-benzylthiourea, 1hr, r.t.

The thiourea (**12**, 0.148mmol, 1.0 equivalents) and α-bromoketone (**11**, 0.177mmol, 1.2 equivalents) were dissolved in DMF (1.5mL) and stirred at 85°C for 16 hours. Polystyrene-bound (PS) benzylthiourea (**13**, 0.118mmol, 0.8 equivalents) was added to the cooled solutions and stirred for a further hour before filtration of the polystyrene beads and evaporation of the solvent *in vacuo*. Purity of compounds was determined by RP-HPLC and NMR. Experimental data is given in Appendix A1.3.

# Chapter 3

# A Novel Assay for NAT Activity

## 3.1 Novel assay development

### 3.1.1 Assays for NAT activity

Determination of the rate of an enzyme catalysed reaction can provide information about the diversity of substrates, the identity and nature of possible inhibitors and allow investigation of the mechanism of enzyme activity. The first aim of this project (Section 1.4, (i)) is to develop an assay for NAT activity that would facilitate the second two aims: (ii) to determine the substrate specificity of MSNAT, and (iii) to be able to screen large libraries of compounds for possible MSNAT inhibitors. To fulfil these aims an assay is required that is:

- Fast, efficient and accurate;
- Independent of the nature of the substrate present;
- Rigorous to a broad range of chemical functionalities.

Previous assays for NAT activity have relied on determining the amount of acceptor substrate acetylated over time. One such method, the detection of arylamine with *p*-dimethylaminobenzaldehyde (DMAB), relies on the nature of the acceptor substrate (Andres *et al.* 1985) although it has been adapted to 96-well format (Coroneos *et al.* 1991). HPLC assay methods, although very sensitive, can be time-consuming and are also substrate specific. The only method previously

used to determine rates of O-acetyl transfer from AcCoA to N-hydroxyarylamines are indirect, involving the quantification of DNA adducts formed after the reaction (Hein *et al.* 1993). Thus a new assay was required that would fit all the above requirements. In this chapter the generation of reagents for the assay is described (Section 3.1.2), followed by development of the assay (Section 3.1.3) and the determination of the acetyl acceptor substrate specificity of MSNAT (Section 3.2).

### 3.1.2 Preparation of pure recombinant MSNAT

Pure, recombinant MSNAT was prepared according to the method of Sandy *et al.* (Sandy *et al.* 2002), sections 2.2.4 and 2.2.5). MSNAT was produced in *E. coli* as a recombinant protein with an *N*-terminus hexahistidine tag and purified using Nickel-NTA affinity resin. MSNAT was eluted from the Ni-NTA resin in the 50mM and 250mM imidazole washes (Figure 3.1). Typically 20mg of pure MSNAT was prepared per litre of growth culture (Table 3.1).

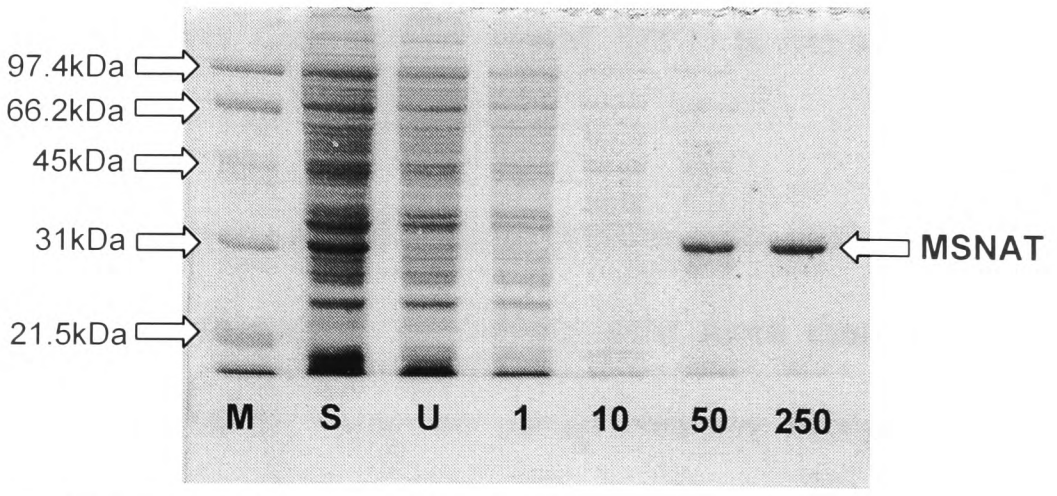


**Figure 3.1 – SDS-PAGE of MSNAT purification**

A 10% SDS-PAGE was performed on samples from the MSNAT purification process (Section 2.2.6). Protein samples (20µL, except S&U: 2µl + 18µl $H_2O$) were added to sample preparation buffer (20µL) before denaturing at 95°C for 10 minutes. 20µL of the mixture was placed in each well and run at 35mA for approximately 45 minutes. Samples are: M - Low Molecular Weight Markers; S - soluble lysate; U - unbound lysate; 1, 10, 50, 250 - imidazole washes of the given concentration in mM.

| | Vol | Protein | Total Protein | Activity | Total Activity: | Specific Activity: | Yield |
|---|---|---|---|---|---|---|---|
| | ml | mg/ml | mg | $nmol.min^{-1}.ml^{-1}$ | $nmol.min^{-1}$ | $nmol.min^{-1}.mg^{-1}$ | % |
| Soluble Lysate | 15 | 24 | 360 | 718 | 10766 | 30 | 100 |
| Unbound Lysate | 15 | 20 | 300 | 10 | 150 | 1 | 1 |
| 1mM wash | 20 | 1.1 | 22 | 0.7 | 14 | 1 | 0 |
| 10mM wash | 20 | 0.5 | 10 | 0.9 | 18 | 2 | 0 |
| 50mM wash | 20 | 0.7 | 14 | 88 | 1320 | 94 | 12 |
| 250mM wash | 20 | 0.6 | 12 | 118 | 1774 | 143 | 16 |

**Table 3.1 – Purification Table for MSNAT Preparation**

The samples shown in Figure 3.1 were tested, after dialysis for the washes, for the acetylation of *p*-anisidine (100μM) in the presence of AcCoA (400μM, Section 2.2.8). Protein concentrations were determined by Bradford Assay or by spectrophotometry for 50mM and 250mM washes (Section 2.2.6). The yield of protein and relative purification are shown.

The assay of MSNAT samples stored at +4°C, -20°C, -70°C and frozen in liquid nitrogen over 18 days resulted in no less than 80% of the initial activity of the protein as determined by acetylation of anisidine. The activity of freshly prepared MSNAT can be determined, as detected by acetylation of 100μM anisidine, both with (161±6 $nmole.min^{-1}.mg^{-1}$) and without (149±5 $nmole.min^{-1}.mg^{-1}$) addition of the thiol reducing agent dithiothreitol (1mM, DTT) to the assay buffer (20mM Tris.HCl, pH 8.0).

Incubation of the N-terminal His-tagged protein with fresh thrombin (5U.$(mg\ protein)^{-1}$), even for 4hrs at 37°C, did not give more than 25% cleavage as determined by SDS-PAGE. However, partial cleavage of the hexahistidine tag resulted in little change in the activity of the protein (uncut, 826$nmol.min^{-1}.mg^{-1}$; cut, 810$nmol.min^{-1}.mg^{-1}$ ± 12$nmol.min^{-1}.mg^{-1}$ as determined by AcCoA hydrolysis (400μM) with 500μM *p*-anisidine). Thus the protein was used uncut in subsequent assays.

### 3.1.3 Detecting NAT activity with DTNB

The acetyltransfer reaction catalysed by NAT uses a 1:1 ratio of arylamine:AcCoA. Dr. Frédérique Pompeo (in the supervisor's laboratory) had previously determined that the free thiol of the CoA formed during the reaction could be detected using the colorimetric agent 5,5'-dithio-bis(2-nitrobenzoic acid) (Ellman's reagent, DTNB). DTNB reacts with any thiol in solution in a 1:1 ratio to produce an asymmetric dithio compound and 5-mercapto-2-nitrobenzoic acid (TNB). This product has a strong absorbance at $\lambda_{max}$=412nm (Riddles *et al.* 1983). DTNB, coupled with a quenching solution of guanidine hydrochloride at 6.4M (Arakawa *et al.* 1984), could thus be used to determine the rate of AcCoA hydrolysis catalysed by NAT. This approach has previously been used to determine the activity of carnitine acetyltransferases (Cederblad *et al.* 1986).

Initial experiments were performed to test the validity of this assay method. TNB showed a molar extinction coefficient of 11.0 $mmol^{-1}.dm^3.cm^{-1}$ at $\lambda_{max}$=412nm in buffer (100mM Tris.HCl, 3.2M guanidine.HCl pH 7.27) measured in a 10mm pathlength cuvette. When a solution of CoA (20mM Tris.HCl, pH 8.0, 100µl) is treated with DTNB solution (6.4M guanidine.HCl, 0.1M Tris.HCl, pH 7.3, 25µl) in a flat-base polystyrene 250µl 96-well plate the TNB has an extinction of 3.3±0.1 $mmol^{-1}.dm^3$ at $\lambda_{max}$=405nm measured in a plate reader (Titertek Multiskan Plus MkII). The liquid depth in the centre of the well is approximately 3.9mm and thus the molar extinction coefficient is 8.5 $mmol^{-1}.dm^3.cm^{-1}$ at this wavelength. A three-fold molar excess of DTNB over AcCoA was used to ensure saturation. The reducing agent DTT releases two equivalents of TNB in the presence of DTNB with an effective molar extinction coefficient of 13.6$mmol^{-1}.dm^3.cm^{-1}$ under these conditions.

When a known MSNAT substrate, isoniazid (INH), AcCoA and MSNAT were incubated in a 96-well plate as described in section 2.2.8 and quenched at various time points with the DTNB solution, an increased coloration was observed over time that correlated with the hydrolysis of the AcCoA (Figure 3.2). Absence of either AcCoA, MSNAT or INH gave no increased colouration with time. The arylamine NAT substrate *p*-anisidine was similarly incubated with MSNAT and AcCoA. Simultaneous detection of *p*-anisidine acetylation by DMAB (section 2.2.7) and AcCoA hydrolysis by DTNB gave identical rates of reaction (Figure 3.3) as expected.

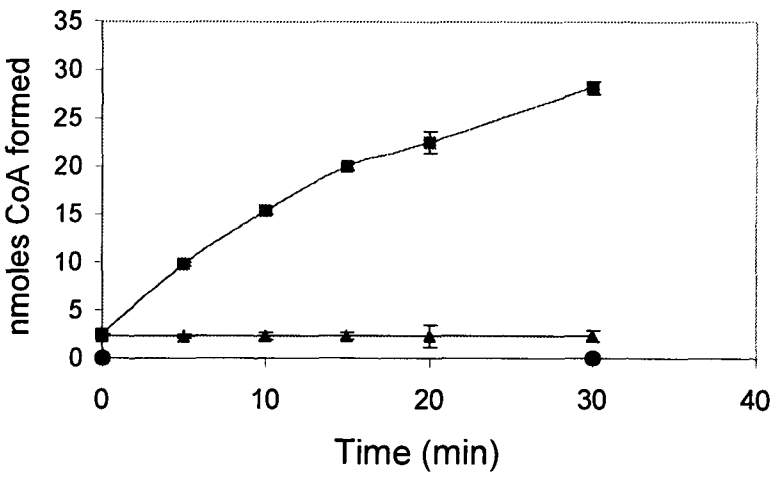


**Figure 3.2 – Detection of MSNAT activity with DTNB**

Following incubation of MSNAT (1.2μg per well), isoniazid (500μM) and AcCoA (400μM) for varying times (x-axis), the reaction was quenched and the quantity of CoA was determined with DTNB (squares). Results for identical experiments except without isoniazid (triangles) or without acetyl CoA (circles) are shown. Results shown are mean values (n=2) with individual values shown as error bars.

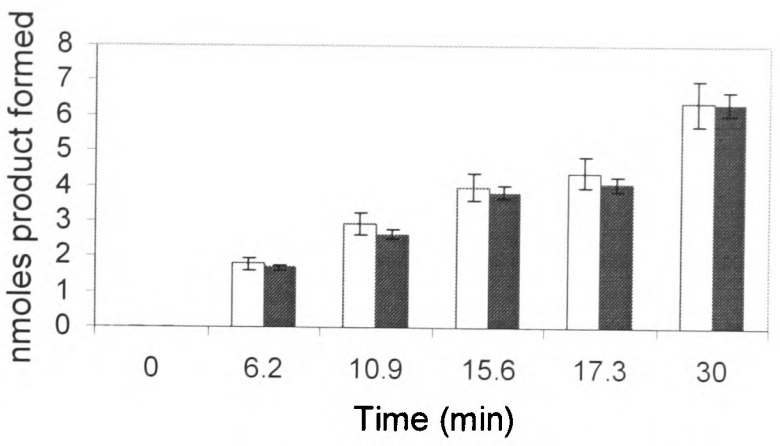


**Figure 3.3 – Comparison of arylamine acetylation and AcCoA hydrolysis**
The rate of acetylation of anisidine (100μM) in the presence of AcCoA (400μM) and MSNAT over varying time periods (x-axis) was determined by simultaneously measuring loss of arylamine (filled bars) and detection of CoA (open bars).

To determine whether this assay method had sufficient accuracy, the Z' factor was calculated (Zhang *et al.* 1999). This value is calculated from the standard deviations of positive and negative controls and the difference in values between them (Equation 3.1). Standard assay conditions were set as 500μM substrate, 400μM AcCoA, sufficient NAT to maintain activity in the linear range and a 15 minute timepoint. Using *p*-anisidine as a positive control and n=4, the standard deviations of positive and negative controls were 0.0096 and 0.0065 AU for a change in absorbance of 0.198AU. This gives a Z' factor of 0.756 which fits into the range for an acceptable assay (0.5<Z'<1.0). Similar values are found with other known substrates.

$$Z' = 1 - \frac{(3\sigma_+ + 3\sigma_-)}{|\mu_+ + \mu_-|}$$

**Equation 3.1 – The Z' factor (from Zhang *et. al.* 1999)**

This assay has also been tested on other sources of NAT. Recombinant hamster NAT2, prepared according to (Sticha *et al.* 1997), was kindly donated by Akane Kawamura of this laboratory. Incubation of *p*-aminobenzoic acid (500μM), AcCoA (400μM) and Hamster NAT2 (0.16μg) at 37°C followed by detection of the CoA with DTNB gave a specific activity of 1310 ± 40 $nmol.min^{-1}.mg^{-1}$ in the

presence of 5% DMSO. Similarly, recombinant NAT1 from *Mesorhizobium loti* was kindly supplied as a glutathione *S*-transferase (GST)-fusion protein by Fernando Rodrigues-Lima (Faculte de Medecine Pitie-Salpetriere, CNRS UMR 7000, Paris 75013). The GST tag was cleaved using thrombin and the cleaved protein (1μg) incubated with AcCoA (400μM) and either *p*-anisidine or 5-aminosalicylate (500μM) as arylamine substrate, followed by addition of DTNB. This gave specific activities of 127 ± 5 $nmol.min^{-1}.mg^{-1}$ for *p*-anisidine and 1440 ± 60 $nmol.min^{-1}.mg^{-1}$ for 5-aminosalicylate.

### 3.1.4 Limitations of the DTNB assay method

These data demonstrate that the determination of NAT activity using DTNB gives an accurate and reproducible assay of the rate of AcCoA hydrolysis and is robust to most chemical functionalities, making it suitable for application to a high-throughput screening format. One potential drawback of this assay is that it cannot be used in the presence of dithiothreitol (DTT) or other thiol-based reducing agents. Although MSNAT has an essential cysteine thiol, MSNAT can be assayed effectively without addition of DTT to the assay buffer. The MSNAT is dialysed into buffer containing DTT (Section 2.2.6) but after protein concentration and dilution into assay buffer the concentration is below 1μM. It has been suggested that several eukaryotic NATs require a thiol reducing agent to maintain activity (Wick *et al.* 1990), and this would have to be investigated for each NAT enzyme to be used in this assay system. The NAT in the assay is present at sub-micromolar levels whereas the concentration of CoA formed is up to 100μM. Hence, the contribution of the protein cysteine residues to the colour development is negligible.

Colorimetric assays are obviously sensitive to the presence of other coloured compounds. The absorbance of other compounds will automatically be taken into account if a time-course has been performed. However, where a time-course is not possible (eg High Throughput Screen, section 2.2.10) the optical density can be measured before and after the addition of DTNB to take account of the contribution to the absorbance by coloured compounds.

### 3.1.5 Acyl donor substrate specificity

The assay developed for detection of hydrolysis of AcCoA can also be used to detect the hydrolysis of other thioester compounds by NAT. Thus it is possible to investigate the substrate specificity of the acyl donor, as well as the acetyl acceptor (Section 3.2.2). The acyl CoA derivatives propionyl CoA (C3CoA), phenylacetyl CoA, butyryl CoA (C4CoA) and all the even numbered acyl CoA derivatives up to C20CoA were purchased. Each was incubated at 400μM with INH (500μM) and MSNAT (1.2μg) and DTNB added after 15 minutes (Section 2.2.9). Under these conditions, the rate of acetyl CoA hydrolysis was 730±5 $nmol.min^{-1}.mg^{-1}$. Propionyl CoA was also hydrolysed by NAT in the presence of isoniazid at a rate of 504±8 $nmol.min^{-1}.mg^{-1}$, 69% of the rate of acetyl CoA hydrolysis. None of the other CoA derivatives were hydrolysed under these conditions. To confirm that the propionyl group was being transferred to the acceptor substrate, propionyl CoA (400μM) was incubated with *p*-anisidine (100μM) and MSNAT before detection of the concentration of arylamine using DMAB (Section 2.2.8). The *p*-anisidine was acylated at rates of 146±3 $nmol.min^{-1}.mg^{-1}$ with acetyl CoA and 117±3 $nmol.min^{-1}.mg^{-1}$ with propionyl CoA.

## 3.2 Substrate Specificity of MSNAT and STNAT

### 3.2.1 Substrate-based applications of novel assay

One advantage of the assay method for detecting the rate of hydrolysis of acetyl CoA using DTNB is that it is not dependent on the nature of the acceptor substrate used in the reaction. Having determined that the assay provides an accurate measure of the rate of a NAT-catalysed reaction (Section 3.1) and is effective with different substrates, the assay has been used to determine the substrate specificity of MSNAT and STNAT.

### 3.2.2 Determining the substrate specificity of MSNAT and STNAT

STNAT was expressed and purified in the same way as MSNAT (Section 2.2.5 and 2.2.6, (Sinclair *et al.* 1998)). STNAT with a hexahistidine tag was eluted in the 50mM and 250mM washes to give 7.6mg of protein. The tag was successfully cleaved with thrombin (40U, 2hrs, 25°C) as determined by SDS-PAGE.

Twenty-one compounds were assayed as acceptor substrates of either MSNAT or STNAT using DTNB to detect hydrolysis of AcCoA (Table 3.2, Figure 3.4, Scheme 3.1). The compounds were selected to include both previously identified substrates of STNAT, human NAT1 and NAT2 and compounds that showed some structural relationship to known substrates (Scheme 3.1). Compounds were divided into four groups comprising arylamine drugs, other arylamines, alkoxyanilines and hydrazines. The rates of hydrolysis of AcCoA in the presence of these compounds and STNAT or MSNAT ranged from 10 to 20,000 $nmoles.min^{-1}.(mg\ protein)^{-1}$. There was no observed production of CoA with any of the substrates in the absence of enzyme over the time periods used.

| Compound (Abbreviation) | Rate [a] | clog P [b] | # α [c] | $E_\alpha$ [d] | $E_\beta$ [e] |
|---|---|---|---|---|---|
| **Arylamine drugs** | | | | | |
| Sulfamethazine (SMZ) | 7±7 | 1.62 | nd | nd | nd |
| Procainamide (PRO) | 54±46 | 1.05 | nd | nd | nd |
| 5-Aminosalicylate (5AS) | 5670±110 | 0.02 | 8 | -6.89±0.26 | -8.88±0.80 |
| **Other arylamines** | | | | | |
| 4-Aminobenzoic acid (pABA) | 30±30 | 0.41 | 1 | -6.69 | -8.54±0.32 |
| 4-Aminopyridine (APY) | 12±8 | -0.06 | nd | nd | nd |
| 4-Trifluoromethylaniline (TFMA) | 121±36 | 2.03 | nd | nd | nd |
| 4-Aminophenol (AMP) | 122±24 | 0.66 | 0 | - | -7.89±0.01 |
| 4-Chloroaniline (CLA) | 430±22 | 1.67 | 1 | -5.58 | -7.56±0.28 |
| 4-Bromoaniline (BRA) | 548±46 | 1.94 | 1 | -5.27 | -7.55±0.28 |
| 4-Iodoaniline (IOA) | 956±61 | 2.35 | nd | nd | nd |
| 4-Phenoxyaniline (POA) | 1620±46 | 3.13 | 10 | -7.29±0.07 | - |
| 2-Aminofluorene* (2AF) | 3610±80 | 2.51 | 10 | -7.87±0.06 | - |
| **Alkoxyanilines** | | | | | |
| 4-Anisidine (ANS) | 1970±100 | 1.18 | 4 | -5.58±0.17 | -7.42±0.31 |
| 4-Aminoveratrole (AMV) | 3000±110 | 1.32 | 8 | -6.09±0.36 | -7.03±1.13 |
| 4-Ethoxyaniline (EOA) | 3560±150 | 1.53 | 8 | -5.95±0.09 | -6.60±0.40 |
| 4-Butoxyaniline* (BOA) | 5670±160 | 2.44 | 10 | -6.96±0.18 | - |
| 4-Hexyloxyaniline* (HOA) | 8510±110 | 3.35 | 10 | -7.81±0.41 | - |
| **Hydrazines** | | | | | |
| 4-Methoxyphenylhydrazine (MPZ) | 395±50 | 1.56 | 9 | -5.99±0.23 | -6.50 |
| Isoniazid (INH) | 1020±42 | -0.64 | 6 | -6.25±0.36 | -7.69±0.13 |
| 4-Chlorobenzoic hydrazide (CBZ) | 3380±70 | 1.25 | 10 | -6.37±0.23 | - |
| Hydralazine (HDZ) | 7060±130 | 0.73 | 10 | -7.58±0.42 | - |

**Table 3.2 – Substrates of MSNAT**

(a) Rate of AcCoA hydrolysis in the presence of MSNAT, AcCoA (400μM) and test compound (500μM) (nmole.min$^{-1}$.(mg protein)$^{-1}$ mean shown ± standard deviation, n=4). * in the presence of 5% DMSO, others 0.5% DMSO.

(b) Calculated partition coefficient between water and 1-octanol determined using ChemDraw Ultra v6.0 (CambridgeSoft).

(c) The number of docking solutions (out of ten) found in the α site. nd: Not determined.

(d) Average "Total Binding Energy" (kcal.mol$^{-1}$, mean ± standard deviation) of solutions found in the α site. -: Not applicable

(e) Average "Total Binding Energy" (kcal.mol$^{-1}$ mean ± standard deviation) of solutions found in the β site. -: Not applicable

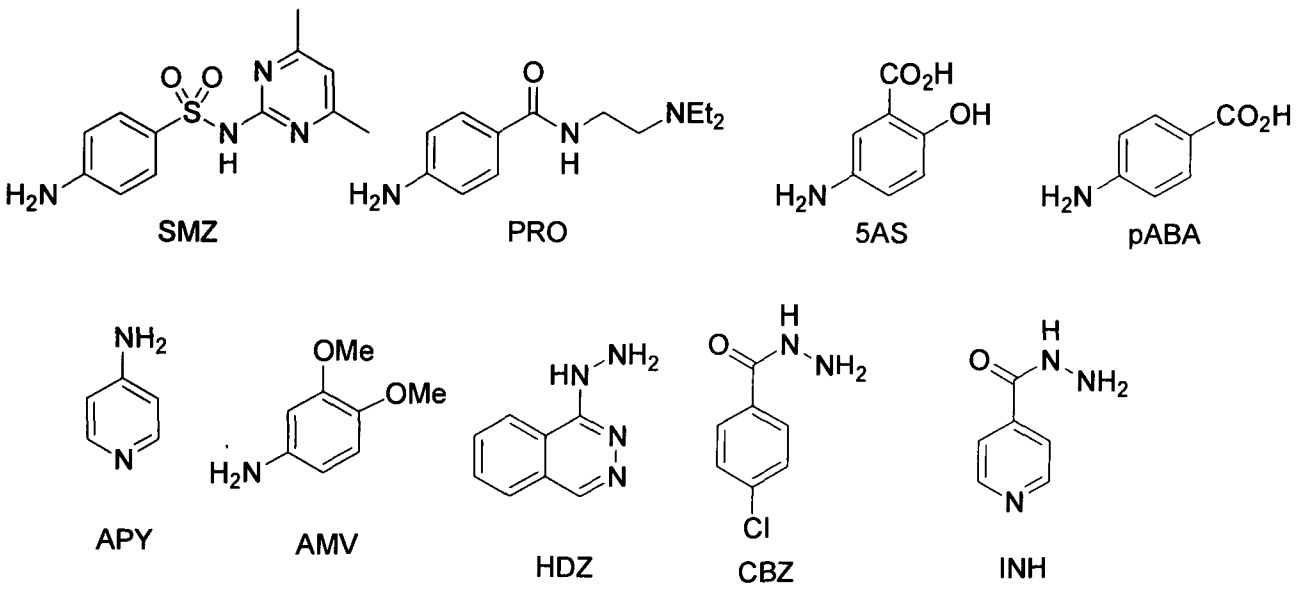


AMP; X = OH
CLA; X = Cl
BRA; X = Br
IOA; X = I
TFMA; X = $CF_3$
POA; X = OPh
ANS; X = OMe
EOA; X = OEt
BOA; X = OBu
HOA; X = OHex

**Scheme 3.1 – Compounds tested as substrates of MSNAT and STNAT**

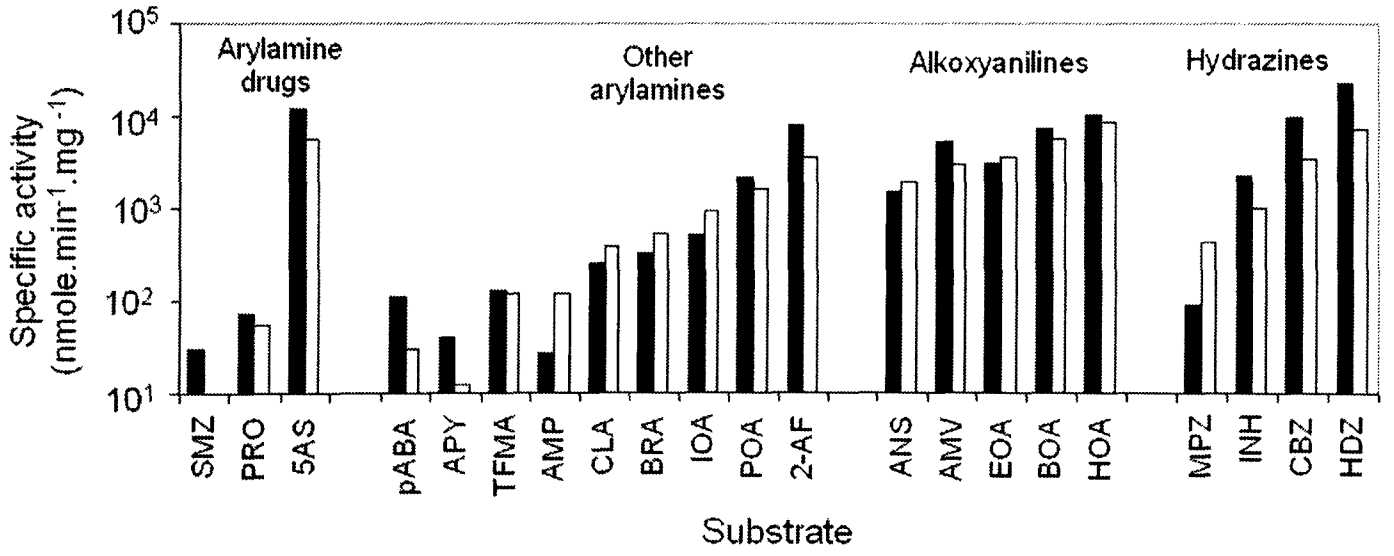


**Figure 3.4 – The substrate specificity of MSNAT and STNAT**

The activity of STNAT (filled columns) and MSNAT (empty columns) is shown, determined by measuring the hydrolysis of acetyl CoA with DTNB (Section 2.2.9) with substrates shown in Table 3.2 (each at 500μM) in assay buffer (20mM Tris.HCl, pH 8.0) containing either 0.5% DMSO or 5% DMSO (2AF, BOA and HOA).

Hydralazine caused the most rapid rate of AcCoA hydrolysis with STNAT, and 4-hexyloxyaniline was the best substrate for MSNAT. 5-Aminosalicylate and 2-aminofluorene were also effective substrates with these proteins in agreement with

previous studies (Delomenie *et al.* 2001). Previously identified STNAT substrates such as 4-anisidine (ANS), 4-aminoveratrole (AMV) and 4-iodoaniline (IOA) are also substrates for MSNAT (Sinclair *et al.* 1998). The human NAT1 substrate 4-aminobenzoic acid (PABA) and the human NAT2 substrate sulfamethazine (SMZ) are both poor substrates for MSNAT and STNAT. Novel NAT substrates identified by this method include the alkoxyanilines (4-ethoxy-, 4-butoxy and 4-hexyloxyaniline, EOA, BOA and HOA respectively) and the isoniazid analogue 4-chlorobenzoic acid hydrazide (Figure 3.4).

The substrate specificity appears to be virtually identical for both STNAT and MSNAT with substrates producing similar rates of reaction with either enzyme. Using the Z' factor as a measure of assay accuracy, activities of less than 200 $nmoles.min^{-1}.(mg\ protein)^{-1}$ under these conditions are below the acceptable limit of accuracy ($Z'<0.5$) and the compounds cannot be classed as MSNAT substrates.

Kinetic analysis was performed with eight of the substrates chosen from each substrate class. Eadie-Hofstee plots showed that the reactions follow apparent Michaelis-Menten kinetics. Apparent kinetic constants (Table 3.3) were determined by non-linear optimisation of the curve to the data as shown for hydralazine and iodoaniline (Figure 3.5). The $k_{cat,\ app}$ values show a 10-fold variation across the series of substrates with turnover numbers for hydralazine of 0.063 $s^{-1}$ and for 4-chloroaniline of 0.0069 $s^{-1}$. The specificity constant, $k_{cat}/K_m$ shows a 200-fold variation with hydralazine and 4-chloroaniline again representing the extremes.

| Substrate | $K_{m,\ app}$ (μM) | $V_{max,\ app}$ (μmole.min$^{-1}$.mg$^{-1}$) | $k_{cat}$ (x10$^3$ s$^{-1}$) | $k_{cat}/K_m$ (s$^{-1}$ M$^{-1}$) |
|---|---|---|---|---|
| Hydralazine | 80 ± 20 | 12 ± 1.0 | 63 | 790 |
| 5-Aminosalicylate | 250 ± 40 | 8.6 ± 0.6 | 44 | 180 |
| 4-Anisidine* | 1800 ± 150 | 5.7 ± 0.6 | 30 | 17 |
| 4-Ethoxyaniline* | 1010 ± 90 | 6.9 ± 0.9 | 36 | 36 |
| 4-Butoxyaniline* | 330 ± 50 | 7.5 ± 0.2 | 39 | 120 |
| 4-Chloroaniline† | 2000 ± 100 | 1.3 ± 0.1 | 6.9 | 3.5 |
| 4-Bromoaniline† | 1800 ± 200 | 1.7 ± 0.2 | 8.6 | 4.8 |
| 4-Iodoaniline† | 1000 ± 100 | 1.9 ± 0.1 | 9.8 | 9.7 |

**Table 3.3 – Kinetic analysis of substrate acetylation**

The rate of acetyl CoA hydrolysis was determined with varying concentrations of the substrates shown. Michaelis-Menten kinetics were confirmed using the Eadie-Hofstee plot (data not shown) and kinetic constants were determined by non-linear optimisation (Figure 3.5). Mean ± difference of two independent measurements are shown. The $K_{m,\ app}$ value for hydralazine is likely to be lower than that showed due to almost complete acetylation of substrate at the lower concentrations. Substrates were tested in the presence of 0%, 2.5%† or 5%* DMSO.

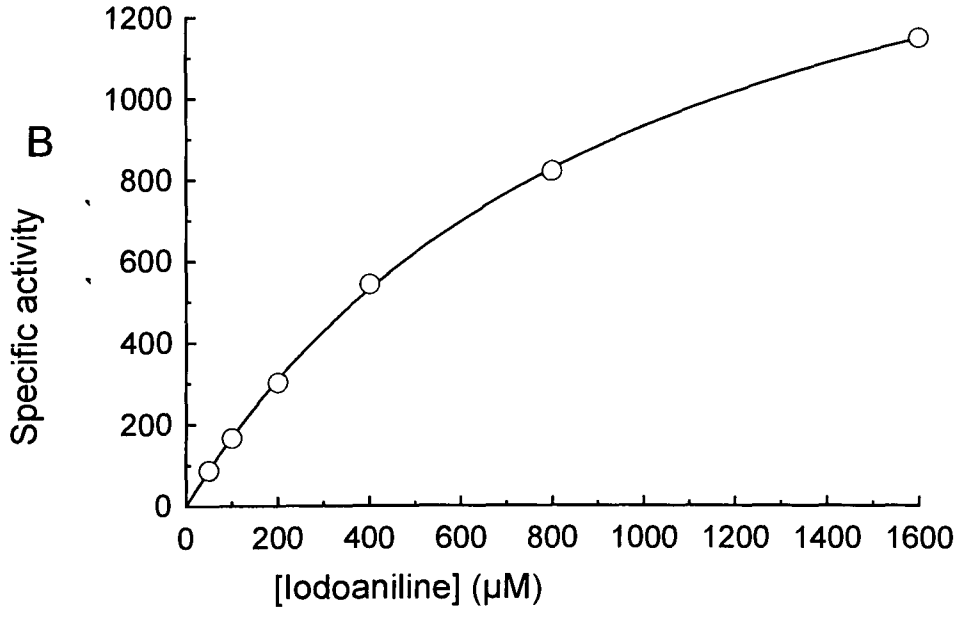


**Figure 3.5 – Kinetics of hydrolysis of Acetyl CoA with iodoaniline**

The specific activity of MSNAT is plotted against the substrate concentration for iodoaniline. 'Best-fit' Michaelis-Menten kinetics were plotted using non-linear optimization (KyPlot v6.0).

### 3.2.3 The lipophilicity of MSNAT Substrates

Apparent differences were observed in the effect of the substituent on the aromatic ring of the substrates on the rate of the reaction. The data suggests that the electronic properties of the aromatic ring have only a moderate effect on the rate of acetylation as the electron-donating 4-aminophenol and the electron-withdrawing 4-trifluoromethylaniline both gave similar values. The series of alkoxyanilines suggested that the lipophilicity of the substrate may be a contributory factor to the rate of acetylation observed and so calculated partition coefficients (clogP) between water and 1-octanol of the substrate molecules were determined using ChemDraw v6.0 (CambridgeSoft) (Table 3.2). Double logarithmic plots of clogP against the MSNAT activity revealed a linear dependence in the rate of reaction with increasing lipophilicity for both the

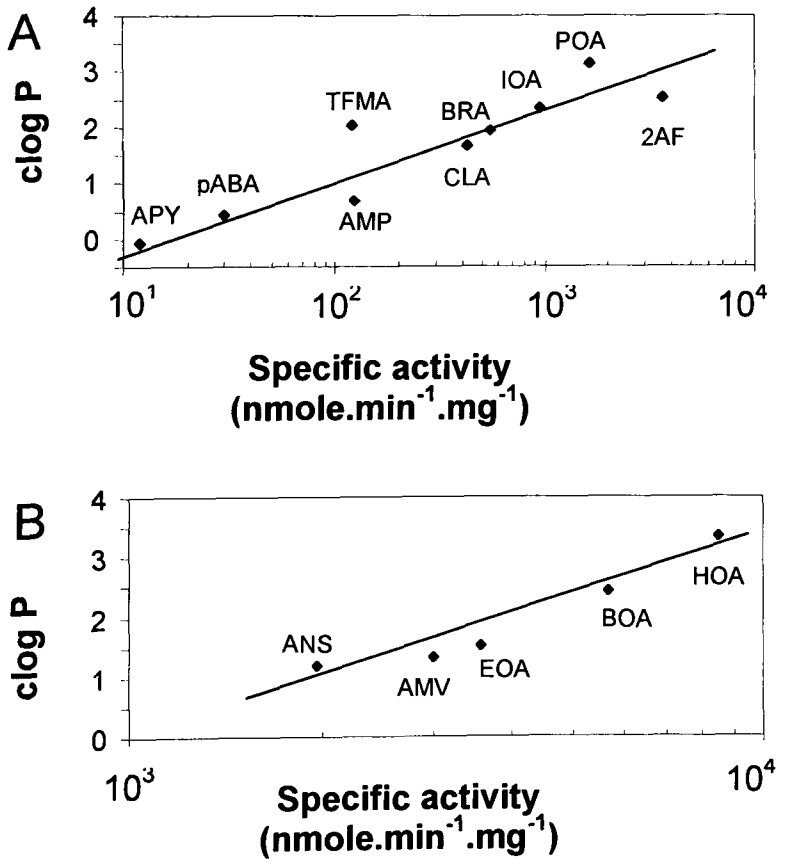


**Figure 3.6 – Effect of substrate lipophilicity on rate of acetylation**

The MSNAT specific activity is plotted on a logarithmic scale against the substrate calculated partition coefficient between 1-octanol and water for the series of (A) arylamines and (B) alkoxyanilines as in Table 3.2. Logarithmic lines of regression are shown.

alkoxyanilines and also the other arylamines (Figure 3.6). However, hydralazine and 5-aminosalicylate are both hydrophilic compounds with high rates of acetylation so other contacts must be involved with these compounds.

### 3.2.4 Simulated annealing of substrates to MSNAT

To determine the contact residues involved in substrate binding, several of the compounds tested were annealed to the MSNAT crystal structure using the Autodock suite of programs (Goodsell *et al.* 1996) (Section 2.2.13). All solutions predict substrate binding into the active site (Table 3.2) with two specific loci: one immediately adjacent to the active cysteine residue (termed the α site) (Mushtaq *et al.* 2002) and one at approximately 11Å from the α site (termed the β site) (Figure 3.7). Average final docked energy values for solutions in the β site across all the compounds were –7.68 kcal.mol$^{-1}$ and those for the α site were –6.65 kcal.mol$^{-1}$. Where compounds bound at both sites, the calculated binding energy at the β site was in all cases more exothermic than at the α site. Six compounds gave solutions only at the α site with an average binding energy of –7.31 kcal.mol$^{-1}$, including four of the five most effective substrates. 4-Aminophenol was predicted to bind only at the β site and is a poor substrate for MSNAT. For the eight compounds that gave binding solutions at both sites, a general correlation was observed between the number of solutions in the alpha site and the specific activity. For alkoxyanilines, the binding energy at the α site was predicted to increase and the binding energy at the β site decrease with increasing specific activity.

It has previously been suggested that substrates bind first to the β site (lower energy) which subsequently allows binding at the α site (Mushtaq *et al.* 2002). Here we show evidence that some of the most effective substrates do not bind to

the β site at all. It may be that the β site is an internal pocket of the protein and, although providing a low energy in docking studies because of the close contact of surrounding residues, cannot in practice be occupied because of steric hindrance.

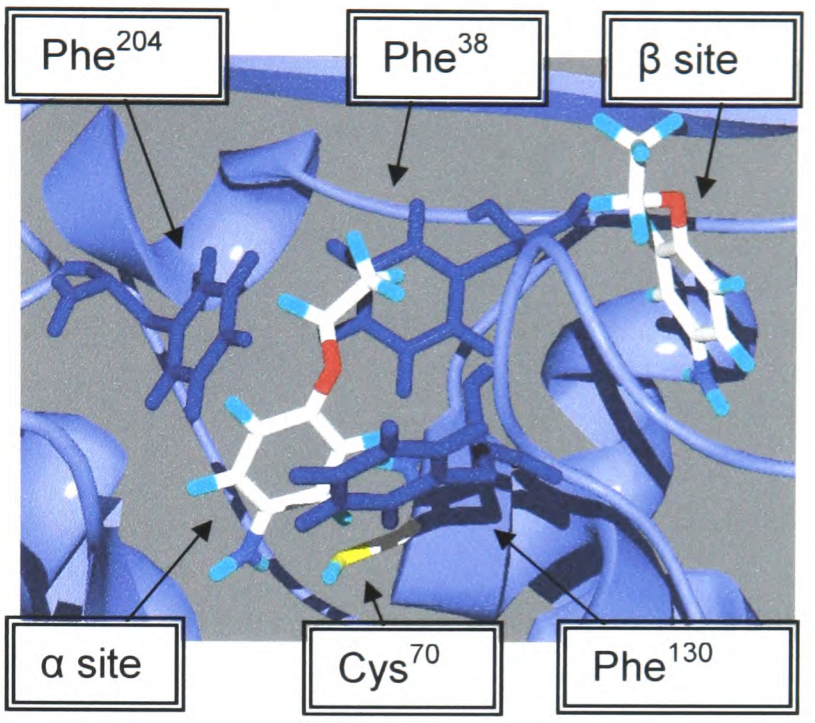


**Figure 3.7 – *In silico* docking of 4-ethoxyaniline to MSNAT**

The 3D structure of MSNAT at 1.7Å is depicted in ribbon format with two of the docking solutions for 4-ethoxyaniline showing the α and β sites of the enzyme. The EOA structures and the Cys[70] sidechain are shown in standard CPK; Phe[38], Phe[130] and Phe[204] are shown in dark blue.

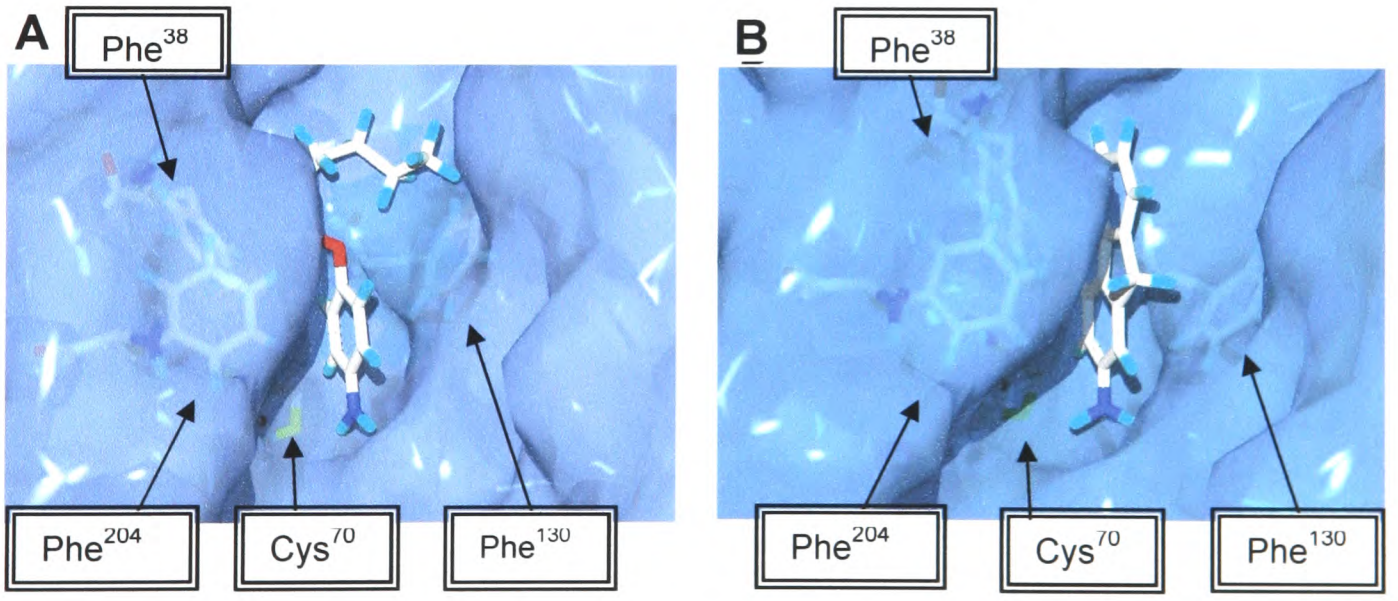


**Figure 3.8 – *In silico* docking of 4-hexyloxyaniline and 2-aminofluorene to MSNAT**

The 3D structure of MSNAT is shown with the lowest energy docking solution for (A) 4-hexyloxyaniline, and (B) 2-aminofluorene. The substrate structures and the enzyme sidechains are shown in standard CPK colouring with the molecular surface of the enzyme in blue.

### 3.2.5 Binding of 5AS to MSNAT

In order to gauge the accuracy of the docking of substrates, it is ideal if a 3D crystallographic structure of the protein with substrate bound can be obtained. In order to generate crystals of MSNAT with bound substrate, 5AS, dissolved in 20mM Tris.HCl pH 8.0, was added to a concentrated MSNAT solution to give final concentrations of 3mM 5AS and 300μM MSNAT. The solution was tested with the Hampton Research Crystal Screen (Section 2.2.12). After three days crystals had formed in several of the wells and condition 25 in Screen 2 (0.01M Cobalt chloride hexahydrate, 0.1M 2-[*N*-morpholino]ethanesulfonic acid (MES) pH 6.5, 1.8M ammonium sulphate) provided suitable crystals. This condition was taken on to further trials by James Sandy (Department of Pharmacology) and a satisfactory crystal was produced at 0.01M cobalt chloride hexahydrate, 0.1M MES pH 6.5 and 2.0M ammonium sulphate. This crystal has undergone X-ray crystallography by Martin Noble (Laboratory of Molecular Biophysics, University of Oxford) and a solution of the structure is currently being resolved.

### 3.2.6 Rationalising the structure-activity relationship of MSNAT substrates

The contact residues between the substrate and the protein in the active site can be used to rationalise the substrate specificity observed. The 3D structures of MSNAT and STNAT are very similar, with a catalytic triad of Cys-His-Asp situated at the base of a cleft in the protein (Sandy *et al.* 2002). The sequence identity over the full length of STNAT and MSNAT is 34% and sequence identity between the first two domains of the two proteins is 52% (Payton *et al.* 2001). The active site cysteine in both these proteins is in a cleft that is approximately 11Å deep and 12Å wide. In MSNAT, the sidechains of residues $Phe^{38}$, $Phe^{130}$ and

$Phe^{204}$ are each within 7Å of the cysteine thiol group and appear to form a hydrophobic lid over the cysteine. In STNAT, $Phe^{38}$, $Phe^{125}$ and $Phe^{199}$ occupy identical positions. Investigation of the docked substrates in the α site showed these residues to be in clear contact with the larger hydrophobic substrates (shown for 4-hexyloxyaniline and 2-aminofluorene, Figure 3.8).

The lipophilic nature of these residues provides a good explanation for the increased activity observed with the more lipophilic substrates and substrates containing large planar ring systems such as 2-aminofluorene. The observed structure/activity relationship may be rationalised by lipophilic-lipophilic and pi-stacking interactions between the phenylalanine residues in the enzyme and the acceptor substrate. Accordingly, the specificity constants ($k_{cat}/K_m$) of the haloanilines and alkoxyanilines increase with the lipophilicity of the substrate yet the catalytic constants ($k_{cat}$) vary to a lesser extent (Table 3.3). The chemical rate of reaction in the absence of enzyme catalysis would be expected to increase with the nucleophilicity of the arylamine nitrogen (Sinclair *et al.* 1998), which can be affected by varying the substituents on the aromatic ring (OR>I>Br>Cl) and this explains the variation observed in $k_{cat}$. However, this influence is essentially constant for the series of alkoxyanilines thus protein-substrate interactions, shown by $k_{cat}/K_m$, must be involved in affecting the varying rates observed in this series.

In contrast, hydralazine and 5-aminosalicylate have high specificity constants and low lipophilicity possibly indicating that they bind in an alternative fashion to the other arylamines. However, these observations do not take into account any conformational change that may occur on binding of the substrate into the active site and a crystal structure containing a substrate molecule will provide valuable insight on the mechanism of the reaction.

The phenylalanine residues that give rise to the observed substrate specificity are also highly conserved throughout the NAT family. $Phe^{38}$ is located in the conserved PFENL region of NATs, $Phe^{199}$ is conserved in all NATs with acetylating activity (Payton *et al.* 2001) and $Phe^{125}$ is found in human NAT1 and highly conserved in prokaryotic NATs. In chimaeric enzyme studies of human NAT1 and NAT2, $Phe^{125}$ has been implicated in causing the different acceptor substrate specificities between the two proteins (Goodfellow *et al.* 2000) and the presence of a serine residue at this position in human NAT2 may allow the acetylation of the more bulky and NAT2 specific substrates such as sulfamethazine and procainamide. Truncation mutants of STNAT with deletions in the third domain hydrolysed AcCoA in the absence of arylamine substrate and one of these mutants was lacking $Phe^{199}$ (Mushtaq *et al.* 2002). The phenylalanines may thus also serve to exclude water from the active site and prevent hydrolysis of the acetyl-cysteine intermediate by general base catalysis.

## 3.3 Conclusions

The development of an assay based on determination of arylamine-dependent AcCoA hydrolysis by NAT has provided a valuable resource. The acetyl acceptor substrate specificity of MSNAT has been determined and key amino acids involved in ligand binding have been postulated through *in silico* modelling. The assay thus provides useful data in the search for an endogenous substrate for MSNAT. Acyl donors other than AcCoA have been investigated and propionyl CoA can also be used as an acyl donor by MSNAT. Previously, the flexibility of other NATs to use C3CoA as an acyl donor has been demonstrated with NAT

purified from hamster liver using an indirect DNA binding assay of N-hydroxyarylamines (Ozawa *et al.* 1990). Here we show direct evidence for the transfer of the propionyl group catalysed by MSNAT.

The MSNAT substrate 5-aminosalicylate (5AS, Table 3.2) is an effective treatment for inflammatory bowel diseases such as Crohn's disease and ulcerative colitis (Loftus *et al.* 2002). It is acetylated rapidly *in vitro* by MSNAT and a study has shown that it is also acetylated by a range of gut flora, presumably by arylamine *N*-acetyltransferases (Delomenie *et al.* 2001). MSNAT has been co-crystallised with 5AS to provide more data about substrate binding in NATs.

The alkoxyanilines proved to be very effective substrates for MSNAT, with the acetylation rate increasing with alkyl chain length. Interestingly, these compounds have been tested for against *M. tuberculosis* and showed moderate anti-tubercular activity with the activity increasing with alkyl chain length (Nodzu, Watanabe *et al.* 1954).

The new assay method will be used to screen a large library of compounds for NAT inhibition in the search for potent inhibitors of MSNAT (section 4.1). Other uses of this assay already tested elsewhere include screening novel NAT proteins for their substrate specificity (e.g. NATs from *M. loti*, *P. aeruginosa*), as a detection assay during NAT purification procedures (e.g. hamster NAT2) and the determination of acetylation of novel drugs by eukaryotic NATs.

# Chapter 4

# Inhibitors of MSNAT

## 4.1 High-Throughput Screening

### 4.1.1 'Hit-to-Lead' development

In this chapter, the discovery of three classes of MSNAT inhibitors by High-Throughput Screening will be described, using the assay developed in the previous chapter. The iterative synthesis and binding to MSNAT of these three classes of compounds will be described: the thiazolidinedione-sultams, the maleimides and the aminothiazoles. Each section includes:

- The synthetic processes used to obtain the compounds and their derivatives,
- the testing of the compounds as inhibitors of MSNAT,
- *in silico* screening of the compounds for structure-based design.

Figure 4.1 shows an overview for this chapter. Initial testing was performed using the detection of CoA released on hydrolysis of AcCoA by MSNAT in the presence of INH by DTNB (Section 2.2.9 and 2.2.10). When DTT was required in the reaction mixture, MSNAT activity was determined using the detection of arylamine concentration with DMAB (Section 2.2.8).

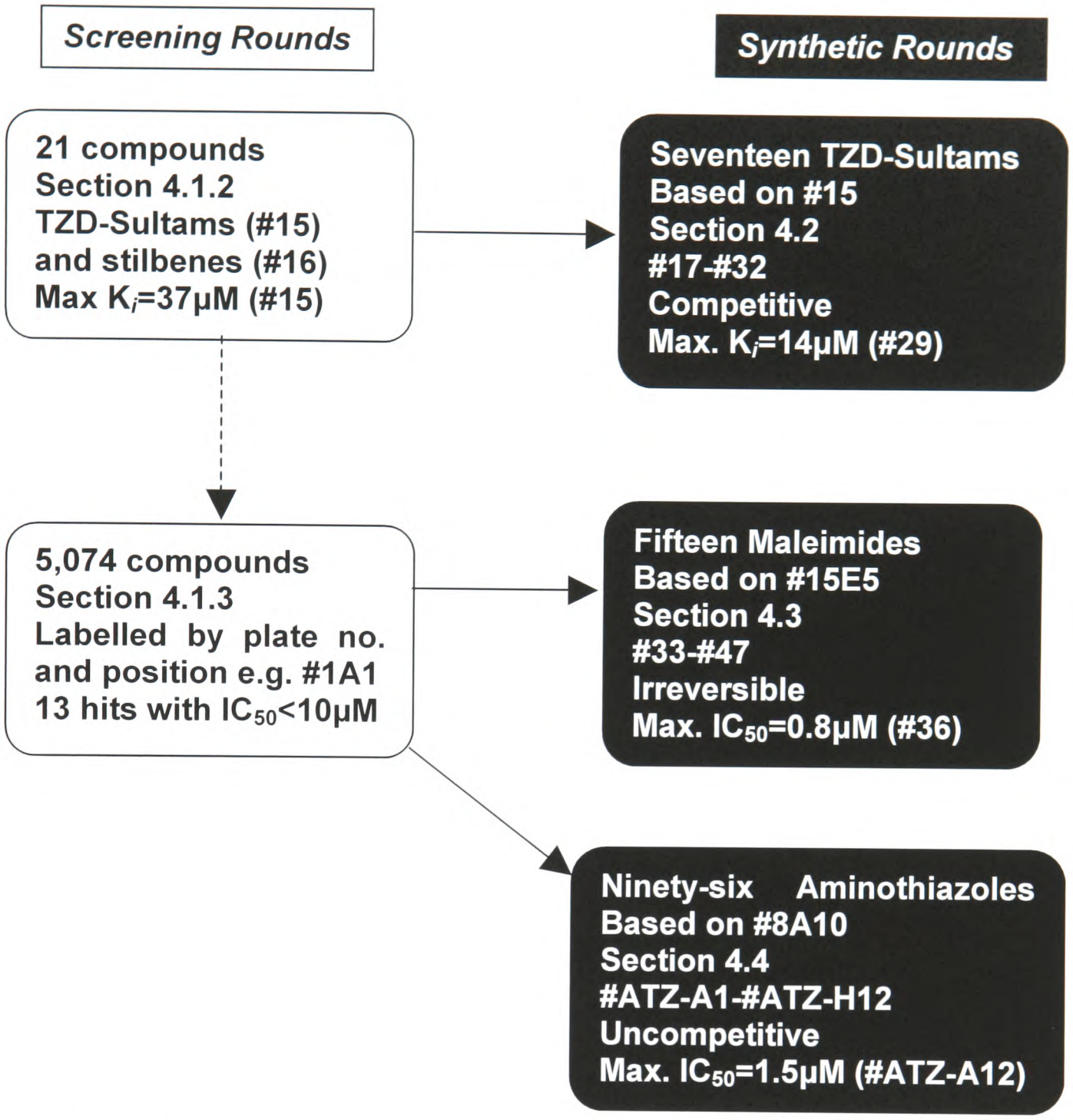


**Figure 4.1 – Overview of NAT inhibitor screening and synthesis**
The initial testing rounds, the subsequent synthetic rounds, nomenclature of different series of compounds, the type of inhibitors made and the maximum inhibitory activity observed are illustrated.

### 4.1.2 Initial Inhibitor Screen

A plate of sixteen compounds kindly donated by Prof. Steve Davies (Dyson Perrins Laboratory, University of Oxford) was tested for NAT inhibition using the method based around the detection of hydrolysed AcCoA with DTNB (Section 2.2.10). The library consisted chiefly of thiazolidinedione-sultams such as **15** (5-(2-cyclohexylmethyl-1,1-dioxo-2,3-dihydro-1*H*-1$\lambda^6$-benzo[e][1,2]thiazin-4-ylidene)-thiazolidine-2,4-dione) and several hydroxyl-substituted stilbenes such as

| Compound | IC50 / μM | Compound | IC50 / μM |
|---|---|---|---|
| 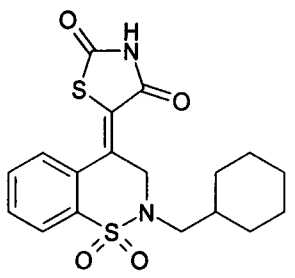 | 20 | 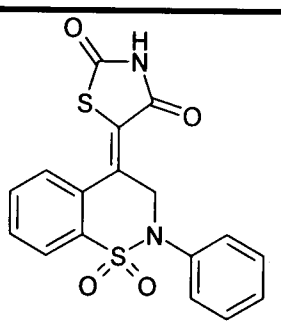 | 170 |
| 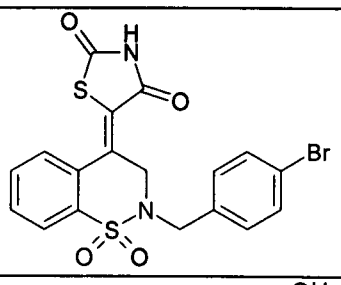 | 65 | 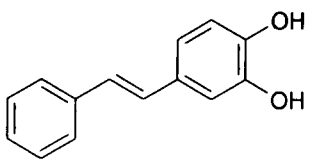 | 180 |
| 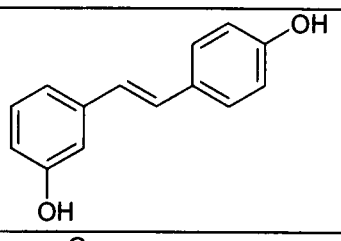 | 70 | 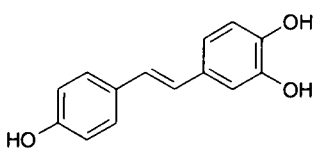 | 180 |
| 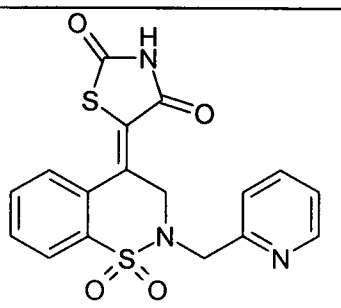 | 90 | 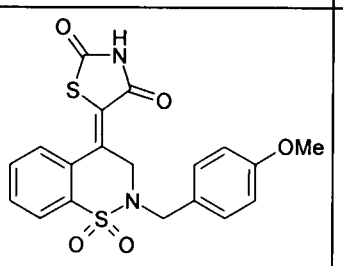 | 200 |
| 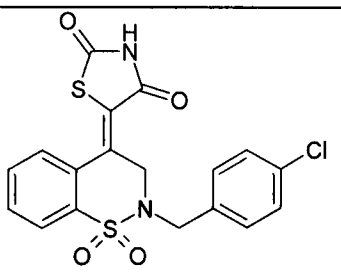 | 100 | 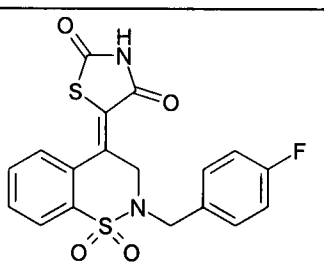 | 200 |
| 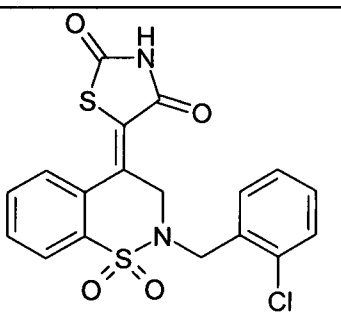 | 110 | 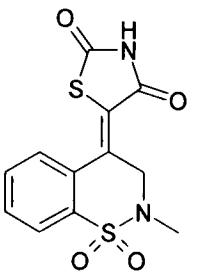 | 200 |
| 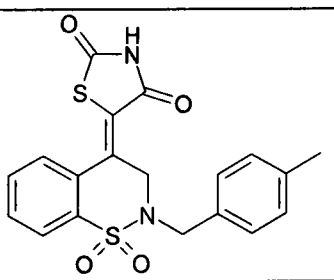 | 150 | 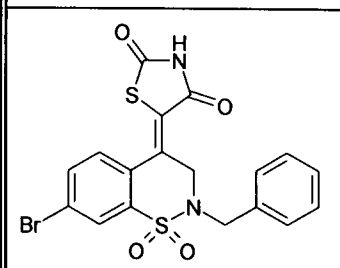 | >500 |
| 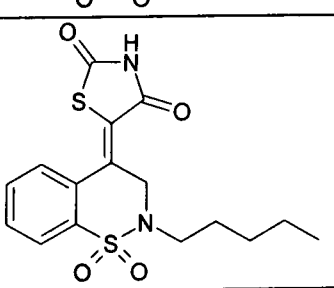 | 170 | 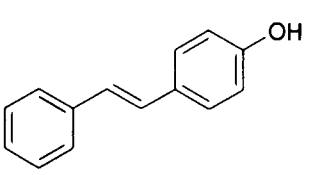 | >500 |

**Table 4.1 – Compounds tested in an initial inhibitor screen**

**16** (Scheme 4.1). Compounds were tested for MSNAT inhibition at concentrations from 0-500μM in the presence of INH (300μM), AcCoA (400μM) and MSNAT. Several of the TZD-sultams showed inhibitory activity particularly the *N*-cyclohexylmethyl-substituted TZD-sultam **15**. The lowest semi-maximal inhibition concentration ($IC_{50}$) for a stilbene was 70μM for **16**.

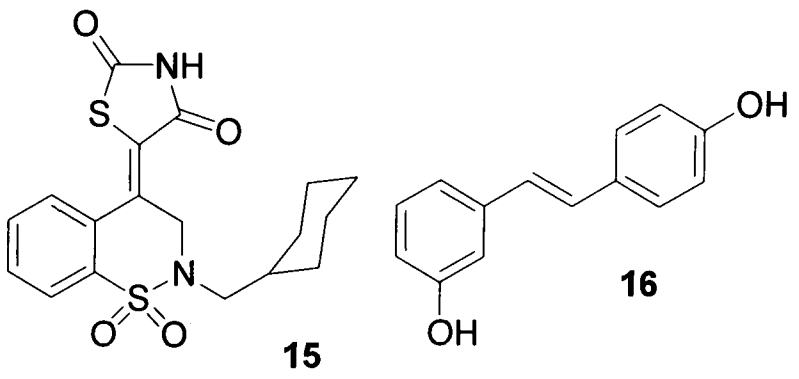


**Scheme 4.1 – *N*-Cyclohexylmethyl substituted TZD-sultam (15) and 4-hydroxy-3'-hydroxystilbene (16).**

Compound **15** inhibited MSNAT in a concentration dependent manner so kinetic analysis was performed to determine the nature of the inhibition. Concentrations of isoniazid were varied from 100 to 450 μM and **15** at concentrations from 12.5 to 100 μM. A double-reciprocal plot of the activities showed that the inhibition was competitive with respect to isoniazid binding. Non-linear regression of the data to the competitive-inhibition model (KyPlot v6.0) gave an inhibition constant ($K_i$) of 37μM (Figure 4.2). Over four determinations in duplicate, the $K_{m,\ app}$ of isoniazid under these conditions was 540μM. On the basis of these results, a library of TZD-sultams was synthesised (Section 4.2).

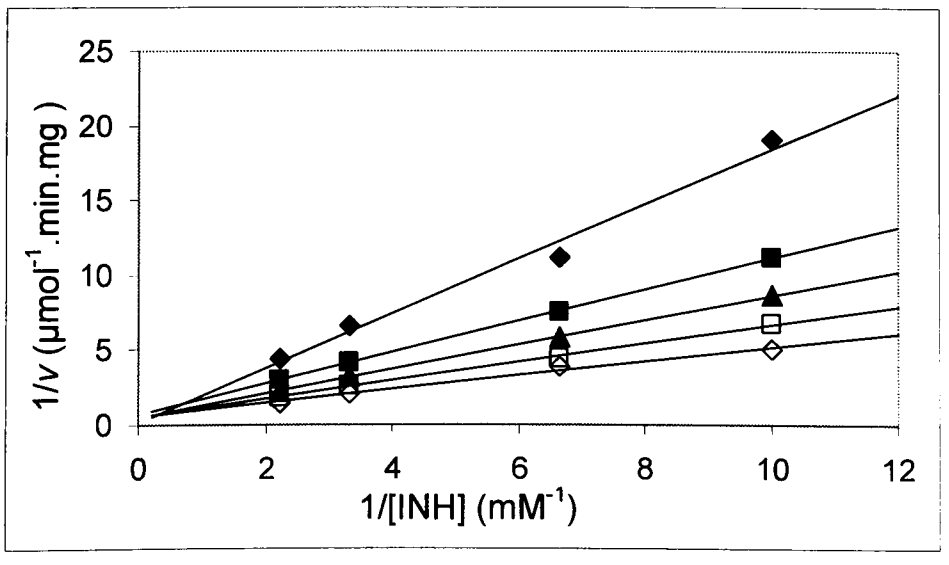


**Figure 4.2 – Inhibition of MSNAT activity by TZD-sultam 15**

The rate of acetylation of INH (100-450μM) was determined in the presence of AcCoA (400μM), MSNAT and the TZD-sultam 15 at 0μM (open diamonds), 12.5μM (open squares), 25μM (triangles), 50μM (closed squares) and 100μM (closed diamonds). Kinetic constants were determined by non-linear optimisation (KyPlot v6.0)

### 4.1.3 High-Throughput Screen

A library of 5,074 compounds was acquired from Chembridge Corporation (San Diego, USA). The library had been picked to include a diverse range of chemical functionalities and structures and all compounds were classified as 'drug-like' by Lipinski's rule of 5 (Lipinski *et al.* 2001). The library was tested for NAT inhibition using the High Throughput Screening Method in Section 2.2.10 with assistance from Isaac Westwood (Department of Pharmacology).

The initial round of testing gave 102 compounds with over 80% inhibition at approximately 96μM (hit-rate of 2.0%). The subsequent rounds of testing gave thirteen compounds with $IC_{50}$ values of below 10μM (0.3%). The structures and $IC_{50}$ values of the hit compounds are shown below (Table 4.2).

To determine the effect of thiol-based reducing agents on the inhibitors, the thirteen hit compounds were re-tested using the detection of arylamine concentration (section 2.2.8) in the presence of DTT at 1mM. Under these conditions, ten of the thirteen compounds lost their inhibitory activity (Figure 4.3). This may be for one of several reasons:

- The compound inhibits the protein by oxidation of the active site cysteine, prevented by the reducing agent DTT (Atmane *et al.* 2003);
- The compound reacts with DTT to produce an adduct that cannot inhibit MSNAT;

The compound, rather than reacting with the protein, reacts with the free CoA formed during the reaction, thus avoiding detection with DTNB and providing false positives.

| Code | MW | Structure | IC50 (μM) |
|---|---|---|---|
| **15E5** | 214.18 | 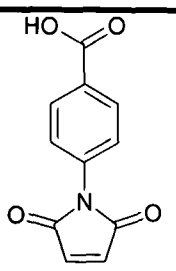 | 1 |
| **40A9** | 264.31 | 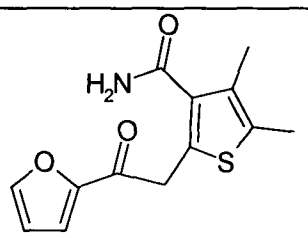 | 1 |
| **10E10** | 245.3 | 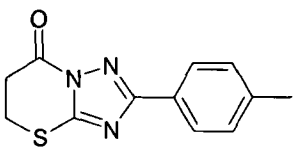 | 2 |
| **8A10** | 484.22 | 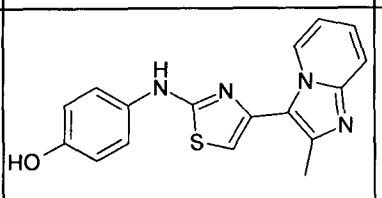 | 3 |
| **37G8** | 327.21 | 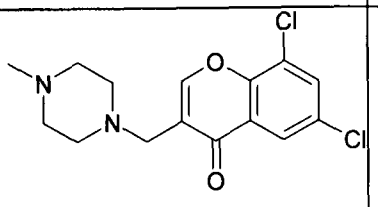 | 4 |
| **31G2** | 300.34 | 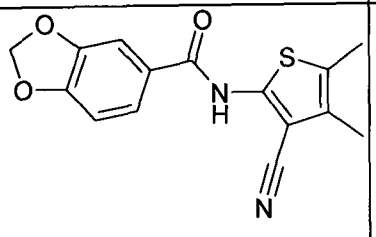 | 5 |
| **19H11** | 295.38 | 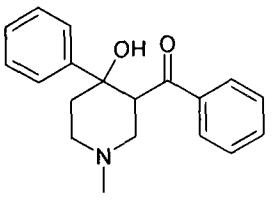 | 6 |

| Code | MW | Structure | IC50 (μM) |
|---|---|---|---|
| **29E1** | 309.39 | 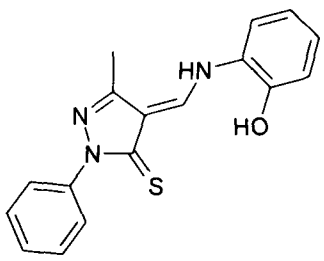 | 6 |
| **15G9** | 358.44 | 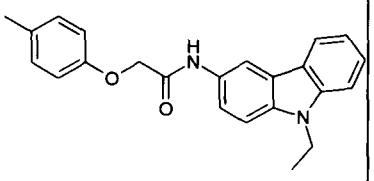 | 7 |
| **2G4** | 403.49 | 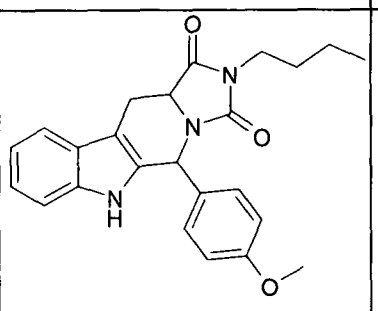 | 8 |
| **30H1** | 344.87 | 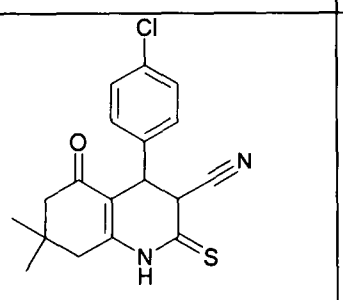 | 8 |
| **19G3** | 216.29 | 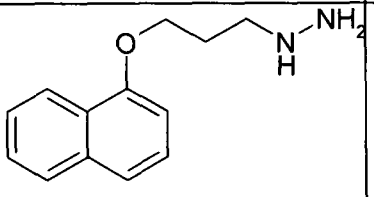 | 10 |
| **40H2** | 302.31 | 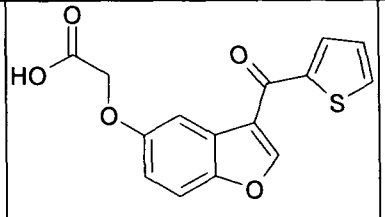 | 10 |

**Table 4.2 – MSNAT inhibitor 'hits' from a High Throughput Screen**

The Table shows the thirteen compounds discovered from a large compound library that showed $IC_{50}$ values of below 10μM (Section 2.2.10). The compound plate number and position, molecular weight, structure and $IC_{50}$ are given.

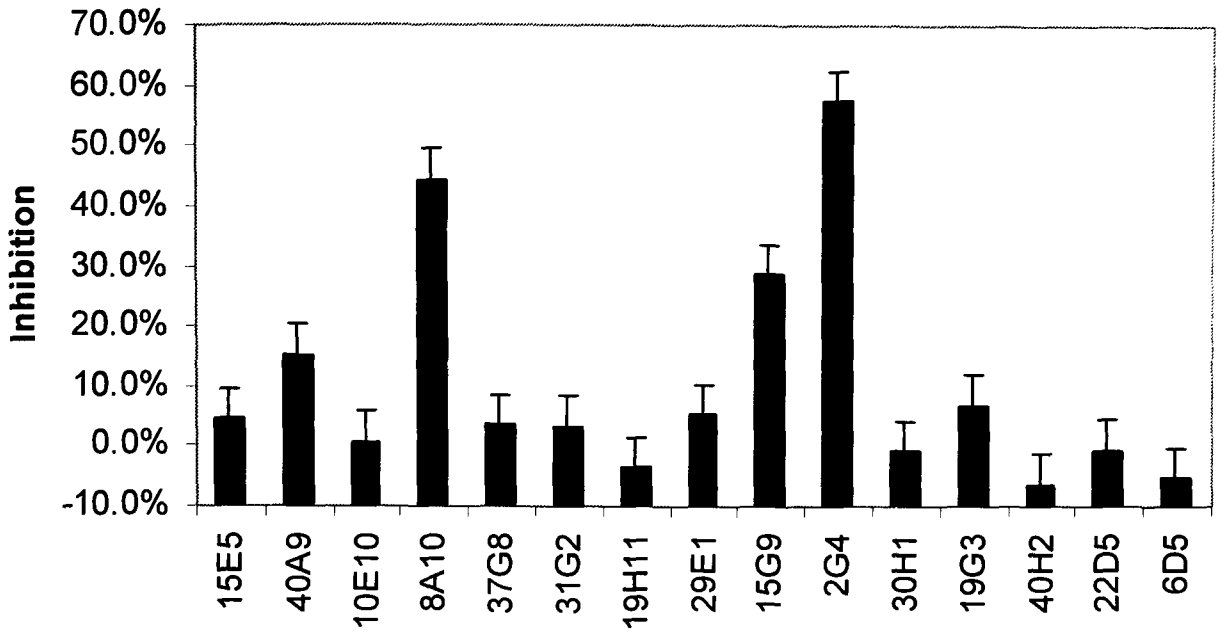


**Figure 4.3 – The effect of DTT on inhibition of MSNAT**

The rate of acetylation of *p*-anisidine (100μM) by MSNAT with AcCoA (200μM) was determined in the presence of the given compounds (20μM, Table 4.2) and DTT at 1mM (Section 2.2.8). Inhibition is given relative to controls containing no compound.

Analysis of the structures of the hit molecules (Table 4.2) shows that five of the thirteen contain an α,β-unsaturated ketone moiety (**15E5, 40A9, 37G8, 30H1** and **40H2**). This functionality can behave as a Michael acceptor which can react with nucleophiles such as thiols under physiological conditions (Schaefer *et al.* 1987). In most living cells, glutathione is present to provide a reducing environment. In *E. coli* concentrations of glutathione can reach 10mM (Fahey *et al.* 1978). Therefore it is likely that the compounds that were inactivated by DTT would be equally inactive within a bacterial cell.

The three compounds which were not inactivated by DTT (**8A10**, **15G9**, **2G4,** Table 4.2) all have a secondary arylamine moiety in their structures. This could be acting as an analogue for an acetylated arylamine intermediate and competing with isoniazid binding in the active site. All thirteen hit molecules were docked into the MSNAT crystal structure as described previously (Section 2.2.13). All compounds were found to be docked into the active site but several orientations were produced for each molecule (Figure 4.4). The average of the mean binding

energies for those compounds deactivated by DTT was 9.24 ± 0.87 kcal.mol$^{-1}$ and the value for those compounds not deactivated by DTT was 10.50 ± 0.21 kcal.mol$^{-1}$ ($p<0.01$). This shows that those hits that are not inactivated by DTT bind more tightly to the active site than those that are inactivated (**15E5, 14A9, 10E10, 37G8, 31G2, 19H11, 29E1, 30H1, 19G3, 40H2, 22D5** and **6D5**) and suggests that the latter group are mechanism based inhibitors.

One series of substituted 1-phenylpyrrole-2,5-dione compounds, termed the maleimides based on compound **15E5**, were further investigated due to their high potency and arylamine-like character (Section 4.3). However, interest was chiefly focused on the three compounds that were not inactivated by DTT (**8A10, 15G9, 2G4,** Table 4.2), and particularly the aminothiazole **8A10** (Section 4.4).

The methodology used for the High Throughput Screen (Section 2.2.10) has several advantages. The assay is quick, easy and reliable, with positive controls always giving a change in absorbance between 0.1 and 0.15AU (approximately 250nmol.min$^{-1}$.mg$^{-1}$). Compounds could be screened in this manner at a rate of up to 6 plates per person per day. It is efficient in the use of MSNAT and AcCoA. The high initial inhibition limit and the multiple rounds of testing greatly minimize the risk of false positives. However, this method also has drawbacks in that it is not suitable for highly coloured compounds and the first round of screening may be prone to produce false negative results. It also can not take into account the effect that reducing conditions may have on certain types of inhibitors. In hindsight it may have been more accurate to perform the first round of screening at a lower concentration in duplicate to reduce the impact of coloured compounds and to minimize the risk of false negatives.

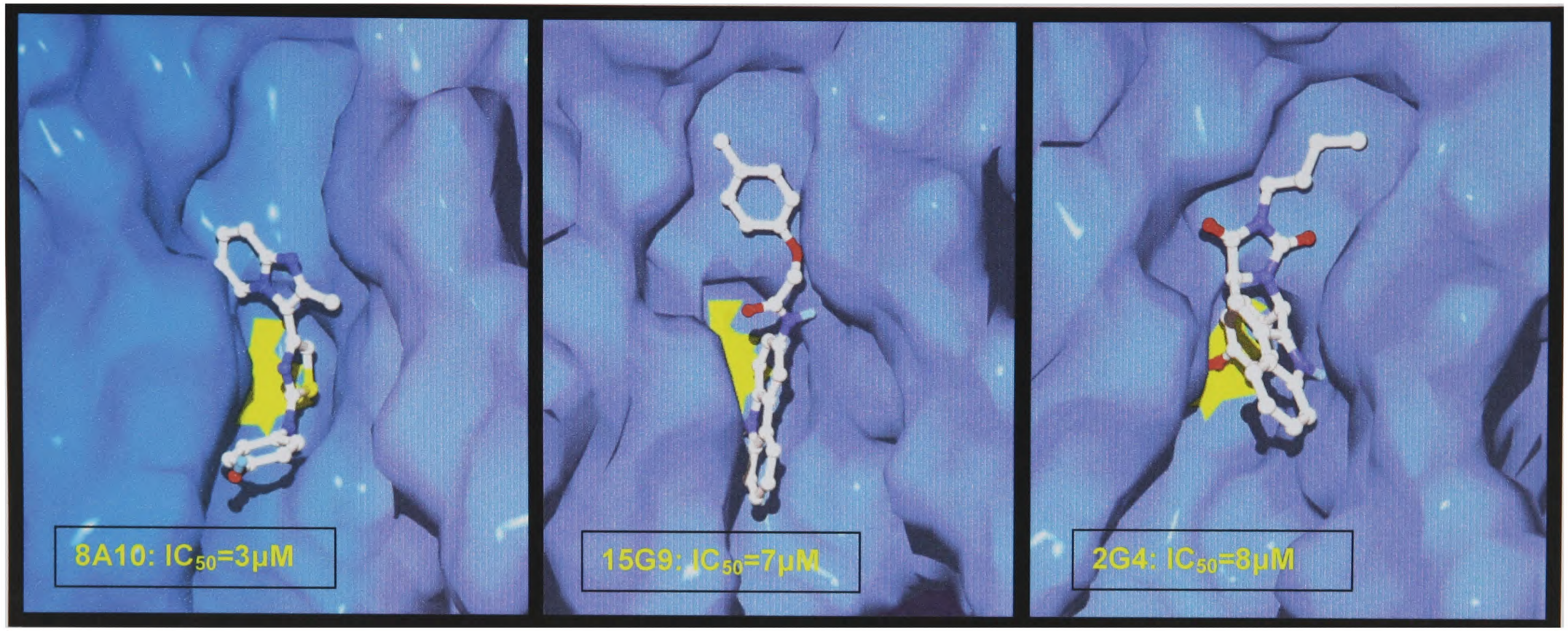


**Figure 4.4 – The binding of 8A10, 15G9 and 2G4 to MSNAT**

The structures of the inhibitors **8A10**, **15G9** and **2G4** (Table 4.1) were docked to the MSNAT crystal structure using the program AutoDock (Section 2.2.13). The highest energy solution for each compound is shown in ball and stick format with the MSNAT molecular surface depicted in blue and the area above $Cys^{70}$ shown in yellow.

## 4.2 Thiazolidinedione-sultams

### 4.2.1 Synthesis of TZD-sultams

The TZD-sultams were synthesized in six steps from saccharin (Scheme 4.2, section 2.3.2, (Brooke *et al.* 2003)) with Dr. Richard Vickers (Dyson Perrins Lab., University of Oxford, UK). N-Diversification was performed on ketal **4** which could be synthesized in high yield. This protected sultam was readily accessible in three steps from sodium saccharin, following work detailed by Zinnes (Zinnes *et al.* 1965; Zinnes *et al.* 1966). Alkylation with chloroacetone and subsequent Gabriel-Colmann ring expansion (Gabriel *et al.* 1900) with two equivalents of NaOEt furnished diketone **3**, as its enolic form, which underwent protection and concomitant de-acylation upon reflux with ethylene glycol under Dean and Stark conditions. Subsequent deprotection of the ketal and condensation with TZD furnished the final products as shown in Scheme 4.2 (identical to Scheme 2.1). However, the final condensation reaction occurs in a very low yield, probably due to the steric interaction between the TZD sulfur and the peri hydrogen in the move from tetrahedral transition state to planar product. The non-aromatic ring is predicted to be twisted from the plane of the aromatic ring to reduce this steric hindrance. Unfortunately, diversification after the condensation step gave a mixture of N-alkylated products. The early position of the diversification step in the synthesis and the low yield of the condensation reaction meant that the library was limited in size and was not amenable to combinatorial methodologies.

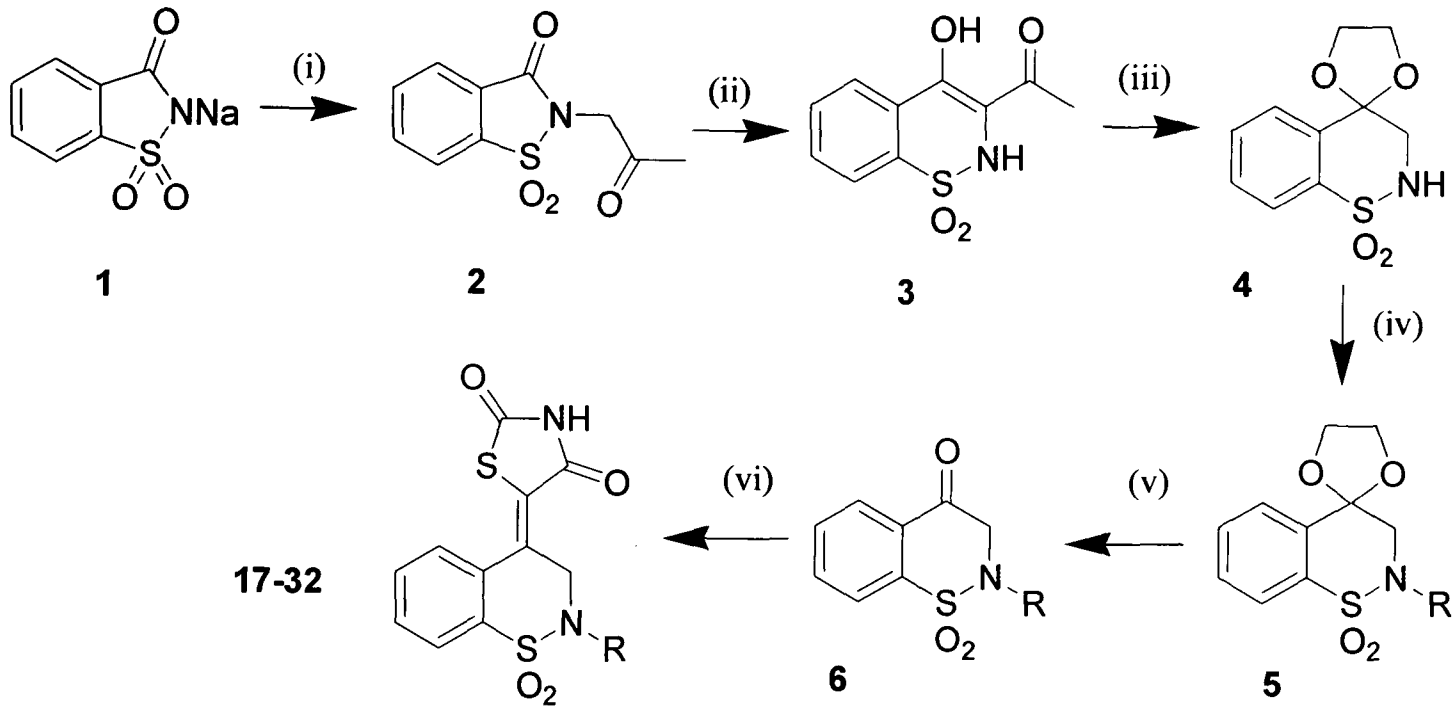


**Scheme 4.2 – The synthesis of *N*-substituted TZD-sultams**

*Reagents and conditions:* (i) $MeCOCH_2Cl$, cetyl trimethylammonium bromide, PhMe, Δ; (ii) NaOEt, EtOH, 55°C then HCl(aq); (iii) ethane-1,2-diol, *p*-TsOH, $C_6H_6$, Δ; (iv) NaH, DMF, RBr, r.t.; (v) HCl, MeOH, Δ; (vi) thiazolidine-2,4-dione, $Et_3N$, $BF_3.OEt_2$, 1,4-dioxane.

Different conditions were tested to improve the yield of the condensation reaction: (i) $BF_3.Et_2O/Et_3N$, 1,4-dioxane, 0°C then RT, 48hours; (ii) $NH_4OAc$, toluene, 110°C, 3 days; (iii) NaOAc/AcOH, reflux, 2 days; (iv) $K_2CO_3$, toluene, molecular sieves, Dean-Stark apparatus, reflux 3 days; (v) TZD + 2 *n*-BuLi, THF/hexane then added to ketone; (vi) TZD + $Br_2$, AcOH, 85°C, 1hr; Br-TZD + $P(OEt)_3$, reflux, 16hours; product added to ketone; (vii) Br-TZD + $PPh_3$, toluene, reflux, 10hr; product added to ketone. Of all these, only the first method provided any final product.

In the diversification step, the sultam nitrogen could be deprotonated either by sodium hydride in THF or the polystyrene-bound base, PS-BEMP (2-*tert*-butylimino-2-diethylamino-1,3-dimethylperhydro-1,3,2-diazaphosphorine, polystyrene bound, (Baxendale *et al.* 2000)). In the case of the polystyrene bound method, excess alkyl halide was sequestered with polystyrene bound potassium thiophenolate (made from PS-thiophenol and potassium trimethylsiloxide).

However, the use of the solid-phase reagents was expensive and did not provide any particular advantage over the solution-phase method.

As noted in Section 3.2.2, MSNAT has a high affinity for lipophilic arylamines of both alkyl chain and planar types (*cf.* hexyloxyaniline and 2-aminofluorene). Thus it was decided to initially diversify the sultam skeleton with a range of straight and branched alkyl chains and planar aryl groups (Table 4.3). Intermediates were characterized by $^{1}H$ and $^{13}C$ NMR, mass spectrometry and melting point and final compounds were fully characterized including high resolution mass spectrometry and IR (Appendix A1.1).

Following synthesis and testing of the original library, it was decided to diversify the sultam nitrogen with more extended aryl π-systems. Several biaryl- and stilbenoid- TZD-sultams were synthesized by Isaac Westwood and Dr. Richard Vickers via the Heck and Suzuki reactions from a bromobenzyl substituted ketal. The testing of these compounds against MSNAT is described in the next section.

### 4.2.2 TZD-sultam inhibition of MSNAT

All the final TZD-sultam adducts and precursors were tested for inhibition of MSNAT catalysed hydrolysis of AcCoA (Section 2.2.10, see overview Figure 4.1). Compounds were initially tested at 100μM and those possessing inhibitory activity were tested at a range of concentrations from 25μM to 200μM. $IC_{50}$ values were determined graphically (Table 4.3).

All intermediate products were tested as MSNAT inhibitors but only the final products containing the TZD moiety possessed any inhibitory activity, whereas TZD itself possessed no inhibitory activity. The most potent compounds possessed either straight-chain alkyl groups of over eight carbon atoms or large

| Compound | R-substituent | Total Yield (%) | MSNAT $IC_{50}$ (μM) | STNAT $IC_{50}$ (μM) |
|---|---|---|---|---|
| 17 | H | 55 | >100 | nd |
| 18 | 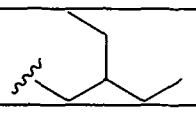 | 10 | 92±5 | >200 |
| 19 | 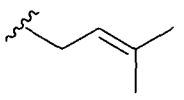 | 28 | >100 | >200 |
| 20 | *n*-octyl | 25 | 61±8 | 150±20 |
| 21 | *n*-decyl | 22 | 22±2 | nd |
| 22 | 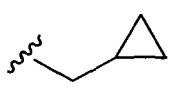 | 16 | >100 | nd |
| 23 |  | 8 | 82±10 | 140±20 |
| 24 | 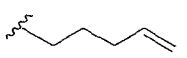 | 6 | >100 | 160±20 |
| 25 | 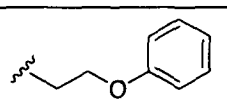 | 19 | >100 | >200 |
| 26 | 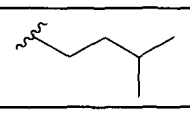 | 15 | >100 | >200 |
| 27 | 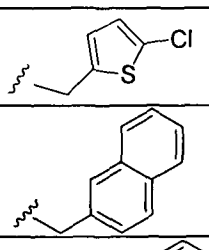 | 24 | 33±1 | 140±10 |
| 28 |  | 20 | 78±5 | 55±5 |
| 29 | 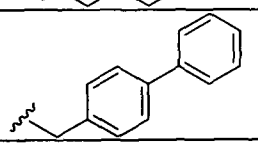 | 10 | 20±1 | 20±1 |
| 30 | *n*-dodecyl | 30 | ins | nd |
| 31 | *n*-tetradecyl | 19 | ins | nd |
| 32 | *n*-hexadecyl | 22 | ins | nd |

**Table 4.3 – Synthesis and testing of a library of TZD-sultams**

Seventeen *N*-substituted TZD-sultams were synthesized (Section 2.3.2) with the R-substituents shown in the table. The yield from ketal **4** is given. The TZD-sultams were tested at concentrations up to 100μM as inhibitors of MSNAT-catalyzed hydrolysis of AcCoA (400μM) in the presence of INH (500μM) (Section 2.2.10) and the concentration giving 50% inhibition of activity is shown as the average of duplicate determinations. The TZD-Sultams were tested at concentrations up to 200μM as inhibitors of STNAT in the same manner. Ins – insoluble under assay conditions, nd – not determined.

conjugated aryl π systems. The chlorothiophene sidechain was also reasonably effective. Despite the presence of 5% DMSO in the assay, some of the more lipophilic TZD-sultams were insoluble at concentrations greater than 100μM. Compounds **29**, **27** and **20** (Table 4.3) also inhibited the acetylation of *p*-anisidine (100μM) by MSNAT with AcCoA (200μM) as determined using DMAB just as effectively with and without the presence of DTT (1mM).

The TZD-Sultams were also tested as inhibitors of STNAT, prepared according to Section 2.2.5 and 2.2.6. Under the same conditions as the MSNAT testing (400μM AcCoA, 500μM INH), the TZD-Sultams were generally less potent against STNAT than they were against MSNAT. The exceptions were the napthyl-substituted **28**, which was more potent against STNAT than MSNAT, and the biphenyl-substituted **29**, which was equipotent against both enzymes (Table 4.3).

To determine the selectivity of the most active TZD-sultams, compounds **27** and **29** (Table 4.3) were tested for inhibition of recombinant hamster NAT2, kindly produced by Akane Kawamura of the supervisor's laboratory (Sticha *et al.* 1997). Hamster NAT2 was incubated with *p*-aminobenzoic acid (500μM), AcCoA (400μM) and compounds **27** and **29** before detection of CoA released by DTNB (Section 2.2.10). At 100μM, the TZD-sultams inhibited AcCoA hydrolysis by 87% (**27**) and 92% (**29**) and at 10μM the inhibition was 5% (**27**) and 23% (**29**). This data suggests that the most potent TZD-sultams are not selective for MSNAT but will also inhibit other bacterial and eukaryotic NATs.

As the biphenyl-substituted TZD-sultam **29** proved to have the most potent activity against MSNAT, a second series of TZD-sultams was synthesized by Isaac Westwood and Dr. Richard Vickers with delocalised aryl systems. The *para*-styryl (**48**) (Brooke, Davies *et al* 2003a), *meta*-biphenyl (**49**) and *ortho*-biphenyl (**50**) TZD-sultams were synthesized using the Heck and Suzuki reactions.

The compounds were tested as MSNAT inhibitors as before. The *p*-styryl substituted TZD-sultam (**48**) was as potent as the *p*-biphenyl TZD-sultam **29** with an $IC_{50}$ of 29±2 μM and a $K_i$ of 14±1 μM (Table 4.4). The *m*-biphenyl TZD-sultam (**49**) and the *o*-biphenyl TZD-sultam (**50**) were weaker inhibitors than the *p*-biphenyl TZD-sultam **29** with $K_i$ values in the order $p<m<o$. Previous studies showed that *meta*- and *ortho*- substituted haloanilines show much lower rates of acetylation than *para*- substituted haloanilines (Sinclair *et al.* 1998) and this trend appears to be matched by the inhibitory activity of the biphenyl-substituted TZD-sultams.

Kinetic analysis was performed for MSNAT inhibition on the most potent compounds by varying inhibitor concentrations from 6.3 to 100μM and isoniazid concentrations from 100 to 500μM (Figure 4.5). In all cases inhibition was found to be competitive with respect to isoniazid with a maximal potency of $K_i$=14μM for compounds **29** and **48** (Table 4.4).

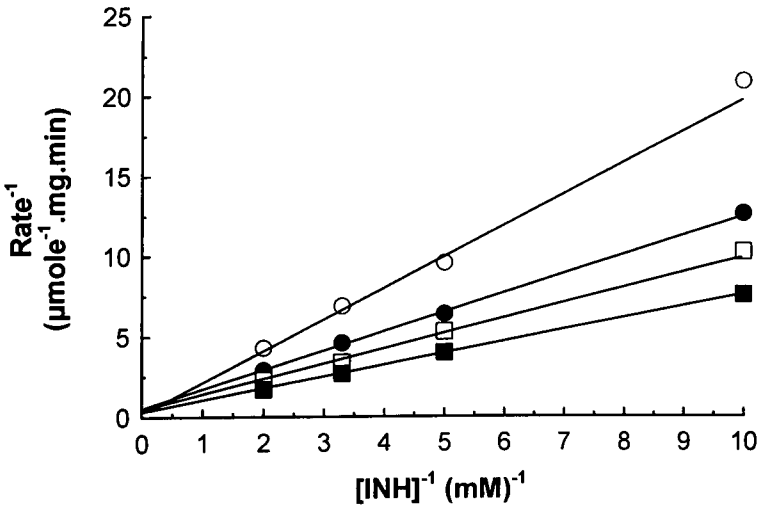


**Figure 4.5 - Inhibition of MSNAT by TZD-sultam 29.**
Double-reciprocal plot of rate against isoniazid concentration in the presence of **29** at 25μM (open circles), 12.5μM (filled circles), 6.25μM (open squares) and 0μM (filled squares). Non-linear regression (KyPlot) shows the inhibition to be competitive with kinetic parameter $K_i$=14μM.

| Compound | $K_i$ (μM) |
|---|---|
| **20** | 43±5 |
| **21** | 15±1 |
| **27** | 27±2 |
| **28** | 70±4 |
| **29** | 14±1 |
| **48** | 14±1 |
| **49** | 41±6 |
| **50** | 120±10 |

**Table 4.4 – Kinetic constants for TZD-sultams.**
Kinetic constants were determined as per Figure 4.5.

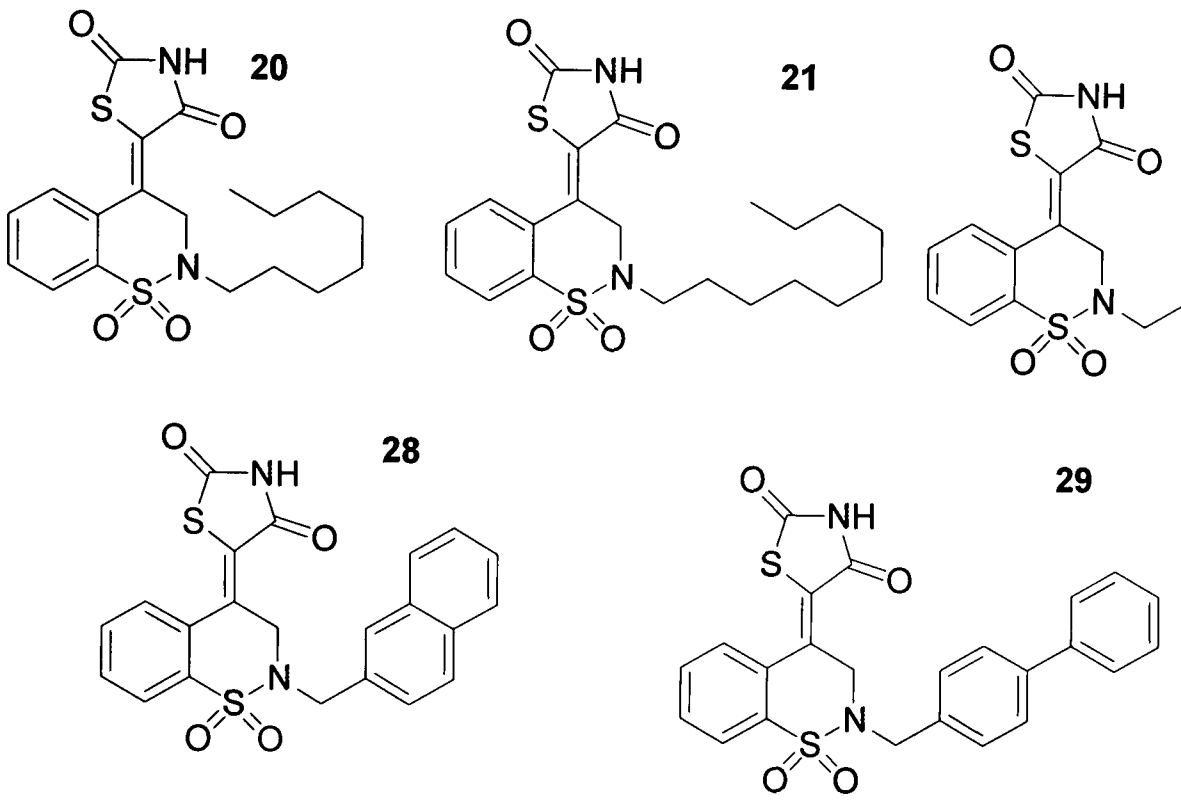


**Scheme 4.3 – TZD-sultams for which kinetic constants determined**

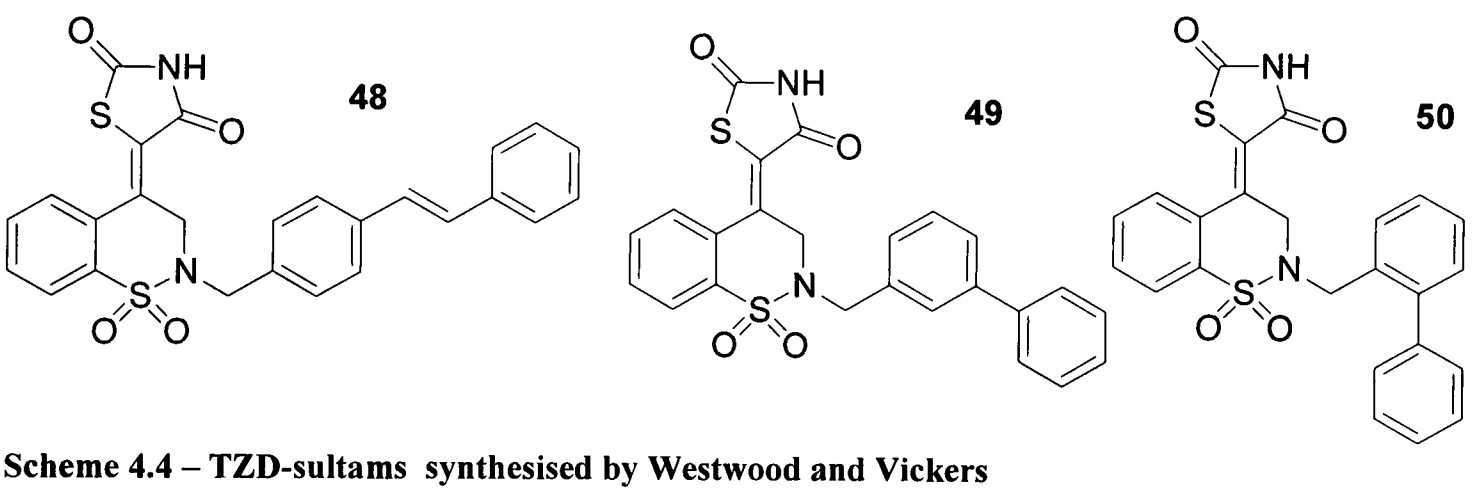


**Scheme 4.4 – TZD-sultams synthesised by Westwood and Vickers**

### 4.2.3 *In silico* screening of TZD-sultams

To help ascertain the binding mode of the TZD-sultams to MSNAT, *in silico* docking studies were performed using the program AutoDock (Goodsell *et al.* 1996; Mushtaq *et al.* 2002). Ten docking solutions were produced for each compound. All compounds showed exothermic energies of binding to the MSNAT structure but, as observed with other docking projects, there was no direct correlation between docking energies and inhibition constants (Siedle *et al.* 2002). However, the lowest energy binding mode of the most potent inhibitors all showed an identical binding orientation (Figure 4.6). This shows the TZD-sultam stretched across the active site cleft in the protein, blocking isoniazid binding. The sultam group is positioned close to the active cysteine residue ($Cys^{70}$). The

tetrahedral arrangement around the sulphur atom may be acting as a homologue of the acetylated arylamine intermediate. Hydrophobic residues surround the sultam nitrogen sidechain. Analysis of the lowest energy docked solution for compound **29** (Table 4.3) was performed using the program LigPlot (Wallace *et al.* 1995) to detect contact residues (Section 2.2.13). All contacts were classed as hydrophobic and the residues were identified as: $Val^{95}$, $Trp^{97}$, $Phe^{130}$, $Gln^{133}$, $His^{203}$, $Phe^{204}$ and $Asn^{223}$. All of these residues except for $His^{203}$ are conserved between MSNAT and TBNAT. The $His^{203}$ residue is involved in a $\pi$ stacking arrangement with the thiazolidinedione ring and may explain the requirement for the TZD functionality for inhibitory activity. The absence of any hydrogen bonds or polar interactions between the TZD-sultams and MSNAT may prove the limiting factor in the potency of this series of compounds as it has not been possible to attain an inhibition constant lower than 14μM.

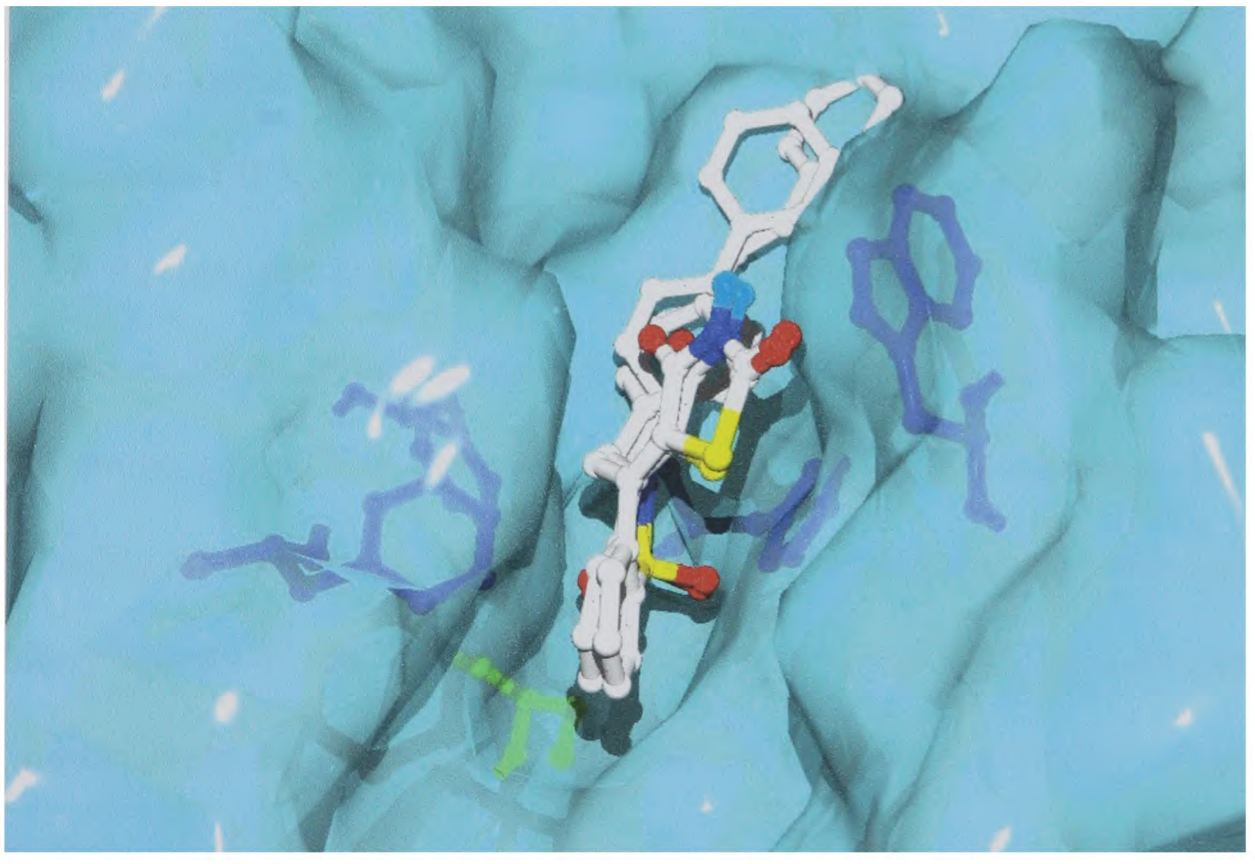

**Figure 4.6 – Docking of the TZD-sultams 29 and 48 to MSNAT**

Compounds **29** and **48** were docked to the MSNAT crystal structure (Section 2.2.13) and the lowest energy docking solutions are shown in ball and stick format. The molecular surface of the protein is shown along with amino acids $Phe^{38}$, $Phe^{130}$, $Phe^{204}$, $Trp^{100}$ (blue) and $Cys^{70}$ (yellow).

## 4.3 Maleimides

### 4.3.1 NAT-specific thiol alkylating agents.

*N*-ethylmaleimide is a thiol-specific alkylating agent that has been used extensively in biochemical studies to determine the role of cysteine residues (Niu *et al.* 2002). Research on the human NATs showed that *N*-ethylmaleimide blocked the enzymic activity irreversibly but that the inactivation was reduced in the presence of AcCoA (Cheon *et al.* 1992). A vinyl fluorenyl ketone was made as a human NAT2 specific affinity label which contains the α,β-unsaturated carbonyl group (Wick *et al.* 1990; Wick *et al.* 1994). Unsaturated vinyl sulfones have been used effectively as inhibitors of cysteine proteases particularly as a possible anti-malaria therapy (Shenai *et al.* 2003). Previously, 2-bromo-*N*-(4-bromophenyl)acetamide has been used as a covalent inhibitor of STNAT in crystallographic studies (Sinclair *et al.* 2000). An arylamine based maleimide may therefore be a useful tool in future studies.

The maleimide **15E5** (Figure 4.1, Table 4.2) was identified as a potent inhibitor of MSNAT through the high throughput screen of the ChemBridge library. The structure contains an arylamine unit of *p*-aminobenzoic acid with a maleimide ring off the amine group. This provides a highly activated α,β-unsaturated carbonyl functionality with structural homology to an acetylated arylamine. Although the inhibitory activity of **15E5** was annulled in the presence of DTT, the high potency and similarity to arylamines was sufficient to synthesise a library of similar compounds.

### 4.3.2 Synthesis of maleimides

The maleimides were synthesised from the corresponding arylamine in two steps (Section 2.3.2, Scheme 4.5). The arylamine (**8**) was stirred with maleic anhydride (furan-2,5-dione) in DMF to produce the uncyclised maleimide (**9**) , characterised by a doublet corresponding to the asymmetric H-C=C-H in the $^1$H NMR spectra and broad $CO_2H$ peak on the IR spectra. Cyclisation was achieved with acetic anhydride and sodium acetate and confirmed by the collapse of the doublet into a 2H singlet at 7.15ppm for the identical protons (**10**, Scheme 4.5). Replacement of the maleic anhydride with succinic anhydride (dihydrofuran-2,5-dione), 3-methylfuran-2,5-dione, 3,4-dimethylfuran-2,5-dione, 3,4-dichlorofuran-2,5-dione or phthalic anhydride (isobenzofuran-1,3-dione) gave the corresponding substituted maleimides. To investigate the relationship between the effectiveness of an arylamine as a substrate and the inhibition of the corresponding maleimide, maleimides were made from the alkoxyanilines, the haloanilines and 2-aminofluorene. Use of the Radleys Carousel allowed the parallel synthesis of ten maleimides, one dimethylmaleimide, one monomethylmaleimide, one succinimide, one dichloromaleimide and one phthalimide (Table 4.5).

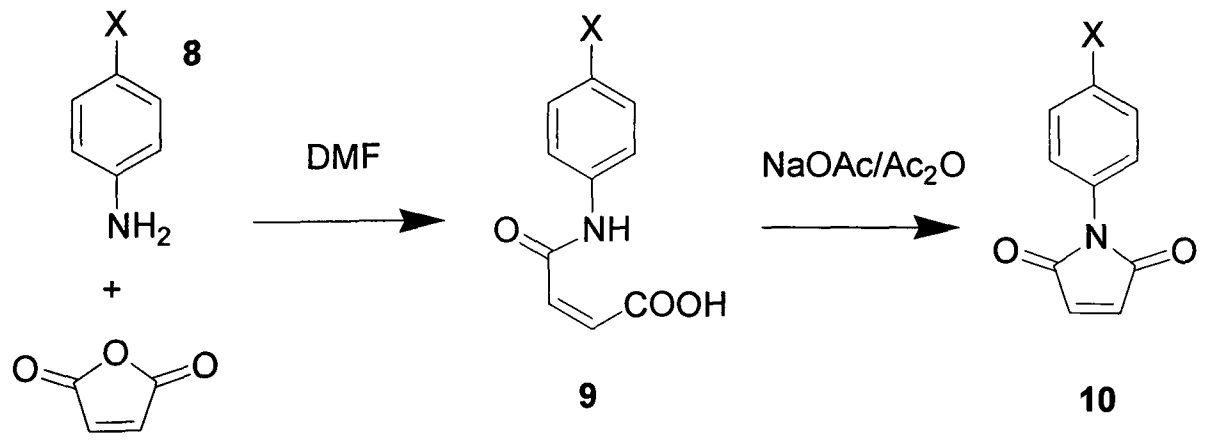


**Scheme 4.5 – The synthesis of *N*-aryl maleimides**
The *N*-aryl maleimides were synthesised in two steps from the corresponding arylamine and maleic anhydride.

### 4.3.3 Maleimide inhibition of MSNAT

The maleimides were tested as inhibitors of MSNAT catalysed hydrolysis AcCoA (400μM) with isoniazid (500μM). The isoniazid, maleimide and MSNAT were preincubated for five minutes before addition of AcCoA and the concentration of maleimide that gave 50% of the rate of controls without maleimide under these conditions was determined graphically (Table 4.5). All of the cyclised maleimides except for the *ortho*-substituted maleimide **42** were potent inactivators of MSNAT but none of the uncyclised compounds possessed any inhibitory activity. Any substitutions on the maleimide C-C double bond **43-45**, **47** resulted in no inhibition and the saturated succinimide **46** was similarly inactive. Testing of *N*-ethylmaleimide under the same conditions gave an $IC_{50}$ of 10μM.

Using direct detection of arylamine acetylation (Section 2.2.8) it was shown that compound **36** (Table 4.5) at 10μM still inhibited the MSNAT catalysed acetylation of 4-anisidine or 4-ethoxyaniline (100μM each) by AcCoA (400μM) and was not sequestering the CoA formed. To determine the type of inhibition involved, MSNAT was incubated with compound **36** for varying times before being added to premixed AcCoA and INH. This showed that the inhibition was both concentration and time dependent (Figure 4.7) as expected for an irreversible inhibitor.

| Compound | Structure | Yield (%) | $IC_{50}$ (μM) |
|---|---|---|---|
| **15E5** | 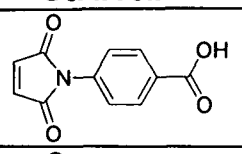 | ns | 0.8 ± 0.1 |
| **33** | 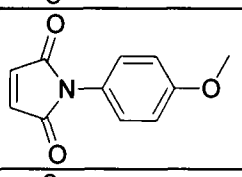 | 49 | 3.3 ± 0.5 |
| **34** | 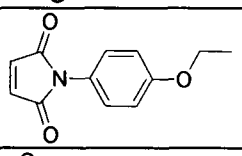 | 32 | 2.0 ± 0.2 |
| **35** | 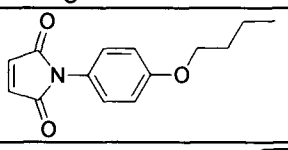 | 49 | 1.0 ± 0.1 |
| **36** | 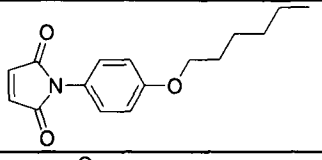 | 47 | 0.8 ± 0.1 |
| **37** | 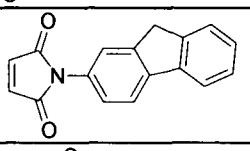 | 53 | 1.6 ± 0.2 |
| **38** | 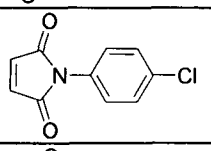 | 79 | 3.2 ± 0.4 |
| **39** | 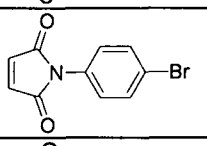 | 64 | 1.6 ± 0.2 |
| **40** | 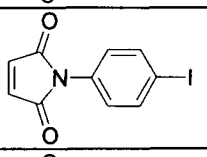 | 71 | 1.4 ± 0.1 |
| **41** | 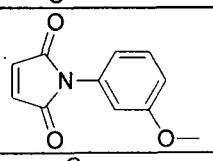 | 31 | 1.4 ± 0.2 |
| **42** | 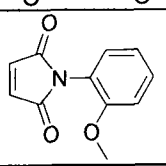 | 25 | >10 |
| **43** | 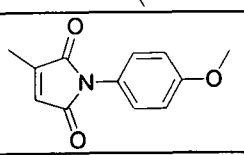 | 48 | >10 |
| **44** | 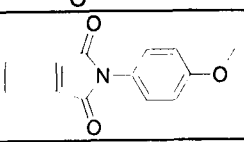 | 55 | >100 |
| **45** | 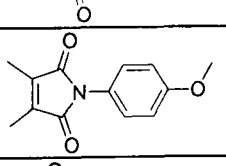 | 71 | >100 |
| **46** | 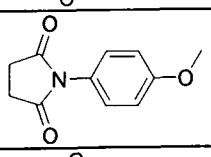 | 50 | >100 |
| **47** | 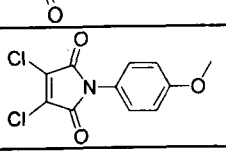 | 80 | >100 |

**Table 4.5 – Synthesis and testing of a library of *N*-aryl maleimides against MSNAT**
Maleimides were tested for inhibition of MSNAT (Section 2.2.10) with INH (500μM) and AcCoA (400μM) and a 5 minute pre-incubation period. The $IC_{50}$ is shown along with total yield over the two steps of the reaction. ns – not synthesized.

The presence of the thiol reagents DTT, glutathione (GSH) and CoA before addition of the maleimide stopped the inhibitory activity but had no effect when added after the maleimide (Figure 4.8). Incubation of compound **34** with DTT (50μM) for 10 minutes at 37°C followed by detection of the thiol concentration of DTT by DTNB showed that the maleimide had reacted with the DTT at close to a 2:1 ratio as would be expected (Figure 4.9).

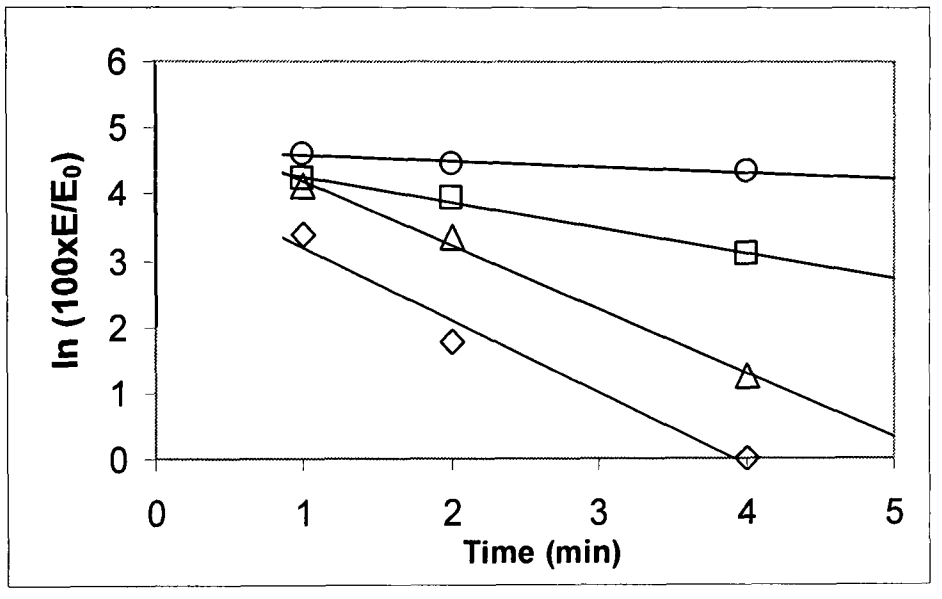


**Figure 4.7 – Time and concentration dependent inhibition by maleimide 36.**
MSNAT was preincubated with **36** for the time shown before addition to preincubated INH (500μM) and AcCoA (400μM) to give final concentrations of **36** of 0μM (circles), 0.5μM (squares), 1μM (triangles) and 2 μM (diamonds). $E/E_0$ is the ratio of the activity observed to the control.

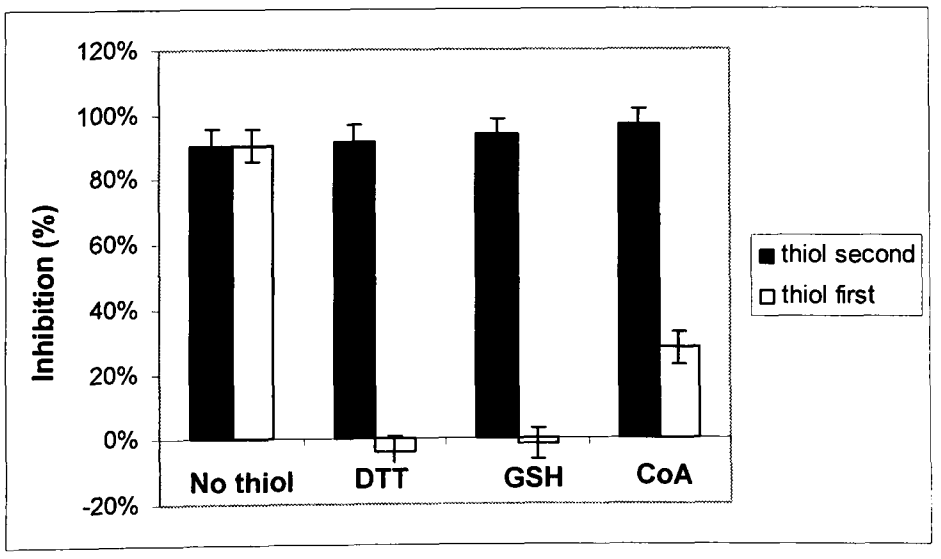


**Figure 4.8 - Prevention of MSNAT inhibition by maleimide 36 using thiols.**
MSNAT was added to compound **36** (10μM final conc.) at 37°C and, after 5minutes, one of the thiols DTT, GSH and CoA (100μM final conc.) was added. In separate tubes the order of addition of protein and thiol was reversed. To all tubes was added premixed ethoxyaniline (100μM) and AcCoA (400μM) and the rate of arylamine acetylation was determined using DMAB (Section 2.2.8).

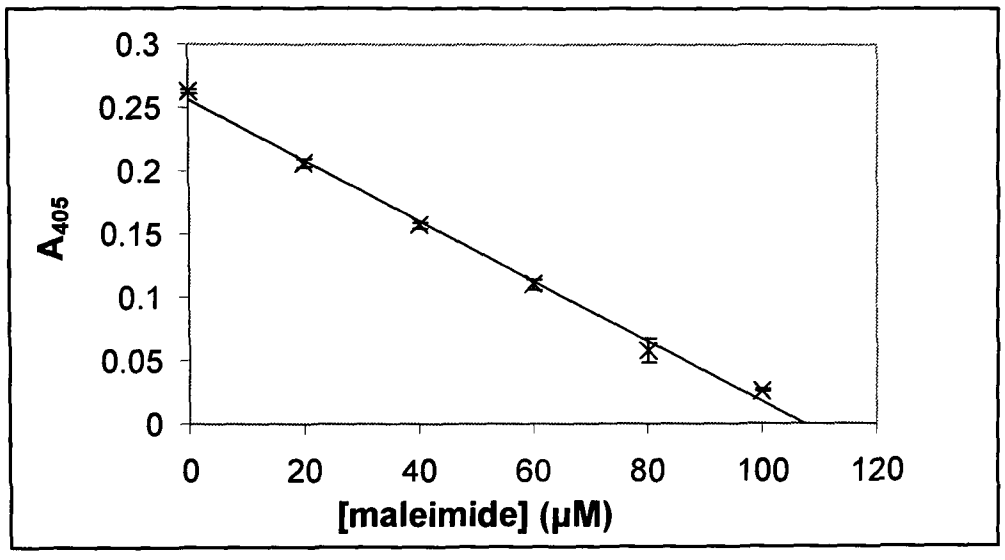


**Figure 4.9 – The action of maleimide 34 on DTT**
DTT (50μM) was incubated with varying concentrations of **34** (final volume 100μL) for 10 minutes at 37°C before addition of 25μL DTNB solution as per the AcCoA hydrolysis assay (Section 2.2.9). The absorbance at 405nm was recorded on a plate-reader.

### 4.3.4 *In silico* docking of maleimides

The maleimides were docked into the crystal structure of MSNAT. The compounds were bound into the active site and had the maleimide orientated at the correct position for nucleophilic attack by the cysteine thiolate (Figure 4.10). For the series of alkoxyanilines, binding energies increased with potency. Although the substituted maleimides still bound to the active site, the double bond was too far from the cysteine to react (Figure 4.10). An oxyanion hole has previously been identified which stabilises the oxyanion formed during the two acetyl transfer steps. This may well also stabilise the oxyanion transition state after maleimide binding.

The maleimides are potent and rapid covalent inhibitors of MSNAT. The alkoxyanilines and haloanilines show that there is some correlation between the activity of an arylamine as a substrate and the inhibitory activity of the corresponding arylamine. However, none of the compounds had a greater activity than the original compound **15E5** (Table 4.2). Although the maleimides are

inactivated by thiols, they may still prove useful as affinity labels or in crystallographic studies (Di Gleria, Nickerson *et al.* 1998).

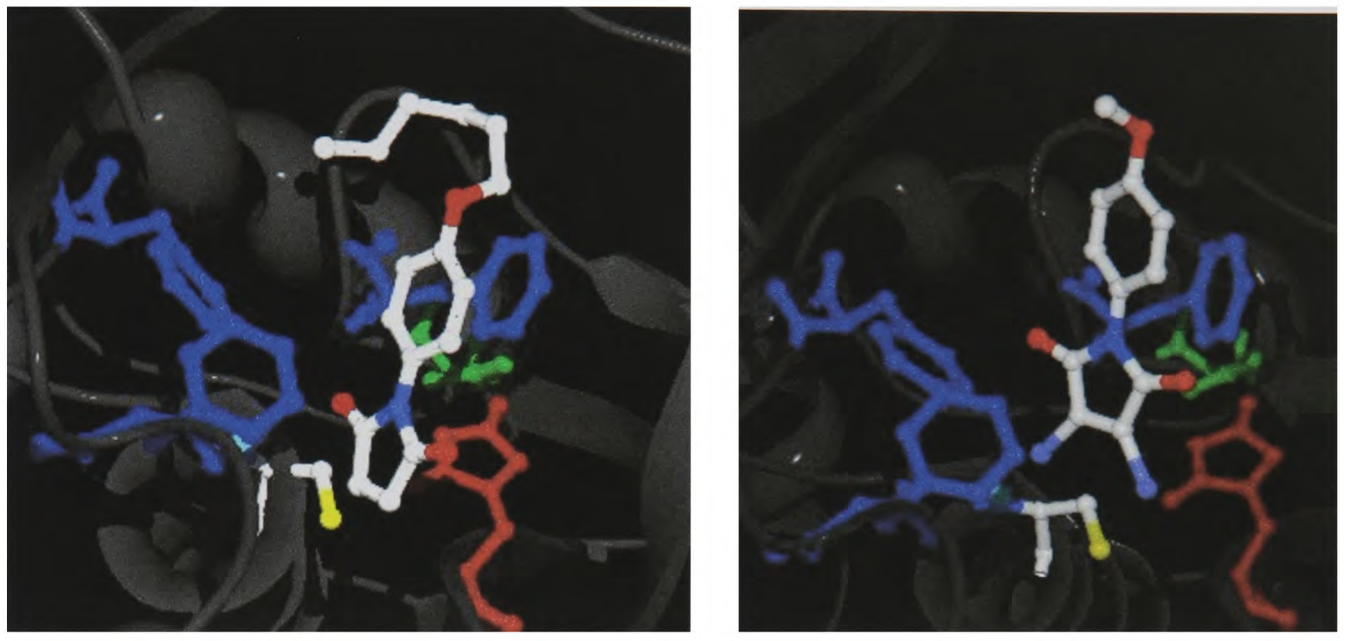

**Figure 4.10 – Binding of maleimides 36 and 47 to MSNAT**

The structures of compounds **36** and **47** were docked to the MSNAT structure (Section 2.2.13). The diagrams show the lowest energy solutions and the active site residue $Cys^{70}$ in CPK colouring with the catalytic triad $His^{110}$ and $Asp^{127}$ in red and green respectively and $Phe^{38}$, $Phe^{130}$ and $Phe^{207}$ in blue.

## 4.4 Aminothiazoles

### 4.4.1 Aminothiazole synthesis

The 2-aminothiazole heterocyclic unit has been studied in a wide range of medicinal chemistry applications (Kearney *et al.* 1998). The aminothiazole **8A10** (4-[4-(2-Methyl-imidazo[1,2-a]pyridin-3-yl)-thiazol-2-ylamino]-phenol, Figure 4.1, Table 4.2) was the most potent inhibitor of MSNAT discovered in the high throughput screen whose inhibitory activity was unaffected by DTT (Section 4.1.3). The first solution-phase synthesis to make 2-aminothiazoles was developed by Hantzsch and Weber (Hantzsch *et al.* 1887). More recently this has been adapted to produce combinatorial libraries of 2-aminothiazoles in both solution-phase (Bailey *et al.* 1996) and solid-phase (Kearney *et al.* 1998). A strategy was adopted that allowed the rapid and effective

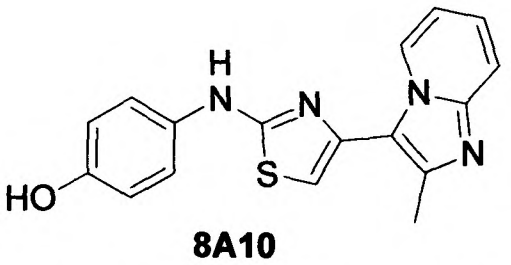


**8A10**

1996) and solid-phase (Kearney *et al.* 1998). A strategy was adopted that allowed the rapid and effective synthesis of similar aminothiazoles in parallel (Section 2.3.4, Scheme 4.6). Refluxing a thiourea **12** with an α-bromoketone **11** at 85°C in DMF for 16 hours furnishes the resulting aminothiazole in high yield. Excess α-bromoketone can be sequestered with polystyrene bound thiourea **13** which is removed easily by filtration. Evaporation of the DMF *in vacuo* provides the solid aminothiazole **14**. The absence of extensive purification procedures, high yield of the reaction and presence of two variable units means that large numbers of aminothiazoles can be synthesised quickly and easily. This makes this type of strategy particularly favourable to medicinal chemists in a hit-to-lead programme.

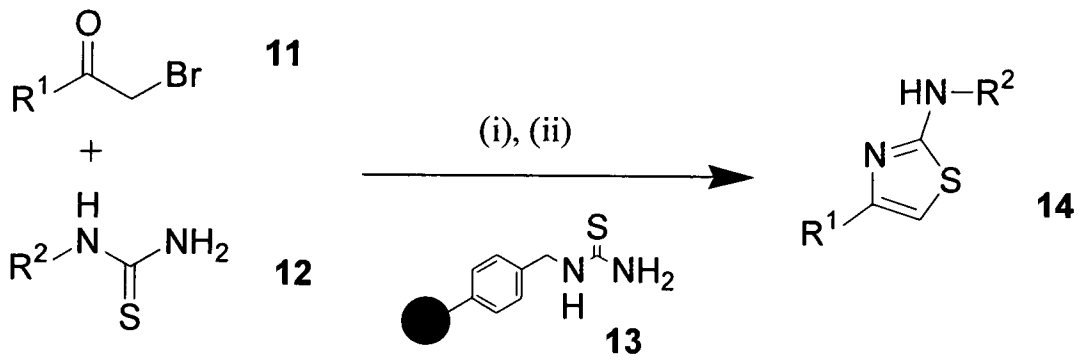


**Scheme 4.6 – The synthesis of aminothiazoles**
(i) DMF, 85°C, 16hrs; (ii) PS-benzylthiourea, 1hr, r.t.

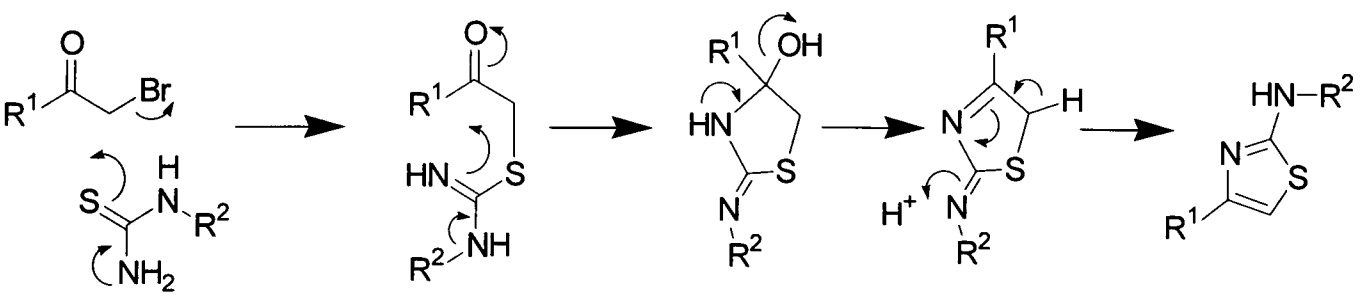

**Scheme 4.7 – Reaction mechanism for aminothiazole synthesis**

A library of 96 aminothiazoles was hence synthesised by Dr. Richard Vickers with assistance from the author (six compounds). Starting reagents were either purchased or synthesised. Thioureas could be made easily from the equivalent

isothiocyanate using 0.5M ammonia in dioxane (Scheme 4.8). The α-bromoketones could be synthesised rapidly from the relevant ketone with $HBr/Br_2$ (Scheme 4.8).

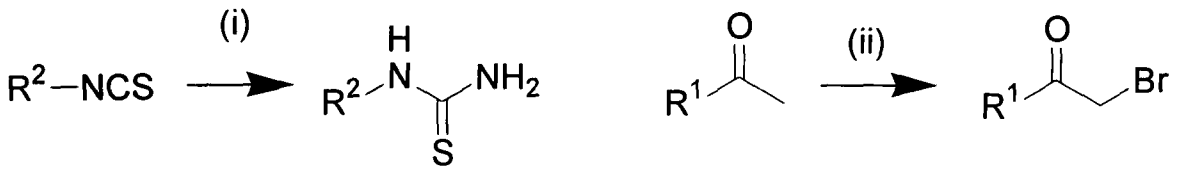


**Scheme 4.8– Synthesis of aminothiazole precursors**
(i) 0.5M $NH_3$/dioxane, 4 days. (ii) $HBr/Br_2$, 70°C, 5 minutes.

Twelve separate thioureas and eight separate α-bromoketones were utilised in a grid format to give ninety-six different aminothiazoles (Scheme 4.9). Yields were high and purity was determined by RP-HPLC and NMR (Appendix A1.3).

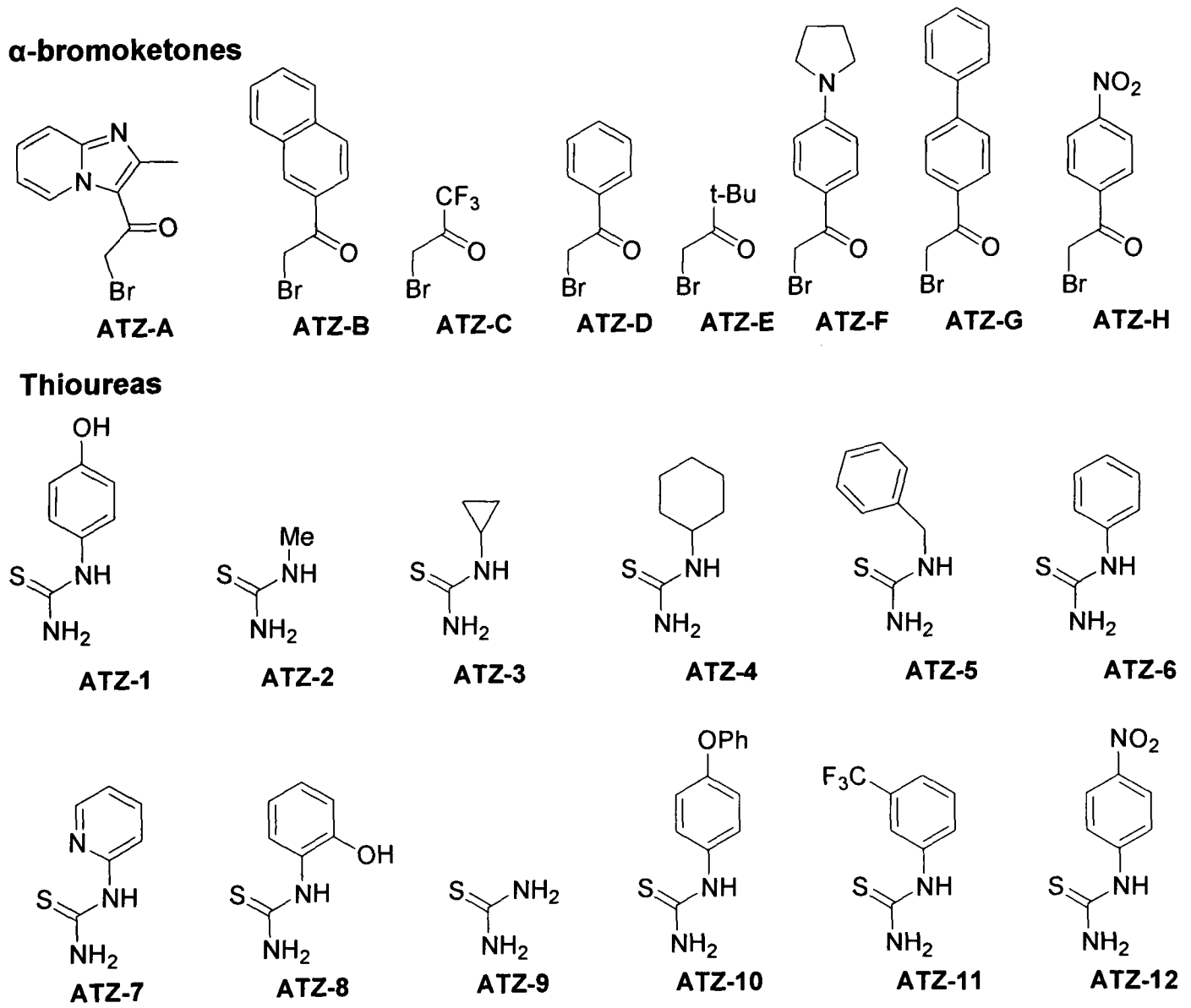


**Scheme 4.9 – Precursors for aminothiazole library**
Each of the α-bromoketones above was reacted with each of the thioureas to give a gridded library of 96 aminothiazoles.

### 4.4.2 Aminothiazole inhibition of MSNAT

The aminothiazoles were tested for inhibition of MSNAT catalysed hydrolysis of AcCoA in the presence of isoniazid (Section 2.2.10). The plate of 96 compounds was tested twice with the aminothiazole at 25μM. Only eight of the aminothiazoles (Appendix A1.3) showed greater than 30% inhibition at this concentration in both tests (denoted by grid position **ATZ-A1**, **ATZ-A5**, **ATZ-A6**, **ATZ-A8**, **ATZ-A12**, **ATZ-B1**, **ATZ-F1** and **ATZ-G1,** Scheme 4.10). All other compounds gave little or no inhibition of MSNAT activity. Interestingly, the compounds that were active at this concentration all possess one of the original R-groups from **8A10**, resynthesised as **ATZ-A1**. Further testing showed that **ATZ-A12** had an $IC_{50}$ value of 1.5μM, a two-fold increase in activity over the original aminothiazole **ATZ-A1** (Figure 4.11). None of the other aminothiazoles had $IC_{50}$ values of less than 30μM.

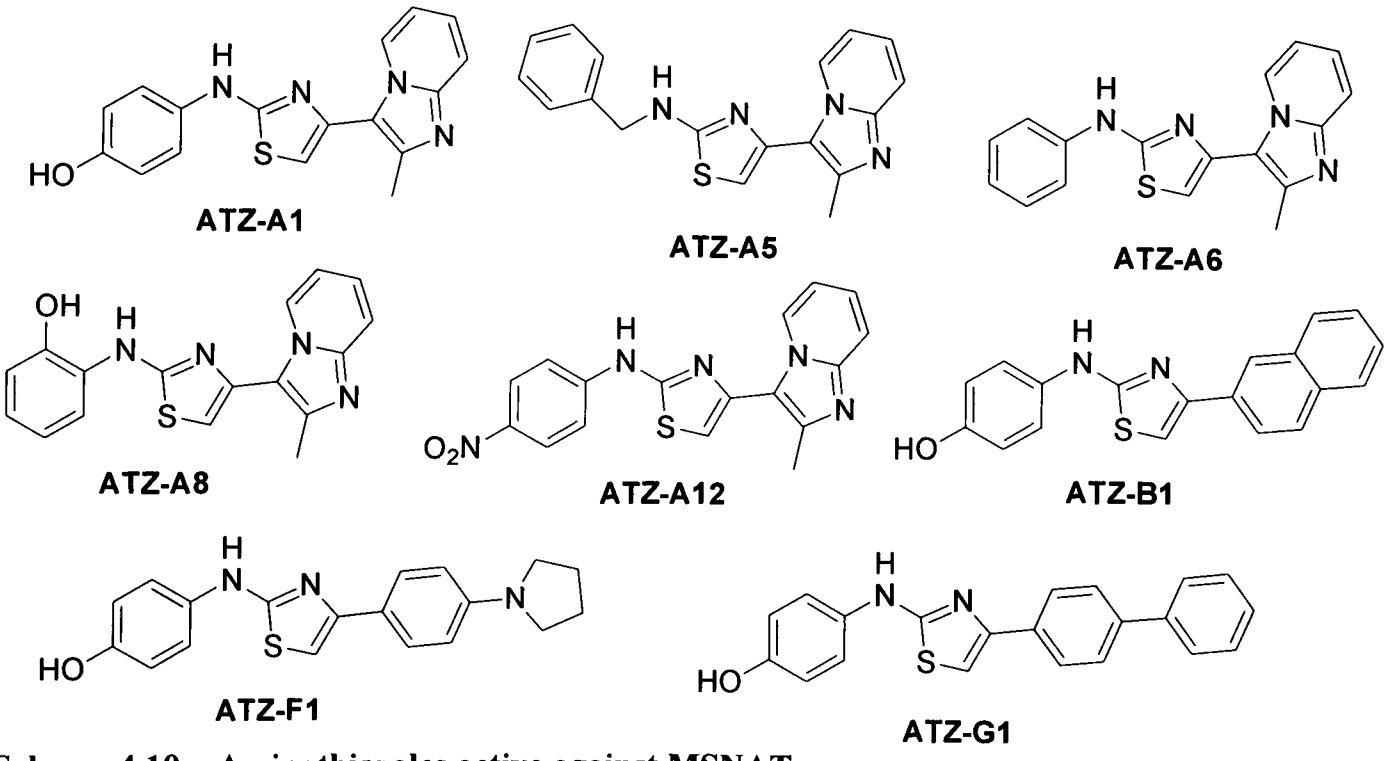


**Scheme 4.10 – Aminothiazoles active against MSNAT**

Some structure-activity relationships can be drawn from this series. Firstly, it is clear that, for this series, either the imidazopyridine group or the *p*-phenol group are required for activity. Secondly, the bromoketone group must contain at least two ring systems, preferably aromatic. The imidazopyridine gave the superior

activity, suggesting an interaction with the ring nitrogen atoms. Thirdly, the thiourea group requires either a phenyl or benzyl functionality, preferentially with a hydrogen-bonding group positioned at the *para* position. The superior activity of the nitro group over the hydroxy group suggests that this group is behaving, either as a hydrogen-bond acceptor to the protein, or by creating a strong electron-withdrawing effect from the phenyl ring.

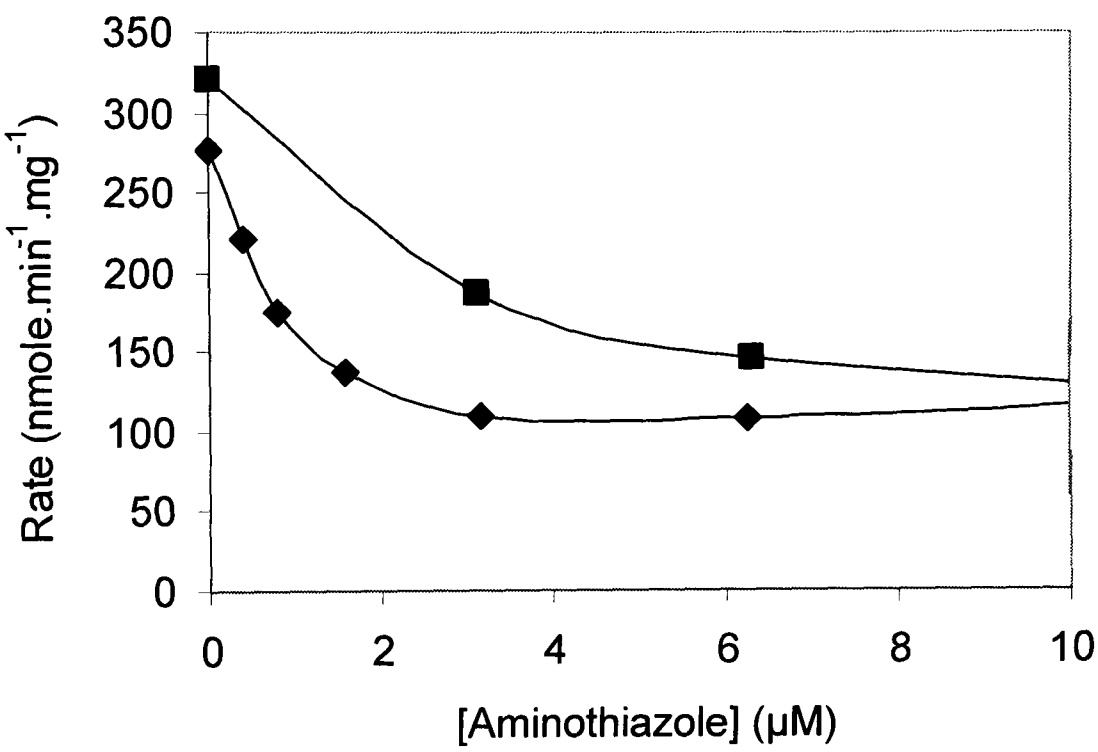


**Figure 4.11 – Inhibition of MSNAT by aminothiazoles ATZ-A1 and ATZ-A12**
The effect of aminothiazoles **ATZ-A1** (squares) and **ATZ-A12** (diamonds) on the initial rate of hydrolysis of AcCoA (100μM) in the presence of MSNAT and isoniazid (500μM) was determined using DTNB (Section 2.2.10).

Kinetic analysis of **ATZ-A1** was performed by varying the concentration of isoniazid and aminothiazole (Figure 4.12). As the concentration of inhibitor increases, the apparent values of $V_{max}$ and $K_m$ decrease leaving the ratio $K_m/V_{max}$ constant. This shows that the inhibition of MSNAT by **ATZ-A1** is uncompetitive with respect to isoniazid. **ATZ-A12** also showed uncompetitive inhibition.

Uncompetitive inhibitors are classically thought of as binding to the enzyme-substrate complex and not to the free enzyme and this could be the case here. However, the same type of inhibition can be seen in a two-substrate reaction

where the inhibitor inhibits the binding of both substrates, creating the reduction of both $K_{m,app}$ and $V_{max,app}$. Thus, as we have increased the potency inhibitors to micromolar levels, we have inhibited the binding of AcCoA to the protein as well as the binding of isoniazid. In terms of drug action, uncompetitive inhibition is favourable over competition as it cannot be completely overcome by increased substrate competition.

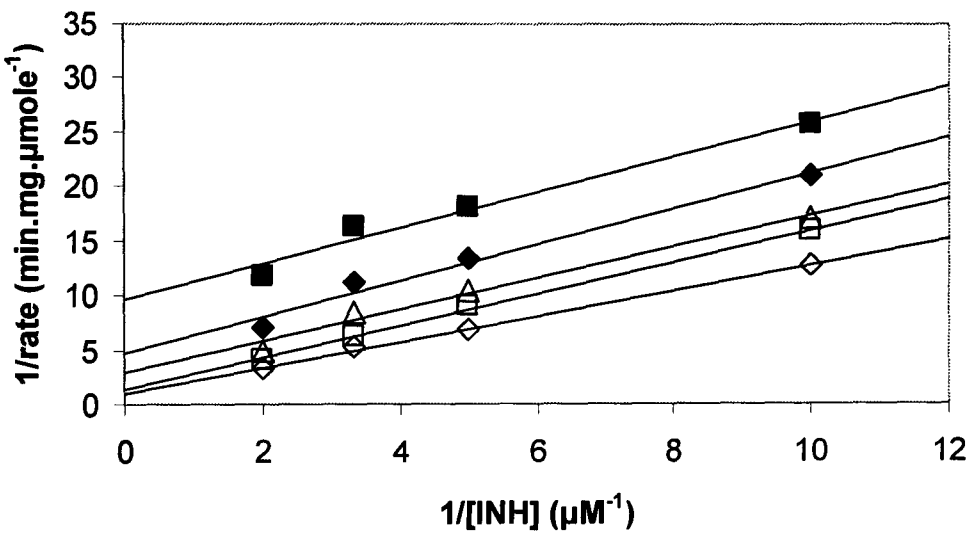


**Figure 4.12 – Inhibition of MSNAT by aminothiazole ATZ-A1**
The effect of aminothiazole **ATZ-A1** at 10 µM (solid squares), 5µM (solid diamonds), 2.5µM (open triangles), 1.3µM (open squares) and 0µM (open diamonds) on the rate of hydrolysis of AcCoA (400µM) by MSNAT was determined in the presence of varying concentrations of isoniazid using DTNB (Section 2.2.10).

### 4.4.3 *In silico* docking of aminothiazoles

The structure of the active aminothiazole **ATZ-A12** was docked into the MSNAT structure. The lowest energy docking solutions for **ATZ-A12** showed that this molecule is a very similar length to the active-site cleft. Docking of **ATZ-A12** showed that it bound in the opposite orientation to **ATZ-A1** (**8A10**, Figure 4.4, Figure 4.13), with the nitro group on $R^2$ binding to $His^{229}$ in the active-site cleft. These compounds have two secondary arylamine moieties at each end of the molecule. **ATZ-A1** has the aminophenol group over $Cys^{70}$ whereas **ATZ-A12** has the imidazopyridine group over $Cys^{70}$. The O-N distance from the nitro group in **ATZ-A12** to $His^{229}$ is 2.8Å, an ideal distance for a hydrogen bond. The minimum

docking energy was -12.2 kcal.mol$^{-1}$ for **ATZ-A1** and -13.3 kcal.mol$^{-1}$ for **ATZ-A12**, reflecting the difference in inhibition observed. His$^{229}$ is conserved in MSNAT and TBNAT so interactions with this residue are very favourable for the design of inhibitors of TBNAT.

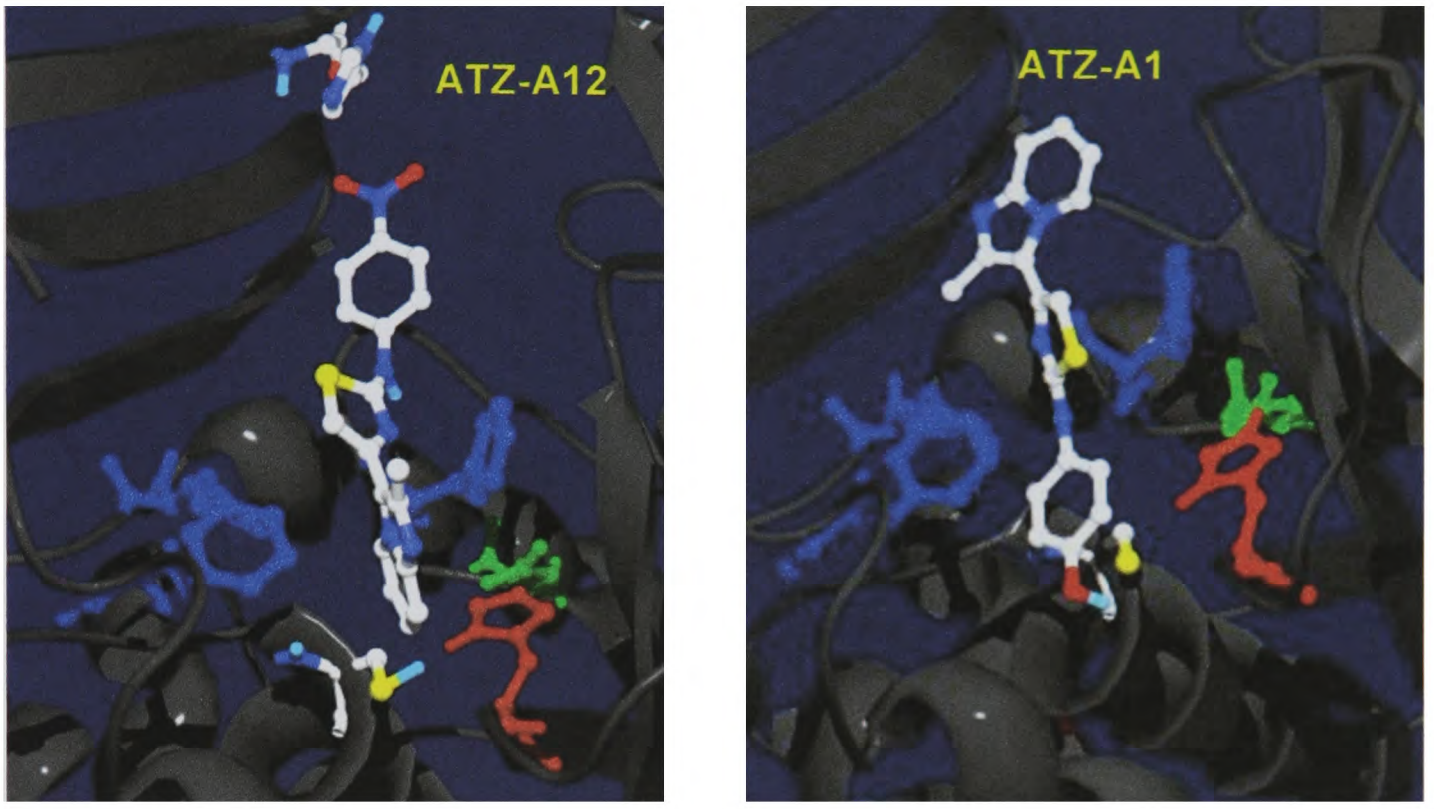


**Figure 4.13 – Docking of aminothiazoles ATZ-A12 and ATZ-A1 to MSNAT**
The structure of compounds **ATZ-A12** and **ATZ-A1** were docked to the MSNAT structure (Section 2.2.13). The diagram shows the lowest energy solution, the active site residue Cys$^{70}$ and His$^{229}$ in CPK colouring with the catalytic triad His$^{110}$ and Asp$^{127}$ in red and green respectively and Phe$^{38}$, Phe$^{130}$ and Phe$^{207}$ in blue.

## 4.5 Conclusions

This chapter has described the chemical synthesis, inhibition analysis and *in silico* docking of three series of compounds in the search for potent inhibitors of MSNAT. High-throughput screening of a large compound library for MSNAT inhibition gave several 'hit' compounds. The TZD-sultams, the maleimides and the aminothiazoles were selected for further development to improve the potency of inhibition. In this manner the best MSNAT inhibition has been improved from **15** ($K_i$=37μM, Figure 4.2) to **ATZ-A12** ($IC_{50}$=1.5μM, Figure 4.11) and **36** ($IC_{50}$=0.8μM, Table 4.5) as shown in Table 4.6. The synthesis of the sultam-TZDs proved to be too time-consuming to make as many members of the series as

| Compound | Structure | Type of Inhibition | Potency |
|---|---|---|---|
| **15 (screened)** | 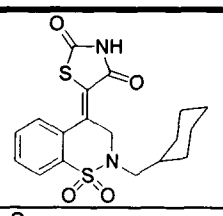 | Competitive | $K_i$=37μM |
| **29 (synthesised)** | 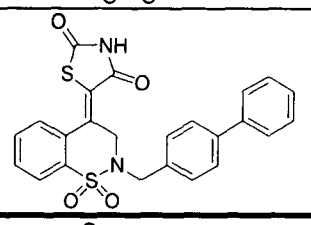 | Competitive | $K_i$=14μM |
| **15E5 (screened)** | 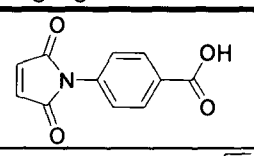 | Irreversible | $IC_{50}$=0.8μM |
| **36 (synthesised)** | 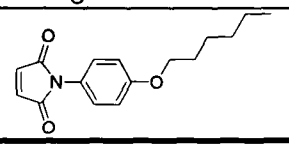 | Irreversible | $IC_{50}$=0.8μM |
| **8A10 (screened)** | 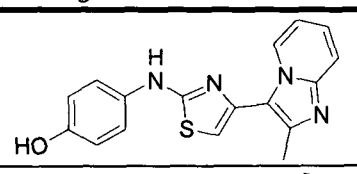 | Uncompetitive | $IC_{50}$=3μM |
| **ATZ-A12 (synthesised)** | 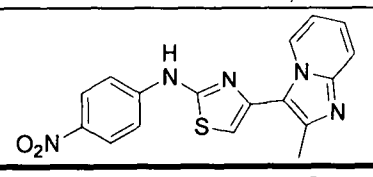 | Uncompetitive | $IC_{50}$=1.5μM |

**Table 4.6 – Screening and synthesis of three classes of MSNAT inhibitor**
The Table shows the most potent inhibitors from three classes of MSNAT inhibitor: the TZD-sultams, the maleimides and the aminothiazoles. Shown is the compound detected through High Throughput Screening and the most potent compound synthesised based upon that compound.

desired. The series reached a maximum potency with compound **29** having a $K_i$ of 14μM. The maleimides are highly potent irreversible inhibitors of MSNAT. They react with the active site cysteine thiolate in a 'Michael'-type reaction, stabilised by a putative oxyanion hole. There is also correlation between the effectiveness of an arylamine as a substrate and the strength of the corresponding maleimide as an inhibitor. However, the high reactivity of the α,β-unsaturated carbonyl group to all thiols in solution means that the series is of limited value *in vivo.*

The aminothiazoles have proved to be the most effective series of compounds. Libraries of aminothiazoles can be synthesised quickly and easily using polymer supported reagents and **ATZ-A1** and **ATZ-A12** (Figure 4.11) display inhibition of MSNAT in the low micromolar range. This is ideal for a hit-to-lead program and the most potent compound **ATZ-A12** will be used in *in vivo* experiments described in Chapter 5.

# Chapter 5

# Effect of MSNAT Inhibitors on Mycobacteria

## 5.1 Introduction

### 5.1.1 The effect of NAT knockouts in mycobacteria

Previous and ongoing studies have created NAT knockouts from the bacteria *Mycobacterium smegmatis* and *M. bovis* BCG (Payton *et al.* 1999; Payton *et al.* 2001); Bhakta S., Upton A. & Sim E. unpublished data). The *M. smegmatis* genetic knockout had two phenotypes:

- an increase in the sensitivity of the bacteria to isoniazid; and
- an increase in the length of the lag-phase of growth.

Closer examination of the *M. bovis* BCG NAT knockout showed a loss of several of the cell-wall lipids compared to the wild-type which made the cells more susceptible to a range of antibiotics (Bhakta S. & Besra G.S., unpublished data).

Other approaches to recreating this phenotype include the use of silencer RNA (siRNA) (Elbashir *et al.* 2001) to inactivate the mRNA for *nat* in the cell or the use of 'chemical genetics' (Schreiber 1998). One aim of this project (Section 1.4, v) is to recreate these phenotypic effects using a chemical genetic approach. As has been

shown in the last chapter, reversible inhibitors of MSNAT have been developed with potency at 1.5μM. Although inhibitors should have nanomolar potency to be included in a chemical genetic study, further rounds of chemical refinement based on these hits are likely to meet this requirement and it was considered prudent to perform the biological *in vivo* assays. The experiments may also provide useful information of how to improve the inhibitors from a medicinal chemistry perspective, including factors such as solubility and cell accessibility.

## 5.2 *In vivo* studies of NAT inhibitors

### 5.2.1 Growth of Mycobacteria

Mycobacteria can be grown in liquid or solid media using the range of 'Middlebrook' media developed for this purpose (Parish *et al.* 1998). *M. smegmatis* and *M. bovis* BCG are grown in liquid Middlebrook 7H9 medium with albumin-dextrose-catalase (ADC) enrichment and on solid 7H10 medium with oleic acid-albumin-dextrose-catalase (OADC) enrichment. A freshly inoculated *M. smegmatis* liquid culture with an absorbance at 600nm of 0.02 (section 2.2.1) will reach the beginning of the logarithmic phase of growth ($A_{600}$=0.2) in approximately 14 hours. The NAT knockout strain of *M. smegmatis* requires an extra 12 hours before logarithmic growth begins (Payton *et al.* 2001). A freshly inoculated *M. bovis* BCG culture ($A_{600}$=0.02) reaches the logarithmic phase in approximately 3 days, with the knockout requiring at least 48 hours more (S. Bhakta, unpublished data).

In determining the effect of the NAT inhibitors on the growth of mycobacteria, solutions of compounds were added to the bacterial medium immediately after the

addition of the bacteria because of the possible role of NAT early in the growth cycle (C. Sholto-Douglas Vernon, unpublished data). Although the compounds had to be dissolved in DMSO, the volume of DMSO was kept to a maximum of 5% to reduce the effect of the cosolvent on the growth. Particularly, DMSO is a commonly known radical scavenger (Kennedy *et al.* 1987) and isoniazid is thought to be activated to, amongst others, a radical form (Johnsson *et al.* 1994). The growth of *M. bovis* BCG was unaffected by 5% v/v DMSO but completely inhibited by 5% v/v ethanol (Section 2.2.1).

The chief compound of interest was the aminothiazole **ATZ-A12** which showed uncompetitive inhibition of MSNAT with an $IC_{50}$ of 1.5μM (Section 4.4.2). This compound is yellow coloured and shows absorbance maxima (20mM Tris.HCl, 5% v/v DMSO) at 307nm and 370nm. The higher absorbance maximum is shifted in 7H9/ADC medium (5% v/v DMSO) to 381nm with an extinction coefficient of 3350 $M^{-1}.cm^{-1}$. The compound was tested at 20μg.$mL^{-1}$ (a) to reduce the risk of non-specific effects of the compounds, and (b) to conserve materials.

### 5.2.2 Growth of *M. smegmatis* with aminothiazole ATZ-A12

*M. smegmatis* was grown with and without the presence of either of the aminothiazoles **ATZ-A1** and **ATZ-A12** and the growth curves compared (Figure 5.1). There was no significant change in the growth patterns in the presence of either aminothiazole. After the bacteria had reached the stationary phase ($A_{600}$=1.0), the cells were harvested by centrifugation as described (section 2.2.4) and the medium

removed. Those bacteria grown in **ATZ-A12** were brightly yellow coloured and the medium had lost the peak of absorbance at 381nm.

*M. smegmatis* was also grown in the presence of varying concentrations of isoniazid with and without **ATZ-A12**. Again, no significant differences were determined between those samples with and without **ATZ-A12** as determined by spectrophotometry (Figure 5.2) and respiration analysis with alamarBlue™ reagent (Section 2.2.3). Similarly, when *M. smegmatis* was grown on solid medium with and without **ATZ-A12** no change in the number of colonies after 24 hours was observed.

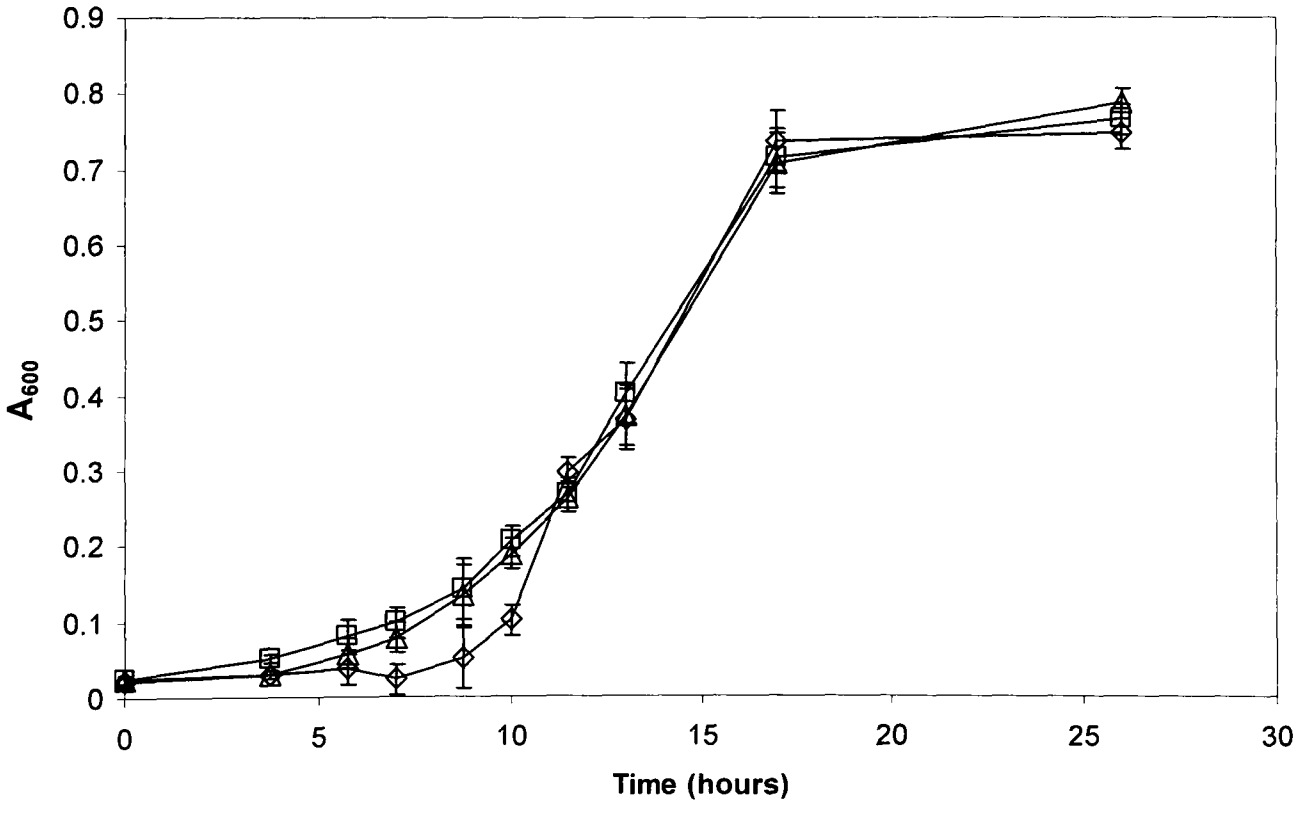


**Figure 5.1 – The growth of *M. smegmatis* with aminothiazoles ATZ-A1 and ATZ-A12**
*M. smegmatis* was grown in the presence of 5% DMSO with compounds **ATZ-A1** (20μg.mL$^{-1}$, open squares), **ATZ-A12** (20μg.mL$^{-1}$, open triangles) or no compound (open diamonds). Bacteria were grown in 20mL culture in 100mL conical flasks and 1mL aliquots were removed periodically (Section 2.2.1). The mean of two independent cultures was taken with the difference as error bars.

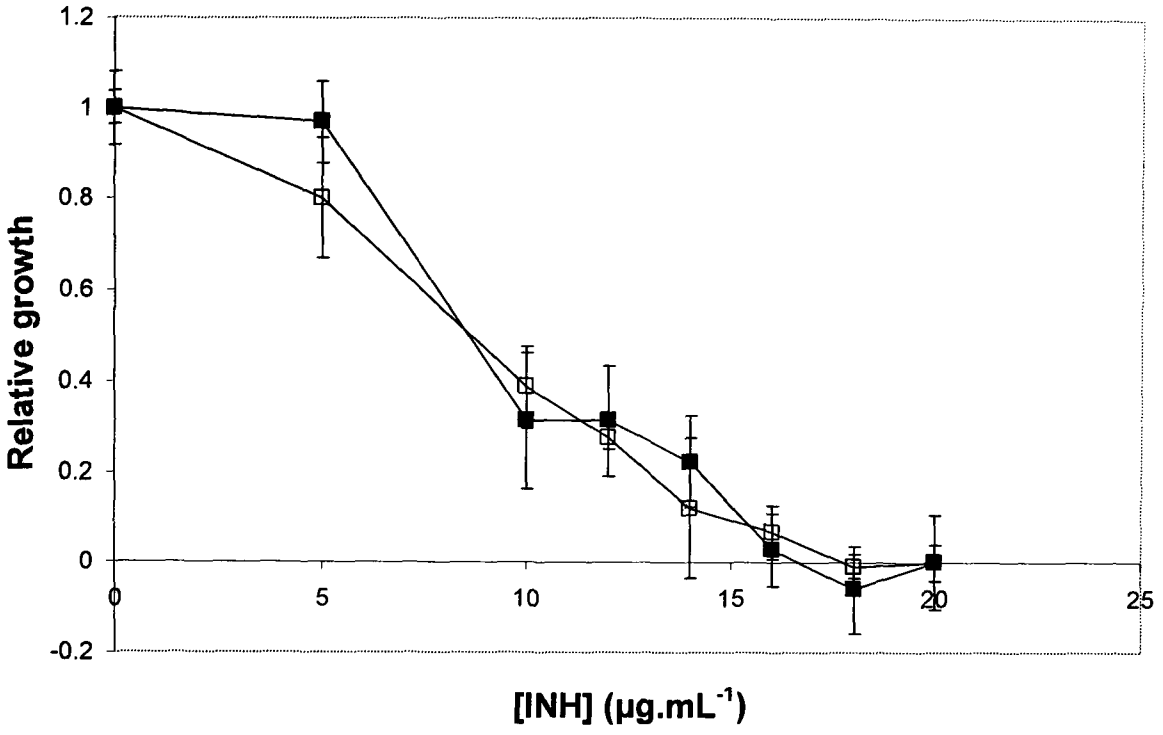


**Figure 5.2 – The effect of aminothiazole ATZ-A12 on *M. smegmatis* growth in isoniazid**
*M. smegmatis* was grown in 96-well plates (Section 2.2.1). Wells contained varying concentrations of isoniazid and were with (filled squares) or without (open squares) **ATZ-A12** at 20μg.mL$^{-1}$. All samples were run in quadruplicate and contained 5% DMSO. After 17 hours the absorbance at 595nm was determined on a plate reader. The relative growth of the samples is shown along with the adjusted standard deviations as error bars.

### 5.2.3 Growth of *M. bovis* BCG with Aminothiazole ATZ-A12

*M. bovis* BCG was also grown in the presence of **ATZ-A12** (Section 2.2.1). Although it is not possible to determine whether **ATZ-A12** is an inhibitor of NAT from *M. bovis* BCG due to the difficulty in expressing and purifying TBNAT (Payton *et al.* 1999), protein structure modelling and conserved residues suggest that the architecture of the active site is similar in the two proteins (Kawamura *et al.* 2003). When grown in the presence of **ATZ-A12** (20μg.mL$^{-1}$, 1% DMSO), no changes were observed in the growth rate of *M. bovis* BCG. Again, the cells were brightly yellow coloured when they had reached the stationary phase. Similarly, growth of the bacteria on solid medium (Section 2.2.1) in the presence of varying concentrations of isoniazid and **ATZ-A12** produced no change in the number of colonies formed.

### 5.2.4 Cell fractionation

To determine the accessibility of **ATZ-A12** to the bacterial cells, cell fractionation was performed on the samples of *M. smegmatis* and *M. bovis* BCG grown in the compound (Section 2.2.4).

When washing the cells with phosphate-buffered saline (PBS) containing 1% Tween 80, the yellow colouration of the cells was extracted into the wash solution (Figure 5.3). By the third wash the colouration was minimal compared to washes of control cells without **ATZ-A12**. The cells were ribolysed and subsequently the cell wall, membrane and cytosol were separated. The cell wall fraction possessed a slight yellow colouration compared to the control but the cell membrane and cytosol contained no detectable **ATZ-A12** by eye or by spectrophotometry (Figure 5.4). The same features were observed with both *M. smegmatis* and *M. bovis* BCG.

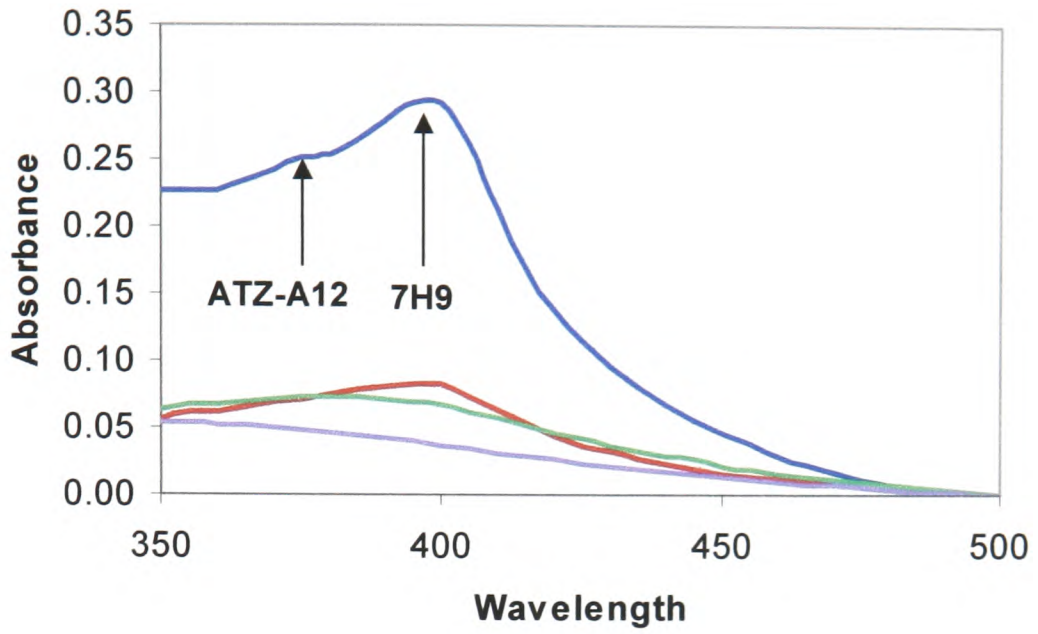


**Figure 5.3 – PBS-Tween washes of *M. smegmatis* grown in aminothiazole ATZ-A12**
*M. smegmatis* was grown in 100mL liquid culture in the presence of **ATZ-A12** at 20μg.mL$^{-1}$ (Section 2.2.1) to an $A_{600}$ of 1.0. The cells were harvested and washed with PBS-Tween (Section 2.2.4). The absorbance spectra of the first (blue), second (red) and third (green) washes were measured and compared to the third wash of cells grown without **ATZ-A12** (purple). Spectra are adjusted to give $A_{500}$=0.

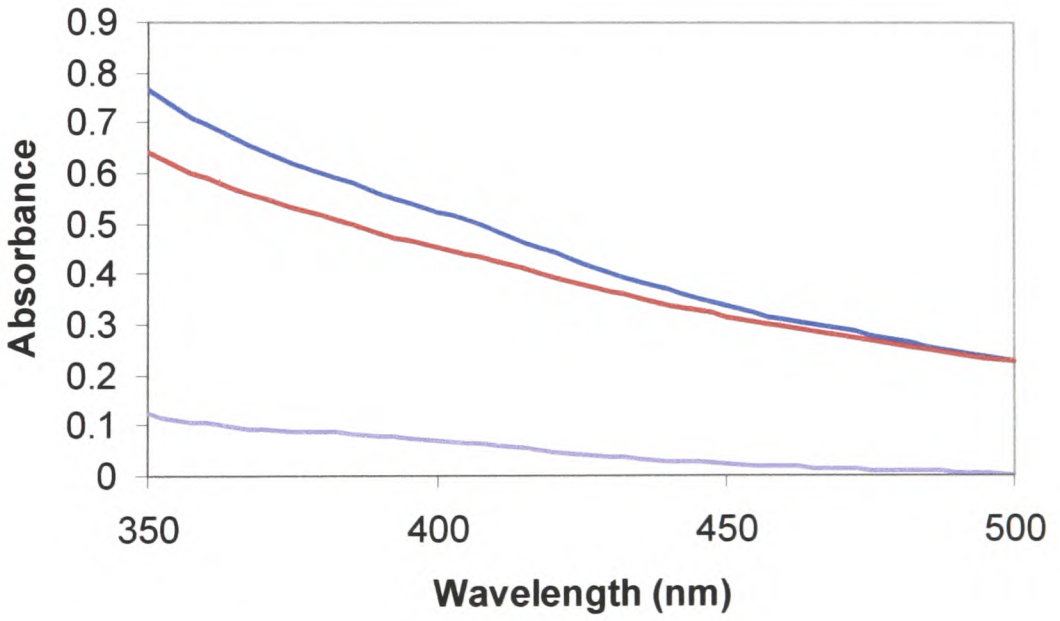


**Figure 5.4 – *M. smegmatis* cytosol after growth in aminothiazole ATZ-A12**
*M. smegmatis* was grown in 100mL liquid culture in the presence of **ATZ-A12** at 20μg.mL$^{-1}$ (Section 2.2.1) to an $A_{600}$ of 1.0. The cells were fractionated (Section 2.2.4) and the absorbance spectra of the cytosolic fraction (blue) was compared to the cytosolic fraction of cells grown without **ATZ-A12** (red). The difference between the two samples is shown in purple.

## 5.3 Conclusions

The mycobacteria, *M. smegmatis* and *M. bovis* BCG, have been grown in the presence of the MSNAT inhibitor **ATZ-A12**. The compound showed no effect on either the growth characteristics of the bacteria, or the sensitivity of the bacteria to isoniazid. Thus it has not been possible to recreate the phenotypic effects of a NAT knockout using the inhibitors that we currently possess. However, it has been shown that **ATZ-A12** is not accessible to the interior of the bacterial cells. The compound binds to the waxy exterior of the cell and can be easily washed off with PBS-Tween solution. This suggests that further efforts to improve the cellular accessibility of these compounds may help in determining the efficacy of this approach and should guide future library synthesis. Similarly, the discovery of more potent NAT inhibitors would decrease the problems associated with cellular accessibility and non-specific binding.

# Chapter 6

# Conclusions

## 6.1 Introduction

The overall aim of this project has been the investigation of protein-ligand interactions in NAT from mycobacteria. NAT in mycobacteria has been shown to acetylate the anti-tubercular drug isoniazid *in vivo* (Upton *et al.* 2001) and inhibition of this acetylation activity may increase the efficacy of isoniazid therapy, for which drug resistance is an all-too-common phenomenon (Slayden *et al.* 2000). The aims stated in Section 1.4 are restated here and how these aims have been met. Possible avenues for future work are discussed in section 6.3. Work from this project has been published in (Brooke *et al.* 2003b) and (Brooke *et al.* 2003a) and the review papers (Brooke *et al.* 2002) and (Brooke *et al.* 2003c).

## 6.2 Review of the Aims of this Project

The aims of this study were:

i. **To develop a rapid and efficient assay for the detection of NAT substrates and inhibitors;**

A novel assay for NAT activity has been developed using the thiol-detecting reagent DTNB (Section 3.1). This assay could be performed on a 96-well plate and is not dependent on the acceptor substrate used. It also works with a range of recombinant NAT proteins.

ii. **To screen a range of possible substrates to gain information about mycobacterial NAT substrate specificity and endogenous roles;**

A range of arylamines were tested as substrates for MSNAT using the new assay methodology. Several novel substrates of MSNAT were discovered, including the alkoxyanilines which have shown anti-tubercular activity (Section 3.2). A relationship was observed between the lipophilicity of a substrate and its acetylation rate by MSNAT. *In silico* docking studies pinpointed several hydrophobic residues which are involved in substrate binding. The substrate specificity of MSNAT gives further evidence as to the role of the enzyme in the detoxification of exogenous arylamines. As yet, no endogenous substrate has been identified.

iii. **To search a large chemical library for novel inhibitors of NAT;**

A library of over 5,000 compounds was tested as inhibitors of MSNAT (Section 4.1). Thirteen compounds had inhibitory activity at concentrations below 10μM, of which three maintained their inhibitory activity in the presence of the thiol-based reducing agent DTT. Both reversible and irreversible inhibitors of MSNAT were discovered and binding modes were investigated by *in silico* docking.

**iv. To perform iterative syntheses and testing to improve inhibitor efficacy;**

Three series of compounds were chosen for subsequent resynthesis and improvement. The TZD-sultams proved difficult to synthesise in large yields or numbers but the competitive inhibition constant was improved from 37μM to 14μM (Section 4.2). The maleimides are irreversible inhibitors of MSNAT with sub-micromolar potency but they are inactivated by DTT and other thiols in solution (Section 4.3). The aminothiazoles are uncompetitive inhibitors of MSNAT that can be synthesised in large numbers and high yields utilising polymer-supported reagents. The most effective compound **ATZ-A12** has an $IC_{50}$ of 1.5μM (Section 4.4).

**v. To determine the effect NAT inhibitors have on the growth of mycobacteria and the sensitivity of mycobacteria to isoniazid.**

The most potent aminothiazole compounds proved to have no detectable effect on the growth of either *M. smegmatis* strain $mc^2155$ or *M. bovis* BCG (Section 5.2). Similarly they did not affect the sensitivity of these two mycobacterial strains to isoniazid. Cell fractionation experiments on the most potent aminothiazole showed that the compounds were not detectable inside the cell.

## 6.3 Future Work

### 6.3.1 The endogenous role of NAT in mycobacteria

Although there is substantial evidence that NAT is playing an important role in mycobacteria, NAT has not been formally identified as a target for drug development. Current work is ongoing on the characterisation of a *M. bovis* BCG NAT knockout which has several very interesting phenotypes (Bhakta S., unpublished data). This data may confirm the position of NAT as a target for drug

discovery. It is also suggested that NAT in *M. bovis* BCG may also be a target for isoniazid in mycobacteria, and other NAT substrates may prove to have anti-mycobacterial action, such as the alkoxyanilines (Section 3.2). It is also important that a NAT knockout is created in active *M. tuberculosis* to provide a more accurate model of the disease state.

### 6.3.2 Future inhibitor development

The inhibitors developed in this project are about one order of magnitude away from being viable inhibitors for chemical genetic and drug discovery projects. Future iterative synthetic programs could improve the potency of the current series of inhibitors, particularly with the aminothiazoles because of the use of combinatorial chemistry and high throughput procedures. Libraries can be based around several of the other hits detected in the high throughput screen and these may furnish more active inhibitors. The use of *in silico* docking will help to guide these iterative synthetic programs. Development of the TBNAT expression and purification system may allow for further work to be performed on the correct enzyme rather than the MSNAT model. We have also shown that it is important to consider the physical properties of future inhibitors in terms of their solubility and cellular accessibility.

Through a range of techniques, skills and collaborations between several departments, we have developed potent inhibitors of a protein involved in isoniazid resistance in *M. tuberculosis*. The continuation of this work has the potential to furnish the researchers with a novel drug or co-drug for the treatment of tuberculosis that may help to solve this global emergency.

# References

Agundez, J. A., J. M. Ladero, M. Olivera, R. Abildua, J. M. Roman and J. Benitez (1995). "Genetic analysis of the arylamine N-acetyltransferase polymorphism in breast cancer patients." Oncology **52**(1): 7-11.

Alanine, A., M. Nettekoven, E. Roberts and A. W. Thomas (2003). "Lead generation--enhancing the success of drug discovery by investing in the hit to lead process." Comb Chem High Throughput Screen **6**(1): 51-66.

Ames, B. N., F. D. Lee and W. E. Durston (1973). "An improved bacterial test system for the detection and classification of mutagens and carcinogens." Proc Natl Acad Sci U S A **70**(3): 782-6.

Andres, H. H., A. J. Klem, L. M. Schopfer, J. K. Harrison and W. W. Weber (1988). "On the active site of liver acetyl-CoA. Arylamine N-acetyltransferase from rapid acetylator rabbits (III/J)." J Biol Chem **263**(16): 7521-7.

Andres, H. H., A. J. Klem, S. M. Szabo and W. W. Weber (1985). "New spectrophotometric and radiochemical assays for acetyl-CoA: arylamine N-acetyltransferase applicable to a variety of arylamines." Anal Biochem **145**(2): 367-75.

Arakawa, T. and S. N. Timasheff (1984). "Protein stabilization and destabilization by guanidinium salts." Biochemistry **23**(25): 5924-9.

Atmane, N., J. Dairou, A. Paul, J. M. Dupret and F. Rodrigues-Lima (2003). "Redox regulation of the human xenobiotic-metabolizing enzyme arylamine N-

acetyltransferase 1 (NAT1) Reversible inactivation by hydrogen peroxide." J Biol Chem **278**: 35086-35092

Bailey, N., A. W. Dean, D. B. Judd, D. Middlemiss, R. Storer and S. P. Watson (1996). "A convenient procedure for the solution phase preparation of 2-aminothiazole combinatorial libraries." Bioorg Med Chem Lett **6**(12): 1409-1414.

Banerjee, A., E. Dubnau, A. Quemard, V. Balasubramanian, K. S. Um, T. Wilson, D. Collins, G. de Lisle and W. R. Jacobs, Jr. (1994). "*inhA*, a gene encoding a target for isoniazid and ethionamide in *Mycobacterium tuberculosis*." Science **263**(5144): 227-30.

Bardou, F., C. Raynaud, C. Ramos, M. A. Laneelle and G. Laneelle (1998). "Mechanism of isoniazid uptake in *Mycobacterium tuberculosis*." Microbiology **144**(9): 2539-44.

Barry, C. E., 3rd, R. E. Lee, K. Mdluli, A. E. Sampson, B. G. Schroeder, R. A. Slayden and Y. Yuan (1998). "Mycolic acids: structure, biosynthesis and physiological functions." Prog Lipid Res **37**(2-3): 143-79.

Basso, L. A., R. Zheng, J. M. Musser, W. R. Jacobs, Jr. and J. S. Blanchard (1998). "Mechanisms of isoniazid resistance in *Mycobacterium tuberculosis*: enzymatic characterization of enoyl reductase mutants identified in isoniazid-resistant clinical isolates." J Infect Dis **178**(3): 769-75.

Baxendale, I. R. and S. V. Ley (2000). "Polymer-supported reagents for multi-step organic synthesis: application to the synthesis of sildenafil." Bioorg Med Chem Lett **10**(17): 1983-6.

## *References*


Berg, M., K. Undisz, R. Thiericke, T. Moore and C. Posten (2000). "Miniaturization of a functional transcription assay in yeast (human progesterone receptor) in the 384- and 1536-well plate format." J Biomol Screen **5**(2): 71-6.

Bernstein, J., W. Lott, B. Steinberg and H. Yale (1952). "Chemotherapy of experimental tuberculosis. V. Isonicotinic acid hydrazide (nydrazid) and related compounds." Am. Rev. Tuberc. **65**: 357-364.

Besra, G. S. and D. Chatterjee (1994). Lipids and carbohydrates of Mycobacterium tuberculosis. Tuberculosis: Pathogenesis, protection and control. B. Bloom. Washington, DC, ASM Press: 285-306.

Bishai, W. (2000). "Lipid lunch for persistent pathogen." Nature **406**(6797): 683-5.

Blum, M., D. M. Grant, W. McBride, M. Heim and U. A. Meyer (1990). "Human arylamine N-acetyltransferase genes: isolation, chromosomal localization, and functional expression." DNA Cell Biol **9**(3): 193-203.

Bradford, M. (1976). "A rapid and sensitive method for the quantition of microgram quantities of protein utilizing the principle of dye-binding." Anal Biochem **72**: 248-254.

Brennan, P. J. and H. Nikaido (1995). "The envelope of mycobacteria." Annu Rev Biochem **64**: 29-63.

Brockmoller, J., I. Cascorbi, R. Kerb and I. Roots (1996). "Combined analysis of inherited polymorphisms in arylamine N-acetyltransferase 2, glutathione S-transferases M1 and T1, microsomal epoxide hydrolase, and cytochrome P450 enzymes as modulators of bladder cancer risk." Cancer Res **56**(17): 3915-25.

***References***

Brooke, E. and E. Sim (2002). "Current developments in drug discovery for tuberculosis - International Symposium." IDrugs **5**(2): 151-153.

Brooke, E. W., S. G. Davies, A. W. Mulvaney, M. Okada, F. Pompeo, E. Sim, R. J. Vickers and I. M. Westwood (2003a). "Synthesis and *in vitro* evaluation of novel small molecule inhibitors of bacterial arylamine N-acetyltransferases (NATs)." Bioorg Med Chem Lett **13**(15): 2527-30.

Brooke, E. W., S. G. Davies, A. W. Mulvaney, F. Pompeo, E. Sim and R. J. Vickers (2003b). "An approach to identifying novel substrates of bacterial arylamine N-acetyltransferases." Bioorg Med Chem **11**(7): 1227-34.

Brooke, E. W., C. Sholto-Douglas-Vernon and E. Sim (2003c). The role of arylamine N-acetyltransferase in bacteria. Recent Research Developments in Bacteriology. S. G. Pandalai. Trivandrum, Research Signpost. 1.

Brosch, R., A. S. Pym, S. V. Gordon and S. T. Cole (2001). "The evolution of mycobacterial pathogenicity: clues from comparative genomics." Trends Microbiol **9**(9): 452-8.

Cederblad, G., P. Harper and K. Lindgren (1986). "Spectrophotometry of carnitine in biological fluids and tissue with a Cobas Bio centrifugal analyzer." Clin Chem **32**(2): 342-6.

Cheon, H. G. and P. E. Hanna (1992). "Effect of group-selective modification reagents on arylamine N-acetyltransferase activities." Biochem Pharmacol **43**(10): 2255-68.

Cohn, D. L. (1997). "Prevention strategies for *Mycobacterium avium-intracellulare* complex (MAC) infection. A review of recent studies in patients with AIDS." Drugs **54** Suppl 2: 8-15; discussion 28-9.

Cole, S. T., R. Brosch, J. Parkhill, T. Garnier, C. Churcher, D. Harris and B. Barrel (1998). "Deciphering the biology of *Mycobacterium tuberculosis* from the complete genome sequence." Nature **393**(6685): 537-544.

Cole, S. T., K. Eiglmeier, J. Parkhill, K. D. James, N. R. Thomson, P. R. Wheeler, N. Honore, T. Garnier, C. Churcher, D. Harris, K. Mungall, D. Basham, D. Brown, T. Chillingworth, R. Connor, R. M. Davies, K. Devlin, S. Duthoy, T. Feltwell, A. Fraser, N. Hamlin, S. Holroyd, T. Hornsby, K. Jagels, C. Lacroix, J. Maclean, S. Moule, L. Murphy, K. Oliver, M. A. Quail, M. A. Rajandream, K. M. Rutherford, S. Rutter, K. Seeger, S. Simon, M. Simmonds, J. Skelton, R. Squares, S. Squares, K. Stevens, K. Taylor, S. Whitehead, J. R. Woodward and B. G. Barrell (2001). "Massive gene decay in the leprosy bacillus." Nature **409**(6823): 1007-11.

Corbett, E. L., R. N. Davidson, S. B. Lucas, N. Shetty and R. F. Miller (1996). "Occult miliary tuberculosis in advanced HIV disease." Genitourin Med **72**(3): 187-92.

Cornish, V. A., K. Pinter, S. Boukouvala, N. Johnson, C. Labrousse, M. Payton, H. Priddle, A. J. Smith and E. Sim (2003). "Generation and analysis of mice with a targeted disruption of the arylamine N-acetyltransferase type 2 gene." Pharmacogenomics J **3**(3): 169-77.

Coroneos, E., J. W. Gordon, S. L. Kelly, P. D. Wang and E. Sim (1991). "Drug metabolising N-acetyltransferase activity in human cell lines." Biochim Biophys Acta **1073**(3): 593-9.

Council, M. R. (1948). "Streptomycin treatment of pulmonary tuberculosis." Brit Med J **2**(769-782).

Deguchi, T. (1992). "Physiology and molecular biology of arylamine N-acetyltransferases." Biomed. Res. **13**: 231-242.

Delomenie, C., S. Fouix, S. Longuemaux, N. Brahimi, C. Bizet, B. Picard, E. Denamur and J. M. Dupret (2001). "Identification and functional characterization of arylamine N-acetyltransferases in eubacteria: evidence for highly selective acetylation of 5-aminosalicylic acid." J Bacteriol **183**(11): 3417-27.

Deretic, V., J. Song and E. Pagan-Ramos (1997). "Loss of *oxyR* in Mycobacterium tuberculosis." Trends Microbiol **5**(9): 367-72.

Dessen, A., A. Quemard, J. S. Blanchard, W. R. Jacobs, Jr. and J. C. Sacchettini (1995). "Crystal structure and function of the isoniazid target of *Mycobacterium tuberculosis*." Science **267**(5204): 1638-41.

Di Gleria, K., D. P. Nickerson, H. A. O. Hill, L. L. Wong and V. Filop (1998). "Covalent attachment of an electroactive sulphydryl reagent in the active site of CP450cam." J Amer Chem Soc **120**: 46.

Drews, J. (2000). "Drug discovery: a historical perspective." Science **287**(5460): 1960-4.

Duncan, K. (2003). "Progress in TB drug development and what is still needed." Tuberculosis (Edinb) **83**(1-3): 201-7.

Dye, C., S. Scheele, P. Dolin, V. Pathania and M. C. Raviglione (1999). "Consensus statement. Global burden of tuberculosis: estimated incidence, prevalence, and mortality by country. WHO Global Surveillance and Monitoring Project." J Amer Med Assoc **282**(7): 677-86.

Elbashir, S. M., J. Harborth, W. Lendeckel, A. Yalcin, K. Weber and T. Tuschl (2001). "Duplexes of 21-nucleotide RNAs mediate RNA interference in cultured mammalian cells." Nature **411**(6836): 494-8.

Evans, D. A. P., K. A. Manley and V. A. McKuisick (1960). "Genetic control of isoniazid acetylation in man." Brit. Med. J. **2**: 485-491.

Fahey, R. C., W. C. Brown, W. B. Adams and M. B. Worsham (1978). "Occurrence of glutathione in bacteria." J Bacteriol **133**(3): 1126-9.

Fitzgerald, J. R. and J. M. Musser (2001). "Evolutionary genomics of pathogenic bacteria." Trends Microbiol **9**(11): 547-53.

Floyd, C. D., C. Leblanc and M. Whittaker (1999). "Combinatorial chemistry as a tool for drug discovery." Prog Med Chem **36**: 91-168.

Fretland, A. J., M. A. Doll, Y. Zhu, L. Smith, M. A. Leff and D. W. Hein (2002). "Effect of nucleotide substitutions in N-acetyltransferase-1 on N-acetylation (deactivation) and O-acetylation (activation) of arylamine carcinogens: implications for cancer predisposition." Cancer Detect Prev **26**(1): 10-4.

Gabriel, S. and J. Colman (1900). Berichte. **33**: 980.

Garnier, T., K. Eiglmeier, J. C. Camus, N. Medina, H. Mansoor, M. Pryor, S. Duthoy, S. Grondin, C. Lacroix, C. Monsempe, S. Simon, B. Harris, R. Atkin, J. Doggett, R. Mayes, L. Keating, P. R. Wheeler, J. Parkhill, B. G. Barrell, S. T. Cole, S. V. Gordon and R. G. Hewinson (2003). "The complete genome sequence of *Mycobacterium bovis*." Proc Natl Acad Sci U S A. **100**(13): 7877-7882

Goodfellow, G. H., J. M. Dupret and D. M. Grant (2000). "Identification of amino acids imparting acceptor substrate selectivity to human arylamine acetyltransferases NAT1 and NAT2." Biochemical Journal **348**(1): 159-66.

Goodsell, D. S., G. M. Morris and A. J. Olson (1996). "Automated docking of flexible ligands: applications of AutoDock." J Mol Recognit **9**(1): 1-5.

Grant, D. M., F. Lottspeich and U. A. Meyer (1989). "Evidence for two closely related isozymes of arylamine N-acetyltransferase in human liver." FEBS Lett **244**(1): 203-7.

Haas, W. H., K. Schilke, J. Brand, B. Amthor, K. Weyer, P. B. Fourie, G. Bretzel, V. Sticht-Groh and H. J. Bremer (1997). "Molecular analysis of *katG* gene mutations in strains of *Mycobacterium tuberculosis* complex from Africa." Antimicrob Agents Chemother **41**(7): 1601-3.

Haemers, A., D. C. Leysen, W. Bollaert, M. Q. Zhang and S. R. Pattyn (1990). "Influence of N substitution on antimycobacterial activity of ciprofloxacin." Antimicrob Agents Chemother **34**(3): 496-7.

Hantzsch, A. R. and J. H. Weber (1887). Berichte. **20**: 3118.

Heifets, L. B. and R. C. Good (1994). Current laboratory methods for the diagnosis of tuberculosis. Tuberculosis: Pathogenesis, protection and control. B. Bloom. Washington, DC, ASM Press: 85-112.

Hein, D. W., M. A. Doll, T. D. Rustan, K. Gray, Y. Feng, R. J. Ferguson and D. M. Grant (1993). "Metabolic activation and deactivation of arylamine carcinogens by recombinant human NAT1 and polymorphic NAT2 acetyltransferases." Carcinogenesis **14**(8): 1633-8.

Herrington, M. B. (1994). "Measurement of the uptake of radioactive *para*-aminobenzoic acid monitors folate biosynthesis in *Escherichia coli* K-12." Anal Biochem **216**(2): 427-30.

Hickman, D., J. Pope, S. D. Patil, G. Fakis, V. Smelt, L. A. Stanley, M. Payton, J. D. Unadkat and E. Sim (1998). "Expression of arylamine N-acetyltransferase in human intestine." Gut **42**(3): 402-9.

Hinshaw, H. C. and W. H. Feldman (1945). "Streptomycin in trreatment of clinical tuberculosis: preliminary report." Proc Staphy Med Mayo Clinic **20**: 313-318.

Hook, V. Y., T. Toneff, W. Aaron, S. Yasothornsrikul, R. Bundey and T. Reisine (2002). "Beta-amyloid peptide in regulated secretory vesicles of chromaffin cells: evidence for multiple cysteine proteolytic activities in distinct pathways for beta-secretase activity in chromaffin vesicles." J Neurochem **81**(2): 237-56.

Hopewell, P. C. (1994). Overview of clinical tuberculosis. Tuberculosis: Pathogenesis, protection and control. B. Bloom. Washington, DC, ASM Press: 25-47.

Hopkins, A. L. and C. R. Groom (2002). "The druggable genome." Nat Rev Drug Discov **1**(9): 727-30.

Hu, Y., A. R. Coates and D. A. Mitchison (2003). "Sterilizing Activities of Fluoroquinolones against Rifampin-Tolerant Populations of *Mycobacterium tuberculosis*." Antimicrob Agents Chemother **47**(2): 653-7.

Jenne, J. W. (1965). "Partial purification and properties of the isoniazid transacetylase in human liver: its relationship to the acetylation of *p*-aminosalicylic acid." J. Clin. Invest. **44**: 1992-2002.

Johnsson, K. and P. G. Schultz (1994). "Mechanistic studies of the oxidation of isoniazid by the catalase-peroxidase from *Mycobacterium tuberculosis*." J. Am. Chem. Soc. **116**: 7425-7426.

Kawamura, A., J. Sandy, A. Upton, M. Noble and E. Sim (2003). "Structural investigation of mutant *Mycobacterium smegmatis* arylamine N-acetyltransferase: a model for a naturally occurring functional polymorphism in *Mycobacterium tuberculosis* arylamine N-acetyltransferase." Protein Expr Purif **27**(1): 75-84.

Kearney, P. C., M. Fernandez and J. A. Flygare (1998). "Solid-phase synthesis of 2-aminothiazoles." J Org Chem **63**: 196-200.

Kelley, C. L., D. A. Rouse and S. L. Morris (1997). "Analysis of *ahpC* gene mutations in isoniazid-resistant clinical isolates of *Mycobacterium tuberculosis*." Antimicrob Agents Chemother **41**(9): 2057-8.

Kennedy, A. R. and M. C. Symons (1987). "'Water structure' versus 'radical scavenger' theories as explanations for the suppressive effects of DMSO and related compounds on radiation-induced transformation in vitro." Carcinogenesis **8**(5): 683-8.

Koch, R. (1932). "Die Aetiologie der Tuberculose (English translation)." American Review of Tuberculosis **25**: 285-323.

Kremer, L., J. D. Douglas, A. R. Baulard, C. Morehouse, M. R. Guy, D. Alland, L. G. Dover, J. H. Lakey, W. R. Jacobs, Jr., P. J. Brennan, D. E. Minnikin and G. S. Besra (2000). "Thiolactomycin and related analogues as novel anti-mycobacterial agents targeting KasA and KasB condensing enzymes in *Mycobacterium tuberculosis*." J Biol Chem **275**(22): 16857-64.

Kremer, L., L. G. Dover, H. R. Morbidoni, C. Vilcheze, W. N. Maughan, A. Baulard, S. C. Tu, N. Honore, V. Deretic, J. C. Sacchettini, C. Locht, W. R. Jacobs, Jr. and G. S. Besra (2003). "Inhibition of InhA activity, but not KasA activity, induces formation of a KasA-containing complex in mycobacteria." J Biol Chem **278**(23): 20547-20554.

Landro, J. A., I. C. Taylor, W. G. Stirtan, D. G. Osterman, J. Kristie, E. J. Hunnicutt, P. M. Rae and P. M. Sweetnam (2000). "HTS in the new millennium: the role of pharmacology and flexibility." J Pharmacol Toxicol Methods **44**(1): 273-89.

Larsen, M. H., C. Vilcheze, L. Kremer, G. S. Besra, L. Parsons, M. Salfinger, L. Heifets, M. H. Hazbon, D. Alland, J. C. Sacchettini and W. R. Jacobs, Jr. (2002). "Overexpression of *inhA*, but not *kasA*, confers resistance to isoniazid and ethionamide in *Mycobacterium smegmatis*, *M. bovis* BCG and *M. tuberculosis*." Mol Microbiol **46**(2): 453-66.

Lee, R. E., M. Protopopova, E. Crooks, R. A. Slayden, M. Terrot and C. E. Barry, 3rd (2003). "Combinatorial lead optimization of [1,2]-diamines based on

ethambutol as potential antituberculosis preclinical candidates." J Comb Chem **5**(2): 172-87.

Lipinski, C. A., F. Lombardo, B. W. Dominy and P. J. Feeney (2001). "Experimental and computational approaches to estimate solubility and permeability in drug discovery and development settings." Adv Drug Deliv Rev **46**(1-3): 3-26.

Loftus, E. V., Jr., P. Schoenfeld and W. J. Sandborn (2002). "The epidemiology and natural history of Crohn's disease in population-based patient cohorts from North America: a systematic review." Aliment Pharmacol Ther **16**(1): 51-60.

Maeda, N., J. Nigou, J. L. Herrmann, M. Jackson, A. Amara, P. H. Lagrange, G. Puzo, B. Gicquel and O. Neyrolles (2003). "The cell surface receptor DC-SIGN discriminates between Mycobacterium species through selective recognition of the mannose caps on lipoarabinomannan." J Biol Chem **278**(8): 5513-6.

Manabe, Y. C. and W. R. Bishai (2000). "Latent *Mycobacterium tuberculosis*-persistence, patience, and winning by waiting." Nature Medicine **6**(12): 1327-9.

McKinney, J. D., K. Honer zu Bentrup, E. J. Munoz-Elias, A. Miczak, B. Chen, W. T. Chan, D. Swenson, J. C. Sacchettini, W. R. Jacobs, Jr. and D. G. Russell (2000). "Persistence of *Mycobacterium tuberculosis* in macrophages and mice requires the glyoxylate shunt enzyme isocitrate lyase." Nature **406**(6797): 735-8.

Mdluli, K., D. R. Sherman, M. J. Hickey, B. N. Kreiswirth, S. Morris, C. K. Stover and C. E. Barry, 3rd (1996). "Biochemical and genetic data suggest that InhA

is not the primary target for activated isoniazid in *Mycobacterium tuberculosis*." J Infect Dis **174**(5): 1085-90.

Mdluli, K., R. A. Slayden, Y. Zhu, S. Ramaswamy, X. Pan, D. Mead, D. D. Crane, J. M. Musser and C. E. Barry, 3rd (1998). "Inhibition of a *Mycobacterium tuberculosis* beta-ketoacyl ACP synthase by isoniazid." Science **280**(5369): 1607-10.

Middlebrook, G. (1954). "Isoniazid-resistance and catalase activity of tubercle bacilli." Am. Rev. Tuberc. **69**: 471-472.

Mikol, V., J. L. Rodeau and R. Giege (1990). "Experimental determination of water equilibration rates in the hanging drop method of protein crystallization." Anal Biochem **186**(2): 332-9.

Mills, J. L. and M. R. Conley (1996). "Folic acid to prevent neural tube defects: scientific advances and public health issues." Curr Opin Obstet Gynecol **8**(6): 394-7.

Minchin, R. F. (1995). "Acetylation of *p*-aminobenzoylglutamate, a folic acid catabolite, by recombinant human arylamine N-acetyltransferase and U937 cells." Biochem J **307**(1): 1-3.

Minchin, R. F., P. T. Reeves, C. H. Teitel, M. E. McManus, B. Mojarrabi, K. F. Ilett and F. F. Kadlubar (1992). "N-and O-acetylation of aromatic and heterocyclic amine carcinogens by human monomorphic and polymorphic acetyltransferases expressed in COS-1 cells." Biochem Biophys Res Commun **185**(3): 839-44.

Mortelmans, K. and E. Zeiger (2000). "The Ames *Salmonella*/microsome mutagenicity assay." Mutat Res **455**(1-2): 29-60.

Mullner, S., T. Neumann and F. Lottspeich (1998). "Proteomics--a new way for drug target discovery." Arzneimittelforschung **48**(1): 93-5.

Mushtaq, A. (2002). "Arylamine N-acetyltransferase from *Salmonella typhimurium*." DPhil Thesis, University of Oxford.

Mushtaq, A., M. Payton and E. Sim (2002). "The COOH terminus of arylamine N-acetyltransferase from *Salmonella typhimurium* controls enzymic activity." J Biol Chem **277**(14): 12175-81.

Musser, J. M., V. Kapur, D. L. Williams, B. N. Kreiswirth, D. van Soolingen and J. D. van Embden (1996). "Characterization of the catalase-peroxidase gene (*katG*) and *inhA* locus in isoniazid-resistant and -susceptible strains of *Mycobacterium tuberculosis* by automated DNA sequencing: restricted array of mutations associated with drug resistance." J Infect Dis **173**(1): 196-202.

Niu, P. and K. Yang (2002). "The 11 beta-hydroxysteroid dehydrogenase type 2 activity in human placental microsomes is inactivated by zinc and the sulfhydryl modifying reagent N-ethylmaleimide." Biochim Biophys Acta **1594**(2): 364-71.

Nodzu, R., H. Watanabe, S. Kuwata, C. Nagaishi and T. Teramatsu (1954). "Studies on Chemotherapy of Tuberculosis. IV. Synthesis of *m*- and *p*-aminophenol alkyl ethers and their bacteriostatic actions on *Mycobacterium tuberculosis*." Journal of the Pharmaceutical Society of Japan **74**: 872-5.

Ozawa, S., M. Abu-Zeid, Y. Kawakubo, S. Toyama, Y. Yamazoe and R. Kato (1990). "Monomorphic and polymorphic isozymes of arylamine N-acetyltransferases in hamster liver: purification of the isozymes and genetic basis of N-acetylation polymorphism." Carcinogenesis **11**(12): 2137-44.

Palomino, J. C., A. Martin, M. Camacho, H. Guerra, J. Swings and F. Portaels (2002). "Resazurin microtiter assay plate: simple and inexpensive method for detection of drug resistance in *Mycobacterium tuberculosis*." Antimicrob Agents Chemother **46**(8): 2720-2.

Parish, T. and N. Stoker (1998a). Mycobacterial Protocols. New Jersey, Human Press.

Parish, T. and P. R. Wheeler (1998b). Preparation of Cell-Free Extracts from Mycobacteria. Mycobacteria Protocols. T. Parish and N. Stoker. New Jersey, Human Press. 101.

Payton, M., R. Auty, R. Delgoda, M. Everett and E. Sim (1999). "Cloning and characterization of arylamine N-acetyltransferase genes from *Mycobacterium smegmatis* and *Mycobacterium tuberculosis*: increased expression results in isoniazid resistance." J Bacteriol **181**(4): 1343-7.

Payton, M., C. Gifford, P. Schartau, C. Hagemeier, A. Mushtaq, S. Lucas, K. Pinter and E. Sim (2001a). "Evidence towards the role of arylamine N-acetyltransferase in *Mycobacterium smegmatis* and development of a specific antiserum against the homologous enzyme of *Mycobacterium tuberculosis*." Microbiology **147**(12): 3295-302.

Payton, M., A. Mushtaq, T. W. Yu, L. J. Wu, J. Sinclair and E. Sim (2001b). "Eubacterial arylamine N-acetyltransferases - identification and comparison of

18 members of the protein family with conserved active site cysteine, histidine and aspartate residues." Microbiology **147**(5): 1137-47.

Phetsukiri, B., A. R. Baulard, A. M. Cooper, D. E. Minnikin, J. D. Douglas, G. S. Besra and P. J. Brennan (1999). "Antimycobacterial activities of Isoxyl and new derivatives through the inhibition of mycolic acid synthesis." Antimicrob Agents Chemother **43**: 1042-51.

Pompeo, F., E. Brooke, A. Kawamura, A. Mushtaq and E. Sim (2002a). "The pharmacogenetics of NAT: structural aspects." Pharmacogenomics **3**(1): 19-30.

Pompeo, F., A. Mushtaq and E. Sim (2002b). "Expression and Purification of the Rifamycin Amide Synthase, RifF, an Enzyme Homologous to the Prokaryotic Arylamine N-Acetyltransferases." Protein Expr Purif **24**(1): 138-51.

Prescott, L. M., J. P. Harley and D. A. Klein (1999). Microbiology. New York, McGraw-Hill.

Pretorius, G. S., P. D. van Helden, F. Sirgel, K. D. Eisenach and T. C. Victor (1995). "Mutations in *katG* gene sequences in isoniazid-resistant clinical isolates of *Mycobacterium tuberculosis* are rare." Antimicrob Agents Chemother **39**(10): 2276-81.

Raczniak, G., M. Ibba and D. Soll (2001). "Genomics-based identification of targets in pathogenic bacteria for potential therapeutic and diagnostic use." Toxicology **160**(1): 181-9.

Ramaswamy, S. and J. Musser (1998). "Molecular genetic basis of antimicrobial agent resistance in *Mycobacterium tuberculosis*: 1998 update." Tubercle Lung Dis. **79**: 3-29.

Rascher, A., Z. Hu, N. Viswanathan, A. Schirmer, R. Reid, W. C. Nierman, M. Lewis and C. R. Hutchinson (2003). "Cloning and characterization of a gene cluster for geldanamycin production in *Streptomyces hygroscopicus* NRRL 3602." FEMS Microbiol Lett **218**(2): 223-30.

Reyrat, J. M. and D. Kahn (2001). "*Mycobacterium smegmatis*: an absurd model for tuberculosis?" Trends Microbiol **9**(10): 472-4.

Riddle, B. and W. P. Jencks (1971). "Acetyl-coenzyme A: arylamine N-acetyltransferase. Role of the acetyl-enzyme intermediate and the effects of substituents on the rate." J Biol Chem **246**(10): 3250-8.

Riddles, P. W., R. L. Blakeley and B. Zerner (1983). "Reassessment of Ellman's reagent." Methods Enzymol **91**: 49-60.

Rodrigues-Lima, F., C. Delomenie, G. H. Goodfellow, D. M. Grant and J. M. Dupret (2001). "Homology modelling and structural analysis of human arylamine N-acetyltransferase NAT1: evidence for the conservation of a cysteine protease catalytic domain and an active-site loop." Biochem J **356**(2): 327-34.

Rodrigues-Lima, F. and J. M. Dupret (2002). "*In silico* sequence analysis of arylamine N-acetyltransferases: evidence for an absence of lateral gene transfer from bacteria to vertebrates and first description of paralogs in bacteria." Biochem Biophys Res Commun **293**(2): 783-92.

Rodriguez, J. W., W. G. Kirlin, R. J. Ferguson, M. A. Doll, K. Gray, T. D. Rustan, M. E. Lee, K. Kemp, P. Urso and D. W. Hein (1993). "Human acetylator genotype: relationship to colorectal cancer incidence and arylamine N-acetyltransferase expression in colon cytosol." Arch Toxicol **67**(7): 445-52.

Rojas-Espinosa, O., K. Wek-Rodriguez, P. Arce-Paredes, F. Aguilar-Torrentera, C. Truyens and Y. Carlier (2002). "Contrary to BCG, MLM fails to induce the production of TNF alpha and NO by macrophages." Int J Lepr Other Mycobact Dis **70**(2): 111-8.

Rosenthal, P. J., P. S. Sijwali, A. Singh and B. R. Shenai (2002). "Cysteine proteases of malaria parasites: targets for chemotherapy." Curr Pharm Des **8**(18): 1659-72.

Rozwarski, D. A., G. A. Grant, D. H. Barton, W. R. Jacobs, Jr. and J. C. Sacchettini (1998). "Modification of the NADH of the isoniazid target (InhA) from *Mycobacterium tuberculosis*." Science **279**(5347): 98-102.

Saito, K., Y. Yamazoe, T. Kamataki and R. Kato (1983). "Mechanism of activation of proximate mutagens in Ames' tester strains: the acetyl-CoA dependent enzyme in *Salmonella typhimurium* TA98 deficient in TA98/1,8-DNP6 catalyzes DNA-binding as the cause of mutagenicity." Biochem Biophys Res Commun **116**(1): 141-7.

Salzberg, S. L., O. White, J. Peterson and J. A. Eisen (2001). "Microbial genes in the human genome: lateral transfer or gene loss?" Science **292**(5523): 1903-6.

Sandy, J., A. Mushtaq, A. Kawamura, J. Sinclair, E. Sim and M. Noble (2002). "The structure of arylamine N-acetyltransferase from *Mycobacterium i*--an enzyme

which inactivates the anti-tubercular drug, isoniazid." J Mol Biol **318**(4): 1071-83.

Schaefer, W. H., T. M. Harris and F. P. Guengerich (1987). "Reaction of the model thiol 2-mercaptoethanol and glutathione with methylvinylmaleimide, a Michael acceptor with extended conjugation." Arch Biochem Biophys **257**(1): 186-93.

Schaeffer, M. L., G. Agnihotri, C. Volker, H. Kallender, P. J. Brennan and J. T. Lonsdale (2001). "Purification and biochemical characterization of the *Mycobacterium tuberculosis* beta-ketoacyl-acyl carrier protein synthases KasA and KasB." J Biol Chem **276**(50): 47029-37.

Schoolnik, G. K. (2002). "Functional and comparative genomics of pathogenic bacteria." Curr Opin Microbiol **5**(1): 20-6.

Schreiber, S. L. (1998). "Chemical genetics resulting from a passion for synthetic organic chemistry." Bioorg Med Chem **6**(8): 1127-52.

Sehgal, A. (2002). "Drug Discovery and development using chemical genomics." Curr. Opin. Drug Discov. Devel. **5**: 526-31.

Senaratne, R. H., H. Mobasheri, K. G. Papavinasasundaram, P. Jenner, E. J. Lea and P. Draper (1998). "Expression of a gene for a porin-like protein of the OmpA family from *Mycobacterium tuberculosis* H37Rv." J Bacteriol **180**(14): 3541-7.

Sharma, V., S. Sharma, K. Hoener zu Bentrup, J. D. McKinney, D. G. Russell, W. R. Jacobs, Jr. and J. C. Sacchettini (2000). "Structure of isocitrate lyase, a

persistence factor of *Mycobacterium tuberculosis*." Nature Struct Biol **7**(8): 663-8.

Shenai, B. R., B. J. Lee, A. Alvarez-Hernandez, P. Y. Chong, C. D. Emal, R. J. Neitz, W. R. Roush and P. J. Rosenthal (2003). "Structure-Activity Relationships for Inhibition of Cysteine Protease Activity and Development of *Plasmodium falciparum* by Peptidyl Vinyl Sulfones." Antimicrob Agents Chemother **47**(1): 154-60.

Shi, T., J. K. Fredrickson and D. L. Balkwill (2001). "Biodegradation of polycyclic aromatic hydrocarbons by *Sphingomonas* strains isolated from the terrestrial subsurface." J Ind Microbiol Biotechnol **26**(5): 283-9.

Siedle, B., S. Cisielski, R. Murillo, B. Loser, V. Castro, C. A. Klaas, O. Hucke, A. Labahn, M. F. Melzig and I. Merfort (2002). "Sesquiterpene lactones as inhibitors of human neutrophil elastase." Bioorg Med Chem **10**(9): 2855-61.

Sim, E., M. Payton, M. Noble and R. Minchin (2000). "An update on genetic, structural and functional studies of arylamine N-acetyltransferases in eucaryotes and procaryotes." Hum Mol Genet **9**(16): 2435-41.

Sinclair, J., R. Delgoda, M. Noble, S. Jarmin, N. Goh and E. Sim (1998). "Purification, characterisation and crystallisation of an N-hydroxyarylamine O-acetyltransferase from *Salmonella typhimurium*." Prot. Exp. Purific. **12**: 371-380.

Sinclair, J. and E. Sim (1997). "A fragment consisting of the first 204 amino-terminal amino acids of human arylamine N-acetyltransferase one (NAT1) and the first transacetylation step of catalysis." Biochem Pharmacol **53**(1): 11-6.

Sinclair, J. C., J. Sandy, R. Delgoda, E. Sim and M. E. Noble (2000). "Structure of arylamine N-acetyltransferase reveals a catalytic triad." Nature Struct Biol **7**(7): 560-4.

Slayden, R. A. and C. E. Barry, 3rd (2000). "The genetics and biochemistry of isoniazid resistance in *Mycobacterium tuberculosis*." Microbes Infect **2**(6): 659-69.

Slayden, R. A. and C. E. Barry, 3rd (2002). "The role of KasA and KasB in the biosynthesis of meromycolic acids and isoniazid resistance in *Mycobacterium tuberculosis*." Tuberculosis (Edinb) **82**(4-5): 149-60.

Smelt, V. A., A. Upton, J. Adjaye, M. A. Payton, S. Boukouvala, N. Johnson, H. J. Mardon and E. Sim (2000). "Expression of arylamine N-acetyltransferases in pre-term placentas and in human pre-implantation embryos." Hum Mol Genet **9**(7): 1101-7.

Smith, C. V., C. C. Huang, A. Miczak, D. G. Russell, J. C. Sacchettini and K. Honer zu Bentrup (2003). "Biochemical and structural studies of malate synthase from *Mycobacterium tuberculosis*." J Biol Chem **278**(3): 1735-43.

Smith, P. G. and Moss, A.R. (1994). Epidemiology of tuberculosis. Tuberculosis: Pathogenesis, protection and control. B. Bloom. Washington, DC, ASM Press: 47-60.

Springer, B., L. Stockman, K. Teschner, G. D. Roberts and E. C. Bottger (1996). "Two-laboratory collaborative study on identification of mycobacteria: molecular versus phenotypic methods." J Clin Microbiol **34**(2): 296-303.

Sreevatsan, S., X. Pan, K. E. Stockbauer, N. D. Connell, B. N. Kreiswirth, T. S. Whittam and J. M. Musser (1997a). "Restricted structural gene polymorphism in the *Mycobacterium tuberculosis* complex indicates evolutionarily recent global dissemination." Proc Natl Acad Sci U S A **94**(18): 9869-74.

Sreevatsan, S., X. Pan, Y. Zhang, V. Deretic and J. M. Musser (1997b). "Analysis of the *oxyR-ahpC* region in isoniazid-resistant and -susceptible *Mycobacterium tuberculosis* complex organisms recovered from diseased humans and animals in diverse localities." Antimicrob Agents Chemother **41**(3): 600-6.

Stanhope, M. J., A. Lupas, M. J. Italia, K. K. Koretke, C. Volker and J. R. Brown (2001). "Phylogenetic analyses do not support horizontal gene transfers from bacteria to vertebrates." Nature **411**(6840): 940-4.

Sticha, K. R., C. A. Sieg, C. P. Bergstrom, P. E. Hanna and C. R. Wagner (1997). "Overexpression and large-scale purification of recombinant hamster polymorphic arylamine N-acetyltransferase as a dihydrofolate reductase fusion protein." Protein Expr Purif **10**(1): 141-53.

Storz, G., L. A. Tartaglia and B. N. Ames (1990). "Transcriptional regulator of oxidative stress-inducible genes: direct activation by oxidation." Science **248**(4952): 189-94.

Stover, C. K., P. Warrener, D. R. VanDevanter, D. R. Sherman, T. M. Arain, M. H. Langhorne, S. W. Anderson, J. A. Towell, Y. Yuan, D. N. McMurray, B. N. Kreiswirth, C. E. Barry and W. R. Baker (2000). "A small-molecule nitroimidazopyran drug candidate for the treatment of tuberculosis." Nature **405**(6789): 962-6.

Sugamori, K. S., S. Wong, A. Gaedigk, V. Yu, H. Abramovici, R. Rozmahel and D. M. Grant (2003). "Generation and functional characterization of arylamine N-acetyltransferase *Nat1/Nat2* double-knockout mice." Mol Pharmacol **64**(1): 170-9.

Takayama, K., L. Wang and H. L. David (1972). "Effect of isoniazid on the *in vivo* mycolic acid synthesis, cell growth, and viability of *Mycobacterium tuberculosis*." Antimicrob. Agents Chemother. **2**: 29.

Upton, A., N. Johnson, J. Sandy and E. Sim (2001a). "Arylamine N-acetyltransferases - of mice, men and microorganisms." Trends Pharmacol Sci **22**(3): 140-6.

Upton, A. M., A. Mushtaq, T. C. Victor, S. L. Sampson, J. Sandy, D. M. Smith, P. V. van Helden and E. Sim (2001b). "Arylamine N-acetyltransferase of *Mycobacterium tuberculosis* is a polymorphic enzyme and a site of isoniazid metabolism." Mol Microbiol **42**(2): 309-17.

Varzim, G., E. Monteiro, R. Silva, C. Pinheiro and C. Lopes (2002). "Polymorphisms of arylamine N-acetyltransferase (NAT1 and NAT2) and larynx cancer susceptibility." ORL J Otorhinolaryngol Relat Spec **64**(3): 206-12.

Victor, T. C., R. Warren, J. L. Butt, A. M. Jordaan, J. V. Felix, A. Venter, F. A. Sirgel, H. S. Schaaf, P. R. Donald, M. Richardson, M. H. Cynamon and P. D. Van Helden (1997). "Genome and MIC stability in *Mycobacterium tuberculosis* and indications for continuation of use of isoniazid in multidrug-resistant tuberculosis." J. Med. Microb. **46**(10): 847-857.

Waksman, S. A. (1964). The Conquest of Tuberculosis. London, Robert Hale Ltd.

Wallace, A. C., R. A. Laskowski and J. M. Thornton (1995). "LIGPLOT: a program to generate schematic diagrams of protein-ligand interactions." Prot Eng **8**(2): 127-34.

Watanabe, M., Y. Aoyagi, H. Mitome, T. Fujita, H. Naoki, M. Ridell and D. E. Minnikin (2002). "Location of functional groups in mycobacterial meromycolate chains; the recognition of new structural principles in mycolic acids." Microbiology **148**(6): 1881-902.

Watanabe, M., Y. Aoyagi, A. Ohta and D. E. Minnikin (1997). "Structures of phenolic glycolipids from *Mycobacterium kansasii*." Eur J Biochem **248**(1): 93-8.

Watanabe, M., T. Sofuni and T. Nohmi (1992). "Involvement of Cys69 residue in the catalytic mechanism of N-hydroxyarylamine O-acetyltransferase of *Salmonella typhimurium*. Sequence similarity at the amino acid level suggests a common catalytic mechanism of acetyltransferase for *S. typhimurium* and higher organisms." J Biol Chem **267**(12): 8429-36.

Watanabe, M., T. Sofuni and T. Nohmi (1993). "Comparison of the sensitivity of *Salmonella typhimurium* strains YG1024 and YG1012 for detecting the mutagenicity of aromatic amines and nitroarenes." Mutat Res **301**(1): 7-12.

Wayne, L. G. and K. Y. Lin (1982). "Glyoxylate metabolism and adaptation of *Mycobacterium tuberculosis* to survival under anaerobic conditions." Infect Immun **37**(3): 1042-9.

Weber, W. W. and D. W. Hein (1985). "N-acetylation pharmacogenetics." Pharmacol Rev **37**(1): 25-79.

Wengenack, N. L., J. R. Uhl, A. L. St Amand, A. J. Tomlinson, L. M. Benson, S. Naylor, B. C. Kline, F. R. Cockerill, 3rd and F. Rusnak (1997). "Recombinant *Mycobacterium tuberculosis* KatG(S315T) is a competent catalase-peroxidase with reduced activity toward isoniazid." J Infect Dis **176**(3): 722-7.

Wick, M. J. and P. E. Hanna (1994). "Inactivation of hamster monomorphic N-acetyltransferase by vinyl fluorenyl ketone." Biochem Pharmacol **48**(9): 1835-8.

Wick, M. J., H. M. Yeh and P. E. Hanna (1990). "An isozyme-selective affinity label for rat hepatic acetyltransferases." Biochem Pharmacol **40**(6): 1389-98.

Wilming, M. a. J., K. (1999). "Spontaneous formation of the bioactive form of the tuberculosis drug isoniazid." Angew. Chem. Int. Ed. **38**: 2588-2590.

Yajko, D. M., J. J. Madej, M. V. Lancaster, C. A. Sanders, V. L. Cawthon, B. Gee, A. Babst and W. K. Hadley (1995). "Colorimetric method for determining MICs of antimicrobial agents for *Mycobacterium tuberculosis*." J Clin Microbiol **33**(9): 2324-7.

Yu, T. W., Y. Shen, Y. Doi-Katayama, L. Tang, C. Park, B. S. Moore, C. Richard Hutchinson and H. G. Floss (1999). "Direct evidence that the rifamycin polyketide synthase assembles polyketide chains processively." Proc Natl Acad Sci U S A **96**(16): 9051-6.

Zhang, J. H., T. D. Chung and K. R. Oldenburg (1999). "A simple statistical parameter for use in evaluation and validation of High Throughput Screening assays." J Biomol Screen **4**(2): 67-73.

Zhang, Y., B. Heym, B. Allen, D. Young and S. Cole (1992). "The catalase-peroxidase gene and isoniazid resistance of *Mycobacterium tuberculosis*." Nature **358**(6387): 591-3.

Zhao, B. Y., R. Pine, J. Domagala and K. Drlica (1999). "Fluoroquinolone action against clinical isolates of *Mycobacterium tuberculosis*: effects of a C-8 methoxyl group on survival in liquid media and in human macrophages." Antimicrob Agents Chemother **43**(3): 661-6.

Zinnes, H., R. A. Comes and J. Shavel Jr. (1966). "1,2-Benzothiazines. III. The Preparation of 2H-1,2-Benzothiazin-4(3H)-one 1,1-Dioxide by the Acid-Catalyzed Deacetylation of ß-Diketone." J Org Chem **31**: 162-165.

Zinnes, H., R. A. Comes, F. R. Zuleski, A. N. Caro and J. Shavel Jr. (1965). "1,2-Benzothiazines. II. The Preparation and Sodium Borohydride Reduction of 3-Acyl-2H-1,2-benzothiazin-4(3H)-one 1,1-Dioxides." J Org Chem **30**: 2241-2246.

# Appendix 1

# Chemical Experimental Data

## A1.1 TZD-Sultams

The TZD-sultams were synthesized by the author and Dr. Richard Vickers (50%:50% work-share) according to Section 2.3.2 and Section 4.2.2.

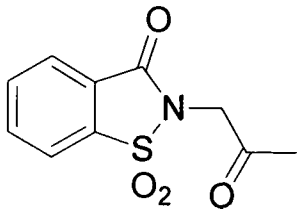


**2**

**2: 1,1-Dioxo-2-(2-oxo-propyl)-1,2-dihydro-1λ$^6$-benzo[*d*]isothiazol-3-one**

Treatment of sodium saccharin (25g, 122mmol) with chloroacetone (16.9g, 183mmol) and cetyltrimethylammonium bromide (12.2g, 31mmol) in refluxing toluene (200mL, 4hrs) furnished the crude product **2** which was recrystallised from hot toluene to give white crystalline product (21.7g, 90.2mmol).
**Yield** (%): 73. **$^1$H NMR** (200MHz, $CDCl_3$): 2.25 (3H, s, C*H*$_3$), 4.44 (2H, s, C*H*$_2$), 7.90-8.06 (4H, m, *Ar*). **$^{13}$C NMR** (60MHz, $CDCl_3$): 26.9 ($CH_3$) 47.0 ($CH_2$) 121.2 125.5 127.1 134.5 135.1 137.7 (Ar) 158.8 (ketone C=O) 198.3 (Amide C=O). **LRMS** (APCI$^+$): m/z 240.06 (100%, MH$^+$). **IR** ($\upsilon_{max}$, disc, cm$^{-1}$): 2978 (C-H), 1728 (C=O), 1538 (C=C, aryl), 1335 ($SO_2$), 1160 ($SO_2$). **M.P.** (°C): 141-142 (lit. 144, Zinnes, H., R. A. Comes, F. R. Zuleski, A. N. Caro and J. Shavel Jr. (1965). J. Org. Chem.**30**, 2241)

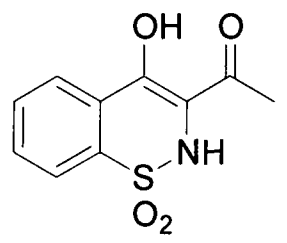


**3**

**3: 1-(4-Hydroxy-1,1-dioxo-1,2-dihydro-1λ$^6$-benzo[*e*][1,2]thiazin-3-yl)-ethanone**

Treatment of **2** (18g, 75mmol) with sodium ethoxide (10.3g, 150mmol) in ethanol (100mL, 50°C) for 30 minutes followed by quenching with 10% aq. HCl (100mL)

furnished crude product **3** which was recrystallised from hot toluene to give colourless crystals (10.6g, 44mmol).
**Yield** (%): 59. **$^1$H NMR** (200MHz, $CDCl_3$): 2.39 (3H, s, C*H*$_3$), 7.95-8.01 (4H, m, *Ar*), 10.20 (1H, br, s, N*H*), 15.05 (1H, br, s, O*H*). **$^{13}$C NMR** (60MHz, $CDCl_3$): 26.0 (*C*$H_3$), 113.3 ($SO_2NHC$), 124.7, 126.8, 128.0, 129.2, 130.8, 133.3 (*Ar*) 159.7 (*C*OH), 200.5 ($CH_3CO$). **LRMS** (APCI$^-$): m/z 238.26 (100%, MH$^-$). **IR** ($\upsilon_{max}$, cm$^{-1}$, disc): 1640 (enolic 1,3-diketone), 1584 (enolic 1,3-diketone), 1317 (S=O), 1179 (S=O). **M.P.** (°C): 152 (lit. 154 Zinnes, H., R. A. Comes, F. R. Zuleski, A. N. Caro and J. Shavel Jr. (1965). J. Org. Chem. **30**, 2241).

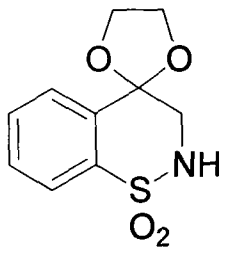


**4**

**4: 1,1-Dioxo-2,3-dihydro-1*H*-1λ$^6$-benzo[*e*][1,2]thiazin-4-one ethylene ketal**

Treatment of **3** (25.0g, 104mmol) with ethylene glycol (32.3g, 521mmol) and fresh tosic acid (7.5g, 39.5mmol) in refluxing toluene (270mL) under a Dean-Stark water separator for 48 hours followed by removal of toluene under vacuum and trituration with 10x25mL diethyl ether furnished crude product **4**. Solid was filtered and washed with ethanol to give white crystals of **4** (16g, 66mmol) .
**Yield** (%): 64. **$^1$H NMR** (200MHz, $CDCl_3$): 3.61 (2H, d, *J*7.4, C*H*$_2$NH), 4.07-4.15 (2H, m, OC*H*HC*H*HO), 4.18-4.26 (2H, m, OCH*H*CH*H*O), 7.55-7.88 (4H, m, *Ar*), 8.64 (1H, t, *J*7.4, $CH_2N$*H*). **$^{13}$C NMR** (60MHz, $CDCl_3$): 48.5 (*C*$H_2$-NH), 66.2 (O-(*C*$H_2$)$_2$-O), 101.4 (ketal *C*), 123.7, 126.4, 128.4, 129.0, 130.9, 133.3 (*Ar*). **LRMS** (APCI$^-$): m/z 242.12 (100%, M$^-$) **IR** (disc): 3186 (N-H), 1328 (S=O), 1160 (S=O). **M.P.** (°C): 190 (lit. 194, Zinnes, H., R. A. Comes and J. Shavel Jr. (1966). J. Org. Chem. **31**, 162)

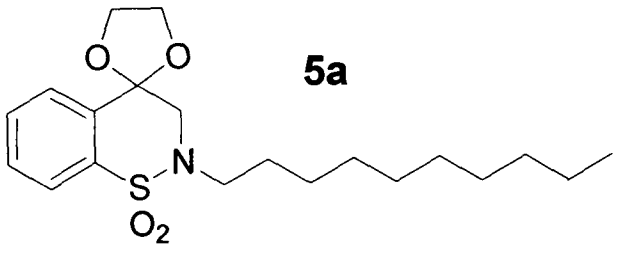


**5a**

**5a: 2-Decyl-1,1-dioxo-2,3-dihydro-1*H*-1λ$^6$-benzo[*e*][1,2]thiazin-4-one ethylene ketal**

Treatment of **4** (750mg, 3.1mmol) with sodium hydride (137mg, 3.4mmol) and 1-bromodecane (752mg, 3.4mmol) in dry DMF (10mL, overnight) followed by extraction into EtOAc and aqueous workup gave crude product that was recrystallised from ether/hexane to give white crystals of **5a** (750mg, 2.0mmol).
**Yield** (%): 63. **$^1$H NMR** (200MHz, $d_6$-DMSO): 0.88 (3H, t, *J*6.5, C*H*$_3$), 1.26(14H, m, (C*H*$_2$)$_7$), 1.63 (bm, 2H, N-$CH_2$-C*H*$_2$), 3.41 (2H, t, *J*7.1, *exo* N-C*H*$_2$), 3.87 (2H, s, *endo* N-C*H*$_2$), 4.10-4.18 (2H, m, OCH*H*CH*H*O), 4.26-4.34 (2H, m, OCH*H*CH*H*O) 7.40-7.80 (4H, m, *Ar*). **$^{13}$C NMR** (60MHz, $d_6$-DMSO): 14.1 (*C*$H_3$), 22.7 26.5 28.4 29.2 29.3 29.5 30.9 31.9 ((*C*$H_2$)$_8$), 48.7 ((ketal)-C*C*$H_2$N), 51.5 (N*C*$H_2$*C*$H_2$), 65.6 (O*C*$H_2$*C*$H_2$O), 101.7 (ketal *C*),123.7 127.5 130.0 132.3 136.4 137.5 (*Ar*). **LRMS** (APCI$^+$): m/z 382.30 (100%, MH$^+$)

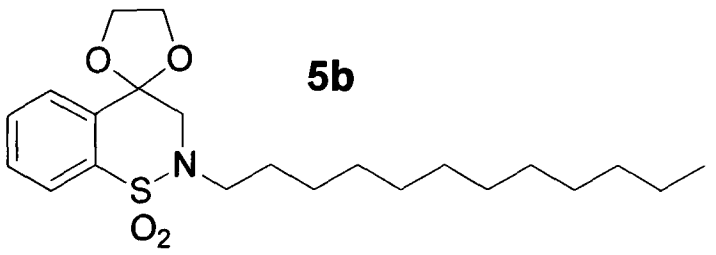


**5b**

**5b: 2-Dodecyl-1,1-dioxo-2,3-dihydro-1*H*-1λ$^6$-benzo[*e*][1,2]thiazin-4-one ethylene ketal**

Treatment of **4** (750mg, 3.1mmol) with sodium hydride (137mg, 3.4mmol) and 1-bromododecane (848mg, 3.4mmol) in dry DMF (10mL, overnight) followed by extraction into EtOAc and aqueous workup gave crude product that was recrystallised from ether/hexane to give pale yellow crystals of **5b** (1.07g, 2.6mmol).

**Yield** (%): 84. **$^1$H NMR** (200MHz, $d_6$-DMSO): 0.88 (3H, t, *J*6.5, C*H*$_3$), 1.26(18H, m, (C*H*$_2$)$_9$), 1.63 (bm, 2H, N-CH$_2$-C*H*$_2$), 3.41 (2H, t, *J*7.1, *exo* N-C*H*$_2$), 3.87 (2H, s, *endo* N-C*H*$_2$), 4.10-4.18 (2H, m, OCH*H*CH*H*O), 4.26-4.34 (2H, m, OCH*H*CH*H*O) 7.40-7.80 (4H, m, *Ar*). **$^{13}$C NMR** (60MHz, $d_6$-DMSO): 14.1 (*C*H$_3$), 22.7 26.5 28.4 29.2 29.3 29.5 30.9 31.9 ((*C*H$_2$)$_{10}$, unresolved), 48.7 ((ketal)-C*C*H$_2$N), 51.5 (N*C*H$_2$CH$_2$), 65.6 (O*C*H$_2$*C*H$_2$O), 101.7 (ketal *C*),123.7 127.5 130.0 132.3 136.4 137.5 (*Ar*). **LRMS** (APCI$^+$): m/z 410.30 (100%, MH$^+$)

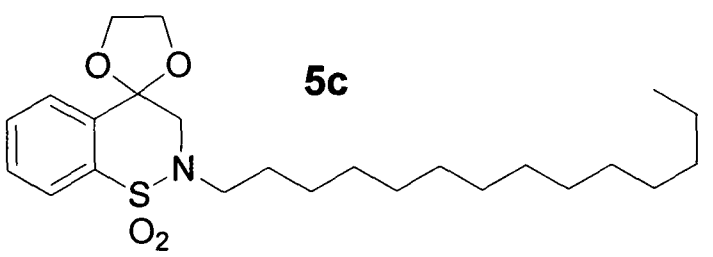


**5c**

**5c: 1,1-Dioxo-2-tetradecyl-2,3-dihydro-1*H*-1λ$^6$-benzo[*e*][1,2]thiazin-4-one ethylene ketal**

Treatment of **4** (750mg, 3.1mmol) with sodium hydride (137mg, 3.4mmol) and 1-bromotetradecane (943mg, 3.4mmol) in dry DMF (10mL, overnight) followed by extraction into EtOAc and aqueous workup gave crude product that was recrystallised from ether/hexane to give pale yellow crystals of **5c** (1.18g, 2.7mmol).

**Yield** (%): 87. **$^1$H NMR** (200MHz, $d_6$-DMSO): 0.88 (3H, t, *J*6.5, C*H*$_3$), 1.26(22H, m, (C*H*$_2$)$_{11}$), 1.63 (2H, m, N-CH$_2$-C*H*$_2$), 3.41 (2H, t, *J*7.1, *exo* N-C*H*$_2$), 3.87 (2H, s, *endo* N-C*H*$_2$), 4.11-4.19 (2H, m, OCH*H*CH*H*O), 4.25-4.33 (2H, m, OCH*H*CH*H*O) 7.40-7.80 (4H, m, *Ar*). **$^{13}$C NMR** (60MHz, $d_6$-DMSO): 14.1 (*C*H$_3$), 22.7 26.5 28.4 29.2 29.3 29.5 29.6 30.9 31.9 ((*C*H$_2$)$_{12}$, unresolved), 48.7 ((ketal)-C*C*H$_2$N), 51.5 (N*C*H$_2$CH$_2$), 65.6 (O*C*H$_2$*C*H$_2$O), 101.7 (ketal *C*),123.7 127.5 130.0 132.3 136.4 137.5 (*Ar*). **LRMS** (APCI$^+$): m/z 438.30 (100%, MH$^+$)

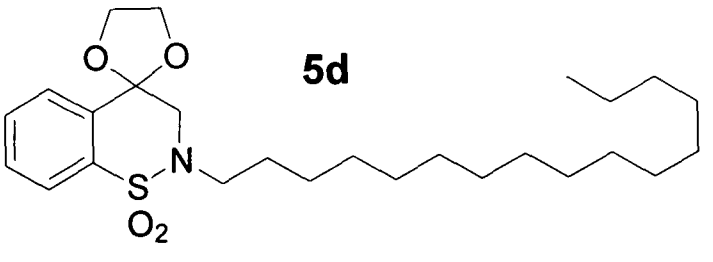


**5d**

**5d: 2-Hexadecyl-1,1-dioxo-2,3-dihydro-1*H*-1λ$^6$-benzo[*e*][1,2]thiazin-4-one ethylene ketal**

Treatment of **4** (750mg, 3.1mmol) with sodium hydride (137mg, 3.4mmol) and 1-bromohexadecane (1038mg, 3.4mmol) in dry DMF (10mL, overnight) followed by extraction into EtOAc and aqueous workup gave crude product that was recrystallised from ether/hexane to give a pale yellow solid of **5d** (963mg, 2.1mmol).

**Yield** (%): 67. **$^1$H NMR** (200MHz, $d_6$-DMSO): 0.88 (3H, t, *J*6.5, C*H*$_3$), 1.26 (26H, m, (C*H*$_2$)$_{13}$), 1.63 (2H, m, N-CH$_2$-C*H*$_2$), 3.41 (2H, t, *J*7.1, *exo* N-C*H*$_2$), 3.87 (2H, s, *endo* N-C*H*$_2$), 4.11-4.19 (2H, m, OCH*H*CH*H*O), 4.25-4.33 (2H, m, OCH*H*CH*H*O) 7.40-7.80 (4H, m, *Ar*). **$^{13}$C NMR** (60MHz, $d_6$-DMSO): 14.1 (*C*H$_3$), 22.7 26.5 28.4 29.2 29.3 29.5 29.6 30.9 31.9 ((*C*H$_2$)$_{14}$, unresolved), 48.7 ((ketal)-C*C*H$_2$N), 51.5 (N*C*H$_2$CH$_2$), 65.6 (O*C*H$_2$*C*H$_2$O), 101.7 (ketal *C*),123.7 127.5 130.0 132.3 136.4 137.5 (*Ar*). **LRMS** (APCI$^+$): m/z 466.34 (100%, MH$^+$)

**5e**

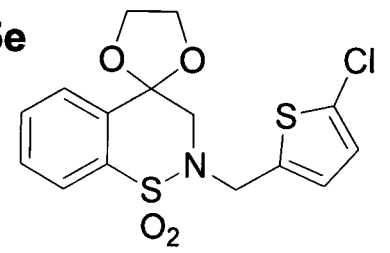


**5e: 2-(5-Chloro-thiophen-2-ylmethyl)-1,1-dioxo-2,3-dihydro-1*H*-1λ$^6$-benzo[*e*][1,2] thiazin-4-one ethylene ketal**

Treatment of **4** (750mg, 3.1mmol) with sodium hydride (137mg, 3.4mmol) and 2-chloro-5-chloromethyl-thiophene (1000mg, 6.0mmol) in dry DMF (10mL, overnight) followed by extraction into EtOAc and aqueous workup gave crude product that was purified *via* flash column chromatography (1:1 hexane/ethyl ether) to give a pale yellow solid of **5e** (730mg, 2.0mmol).

**Yield** (%): 63. **$^1$H NMR** (200MHz, $d_6$-DMSO): 3.80 (2H, s, *endo* N-C*H*$_2$), 4.00-4.08 (2H, m, OCH*H*CH*H*O), 4.24-4.32 (2H, m, OCH*H*CH*H*O), 4.71(2H, s, *exo* N-C*H*$_2$), 6.82 (2H, m, thiophene C*H*-C*H*), 7.50-7.85 (4H, m, *Ar*). **$^{13}$C NMR** (60MHz, $d_6$-DMSO): 47.4 ((ketal)-C*C*H$_2$N), 49.5 (N*C*H$_2$-thiophene), 65.6 (O*C*H$_2$*C*H$_2$O), 101.5 (ketal *C*), 123.8 125.9 127.4 127.8 130.3 130.7 132.8 136.3 136.8 137.0 (*Ar* and *thiophene*).

**5f**

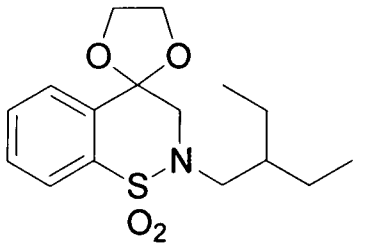


**5f: 2-(2-Ethyl-butyl)-1,1-dioxo-2,3-dihydro-1*H*-1λ$^6$-benzo[*e*][1,2]thiazin-4-one ethylene ketal**

Treatment of **4** (750mg, 3.1mmol) with sodium hydride (137mg, 3.4mmol) and 1-bromo-2-ethylbutane (561mg, 3.4mmol) in dry DMF (10mL, overnight) followed by extraction into EtOAc and aqueous workup gave crude product that was purified *via* flash column chromatography (1:1 hexane/ethyl ether) to give a clear oil of **5f** (640mg, 2.0mmol).

**Yield** (%): 63. **$^1$H NMR** (200MHz, $d_6$-DMSO): 0.84 (6H, t, *J*7.4, 2xC*H*$_3$), 1.29 (4H, m, 2xC*H*$_2$CH$_3$), 1.48 (1H, m, NCH$_2$C*H*), 3.27 (2H, d, *J*7.0, NC*H*$_2$), 3.81 (2H,

s, *endo* N-C$H_2$), 4.00-4.08 (2H, m, OCH*H*CH*H*O), 4.16-4.24 (2H, m, OCH*H*CH*H*O), 7.50-7.80 (4H, m, *Ar*). **$^{13}$C NMR** (60MHz, $d_6$-DMSO): 10.5 (2x*C*$H_3$), 23.0 (2x*C*$H_2$CH$_3$), 39.2 (*C*H), 51.5 ((ketal)-C*C*$H_2$N), 51.6 (N*C*$H_2$CH), 65.6 (O*C*$H_2$*C*$H_2$O), 101.4 (ketal *C*), 123.4 127.8 129.9 132.4 136.6 137.5 (*Ar*). **LRMS** (APCI$^+$): m/z 326.19 (100%, MH$^+$)

**5g**

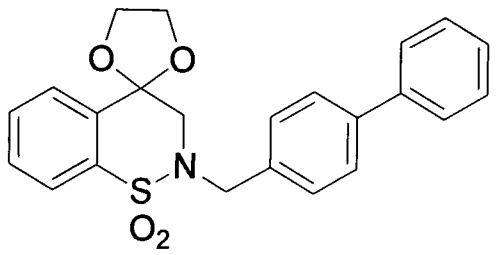


**5g: 2-Biphenyl-4-ylmethyl-1,1-dioxo-2,3-dihydro-1*H*-1λ$^6$-benzo[*e*][1,2]thiazin-4-one ethylene ketal**

Treatment of **4** (750mg, 3.1mmol) with sodium hydride (137mg, 3.4mmol) and 4-phenylbenzyl chloride (689mg, 3.4mmol) in dry DMF (10mL, overnight) followed by extraction into EtOAc and aqueous workup gave crude product that was purified *via* flash column chromatography (1:1 hexane/ethyl ether) to give a white solid of **5g** (1.08g, 2.7mmol).

**Yield** (%): 86. **$^1$H NMR** (400MHz, $d_4$-$CDCl_3$): 3.74 (2H, s, *endo* N-C$H_2$), 3.95-4.05 (2H, m, OCH*H*CH*H*O), 4.22-4.30 (2H, m, OCH*H*CH*H*O), 4.68 (2H, s, *exo* N-C$H_2$), 7.30-7.80 (13H, m, *Ar*). **$^{13}$C NMR** (100MHz, APT, $d_4$-$CDCl_3$): 49.59 (*exo* N-*C*$H_2$), 51.58 (*endo* N-*C*$H_2$), 65.45 (O*C*$H_2$*C*$H_2$O), 101.70 (ketal *C*), 123.85 127.05 127.38 127.47 127.76 128.83 129.36 130.23 132.58 (9x aromatic *C*-H environments), 134.41 136.41 137.27 140.54 140.92 (5x aromatic *C*).

**6a**

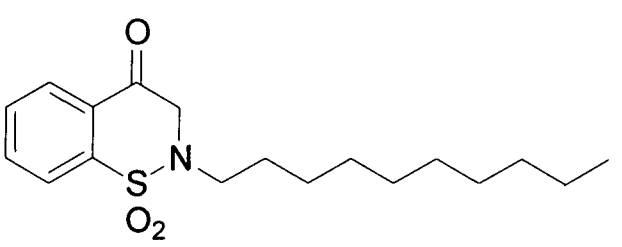


**6a: Crude 2-Decyl-1,1-dioxo-2,3-dihydro-1*H*-1λ$^6$-benzo[*e*][1,2]thiazin-4-one**

Treatment of ketal **5a** (650mg, 1.7mmol) with methanolic HCl (9%, 6.8mL) under reflux for 45 minutes, followed by extraction into EtOAc and aqueous workup furnished the ketone **6a** (520mg, 1.5mmol) as an orange oil.

**Yield** (%): 91. **$^1$H NMR** (200MHz, $d_6$-DMSO): 0.87 (3H, t, *J*6.5, C*H*$_3$), 1.24 (14H, m, (C*H*$_2$)$_7$), 1.56 (2H, m, N-CH$_2$-C*H*$_2$), 3.18 (2H, t, *J*7.1, *exo* N-C*H*$_2$), 4.42 (2H, s, *endo* N-C*H*$_2$), 7.50-8.10 (4H, m, *Ar*). **$^{13}$C NMR** (60MHz, $d_6$-DMSO): 14.1 (*C*H$_3$), 22.6 26.4 26.6 27.7 29.0 29.2 29.4 31.8 ((*C*H$_2$)$_8$), 50.6 (N*C*H$_2$CH$_2$), 57.9 (CO-*C*H$_2$-N), 124.5 128.1 132.9 135.2 135.7 139.6 (*Ar*), 190.2 (*C*O).

**6b**

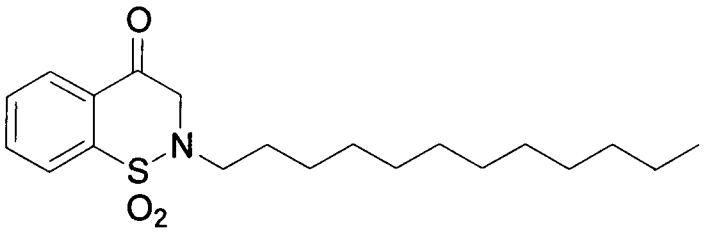

**6b: Crude 2-Dodecyl-1,1-dioxo-2,3-dihydro-1*H*-1λ$^6$-benzo[*e*][1,2]thiazin-4-one**

Treatment of ketal **5b** (970mg, 2.4mmol) with methanolic HCl (9%, 9.4mL) under reflux for 45 minutes, followed by extraction into EtOAc and aqueous workup furnished the ketone **6b** (850mg, 2.2mmol) as an orange oil.
**Yield** (%): 93. **$^1$H NMR** (200MHz, $d_6$-DMSO): 0.86 (3H, t, *J*6.5, C*H*$_3$), 1.15-1.30 (18H, m, (C*H*$_2$)$_9$), 1.55 (2H, m, N-CH$_2$-C*H*$_2$), 3.17 (2H, t, *J*7.2, *exo* N-C*H*$_2$), 4.42 (2H, s, *endo* N-C*H*$_2$), 7.50-8.08 (4H, m, *Ar*). **$^{13}$C NMR** (60MHz, $d_6$-DMSO): 14.1 (*C*H$_3$), 22.6 26.4 26.6 27.7 28.8 29.0 29.3 29.5 30.4 31.9 ((*C*H$_2$)$_{10}$), 50.6 (N*C*H$_2$CH$_2$), 57.9 (CO-*C*H$_2$-N), 124.5 128.1 131.5 132.9 135.7 139.6 (*Ar*), 190.1 (*C*O).

**6c**

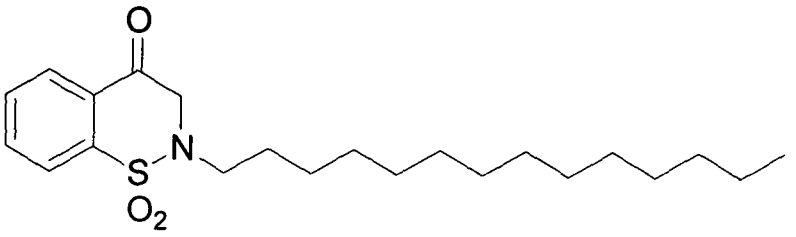


**6c: Crude 1,1-Dioxo-2-tetradecyl-2,3-dihydro-1*H*-1λ$^6$-benzo[*e*][1,2]thiazin-4-one**

Treatment of ketal **5c** (1080mg, 2.5mmol) with methanolic HCl (9%, 9.8mL) under reflux for 45 minutes, followed by extraction into EtOAc and aqueous workup furnished the ketone **6c** (630mg, 1.6mmol) as white crystals.
**Yield** (%): 65. **$^1$H NMR** (200MHz, $d_6$-DMSO): 0.87 (3H, t, *J*6.4, C*H*$_3$), 1.15-1.30 (22H, m, (C*H*$_2$)$_{11}$), 1.56 (2H, m, N-CH$_2$-C*H*$_2$), 3.18 (2H, t, *J*7.2, *exo* N-C*H*$_2$), 4.42 (2H, s, *endo* N-C*H*$_2$), 7.50-8.05 (4H, m, *Ar*). **$^{13}$C NMR** (60MHz, $d_6$-DMSO): 14.1 (*C*H$_3$), 22.7 26.4 27.7 28.8 29.0 29.3 29.4 29.5 29.6 31.9 ((*C*H$_2$)$_{12}$ unresolved), 50.6 (N*C*H$_2$CH$_2$), 57.9 (CO-*C*H$_2$-N), 124.5 128.1 131.5 132.9 135.2 139.7 (*Ar*), 190.1 (*C*O).

**6d**

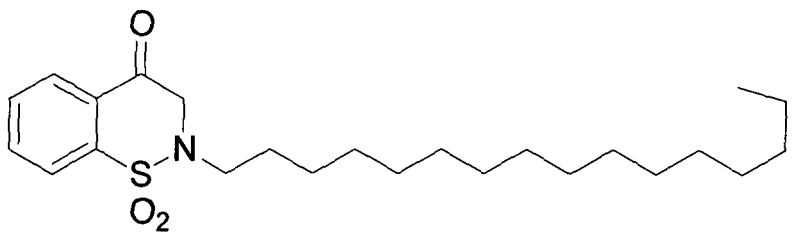


**6d: Crude 2-Hexadecyl-1,1-dioxo-2,3-dihydro-1*H*-1λ$^6$-benzo[*e*][1,2]thiazin-4-one**

Treatment of ketal **5d** (860mg, 1.9mmol) with methanolic HCl (9%, 7.4mL) under reflux for 45 minutes, followed by extraction into EtOAc and aqueous workup furnished the ketone **6d** (680mg, 1.6mmol) as yellow crystals.
**Yield** (%): 87. **$^1$H NMR** (200MHz, $d_6$-DMSO): 0.87 (3H, t, *J*6.4, C*H*$_3$), 1.15-1.30 (22H, m, (C*H*$_2$)$_{11}$), 1.56 (2H, m, N-CH$_2$-C*H*$_2$), 3.18 (2H, t, *J*7.2, *exo* N-C*H*$_2$), 4.42 (2H, s, *endo* N-C*H*$_2$), 7.50-8.05 (4H, m, *Ar*). **$^{13}$C NMR** (60MHz, $d_6$-DMSO): 14.1 (*C*H$_3$), 22.7 26.4 27.7 28.8 29.0 29.3 29.4 29.5 29.6 31.9 ((*C*H$_2$)$_{14}$ unresolved), 50.6 (N*C*H$_2$CH$_2$), 57.9 (CO-*C*H$_2$-N), 124.5 128.1 131.5 132.9 135.2 139.7 (*Ar*), 190.1 (*C*O).

**6e**

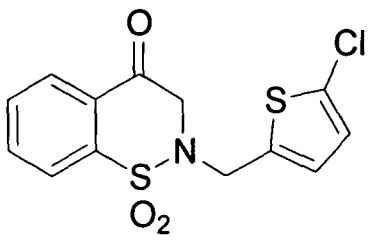


**6e: Crude 2-(5-Chloro-thiophen-2-ylmethyl)-1,1-dioxo-2,3-dihydro-1*H*-1λ$^6$-benzo[*e*][1,2]thiazin-4-one**

Treatment of ketal **5e** (630mg, 1.7mmol) with methanolic HCl (9%, 6.8mL) under reflux for 45 minutes, followed by extraction into EtOAc and aqueous workup furnished the ketone **6e** (490mg, 1.5mmol) as orange crystals.
**Yield** (%): 88. **$^1$H NMR** (200MHz, $d_6$-DMSO): 4.41 (2H, s, *endo* N-C*H*$_2$), 4.52 (2H, s, *exo* N-C*H*$_2$), 6.70 (2H, m, *H*CC*H*), 7.50-8.00 (4H, m, *Ar*). **$^{13}$C NMR** (60MHz, $d_6$-DMSO): 49.3 (*exo* NCH$_2$), 57.9 (CO-*C*H$_2$-N), 123.8 124.4 125.7 126.9 128.2 129.2 131.9 133.0 135.0 139.7 (10x*Ar*), 189.2 (*C*O).

**6f**

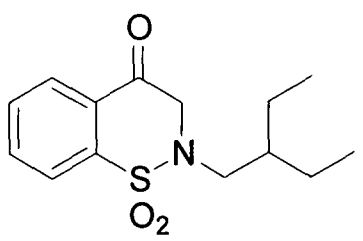


**6f: Crude 2-(2-Ethyl-butyl)-1,1-dioxo-2,3-dihydro-1*H*-1λ$^6$-benzo[*e*][1,2]thiazin-4-one**

Treatment of ketal **5f** (420mg, 1.3mmol) with methanolic HCl (9%, 5.2mL) under reflux for 45 minutes, followed by extraction into EtOAc and aqueous workup furnished the ketone **6f** (340mg, 1.2mmol) as a clear oil.
**Yield** (%): 93. **$^1$H NMR** (200MHz, $d_6$-DMSO): 0.75-0.95 (6H, m, 2xC*H*$_3$), 1.15-1.35 (4H, m, 2xC*H*$_2$CH$_3$), 1.56 (1H, m, N-CH$_2$-C*H*$_2$), 2.98 (2H, d, *J*7.2, *exo* N-C*H*$_2$), 4.40 (2H, s, *endo* N-C*H*$_2$), 7.50-8.10 (4H, m, *Ar*). **$^{13}$C NMR** (60MHz, $d_6$-DMSO): 10.3 (2x*C*H$_3$), 22.8 (2x*C*H$_2$CH$_3$), 38.8 (NCH$_2$*C*H), 53.8 (NCH$_2$CH$_2$), 57.7 (CO-*C*H$_2$-N), 124.5 128.1 132.9 135.2 135.7 139.6 (*Ar*), 190.2 (*C*O).

**6g**

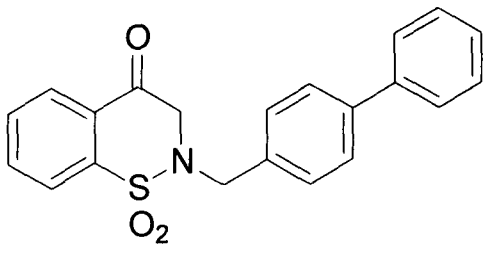


**6g: Crude 2-Biphenyl-4-ylmethyl-1,1-dioxo-2,3-dihydro-1*H*-1λ$^6$-benzo[*e*][1,2]thiazin-4-one**

Treatment of ketal **5g** (980mg, 2.4mmol) with methanolic HCl (9%, 9.6mL) under reflux for 45 minutes, followed by extraction into EtOAc and aqueous workup furnished the ketone **6g** (765mg, 2.1mmol) as white crystals.
**Yield** (%): 87. **$^1$H NMR** (200MHz, $d_6$-DMSO): 4.37 (2H, s, *endo* N-C*H*$_2$), 4.45 (2H, s, *exo* N-C*H*$_2$), 7.20-8.00 (13H, m, *Ar*). **$^{13}$C NMR** (60MHz, $d_6$-DMSO): 54.2 (*exo* NCH$_2$), 57.1 (CO-*C*H$_2$-N), 124.5 127.1 127.4 127.5 127.6 128.1 128.6 128.8 129.3 129.5 131.7 132.3 132.9 134.2 135.1 139.6 140.3 141.5 (18x*Ar*), 189.7 (*C*O).

For all TZD-sultams **17-32**:
Treatment of the corresponding *N*-substituted ketone (1.0 equivalent) in 5-10ml dioxane with thiazolidine-2,4-dione (1.0 equivalent) in the presence of boron trifluoride etherate (4.0 equivalents) and triethylamine (2.0 equivalents) for 48 hours followed by ethyl acetate extraction and aqueous work-up furnished a crude mixture from which the TZD-sultam was purified *via* flash column chromatography (1:1 hexane/ethyl ether). Not all ketal and ketone products (**5** and **6**) were purified before synthesis of the final thiazolidinedione.

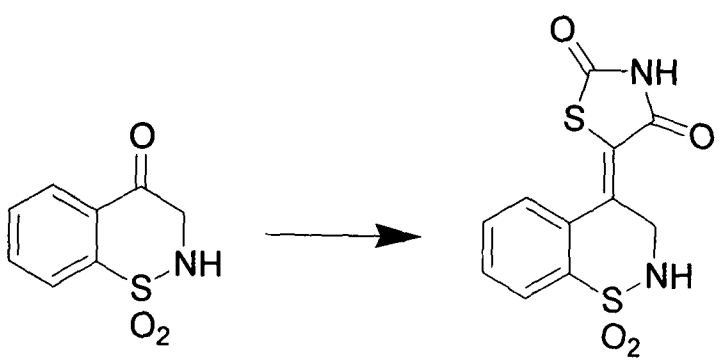

**17a** **17**

**17: 5-(1,1-Dioxo-2,3-dihydro-1*H*-1λ$^6$-benzo[*e*][1,2]thiazin-4-ylidene)-thiazolidine-2,4-dione**

From 990mg (5.1mmol) of crude unsubstituted ketone 17a, 820mg (2.8mmol) of pale yellow powder **17** was produced.
**Yield** (%): 55. **$^1$H NMR** (400MHz, $d_6$-DMSO): 4.78 (2H, d, 6.9Hz, C$H_2$), 7.50-7.90 (m, 4H). **$^{13}$C NMR** (60MHz, $d_6$-DMSO): 53.52 (*C*$H_2$), 124.11 124.51 129.41 131.86 133.46 133.65 138.19 140.49 (*Ar* and *C*=*C*) 167.30 168.41 (*C*O). **LRMS** (APCI$^-$): 294.60 (100%, M$^-$) **HRMS** (ESIMS): $C_{11}H_8N_2O_4S_2$ requires 294.9847 Found 294.9845. **IR** (disc): 1178.9 (S=O), 1317.4 (S=O), 1456.7 (aromatic), 1698.8 (C=O), 1725.4 (C=O). **M.P.** (°C): 195 (decomposed)

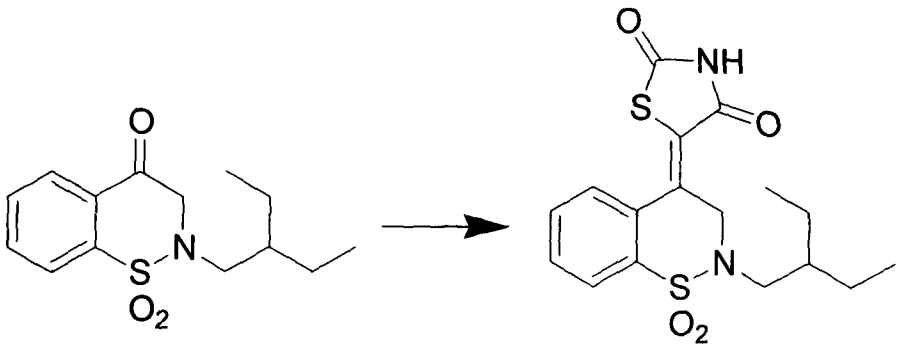

**6f** **18**

**18: 5-[2-(2-Ethyl-butyl)-1,1-dioxo-2,3-dihydro-1*H*-1λ$^6$-benzo[*e*][1,2]thiazin-4-ylidene]-thiazolidine-2,4-dione**

From 401mg of crude ketone **6f** (1.2mmol), 68mg (0.18mmol) of white solid **18** was produced.
**Yield** (%): 17. **$^1$H NMR** (200MHz, $d_6$-DMSO): 0.77 (6H, m, 2xC$H_3$), 1.30 (4H, m, C$H_2$CH$_3$), 1.53 (1H, m, C*H*), 2.61 (2H, d, 7Hz, NC$H_2$CH), 4.96 (2H, s, *endo* N-C$H_2$), 7.70-7.92 (4H, m, *Ar*). **$^{13}$C NMR** (60MHz, $d_6$-DMSO): 10.3 (2x*C*H$_3$), 22.8 (2x*C*H$_2$CH$_3$), 38.9 (NCH$_2$*C*H), 53.5 (C=C-*C*H$_2$-N), 54.0 (NCH$_2$*C*H$_2$), 123.2 125.3 128.52 131.1 132.4 132.6 137.4 138.7 (*Ar* and *C*=*C*), 165.4 166.9 (*C*O). **LRMS** (APCI$^-$): 378.57 (100%, M$^-$). **HRMS** (ESIMS): $C_{17}H_{20}N_2O_4S_2$ Requires 379.0786 Found 379.0786. **IR** (disc): 1171.3 (S=O), 1338.5 (S=O), 1457.8 (aromatic), 1716.2 (C=O), 1737.9 (C=O). **M.P.** (°C): 134-135

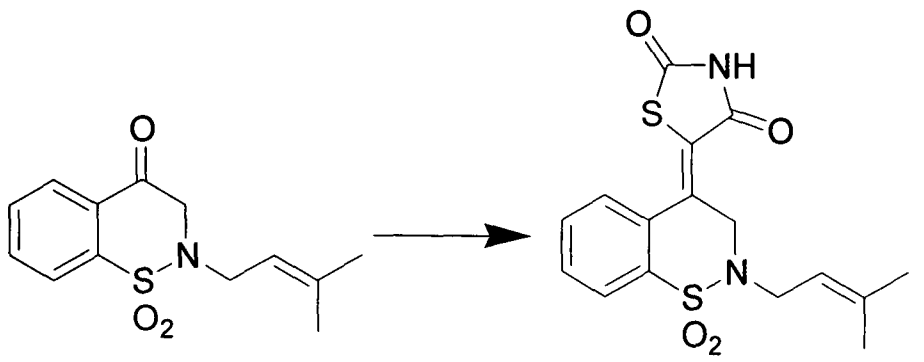

**19a** **19**

**19: 5-[2-(3-Methyl-but-2-enyl)-1,1-dioxo-2,3-dihydro-1*H*-1λ$^6$-benzo[*e*][1,2]thiazin-4-ylidene]-thiazolidine-2,4-dione**

From 290mg of crude ketone **19a** (1.1mmol),160mg (0.44mmol) of a white solid **19** was produced.

**Yield** (%): 40. **$^1$H NMR** (200MHz, $d_6$-DMSO): 1.49 (3H, s, C*H*$_3$), 1.57 (3H, s, C*H*$_3$), 3.54 (1H, m, C*H*=C), 3.70 (2H, s, NC*H*$_2$CH), 4.91 (2H, s, *endo* N-C*H*$_2$), 7.75-7.90 (4H, m, *Ar*), 10.01 (1H, br s, N*H*). **$^{13}$C NMR** (60MHz, $d_6$-DMSO): 17.8 (C*H*$_3$), 25.5 (C*H*$_3$), 47.8 (N-*C*H$_2$-CH), 51.8 (*endo C*H$_2$-N), 66.9 115.4 (*C*H=*C*), 123.2 125.0 127.2 131.1 132.7 137.6 138.1 139.4 (*Ar* and *C*=*C*) 165.8 167.4 (*C*O). **LRMS** (APCI$^-$): 362.54 (100%, M$^-$). **HRMS** (ESIMS):$C_{16}H_{16}N_2O_4S_2$ Requires 363.0473 Found 363.0460. **M.P.** (°C): 112-113

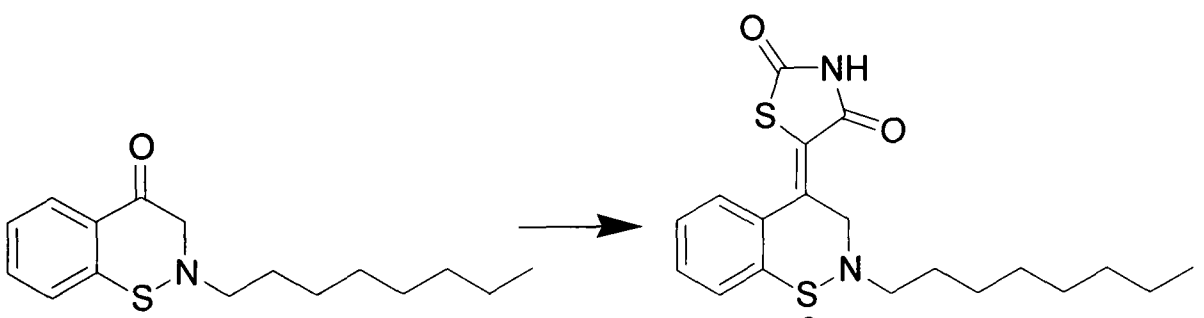

**20a** **20**

**20: 5-(2-Octyl-1,1-dioxo-2,3-dihydro-1*H*-1λ$^6$-benzo[*e*][1,2]thiazin-4-ylidene)-thiazolidine-2,4-dione**

From 188mg of crude **20a** (0.62mmol), 25mg (0.062mmol) of a clear oil **20** was produced that did not solidify.

**Yield** (%): 10. **$^1$H NMR** (200MHz, $d_6$-DMSO): 0.87 (3H, t, *J*6.5, C*H*$_3$), 1.22 (10H, m, (C*H*$_2$)$_5$), 1.50 (2H, m, NCH$_2$C*H*$_2$), 2.81 (2H, t, *J*7.2, NC*H*$_2$CH$_2$), 4.99 (2H, s, *endo* N-C*H*$_2$) 7.6-8.0 (4H, m, *Ar*), 8.95 (1H, s, N*H*). **$^{13}$C NMR** (60MHz, $d_6$-DMSO): 14.1 (C*H*$_3$), 22.6 26.5 27.8 29.1 29.4 31.8 ((*C*H$_2$)$_6$), 50.6 (N-*C*H$_2$-CH$_2$), 53.0 (*endo C*H$_2$-N), 123.1 125.1 128.3 131.1 132.4 132.6 137.7 138.8 (*Ar* and *C*=*C*), 165.1 166.5 (*C*=O). **LRMS** (APCI$^-$): 406.28 (100%, M$^-$). **HRMS** (ESIMS): $C_{19}H_{24}N_2O_4S_2$ Requires 407.1099 Found 407.1099 . **M.P.** (°C): none

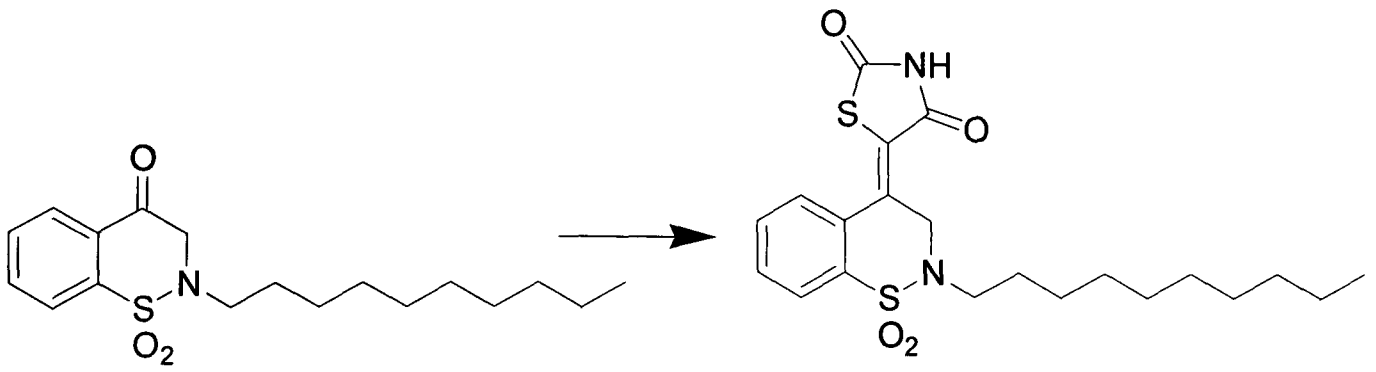

**6a** **21**

**21: 5-(2-Decyl-1,1-dioxo-2,3-dihydro-1*H*-1λ$^6$-benzo[*e*][1,2]thiazin-4-ylidene)-thiazolidine-2,4-dione**

From 450mmol of crude **6a** (1.23mmol), 220mg (0.48mmol) of a white solid **21** was produced.
**Yield** (%): 39. **$^1$H NMR** (200MHz, $d_6$-DMSO): 0.87 (3H, t, *J*6.5, C*H*$_3$), 1.22 (14H, m, (C*H*$_2$)$_7$), 1.50 (2H, m, NCH$_2$C*H*$_2$), 2.81 (2H, t, *J*7.2, NC*H*$_2$CH$_2$), 4.99 (2H, s, *endo* N-C*H*$_2$) 7.6-8.0 (4H, m, *Ar*), 8.95 (1H, s, N*H*). **$^{13}$C NMR** (60MHz, $d_6$-DMSO): 14.1 (C*H*$_3$), 22.6 26.5 27.8 29.1 29.2 29.4 31.8 ((*C*H$_2$)$_8$ unresolved), 50.6 (N-*C*H$_2$-CH$_2$), 53.0 (*endo C*H$_2$-N), 123.1 125.1 128.3 131.1 132.4 132.6 137.7 138.8 (*Ar* and *C*=*C*), 165.1 166.5 (*C*O). **LRMS** (APCI$^-$): 462.83 (100%, M$^-$). **HRMS** (ESIMS): $C_{21}H_{28}N_2O_4S_2$ Requires 463.1725 Found 463.1730. **M.P.** (°C): 86-87

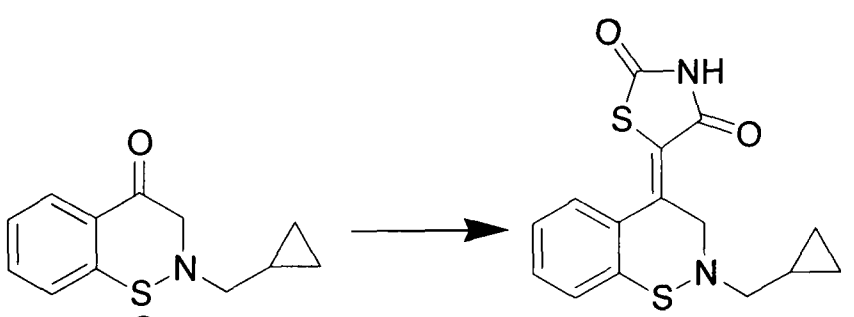

**22a** **22**

**22: 5-(2-Cyclopropylmethyl-1,1-dioxo-2,3-dihydro-1*H*-1λ$^6$-benzo[*e*][1,2]thiazin-4-ylidene)-thiazolidine-2,4-dione**

From 300mg of crude **22a** (1.2mmol), 74mg (0.21 mmol) of a white solid **22**.
**Yield** (%): 16. **$^1$H NMR** (200MHz, $d_6$-DMSO): 0.09 (2H, m, C*H*$_2$-C*H*$_2$), 0.38 (2H, m, C*H*$_2$-C*H*$_2$), 0.75 (1H, m, C*H*), 2.88 (2H, d, *J*7.0, NC*H*$_2$CH), 5.01 (2H, s, *endo* N-C*H*$_2$), 7.55-7.93 (4H, m, *Ar*). **$^{13}$C NMR** (60MHz, $d_6$-DMSO): 3.8 (*C*H$_2$-CH$_2$), 8.9 (*C*H) 52.8 (N-*C*H$_2$-CH), 55.2 (*endo C*H$_2$-N), 123.0 124.8 128.3 131.0 132.6 138.3 139.0 (*Ar* and *C*=*C*), 165.8 167.4 (*C*O). **LRMS** (APCI$^-$): 348.33 (100%, M$^-$). **HRMS** (ESIMS): $C_{15}H_{14}N_2O_4S_2$ Requires 349.0315 Found 349.0317. **IR** (disc): 1176.1 (S=O), 1323.7 (S=O), 1462.9 (aromatic), 1700.5 (C=O), 1746.5 (C=O). **M.P.** (°C): 160-162

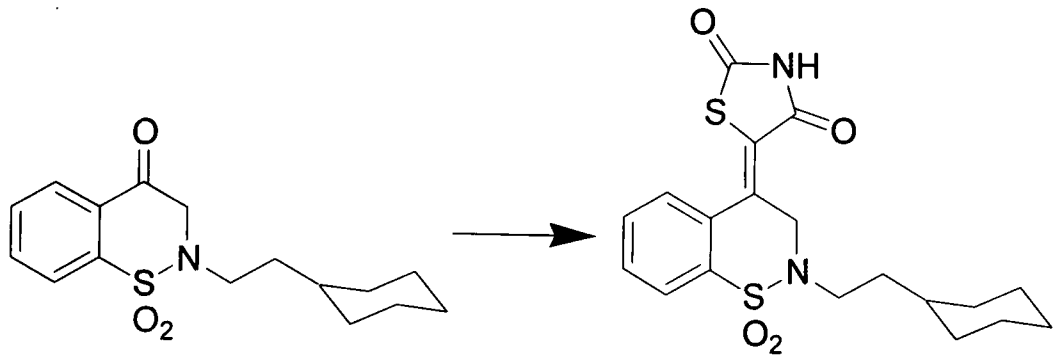

**23a** **23**

**23: 5-[2-(2-Cyclohexyl-ethyl)-1,1-dioxo-2,3-dihydro-1*H*-1λ$^6$-benzo[*e*][1,2]thiazin-4-ylidene]-thiazolidine-2,4-dione**

48mg (0.12mmol) of white solid **23**.
**Yield** (%): 12. **$^1$H NMR** (200MHz, $d_6$-DMSO): 0.87 (2H, m, $NCH_2CH_2$), 1.05-1.30 (6H, m, $CH_2CH_2CH_2$), 1.66 (m, 5H, ring $CH_2CHCH_2$), 2.85 (2H, t, *J*7.0, $NCH_2CH_2$), 4.97 (2H, s, *endo* N-$CH_2$) 7.55-7.93 (4H, m, *Ar*). **$^{13}$C NMR** (60MHz, $d_6$-DMSO): 26.1 26.4 32.9 34.8 35.1 35.6 ($CH_2$-*cyclohexyl* unresolved), 48.5 ($NCH_2CH_2$) 52.8 (*endo* $CH_2N$) 123.1 125.2 128.2 131.1 132.4 132.6 137.6 138.8 (*Ar* and *C*=*C*), 165.5 167.1 (*C*O). **LRMS** (APCI$^-$): 404.35 (100%, M$^-$). **HRMS** (ESIMS): $C_{19}H_{22}N_2O_4S_2$ Requires 405.0943 Found 405.0947. **M.P.** (°C): 78-79

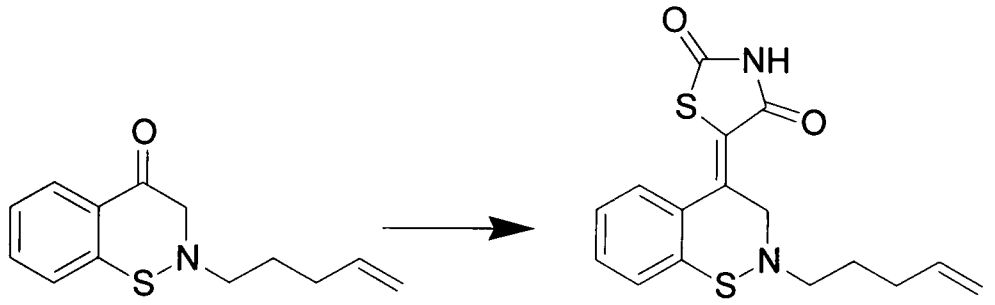

**24a** **24**

**24: 5-(1,1-Dioxo-2-pent-4-enyl-2,3-dihydro-1*H*-1λ$^6$-benzo[*e*][1,2]thiazin-4-ylidene)-thiazolidine-2,4-dione**

From 792mg (3.0mmol) of crude ketone **24a**, 110mg (0.30mmol) of pale yellow solid **24** was produced.
**Yield** (%): 10. **$^1$H NMR** (200MHz, $d_6$-DMSO): 1.60 (2H, m, $NCH_2CH_2$), 2.04 (2H, m, $NCH_2CH_2CH_2$), 2.83 (2H, t, $NCH_2$), 4.98 (4H, m, C=$CH_2$ & *endo* N-$CH_2$), 5.73 (1H, m, $CH$=$CH_2$), 7.55-7.92 (4H, m, *Ar*). **$^{13}$C NMR** (60MHz, $d_6$-DMSO): 27.0 30.4 ($NCH_2CH_2CH_2$) 50.1 ($NCH_2CH_2$) 53.2 (*endo* $CH_2$-N), 115.6 123.3 125.1 128.3 131.2 132.4 132.8 137.1 137.5 138.6 ($CH$=$CH_2$, *C*=*C* & *Ar*), 165.8 167.4 (*C*O). **LRMS** (APCI$^-$): 362.52 (100%, M$^-$). **HRMS** (ESIMS): $C_{16}H_{16}N_2O_4S_2$ Requires 363.0473 Found 363.0465. **IR** (disc): 1172.9 (S=O), 1334.9 (S=O), 1452.9 (aromatic), 1698.9 (C=O), 1724.6 (C=O). **M.P.** (°C): 141-142

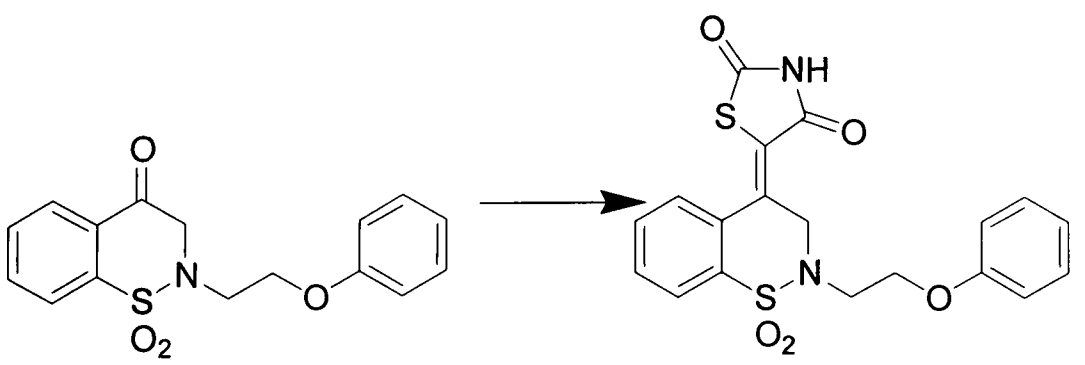

**25a** **25**

**25: 5-[1,1-Dioxo-2-(2-phenoxy-ethyl)-2,3-dihydro-1*H*-1λ$^6$-benzo[*e*][1,2]thiazin-4-ylidene]-thiazolidine-2,4-dione**

From 662mg (1.86mmol) of crude ketone **25a**, 180mg (0.41mmol) of a clear oil **25** was produced that did not solidify under vacuum or cooling.
**Yield** (%): 22. **$^1$H NMR** (200MHz, $d_6$-DMSO): 3.77 (2H, m, OC*H*$_2$) 4.02 (2H, m, NC*H*$_2$CH$_2$), 4.88 (2H, s, *endo* N-C*H*$_2$), 6.63 (2H, m, OCCHC*H*) 6.88 (1H, m, OCCHCHC*H*) 7.14 (2H, m, OCC*H*) 7.50-7.90 (4H, m, *Ar*). **$^{13}$C NMR** (60MHz, $d_6$-DMSO): 37.1 (OCH$_2$) 57.2 (*endo* *C*H$_2$-N) 67.3 (NCH$_2$CH$_2$) 110.4 115.6 122.5 125.2 130.9 134.2 136.7 145.8 159.0 159.9 (*Ar*, OAr & *C*=*C* unresolved) 164.2 166.5 (*C*O). **LRMS** (APCI$^-$): 434.15 (100%, M$^-$). **IR** (disc): 1175 (S=O), 1338 (S=O), 1699 (C=O), 1733 (C=O). **M.P.** (°C): none

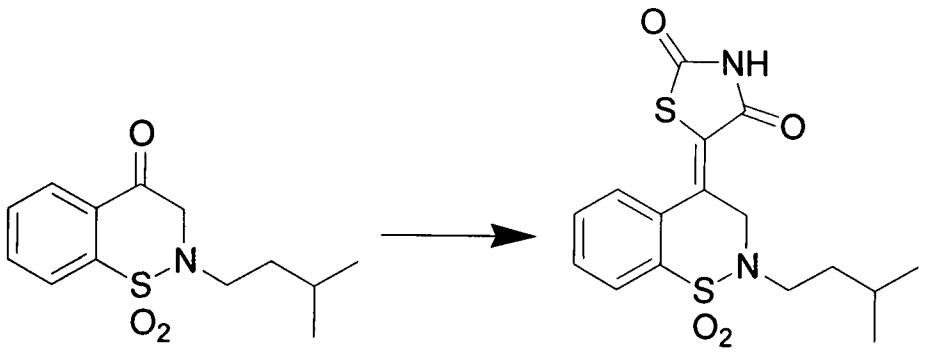


**26a** **26**

**26: 5-[2 (3-methyl-butyl)-1,1-dioxo-2,3-dihydro-1*H*-1λ$^6$-benzo[*e*][1,2]thiazin-4-ylidene]-thiazolidine-2,4-dione**

From 340mg (1.3mmol) of crude ketone **26a**, 85mg (0.23mmol) of a clear oil **26** was produced that did not solidify under vacuum or cooling.
**Yield** (%): 18. **$^1$H NMR** (200MHz, $d_6$-DMSO): 0.86 (6H, d, *J*6.4, C*H*$_3$CH C*H*$_3$), 1.45 (2H, m, NCH$_2$C*H*$_2$), 1.67 (1H, m, C*H*), 2.84 (2H, t, *J*7.2, NC*H*$_2$CH$_2$), 4.97 (2H, s, *endo* N-C*H*$_2$), 7.61-7.95 (4H, m, *Ar*) 9.32 (1H, br s, N*H*). **$^{13}$C NMR** (60MHz, $d_6$-DMSO): 10.6 (2x*C*H$_3$), 25.4 (*C*H), 35.4 (NCH$_2$*C*H$_2$), 53.5 (C=C-*C*H$_2$-N), 54.0 (N*C*H$_2$CH$_2$), 123.2 125.3 128.52 131.1 132.4 132.6 137.4 138.7 (*Ar* and *C*=*C*), 165.4 166.9 (*C*O). **LRMS** (APCI$^-$): 364.59 (100%, M$^-$). **HRMS** (ESIMS): $C_{16}H_{18}N_2O_4S_2$ Requires 365.0630 Found 365.0639. **M.P.** (°C): none

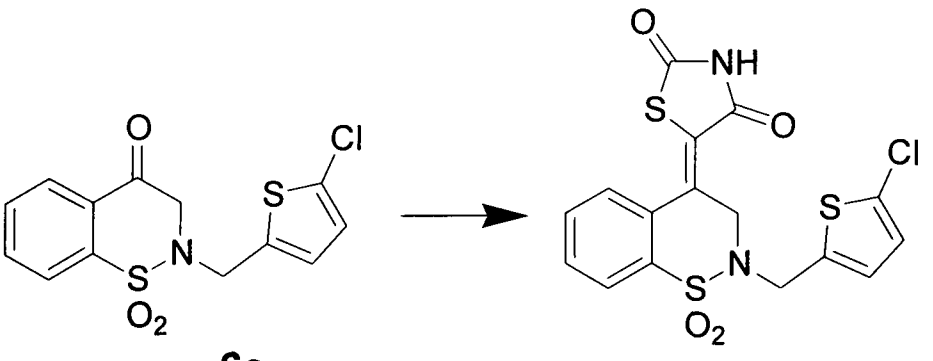


**6e** **27**

**27: 5-[2-(5-Chloro-thiophen-2-ylmethyl)-1,1-dioxo-2,3-dihydro-1*H*-1λ$^6$-benzo[*e*][1,2]thiazin-4-ylidene]-thiazolidine-2,4-dione**

From 380mg (1.2mmol) of ketone **6e**, 95mg (0.22mmol) of a white solid **27** was produced.
**Yield** (%): 19. **$^1$H NMR** (200MHz, $d_6$-DMSO): 4.26 (2H, s, *exo* N-C*H*$_2$), 5.00(2H, s, *endo* N-C*H*$_2$), 6.63 (2H, m, C*H*C*H*CCl), 7.65-7.97 (4H, m, *Ar*), 8.96(1H, br, N*H*). **$^{13}$C NMR** (60MHz, $d_6$-DMSO): 49.0 (*exo* N-C*H*$_2$), 52.0 (*endo* N-C*H*$_2$), 123.2 125.0 125.9 127.3 128.3 131.0 132.4 132.8 135.2 138.0 138.2 (*Ar*,

*thiophene & C=C* unresolved) 165.0 166.4 (*C*O). **LRMS** (APCI⁻): 423.85 (100%, M⁻). **HRMS** (ESIMS): $C_{16}ClH_{11}N_2O_4S_3$ Requires 424.9491 Found 424.9485. **IR** (disc): 1172.3 (S=O), 1336.7 (S=O), 1462.0 (aromatic), 1709.4 (C=O), 1738.1 (C=O). **M.P.** (°C): 157-158

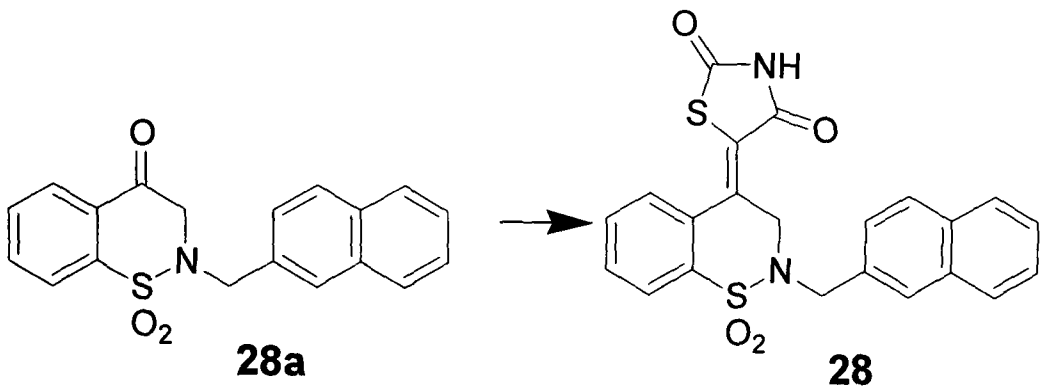


**28a** **28**

**28: 5-(2-Naphthalen-2-ylmethyl-1,1-dioxo-2,3-dihydro-1*H*-1λ⁶-benzo[*e*][1,2]thiazin-4-ylidene)-thiazolidine-2,4-dione**

From 500mg (1.48mmol) of crude ketone **28a**, 162mg (0.37mmol) of a brown solid **28** was produced.

**Yield** (%): 25. **$^1$H NMR** (200MHz, $d_6$-DMSO): 4.21 (2H, s, *exo* N-C$H_2$), 4.95 (2H, s, *endo* N-C$H_2$), 7.50 (4H, m, nap C*H*C*H*C*H*C*H*), 7.70-7.92 (6H, m, *Ar* & naphthyl *H*CCCC*H*), 8.05 (1H, d, *J*7.1, nap NCH$_2$CC*H*CH). **$^{13}$C NMR** (60MHz, $d_6$-DMSO): 52.8 (*endo* N-C$H_2$), 54.3 (*exo* N-C$H_2$), 125.0 125.5 127.0 127.5 127.8 128.2 128.5 128.6 129.2 132.0 133.3 133.4 133.5 133.6 134.1 136.6 137.3 (*Ar*, *nap* & *C=C* unresolved), 167.3 168.3 (*C*O). **LRMS** (APCI⁻): 434.01 (100%, M⁻). **HRMS** (ESIMS): $C_{22}H_{16}N_2O_4S_2$ Requires 435.0473 Found 435.0478. **IR** (disc): 1165.6 (S=O), 1334.6 (S=O), 1463.6 (aromatic), 1705.6 (C=O), 1741.5 (C=O). **M.P.** (°C): 142-143.

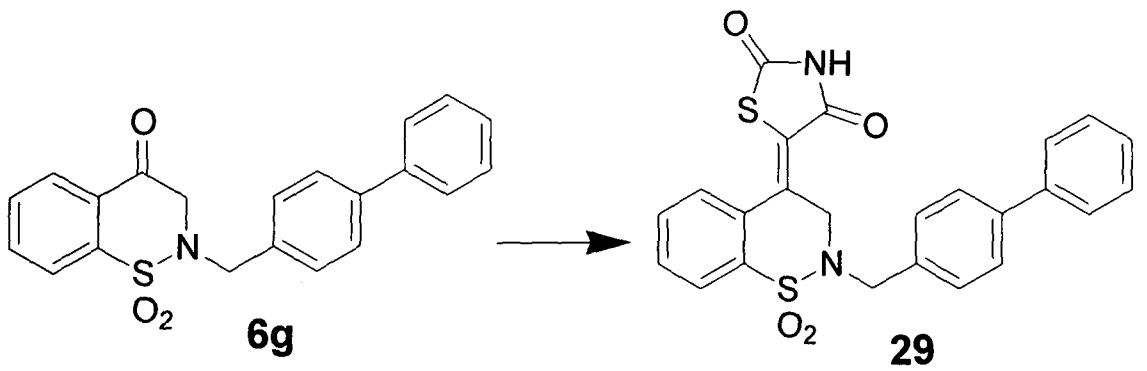


**6g** **29**

**29: 5-(2-Biphenyl-4-ylmethyl-1,1-dioxo-2,3-dihydro-1*H*-1λ⁶-benzo[*e*][1,2]thiazin-4-ylidene)-thiazolidine-2,4-dione**

From 670mg (1.8mmol) of crude ketone **6g**, 260mg (0.57mmol) of a white solid **29** was produced.

**Yield** (%): 31. **$^1$H NMR** (200MHz, $d_6$-DMSO): 4.13 (2H, s, *exo* N-C$H_2$), 4.96(2H, s, *endo* N-C$H_2$), 7.20-7.80 (12H, m, *Ar* & *biphenyl*), 8.01 (1H, m, bip CHC*H*CH), 9.22 (1H, br, N*H*). **$^{13}$C NMR** (60MHz, $d_6$-DMSO): 52.2 (*endo* N-C$H_2$), 53.9 (*exo* N-C$H_2$), 123.2 125.2 127.0 127.4 128.3 128.8 129.0 129.4 129.6 131.1 132.5 132.7 133.0 137.8 138.4 140.4 141.1 (*Ar*, *C=C* & *biphenyl*), 165.2 166.7 (*C*O). **LRMS** (APCI⁻): 460.20 (100%, M⁻). **HRMS** (ESIMS): $C_{24}H_{18}N_2O_4S_2$ Requires 461.0630 Found 461.0637. **IR** (disc): 1169.9 (S=O), 1340.4 (S=O), 1487.5 (aromatic), 1708.5 (S=O), 1744.0 (S=O). **M.P.** (°C): 178-179

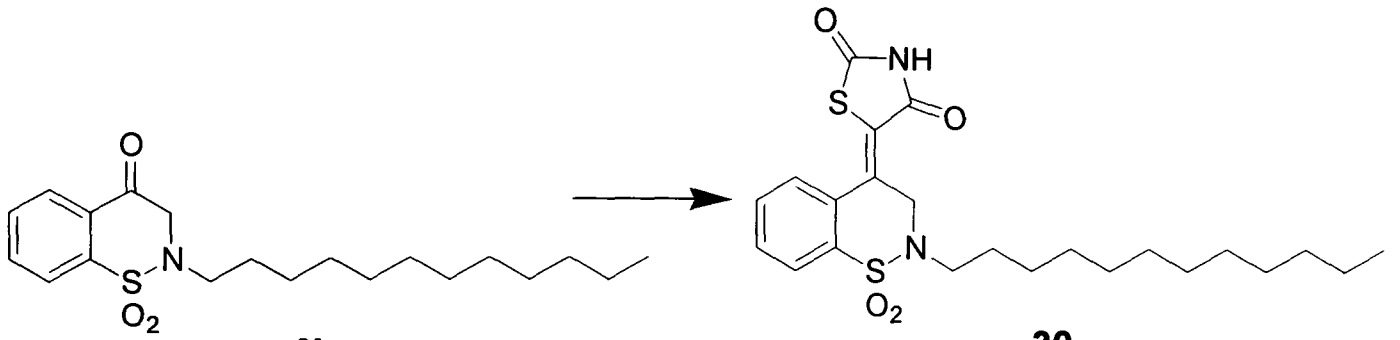

**6b** **30**

**30: 5-(2-Dodecyl-1,1-dioxo-2,3-dihydro-1*H*-1λ$^6$-benzo[*e*][1,2]thiazin-4-ylidene)-thiazolidine-2,4-dione**

From 700mg (1.9mmol) of crude **6b**, 345mg (0.75mmol) of a white solid **30** was produced.

**Yield** (%): 39. **$^1$H NMR** (200MHz, $d_6$-DMSO): 0.87 (3H, t, *J*6.5, C*H*$_3$CH$_2$), 1.22 (18H, m, (C*H*$_2$)$_9$), 1.50 (2H, m, NCH$_2$C*H*$_2$), 2.81 (2H, t, *J*7.2, NC*H*$_2$CH$_2$), 4.99 (2H, s, *endo* N-C*H*$_2$) 7.61-8.01 (4H, m, *Ar*), 9.58 (1H, br, N*H*). **$^{13}$C NMR** (60MHz, $d_6$-DMSO): 14.1 (*C*H$_3$) 22.7 26.5 27.8 29.1 29.3 29.5 29.6 30.4 31.9 35.6 ((*C*H$_2$)$_{10}$), 50.7 (*endo* N-C*H*$_2$), 53.0 (*exo* N-C*H*$_2$), 123.1 125.1 128.3 131.1 132.4 132.6 137.7 138.8 (*C*=*C* & *Ar*), 165.5 166.9 (*C*O). **LRMS** (APCI$^-$): 462.83 (100%, M$^-$). **HRMS** (ESIMS): $C_{23}H_{32}N_2O_4S_2$ Requires 463.1725 Found 463.1730. **M.P.** (°C): 84-85

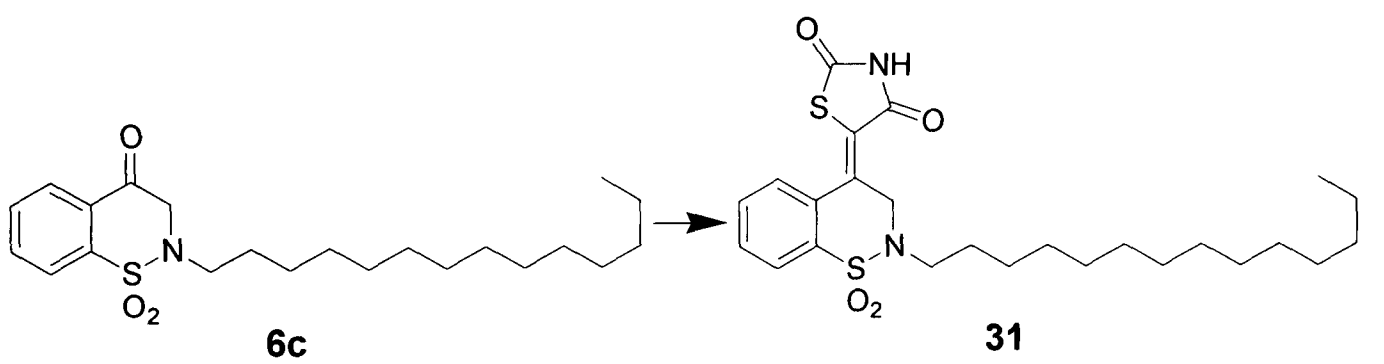

**6c** **31**

**31: 5-(1,1-Dioxo-2-tetradecyl-2,3-dihydro-1*H*-1λ$^6$-benzo[*e*][1,2]thiazin-4-ylidene)-thiazolidine-2,4-dione**

260mg (0.53mmol) of pale yellow solid **31**.

**Yield** (%): 33. **$^1$H NMR** (200MHz, $d_6$-DMSO): 0.86 (3H, t, *J*6.5, C*H*$_3$), 1.22 (22H, br, (C*H*$_2$)$_{11}$), 1.45 (2H, m, NCH$_2$C*H*$_2$), 2.81( 2H, t, *J*7.2Hz, NC*H*$_2$CH$_2$), 4.99 (2H, s, *endo* N-C*H*$_2$), 7.55-8.02 (4H, m, *Ar*). **$^{13}$C NMR** (60MHz, $d_6$-DMSO): 14.1 (*C*H$_3$) 22.7 26.5 27.8 28.0 28.6 29.1 29.3 29.5 29.6 31.2 31.9 ((*C*H$_2$)$_{12}$ unresolved) 50.6 (*endo* N-*C*H$_2$), 53.0 (*exo* N-*C*H$_2$), 123.1 125.1 128.2 131.1 132.4 132.6 137.7 138.7 (*C*=*C* & *Ar*) 165.5 166.9 (*C*O). **LRMS** (APCI$^-$): 490.43 (100%, M$^-$). **HRMS** (ESIMS): $C_{25}H_{36}N_2O_4S_2$ Req 491.2038 Fnd 491.2030. **M.P.** (°C): 75-76

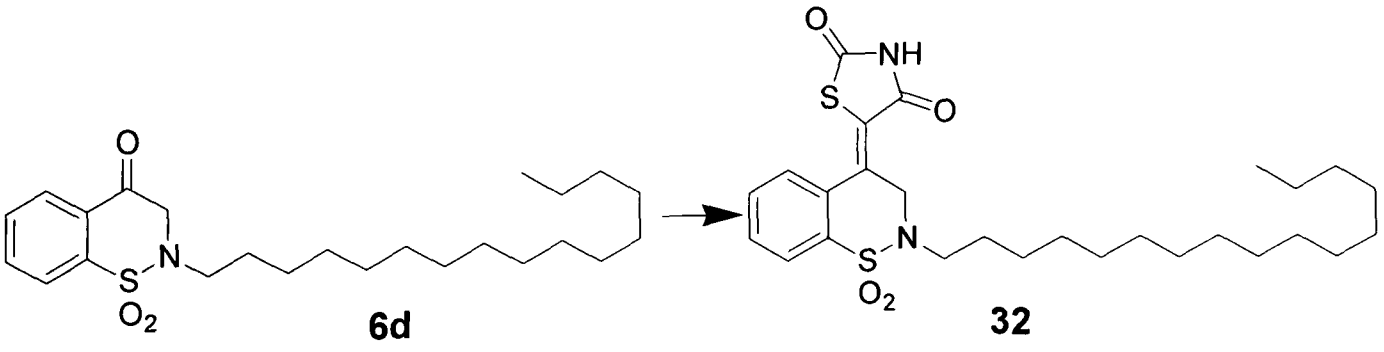

**6d** **32**

**32: 5-(2-Hexadecyl-1,1-dioxo-2,3-dihydro-1*H*-1λ$^6$-benzo[*e*][1,2]thiazin-4-ylidene)-thiazolidine-2,4-dione**

From 550mg (1.3mmol) of crude ketone **6d**, 260mg (0.50mmol) of a white solid **32** was produced.

**Yield** (%): 38. **$^1$H NMR** (200MHz, $d_6$-DMSO): 0.86 (3H, t, *J*6.5, C$H_3$), 1.25 (26H, br, (C$H_2$)$_{13}$), 1.50 (2H, m, NCH$_2$C$H_2$), 2.80 (2H, t, *J*7.2, NC$H_2$CH$_2$), 4.99 (2H, s, *endo* N-C$H_2$) 7.55-8.02 (4H, m, *Ar*), 9.50 (1H, br, N*H*). **$^{13}$C NMR** (60MHz, $d_6$-DMSO): 14.1 (CH$_3$), 22.7 26.5 27.8 29.1 29.3 29.5 29.7 31.9 ((*C*H$_2$)$_{14}$ unresolved), 50.7 (*endo* N-*C*H$_2$), 53.0 (*exo* N-*C*H$_2$), 123.1 125.1 128.2 131.1 132.4 132.6 137.7 138.8 (*C*=*C* & *Ar*), 165.6 167.0 (*C*O). **LRMS** (APCI$^-$): 518.42 (100%, M$^-$). **HRMS** (ESIMS): $C_{27}H_{40}N_2O_4S_2$ Requires 519.2351 Found 519.2343. **IR** (disc): 1179.3 (S=O), 1350.7 (S=O), 1464.3 (aromatic), 1692.4 (C=O), 1752.7 (C=O). **M.P.** (°C): 92-93.

## A1.2 Maleimides

**9a**

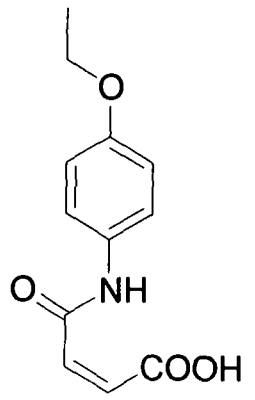


**9a: 3-(4-Ethoxy-phenylcarbamoyl)-acrylic acid**

Treatment of 4-ethoxyaniline (667mg, 4.9mmol) with maleic anhydride (500mg, 5.1mmol) in DMF (5 mL) for 14 hours produced crude product that was purified by recrystallisation from hot methanol to give yellow crystals of **9a** (507mg, 2.2mmol).

**Yield** (%): 44. **$^1$H NMR** (400MHz, $d_6$-DMSO): 1.30 (3H, t, *J*7.0, C$H_3$), 3.99 (2H, q, *J*10.0, C$H_2$), 6.37 (2H, m, *H*-C=C-*H*), 6.90 (2H, m, *Ar*), 7.53 (2H, m, *Ar*). **$^{13}$C NMR** (100MHz, $d_6$-DMSO): 15.52 (*C*$H_3$), 63.95 (*C*$H_2$), 96.09, 96.07 (*C*=*C*) 115.31 122.01 131.74 (Ar *C*-H) 132.16 (Ar *C*-O) 132.51 (Ar *C*-H) 155.92 (*C*-N) 163.66 167.52 (*C*=O). **LRMS** (APCI$^+$): 217.85 (M-OH$^-$). **IR** (disc): 847.4 (aromatic), 1175.1 (C-N), 1256.1 (C-O-C), 1513.0 (aromatic), 1706.0 (C=O), 3111.8 (br, $CO_2$H). **M.P.** (°C): 177-178.

**9b**

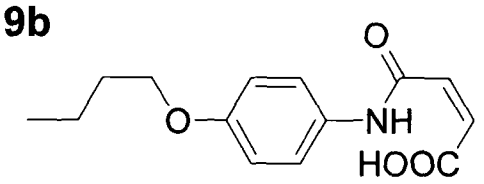


**9b: 3-(4-Butoxy-phenylcarbamoyl)-acrylic acid**

Treatment of 4-butoxyaniline (808mg, 4.9mmol) with maleic anhydride (500mg, 5.1mmol) in DMF (5 mL) for 14 hours produced crude product that was purified by recrystallisation from hot methanol to give yellow crystals of **9b** (755mg, 2.9mmol).

**Yield** (%): 58. **$^1$H NMR** (400MHz, $d_6$-DMSO): 0.93 (3H, t, *J*7.0, C$H_3$), 1.42 (2H, m, C$H_2$), 1.68 (2H, m, C$H_2$), 3.93 (2H, t, *J*6.5, C$H_2$), 6.36 (2H, m, *H*-C=C-*H*), 6.90 (2H, m, *Ar*), 7.50 (2H, m, *Ar*). **$^{13}$C NMR** (100MHz, $d_6$-DMSO): 14.56 (*C*$H_3$), 19.59 31.62 68.09 (*C*$H_2$), 96.07 (*C*=*C*) 115.35 122.00 131.81 (Ar *C*H), 132.15 (Ar *C*-O), 132.49 (Ar *C*H), 156.11 (Ar *C*-N), 163.66 167.51 (*C*=O). **LRMS** (APCI$^+$): 245.85 (M-OH$^-$). **IR** (disc): 853.3 (aromatic), 1179.3 (C-N), 1247.4 (C-O-C), 1512.0 (aromatic), 1707.6 (C=O), 3096.1 ($CO_2$H). **M.P.** (°C): 162-164.

**9c**

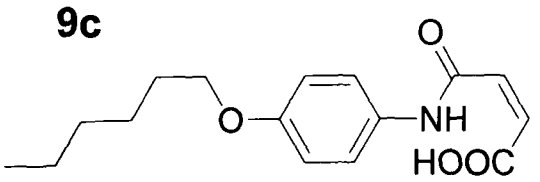


**9c: 3-(4-Hexyloxy-phenylcarbamoyl)-acrylic acid**

Treatment of 4-hexyloxyaniline (946mg, 4.9mmol) with maleic anhydride (500mg, 5.1mmol) in DMF (5 mL) for 14 hours produced crude product that was purified

by recrystallisation from hot methanol to give brown crystals of **9c** (870mg, 3.0mmol).
**Yield** (%): 61. **$^1$H NMR** (400MHz, $d_6$-DMSO): 0.87 (3H, t, *J*7.0, C*H*$_3$), 1.29 (4H, m, 2xC*H*$_2$), 1.39 (2H, m, C*H*$_2$), 1.68 (2H, m, C*H*$_2$), 3.93 (2H, t, *J*6.5, C*H*$_2$), 6.36 (2H, m, *H*-C=C-*H*), 6.90 (2H, m, *Ar*), 7.50 (2H, m, *Ar*). **$^{13}$C NMR** (100MHz, $d_6$-DMSO): 14.78 (*C*H$_3$), 22.94 26.05 29.52 31.87 68.39 (*C*H$_2$) 96.08 (*C*=*C*) 115.35 122.00 131.78 (Ar *C*H) 132.15 (Ar *C*-O) 132.49 (Ar *C*H) 156.10 (Ar *C*-N) 163.65 167.51 (*C*=O). **LRMS** (APCI$^+$): 274.00 (M-OH$^-$). **IR** (disc): 845.3 (aromatic), 1180.4 (C-N), 1246.7 (C-O-C), 1515.9 (aromatic), 1715.7 (C=O). **M.P.** (°C): 151-152.

**9d**

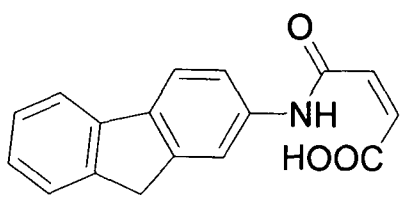


**9d: 3-(9*H*-Fluoren-2-ylcarbamoyl)-acrylic acid**

Treatment of 2-aminofluorene (887mg, 4.9mmol) with maleic anhydride (500mg, 5.1mmol) in DMF (5 mL) for 14 hours produced crude product that was washed with methanol, ethanol and acetonitrile to give a yellow powder of crude **9d** (912mg, 3.2mmol).
**Yield** (%): 65. **$^1$H NMR** (400MHz, $d_6$-DMSO): 3.92 (2H, s, C*H*$_2$), 6.42 (2H, m, *H*-C=C-*H*), 7.26 (1H, m, *Ar*), 7.37 (1H, m, *Ar*), 7.58 (2H, m, *Ar*), 7.84 (2H, m, *Ar*), 7.98 (1H, s, *H*-CC-N). **$^{13}$C NMR** (100MHz, APT, $d_6$-DMSO): 37.37 (*C*H$_2$), 96.09 (*C*=*C*), 117.17 119.15 121.06 125.9 127.62 131.45 132.47 (Ar *C*H), 137.83 138.39 141.71 143.74 (Ar *C*) 144.66 (Ar *C*-N) 164.00 167.76 (*C*O). **LRMS** (APCI$^+$): 262.22 (M-OH$^-$). **IR** (disc): 842.6 (aromatic), 1157.8 (C-N), 1524.7 (aromatic), 1695.1 (C=O), 3101.2 ($CO_2H$). **M.P.** (°C): 212-213.

**9e**

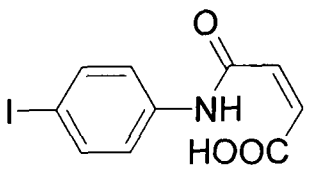


**9e: 3-(4-Iodo-phenylcarbamoyl)-acrylic acid**

Treatment of 4-iodoaniline (1073mg, 4.9mmol) with maleic anhydride (500mg, 5.1mmol) in DMF (5 mL) for 14 hours produced crude product that was purified by recrystallisation from hot methanol to give light brown crystals of **9a** (670mg, 2.1mol).
**Yield** (%): 43. **$^1$H NMR** (400MHz, $d_6$-DMSO): 6.39 (2H, m, *H*-C=C-*H*), 7.45 (2H, m, *Ar*), 7.66 (2H, m, *Ar*). **$^{13}$C NMR** (100MHz, $d_6$-DMSO): 88.27 (Ar *C*I), 96.08 (*C*=*C*), 122.42 131.09 132.44 138.31 (Ar *C*H) 139.33 (Ar *C*-N) 164.19 167.77 (*C*O). **LRMS** (APCI$^+$): 299.00 (M-OH$^-$). **IR** (disc): 612.0 (C-I), 852.6 (aromatic), 1484.8 (aromatic), 1704.5 (C=O), 3081.0 (br, $CO_2H$). **M.P.** (°C): 182-185.

**33**

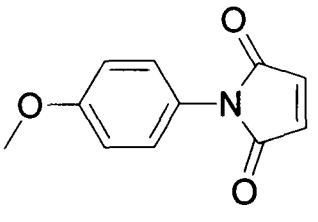

**33: 1-(4-Methoxy-phenyl)-pyrrole-2,5-dione**

Treatment of 4-methoxyaniline (500mg, 4.1mmol) with maleic anhydride (418mg, 4.3mmol) in DMF (5 mL) for 14 hours produced the crude uncyclised maleimide that was purified by recrystallisation from hot methanol to give bright yellow solid (470mg, 2.1mmol, 49%). Treatment of this solid (350mg, 1.6mmol) with sodium acetate (20mg, 0.2mmol) in acetic anhydride (2ml) for 3 hours at 65°C furnished crude product that was recrystallised from hot methanol to give a yellow powder **33** (160mg, 0.79mmol, 49%).
**$^1$H NMR** (400MHz, $d_6$-DMSO): 3.84 (3H, s, C$H_3$O), 7.04 (2H, m, O-CC-*H*), 7.15 (2H, s, *H*CC*H*), 7.24 (2H, d, N-CC-*H*). **$^{13}$C NMR** (100MHz, $d_6$-DMSO): 56.23 (*C*$H_3$), 115.01 115.23 (2x*C*CO), 124.80 (C-N), 127.94 129.18 (2x*C*CN), 135.44 (H*C*=*C*H) 158.94 (*C*-O), 171.04 (2x*C*=O). **LRMS** (APCI$^+$): 203.17 ($M^+$). **IR** (disc): 826.8 (aromatic), 1156.7 (C-N), 1247.6 (C-O-C), 1510.7 (aromatic), 1708.4 (C=O). **M.P.** (°C): 118-124.

**34**

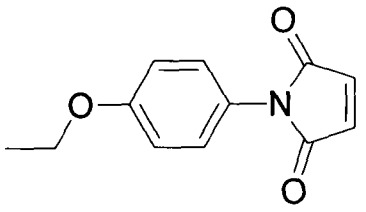


**34: 1-(4-Ethoxy-phenyl)-pyrrole-2,5-dione**

Treatment of **9a** (483mg, 2.0mmol) with sodium acetate (20mg, 0.2mmol) in acetic anhydride (3ml) for 3 hours at 65°C furnished crude product that was recrystallised from hot methanol to give yellow crystals of **34** (143mg, 0.66mmol, 32%).
**$^1$H NMR** (400MHz, $d_4$-MeOD): 1.36 (3H, t, *J*7.0, C$H_3$), 4.08 (2H, q, 7.0Hz, C$H_2$), 7.03 (2H, m, Ar *H*-CC-O), 7.18 (2H, s, HC=CH), 7.24 (2H, d, Ar *H*-CC-N). **$^{13}$C NMR** (100MHz, APT, $d_4$-MeOD): 14.07 (*C*$H_3$), 63.75 (*C*$H_2$), 114.63 114.72 (H-*C*-C-O), 122.16 (*C*-N), 128.08 (2x H-*C*-C-N), 134.41 (H*C*=*C*H), 171.04 (2x*C*=O). **LRMS** (APCI$^+$): 217.61 ($M^+$). **IR** (disc): 833.9 (aromatic), 1154.7 (C-N), 1257.3 (C-O-C), 1519.3 (aromatic), 1703.3 (C=O). **M.P.** (°C): 128-130 (lit. 133.5-134.5, Roderick R.W. (1957), J. Amer. Chem. Soc. **79**, 1710).

**35**

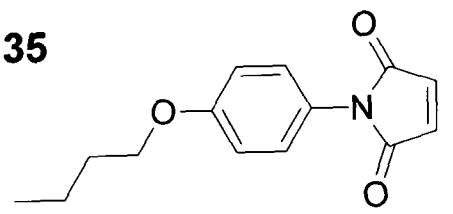


**35: 1-(4-Butoxy-phenyl)-pyrrole-2,5-dione**

Treatment of **9b** (686mg, 2.6mmol) with sodium acetate (20mg, 0.2mmol) in acetic anhydride (3ml) for 3 hours at 65°C furnished crude product that was recrystallised from hot methanol to give brown crystals of **35** (312mg, 1.3mmol, 49%).
**$^1$H NMR** (400MHz, $d_6$-DMSO): 0.88 (3H, t, *J*7.0, C$H_3$), 1.45 (2H, m, C$H_2$), 1.69 (2H, m, C$H_2$), 3.94 (2H, t, O-C$H_2$), 7.04 (2H, m, O-CC-*H*), 7.14 (2H, s, *H*CC*H*), 7.21 (2H, m, N-CC-*H*). **$^{13}$C NMR** (100MHz, APT, $d_6$-DMSO): 14.52 (*C*$H_3$), 19.57 31.52 68.26 (*C*$H_2$), 115.71 115.48 (H-*C*C-O), 124.80 (*C*-N), 129.15 (2xH*C*CN), 135.43 (H*C*=*C*H), 158.94 (*C*-O) 171.04 (2x*C*=O). **LRMS** (APCI$^+$): 245.20 ($M^+$). **IR** (disc): 832.5 (aromatic), 1151.5 (C-N), 1252.9 (C-O-C), 1517.1 (aromatic), 1704.1 (C=O). **M.P.** (°C): 49-51.

**36**

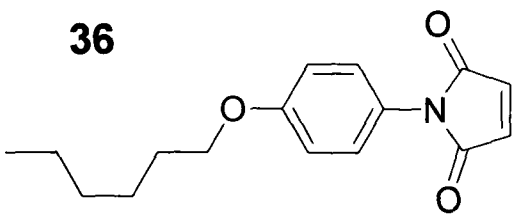

**36: 1-(4-Hexyloxy-phenyl)-pyrrole-2,5-dione**

Treatment of **9c** (801mg, 2.8mmol) with sodium acetate (20mg, 0.2mmol) in acetic anhydride (3ml) for 3 hours at 65°C furnished crude product that was recrystallised from hot methanol to give a brown powder of **36** (350mg, 1.3mmol, 48%).
**$^1$H NMR** (400MHz, $d_6$-DMSO): 0.93 (3H, t, C*H*$_3$), 1.32 (6H, m, 3xC*H*$_2$), 1.42 (2H, m, C*H*$_2$), 1.73 (2H, m, C*H*$_2$), 3.97 (2H, t, O-C*H*$_2$), 6.99 (2H, m, O-CC-*H*), 7.14 (2H, s, *H*CC*H*), 7.21 (2H, m, N-CC-*H*). **$^{13}$C NMR** (100MHz, APT, $d_6$-DMSO): 14.75 (*C*H$_3$), 22.92 26.01 29.43 31.84 68.57 (5x*C*H$_2$), 115.48 115.70 (H-*C*C-O), 124.80 (*C*-N),129.14 (2xH-*C*C-N), 135.43 (HC*C*H), 158.93 (*C*-O), 171.04 (2x*C*=O). **LRMS** (APCI$^+$): 273.17. **IR** (disc): 831.8 (aromatic), 1155.4 (C-N), 1254.4 (C-O-C), 1517.9 (aromatic), 1707.6 (C=O). **M.P.** (°C): 53-54.

**37**

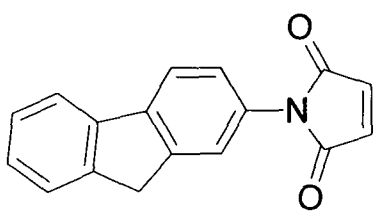

**37: 1-(9*H*-Fluoren-2-yl)-pyrrole-2,5-dione**

Treatment of **9d** (905mg, 3.2mmol) with sodium acetate (20mg, 0.2mmol) in acetic anhydride (3ml) for 3 hours at 65°C furnished crude product that was recrystallised from hot methanol to give a yellow powder of **37** (447mg, 1.7mmol, 53%).
**$^1$H NMR** (400MHz, $d_6$-DMSO): 3.98 (2H, s, C*H*$_2$), 7.21 (2H, s, *H*CC*H*), 7.40 (3H, m) 7.54 (1H, s, *H*-CC-N), 7.62 (1H, d, 7.2Hz, *H*-CCC-N), 7.94 (1H, d, 7.4Hz, *H*-CC-N) 8.00 (1H, d, 8.1Hz). **$^{13}$C NMR** (100MHz, APT, $d_6$-DMSO): 37.29 (*C*H$_2$), 120.97 121.18 124.62 126.07 126.50 127.74 127.98 (Ar *C*H), 130.93 (*C*-N), 135.56 (2xHC*C*H), 141.12 141.46 144.22 144.41 (Ar *C*), 170.97 (2x*C*=O). **IR** (disc): 836.0 (aromatic), 1150.1 (C-N), 1397.2 1427.6 1458.3 1488.4 (aromatics), 1712.2 (C=O). **M.P.** (°C): 175-178.

**38**

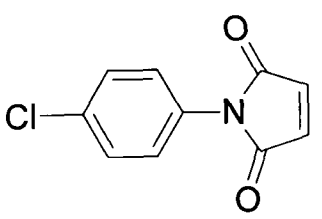

**38: 1-(4-Chloro-phenyl)-pyrrole-2,5-dione**

Treatment of 4-chloroaniline (625mg, 4.9mmol) with maleic anhydride (500mg, 5.1mmol) in DMF (5 mL) for 14 hours produced the crude uncyclised maleimide that was purified by recrystallisation from hot methanol to give white crystals (520mg, 2.3mmol, 47%). Treatment of this solid (516mg, 2.3mmol) with sodium acetate (20mg, 0.2mmol) in acetic anhydride (3ml) for 3 hours at 65°C furnished crude product that was recrystallised from hot methanol to give pale yellow needles of **38** (377mg, 1.8mmol, 79%).

**$^1$H NMR** (400MHz, $d_6$-DMSO): 7.19 (2H, s, *H*CC*H*), 7.40 (2H, d, 10.4Hz, *H*-CC-N), 7.56 (2H, d, 8.7Hz, *H*-CC-Cl). **$^{13}$C NMR** (100MHz, APT, $d_6$-DMSO): 129.25 129.76 (4x*C*-H), 131.35 (*C*-Cl), 132.96 (*C*-N), 135.62 (H*C*CH), 170.51 (2x*C*=O). **LRMS** (APCI$^+$): 207.28 ($M^+$). **IR** (disc): 684.7 (C-Cl), 836.0 (aromatic), 1149.0 (C-N), 1497.7 (aromatic), 1712.3 (C=O). **M.P.** (°C): 112-114

**39**

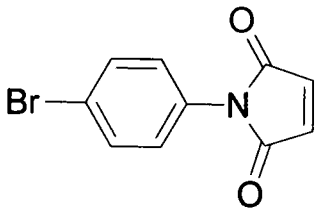


**39: 1-(4-Bromo-phenyl)-pyrrole-2,5-dione**

Treatment of 4-bromoaniline (843mg, 4.9mmol) with maleic anhydride (500mg, 5.1mmol) in DMF (5 mL) for 14 hours produced the crude uncyclised maleimide that was purified by recrystallisation from hot methanol to give pale yellow crystals (720mg, 2.7mmol, 54%). Treatment of this solid (598mg, 2.2mmol) with sodium acetate (20mg, 0.2mmol) in acetic anhydride (3ml) for 3 hours at 65°C furnished crude product that was recrystallised from hot methanol to give pale yellow needles of **39** (357mg, 1.4mmol, 64%).

**$^1$H NMR** (400MHz, $d_6$-DMSO): 7.21 (2H, s, *H*CC*H*), 7.32 (2H, d, *J*8.8, *H*-CC-N), 7.71 (2H, d, *J*8.8, *H*-CC-Br). **$^{13}$C NMR** (100MHz, APT, $d_6$-DMSO): 121.37 (*C*-N), 129.53 (2xH-*C*C-N), 131.80 (*C*-Br), 132.71 (2xH-*C*C-Br), 135.63 (H*C*CH), 170.46 (2x*C*=O). **LRMS** (APCI$^+$): 251.02 ($M^+$). **IR** (disc): 687.5 (C-Br), 826.0 (aromatic), 1154.5 (C-N), 1488.9 (aromatic), 1712.9 (C=O). **M.P.** (°C): 118-120, (lit. 118-120, Froborg, J., Magnusson, G. and Thoren S. (1975) J. Org. Chem., **40**, 1595)

**40**

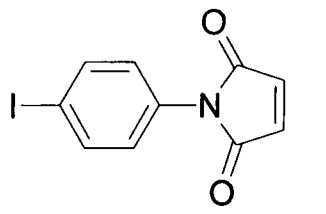


**40: 1-(4-Iodo-phenyl)-pyrrole-2,5-dione**

Treatment of **9e** (527mg, 1.7mmol) with sodium acetate (20mg, 0.2mmol) in acetic anhydride (3ml) for 3 hours at 65°C furnished crude product that was recrystallised from hot methanol to give beige needles of **40** (355mg, 1.2mmol, 71%).

**$^1$H NMR** (400MHz, $d_6$-DMSO): 7.16 (2H, s, *H*CC*H*), 7.23 (2H, d, *J*9.0 *H*-CC-N), 7.88 (2H, d, *J*9.0, *H*-CC-I). **$^{13}$C NMR** (100MHz, APT, $d_6$-DMSO): 129.57 (2xH*C*CN), 132.11 (*C*-I), 132.25 (*C*-N), 135.63 (H*C*CH), 138.57 (2xH*C*CI), 170.44 (2x*C*=O). **LRMS** (APCI$^+$): 299.01 ($M^+$). **IR** (disc): 585.6 (C-I), 826.1 (aromatic), 1153.2 (C-N), 1486.0 (aromatic), 1703.3 (C=O). **M.P.** (°C): 153-154

**41**

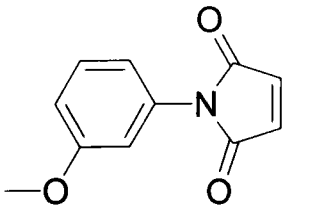


**41: 1-(3-Methoxy-phenyl)-pyrrole-2,5-dione**

Treatment of 3-methoxyaniline (602mg, 4.9mmol) with maleic anhydride (500mg, 5.1mmol) in DMF (5 mL) for 14 hours produced the crude uncyclised maleimide

that was purified by recrystallisation from hot methanol to give a pale brown solid (570mg, 2.6mmol, 52%). Treatment of this solid (449mg, 2.0mmol) with sodium acetate (20mg, 0.2mmol) in acetic anhydride (3ml) for 3 hours at 65°C furnished crude product that was recrystallised from hot methanol to give a beige powder **41** (130mg, 0.65mmol, 31%).
**$^1$H NMR** (400MHz, $d_6$-DMSO): 3.77 (3H, s, C*H*$_3$), 6.91 (1H, d, 9.5Hz, N-CC-*H*), 6.92 (1H, s, N-CC-*H*), 6.99 (1H, d, 8.4Hz, O-CC-*H*), 7.18 (s, 2H, *H*CC*H*), 7.39 (1H, t, 8.1Hz, N-CCC-*H*). **$^{13}$C NMR** (100MHz, APT, $d_6$-DMSO): 56.18 (*C*H$_3$), 113.66 114.18 119.89 130.46 (Ar *C*H), 133.49 (*C*-N), 135.52 (HC*C*H), 160.31 (*C*-O), 170.69 (2x*C*=O). **LRMS** (APCI$^+$): 203.24 ($M^+$). **IR** (disc): 697.0 774.1 (aromatic), 1146.9 (C-N), 1256.5 (C-O-C), 1497.1 (aromatic), 1715.9 (C=O). **M.P.** (°C): 65-66 (lit. 66-67.5, Phos Sulf Sil Rel Elements (1993), **79**, 187)

**42**

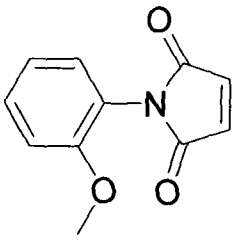

**42: 1-(2-Methoxy-phenyl)-pyrrole-2,5-dione**

Treatment of 2-methoxyaniline (602mg, 4.9mmol) with maleic anhydride (500mg, 5.1mmol) in DMF (5 mL) for 14 hours produced the crude uncyclised maleimide that was purified by recrystallisation from hot methanol to give a pale brown solid (330mg, 1.5mmol, 31%). Treatment of this solid (306mg, 1.4mmol) with sodium acetate (20mg, 0.2mmol) in acetic anhydride (3ml) for 3 hours at 65°C furnished crude product that was recrystallised from hot methanol to give beige plate-shaped crystals of **42** (71mg, 0.35mmol, 25%).
**$^1$H NMR** (400MHz, $d_6$-DMSO): 3.74 (3H, s, C*H*$_3$), 7.05 (1H, t, *J*6.6, O-CCC-*H*), 7.14 (1H, m, N-CC-H), 7.16 (2H, s, *H*CC*H*), 7.25 (1H, d, *J*7.0, O-CC-*H*), 7.45 (1H, t, *J*6.8, N-CCC-*H*). **$^{13}$C NMR** (100MHz, APT, $d_6$-DMSO): 56.64 (*C*H$_3$), 113.17 (Ar *C*H), 120.73 (*C*-N), 121.37 131.21 131.40 (Ar *C*H), 135.83 (HC*C*H), 156.16 (*C*-O), 170.75 (2x*C*=O). **LRMS** (APCI$^+$): 203.48 ($M^+$). **IR** (disc): 754.8 (aromatic), 1155.6 (C-N), 1254.7 (C-O-C), 1509.0 (aromatic), 1703.2 (C=O). **M.P.** (°C): 118-120 (lit. 119-120, Zh Obshch Khim (1956), **26**, 208).

**43**

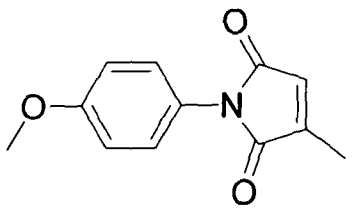

**43: 1-(4-Methoxy-phenyl)-3-methyl-pyrrole-2,5-dione**

Treatment of 4-methoxyaniline (500mg, 4.1mmol) with 3-methyl maleic anhydride (478mg, 4.3mmol) in DMF (5 mL) for 14 hours produced the crude uncyclised maleimide that was purified by recrystallisation from hot methanol to give a fine yellow solid (863mg, 3.7mmol, 90%). Treatment of this solid (860mg, 3.7mmol) with sodium acetate (20mg, 0.2mmol) in acetic anhydride (3ml) for 3 hours at 65°C furnished crude product that was recrystallised from hot methanol to give yellow solid **43** (420mg, 1.9mmol, 51%).
**$^1$H NMR** (400MHz, $d_4$-MeOD): 2.17 (3H, s, C-C*H*$_3$), 3.83 (3H, s, C*H*$_3$-O), 6.92 (2H, m, *H*-C-C-O), 6.95 (1H, s, *H*C=C), 7.48 (2H, m, *H*-C-C-N). **$^{13}$C NMR** (100MHz, APT, $d_6$-DMSO): 11.48 (C-*C*H$_3$), 56.19 (O-*C*H$_3$) 115.13 115.40 (Ar

*C*H), 123.97 (*C*-N), 127.45 (Ar *C*H), 137.48 (H-*C*=C-$CH_3$), 139.44 (H-C=*C*-$CH_3$), 149.65 (*C*-O), 158.85 169.60 (*C*=O). **LRMS** ($APCI^+$): 217.57 ($M^+$). **IR** (disc): 832.1 (aromatic), 1177.7 (C-N), 1250.0 (C-O-C), 1504.1 (aromatic), 1775.4 (C=O). **M.P.** (°C): 110-111.

**44**

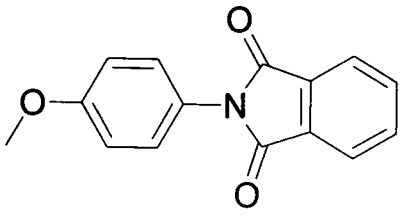

**44: 2-(4-Methoxy-phenyl)-isoindole-1,3-dione**

Treatment of 4-methoxyaniline (500mg, 4.1mmol) with pthalic anhydride (631mg, 4.3mmol) in DMF (5 mL) for 14 hours produced the crude uncyclised maleimide that was purified by recrystallisation from hot methanol to give a yellow solid (390mg, 1.4mmol, 35%). Treatment of this solid (350mg, 1.3mmol) with sodium acetate (20mg, 0.2mmol) in acetic anhydride (3ml) for 3 hours at 65°C furnished crude product that was recrystallised from hot methanol to give fine yellow crystals of **44** (180mg, 0.71mmol, 55%).
**$^1$H NMR** (400MHz, $d_6$-DMSO): 3.82 (3H, s, C$H_3$-O), 7.08 (2H, d, *J*9.1, O-CC-*H*), 7.36 (2H, d, *J*9.1, N-CC-*H*), 7.93 (4H, m, *C*H*C*H*C*H*C*H). **$^{13}$C NMR** (100MHz, APT, $d_6$-DMSO): 56.26 (C$H_3$), 96.08 (*C*=*C*), 114.99 (2xH*C*CO), 124.18 (2xpthal *C*-H), 129.62 (2xH*C*CN), 132.45 (C-N), 135.47 (2xpthal *C*-H), 158.85 (*C*-O), 168.53 (2x*C*=O). **LRMS** ($APCI^+$): 253.31 ($M^+$). **IR** (disc): 713.8 (indole aromatic), 825.9 (aromatic), 1175.9 (C-N), 1257.1 (C-O-C), 1516.0 (aromatic), 1716.7 (C=O). **M.P.** (°C): 158-160 (lit. 162, J Chem Soc pt 1 (1973) 272).

**45**

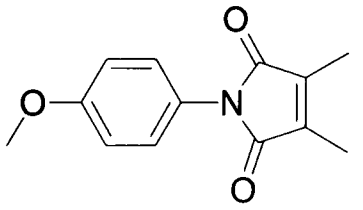

**45: 1-(4-Methoxy-phenyl)-3,4-dimethyl-pyrrole-2,5-dione**

Treatment of 4-methoxyaniline (465mg, 3.8mmol) with 2,3-dimethyl maleic anhydride (500mg, 4.0mmol) in DMF (5 mL) for 14 hours produced the crude uncyclised maleimide that was purified by recrystallisation from hot methanol to give beige crystals (705mg, 2.9mmol, 75%). Treatment of this solid (650mg, 2.6mmol) with sodium acetate (20mg, 0.2mmol) in acetic anhydride (3ml) for 3 hours at 65°C furnished crude product that was recrystallised from hot methanol to give fine yellow crystals of **45** (435mg, 1.9mmol, 73%).
**$^1$H NMR** (400MHz, $d_6$-DMSO): 1.97 (6H, s, C$H_3$C=CC$H_3$), 3.78 (3H, s, C$H_3$O), 7.02 (2H, d, *J*9.1 O-CC-*H*), 7.22 (2H, d, *J*9.1, *H*-CC-N). **$^{13}$C NMR** (100MHz, APT, $d_6$-DMSO): 9.45 (*C*$H_3$C=C*C*$H_3$), 56.20 (*C*$H_3$O), 114.97 (2xH*C*CO), 125.47 (*C*-N), 128.86 (2xH*C*CN), 137.71 (*C*=*C*), 159.29 (*C*-O), 171.74 (2x*C*=O). **LRMS** ($APCI^+$): 231.24 ($M^+$). **IR** (disc): 833.5 (aromatic), 1177.6 (C-N), 1249.6 (C-O-C), 1511.4 (aromatic), 1704.4 (C=O). **M.P.** (°C): 136-137 (lit. 139, Gazz. Chim. Ital. (1910), **40**, 548).

**46**

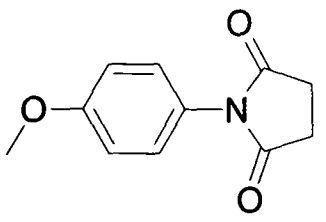

**46: 1-(4-Methoxy-phenyl)-pyrrolidine-2,5-dione**

Treatment of 4-methoxyaniline (610mg, 4.9mmol) with succinic anhydride (500mg, 5.1mmol) in DMF (5mL) for 14 hours produced the crude uncyclised maleimide that was purified by recrystallisation from hot methanol to give beige crystals (277mg, 1.2mmol, 25%). Treatment of this solid (238mg, 1.1mmol) with sodium acetate (20mg, 0.2mmol) in acetic anhydride (3ml) for 3 hours at 65°C furnished crude product that was recrystallised from hot methanol to give white crystals of **46** (109mg, 0.53mmol, 50%).
**$^1$H NMR** (400MHz, $d_6$-DMSO): 2.76 (4H, s, $H_2$C-C$H_2$), 3.79 (3H, s, C$H_3$O), 7.03 (2H, d, *J*10.0, *H*-CC-O), 7.17 (2H, d, *J*10.0, *H*-CC-N). **$^{13}$C NMR** (100MHz, APT, $d_6$-DMSO): 29.23 (*C*$H_2$CC*C*$H_2$), 56.20 (*C*$H_3$-O), 114.90 (2xH*C*CO), 126.15 (*C*-N), 129.14 (2xH*C*CN), 159.64 (*C*-O), 177.95 (2x*C*=O). **LRMS** (APCI$^+$): 205.21 ($M^+$). **IR** (disc): 840.4 (aromatic), 1175.8 (C-N), 1252.0 (C-O-C), 1511.1 (aromatic), 1704.6 (C=O). **M.P.** (°C): 158-159 (lit. 162-163, Chem. Ber. (1896) **29**, 84).

**47**

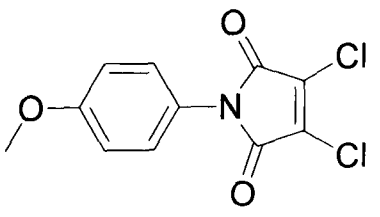

**47: 3,4-Dichloro-1-(4-methoxy-phenyl)-pyrrole-2,5-dione**

Treatment of 4-methoxyaniline (500mg, 4.1mmol) with 2,3-dichloro maleic anhydride (713mg, 4.3mmol) in DMF (5 mL) for 14 hours produced the crude uncyclised maleimide that was purified by recrystallisation from hot methanol to give a fine yellow solid (1008mg, 3.5mmol, 84%). Treatment of this solid (1008mg, 3.5mmol) with sodium acetate (20mg, 0.2mmol) in acetic anhydride (3ml) for 3 hours at 65°C furnished crude product that was recrystallised from hot methanol to give yellow crystals of **47** (140mg, 0.5mmol, 15%).
**$^1$H NMR** (400MHz, $d_4$-$CDCl_3$): 3.85 (3H, s, C$H_3$-O), 7.00 (2H, d, *J*9.0, O-C-C-*H*), 7.24 (2H, d, *J*8.9, N-C-C-*H*). **$^{13}$C NMR** (100MHz, APT, $d_4$-$CDCl_3$): 55.51 (*C*$H_3$), 114.65 (2xH*C*CO), 123.03 (*C*-N), 127.59 (2xH*C*CN), 133.48 (Cl-*C*=*C*-Cl), 159.65 (C-O), 162.23 (2xC=O). **LRMS** (APCI$^+$): 271.23 ($M^+$). **IR** (disc): 525.2 (C-Cl), 824.8 (aromatic), 1172.2 (C-N), 1253.9 (C-O-C), 1520.0 (aromatic), 1732.2 (C=O). **M.P.** (°C): 201-202 .

## A1.3 Aminothiazoles

Ninety-six aminothiazoles were synthesized according to Section 2.3.4 and Section 4.4.1 by Dr. Richard Vickers with **ATZ-D1** to **ATZ-D6** synthesised by the author. Full experimental data is given for **ATZ-A1** and **ATZ-A12** and partial data is given for the rest of the library. The purity was determined by RP-HPLC and, for some compounds, estimated from 400MHz NMR (in brackets). The author synthesized compounds **ATZ-D1** to **ATZ-D6**.

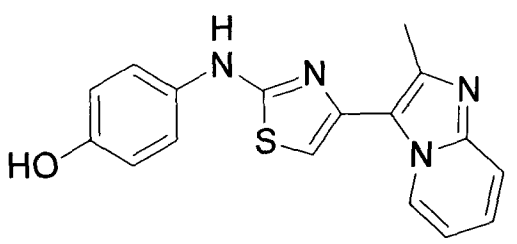


**ATZ-A1: 4-[4-(2-Methyl-imidazo[1,2-a]pyridin-3-yl)-thiazol-2-ylamino]-phenol**

**Yield** (%): 78. **HPLC**: Retention time 6.62mins, % Area 100. **$^1$H NMR** (400MHz, $d_4$-MeOD): 2.71 (3H, s, C*H*$_3$), 6.80 (2H, d, *J*12.3, phenol C-*H*), 7.16 (1H, s, S-C*H*), 7.40 (2H, d, *J*12.9, phenol C-*H*), 7.48 (1H, m, pyridine $N_2$-C-C-*H*), 7.95 (2H, m, pyridine *H*-C-C-*H*), 9.27 (1H, m, pyridine N-C-*H*). **LRMS** (APCI$^+$): 323.17 ($MH^+$).

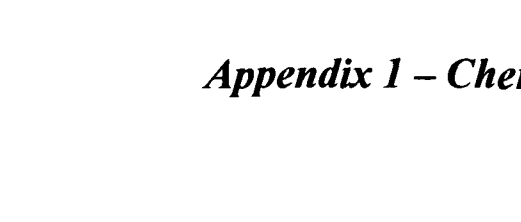


**ATZ-A12: [4-(2-Methyl-imidazo[1,2-a]pyridin-3-yl)-thiazol-2-yl]-(4-nitro-phenyl)-amine**

**Yield** (%): 100. **HPLC**: Retention time 6.88mins, % Area 100. **$^1$H NMR** (400MHz, $d_4$-MeOD): 2.65 (3H, s, C*H*$_3$), 7.53 (2H, m, pyridine $N_2$-C-C-*H*), 7.64 (1H, s, S-C*H*), 7.85 (2H, d, *J*9.9, nitrophenyl C-*H*), 7.90 (2H, m, pyridine *H*-C-C-*H*), 8.25 (2H, d, *J*9.3, nitrophenyl C-*H*), 9.07 (1H, d, *J*6.9, pyridine N-C-*H*). **LRMS** (APCI$^+$): 352.65 ($MH^+$).

| | compound | formula | M.W. | yield (%) | Estimated purity (%) |
|---|---|---|---|---|---|
| 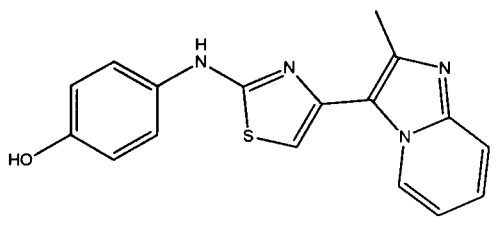 | **ATZ-A1** | $C_{17}H_{14}N_4OS$ | 322.3838 | 78 | 100 |
| 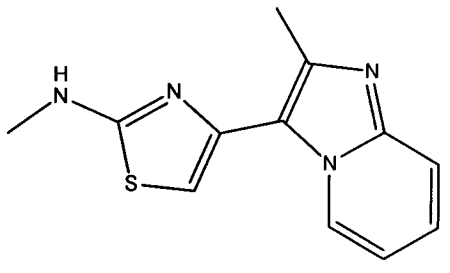 | **ATZ-A2** | $C_{12}H_{12}N_4S$ | 244.3136 | 100 | 55 (85+) |
| 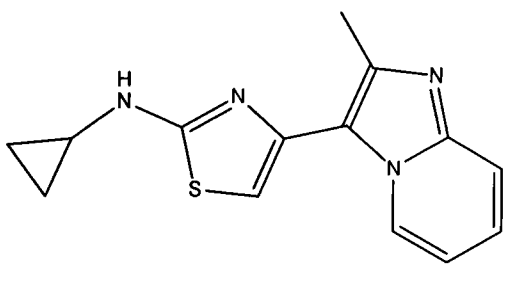 | **ATZ-A3** | $C_{14}H_{14}N_4S$ | 270.3514 | 68 | 44 (85+) |
| 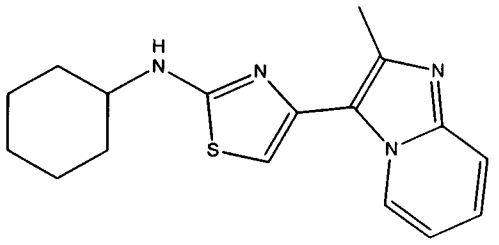 | **ATZ-A4** | $C_{17}H_{20}N_4S$ | 312.4318 | 62 | 99 |
| 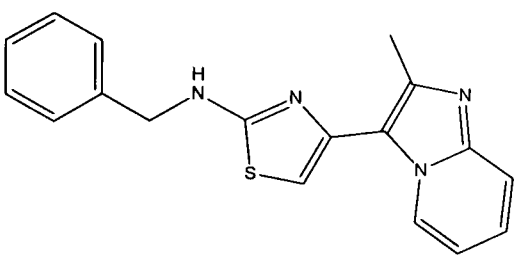 | **ATZ-A5** | $C_{18}H_{16}N_4S$ | 320.4112 | 49 | 89 |
| 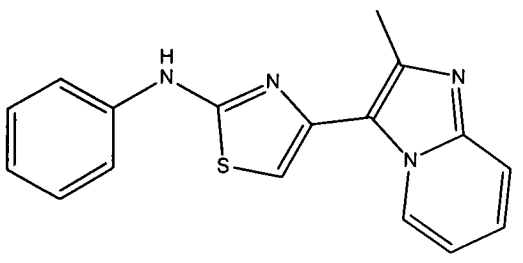 | **ATZ-A6** | $C_{17}H_{14}N_4S$ | 306.3844 | 73 | 97 |
| 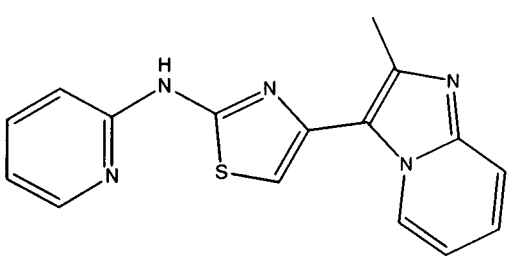 | **ATZ-A7** | $C_{16}H_{13}N_5S$ | 307.3722 | 100 | 95 |

| compound | formula | M.W. | yield (%) | purity (%) |
|---|---|---|---|---|
| 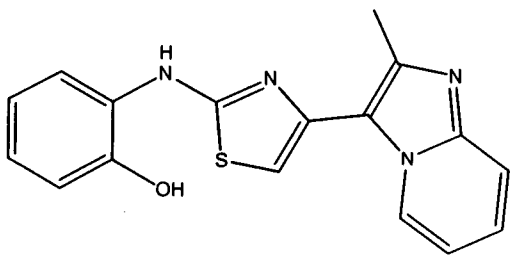 | **ATZ-A8** | $C_{17}H_{14}N_4SO$ | 322.3838 | 99 | 100 |
| 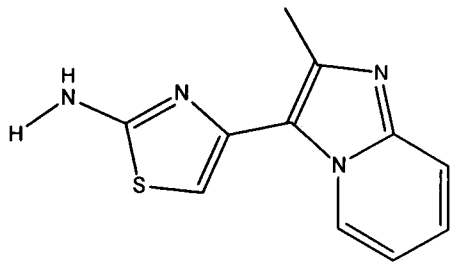 | **ATZ-A9** | $C_{11}H_{10}N_4S$ | 230.2868 | 100 | 86 |
| 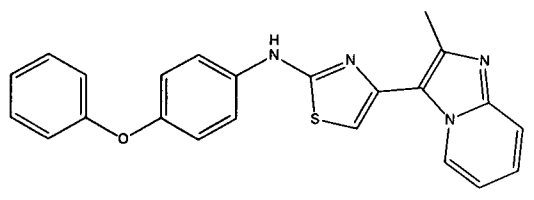 | **ATZ-A10** | $C_{23}H_{18}N_4SO$ | 398.4814 | 100 | 91 |
| 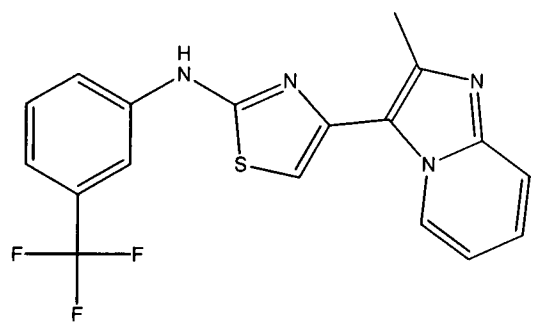 | **ATZ-A11** | $C_{18}H_{13}N_4SF_3$ | 374.3827 | 96 | 100 |
| 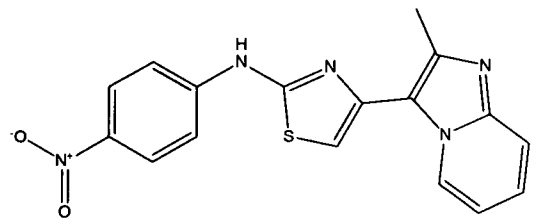 | **ATZ-A12** | $C_{17}H_{13}N_5SO_2$ | 351.382 | 100 | 100 |
| 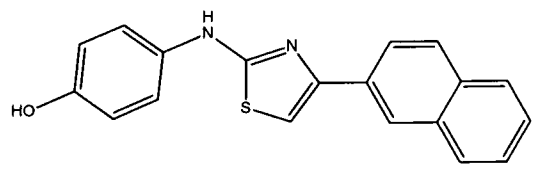 | **ATZ-B1** | $C_{19}H_{14}N_2SO$ | 318.3924 | 97 | 93 |
| 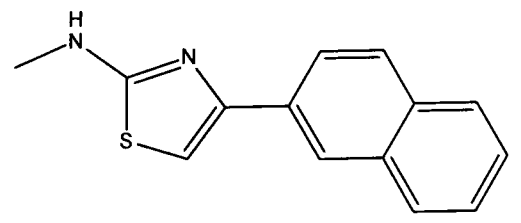 | **ATZ-B2** | $C_{14}H_{12}N_2S$ | 240.3222 | 96 | 64 (80+) |
| 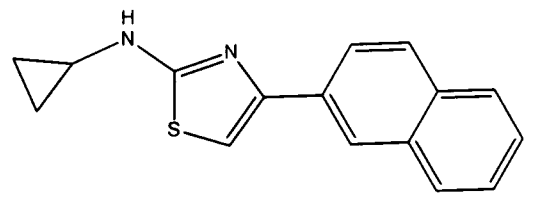 | **ATZ-B3** | $C_{16}H_{14}N_2S$ | 266.36 | 100 | 56 (70+) |

| | compound | formula | M.W. | yield (%) | purity (%) |
|---|---|---|---|---|---|
| 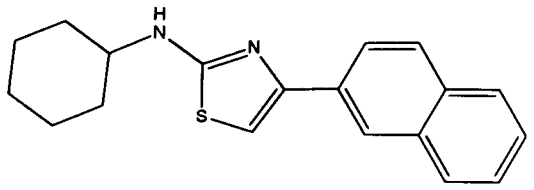 | **ATZ-B4** | $C_{19}H_{20}N_2S$ | 308.4404 | 100 | 91 |
| 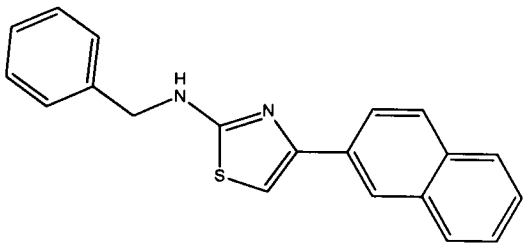 | **ATZ-B5** | $C_{20}H_{16}N_2S$ | 316.4198 | 76 | 74 |
| 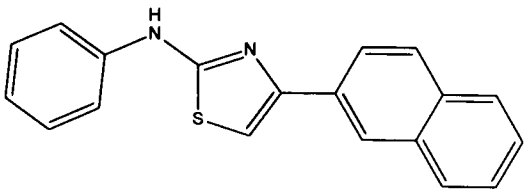 | **ATZ-B6** | $C_{19}H_{14}N_2S$ | 302.393 | 100 | 95 |
| 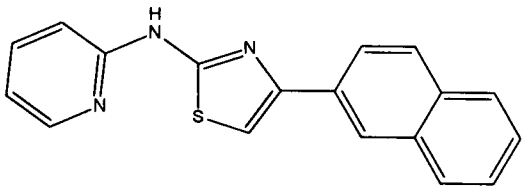 | **ATZ-B7** | $C_{18}H_{13}N_3S$ | 303.3808 | 99 | 95 |
| 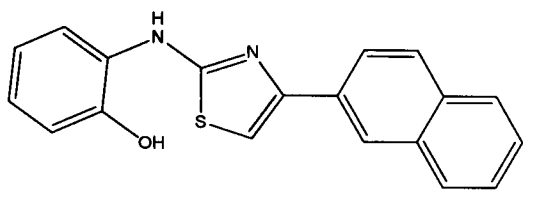 | **ATZ-B8** | $C_{19}H_{14}N_2SO$ | 318.3924 | 92 | 95 |
| 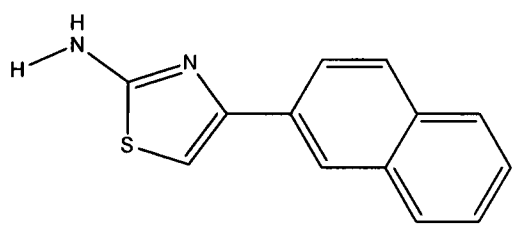 | **ATZ-B9** | $C_{13}H_{10}N_2S$ | 226.2954 | 100 | 81 |
| 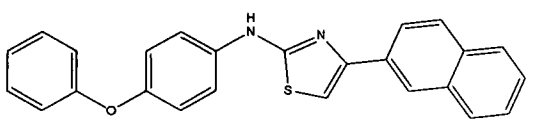 | **ATZ-B10** | $C_{25}H_{18}N_2SO$ | 394.49 | 81 | 88 |
| 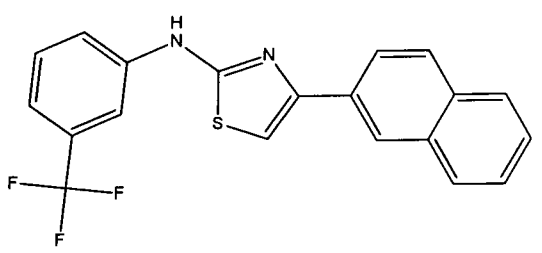 | **ATZ-B11** | $C_{20}H_{13}N_2SF_3$ | 370.3913 | 100 | 98 |
| 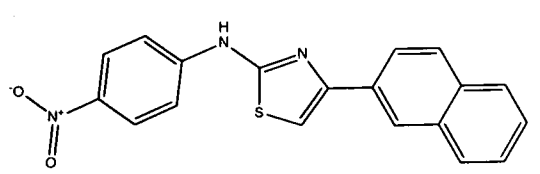 | **ATZ-B12** | $C_{19}H_{13}N_3SO_2$ | 347.3906 | 100 | 97 |
| 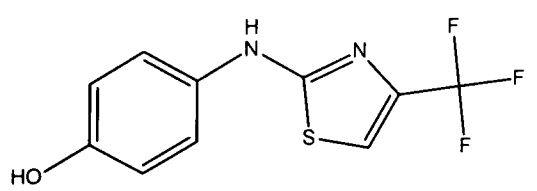 | **ATZ-C1** | $C_{10}H_7F_3N_2OS$ | 260.2333 | 97 | 96 |

| | compound | formula | M.W. | yield (%) | purity (%) |
|---|---|---|---|---|---|
| 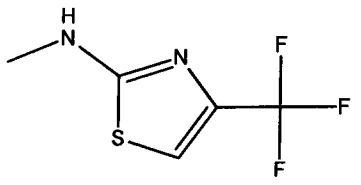 | **ATZ-C2** | $C_5H_5F_3N_2S$ | 182.1631 | 92 | 100 |
| 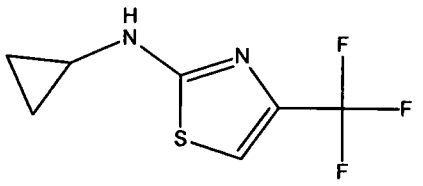 | **ATZ-C3** | $C_7H_7F_3N_2S$ | 208.2009 | 77 | 98 |
| 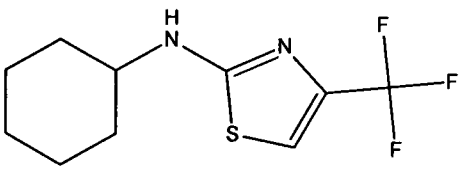 | **ATZ-C4** | $C_{10}H_{13}F_3N_2S$ | 250.2813 | 100 | 92 |
| 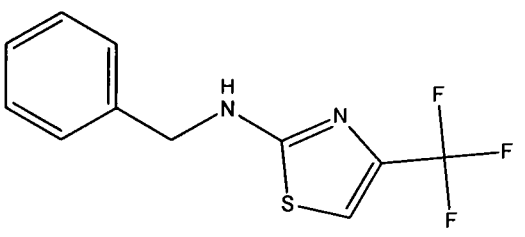 | **ATZ-C5** | $C_{11}H_9F_3N_2S$ | 258.2607 | 100 | 94 |
| 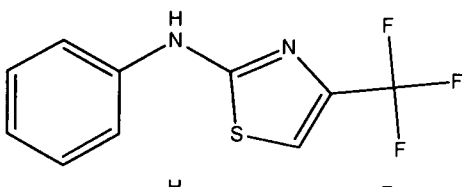 | **ATZ-C6** | $C_{10}H_7F_3N_2S$ | 244.2339 | 99 | 100 |
| 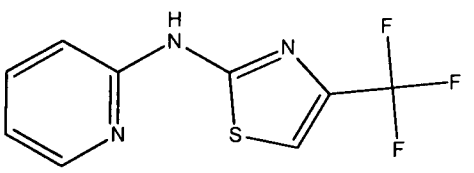 | **ATZ-C7** | $C_9H_6F_3N_3S$ | 245.2217 | 100 | 100 |
| 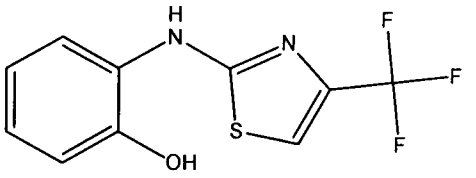 | **ATZ-C8** | $C_{10}H_7F_3N_2SO$ | 260.2333 | 100 | 100 |
| 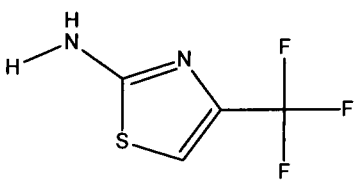 | **ATZ-C9** | $C_4H_3F_3N_2S$ | 168.1363 | 84 | 98 |
| 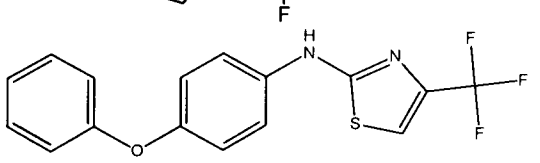 | **ATZ-C10** | $C_{16}H_{11}F_3N_2SO$ | 336.3309 | 97 | 57 (95+) |
| 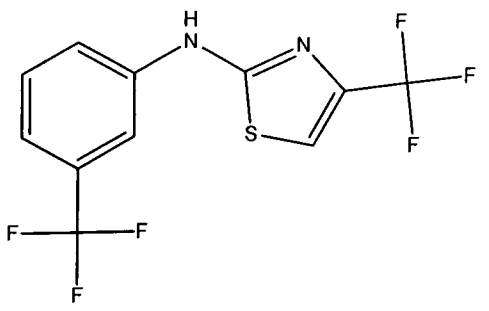 | **ATZ-C11** | $C_{11}H_6F_6N_2S$ | 312.2322 | 100 | 99 |
| 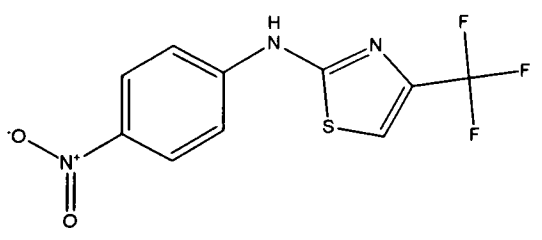 | **ATZ-C12** | $C_{10}H_6F_3N_3SO_2$ | 289.2315 | 100 | 98 |

| | compound | formula | M.W. | yield (%) | purity (%) |
|---|---|---|---|---|---|
| 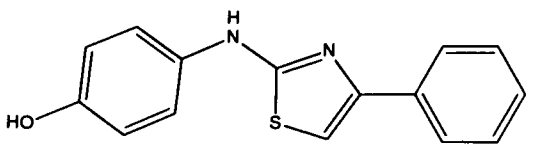 | **ATZ-D1** | $C_{15}H_{12}N_2SO$ | 268.3326 | 87 | 99 |
| 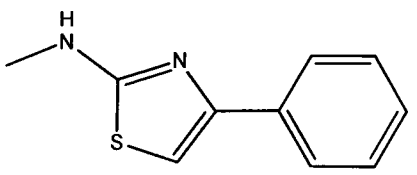 | **ATZ-D2** | $C_{10}H_{10}N_2S$ | 190.2624 | 82 | 95 |
| 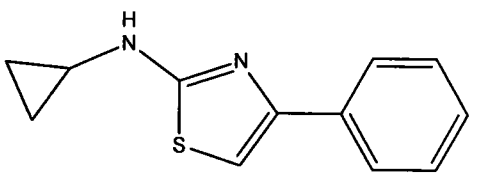 | **ATZ-D3** | $C_{12}H_{12}N_2S$ | 216.3002 | 100 | 51 (85+) |
| 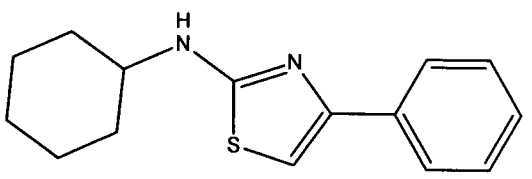 | **ATZ-D4** | $C_{15}H_{18}N_2S$ | 258.3806 | 54 | 35 (90+) |
| 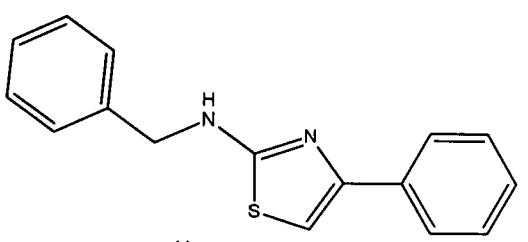 | **ATZ-D5** | $C_{16}H_{14}N_2S$ | 266.36 | 58 | 97 |
| 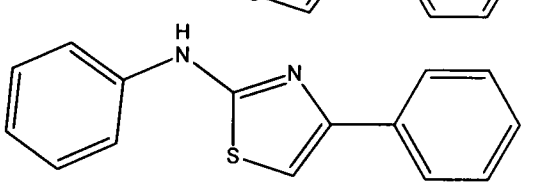 | **ATZ-D6** | $C_{15}H_{12}N_2S$ | 252.3332 | 100 | 82 |
| 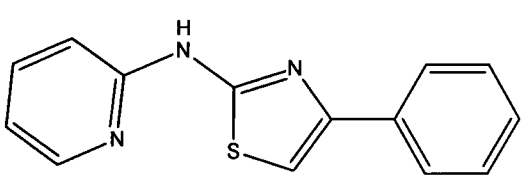 | **ATZ-D7** | $C_{14}H_{11}N_3S$ | 253.321 | 96 | 98 |
| 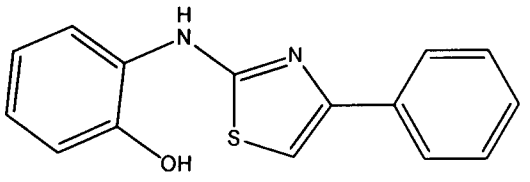 | **ATZ-D8** | $C_{15}H_{12}N_2SO$ | 268.3326 | 100 | 95 |
| 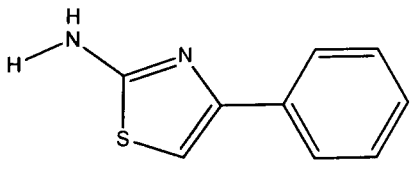 | **ATZ-D9** | $C_9H_8N_2S$ | 176.2356 | 100 | 88 |
| 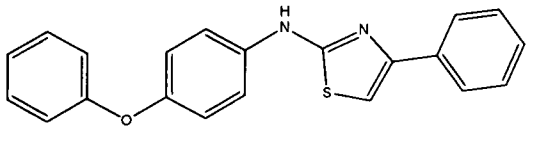 | **ATZ-D10** | $C_{21}H_{16}N_2SO$ | 344.4302 | 98 | 82 |
| 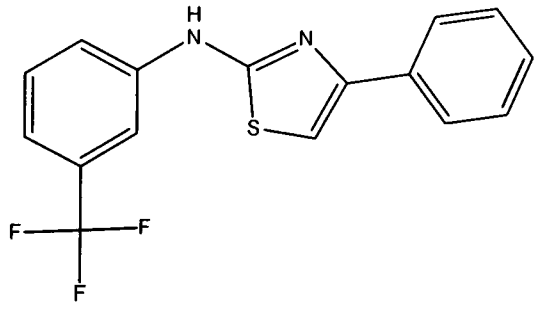 | **ATZ-D11** | $C_{16}H_{11}N_2SF_3$ | 320.3315 | 99 | 97 |

| | compound | formula | M.W. | yield (%) | purity (%) |
|---|---|---|---|---|---|
| 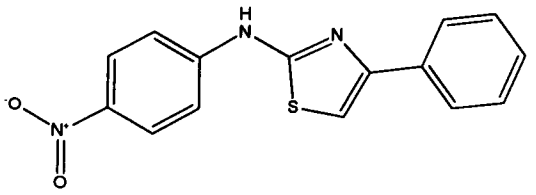 | **ATZ-D12** | $C_{15}H_{11}N_3SO_2$ | 297.3308 | 100 | 98 |
| 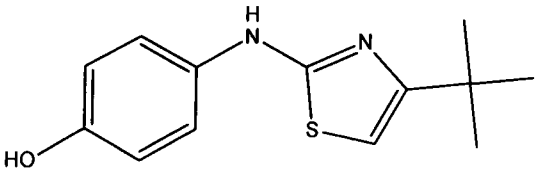 | **ATZ-E1** | $C_{13}H_{16}N_2SO$ | 248.3422 | 72 | 81 (95) |
| 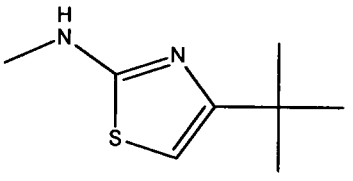 | **ATZ-E2** | $C_8H_{14}N_2S$ | 170.272 | 50 | 94 |
| 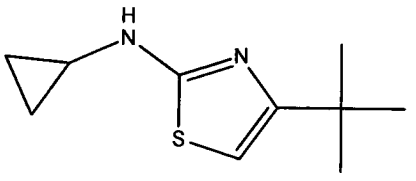 | **ATZ-E3** | $C_{10}H_{16}N_2S$ | 196.3098 | 100 | 87 |
| 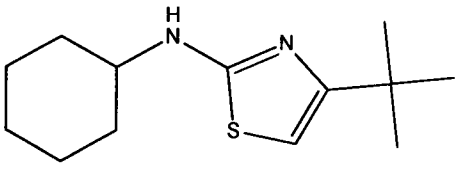 | **ATZ-E4** | $C_{13}H_{22}N_2S$ | 238.3902 | 60 | 64 (90+) |
| 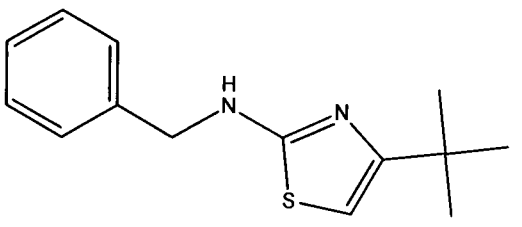 | **ATZ-E5** | $C_{14}H_{18}N_2S$ | 246.3696 | 100 | 86 |
| 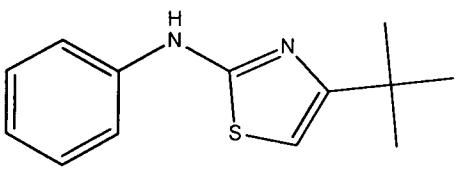 | **ATZ-E6** | $C_{13}H_{16}N_2S$ | 232.3428 | 98 | 100 |
| 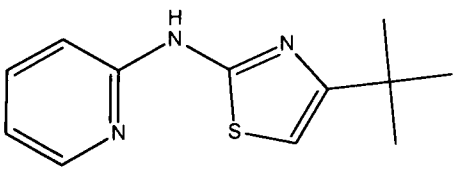 | **ATZ-E7** | $C_{12}H_{15}N_3S$ | 233.3306 | 100 | 100 |
| 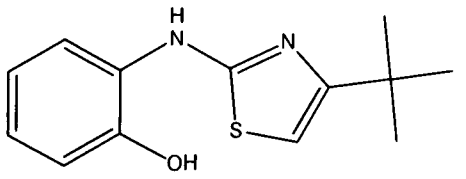 | **ATZ-E8** | $C_{13}H_{16}N_2SO$ | 248.3422 | 89 | 93 |
| 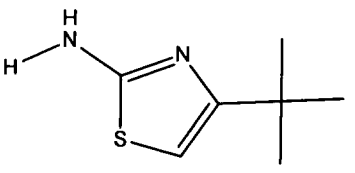 | **ATZ-E9** | $C_7H_{12}N_2S$ | 156.2452 | 100 | 100 |
| 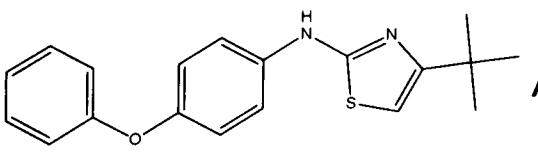 | **ATZ-E10** | $C_{19}H_{20}N_2SO$ | 324.4398 | 100 | 92 |

| | compound | formula | M.W. | yield (%) | purity (%) |
|---|---|---|---|---|---|
| 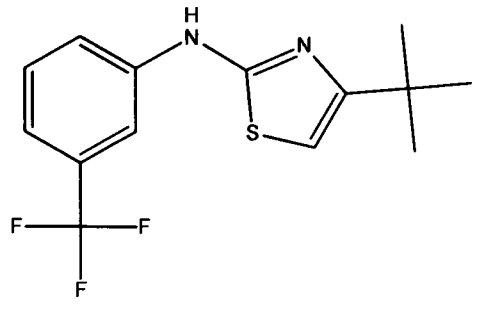 | **ATZ-E11** | $C_{14}H_{15}N_2SF_3$ | 300.3411 | 100 | 95 |
| 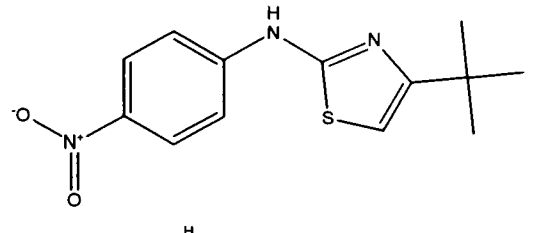 | **ATZ-E12** | $C_{13}H_{15}N_3SO_2$ | 277.3404 | 100 | 87 |
| 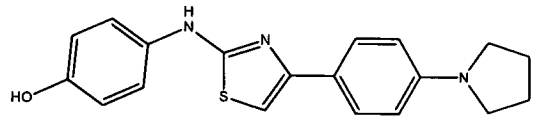 | **ATZ-F1** | $C_{19}H_{19}N_3SO$ | 337.4386 | 100 | 49 (90+) |
| 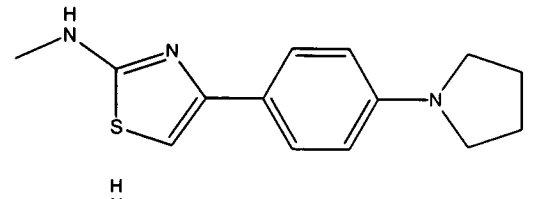 | **ATZ-F2** | $C_{14}H_{17}N_3S$ | 259.3684 | 100 | 78 (90+) |
| 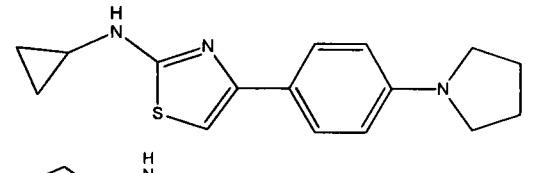 | **ATZ-F3** | $C_{16}H_{19}N_3S$ | 285.4062 | 100 | 64 (80+) |
| 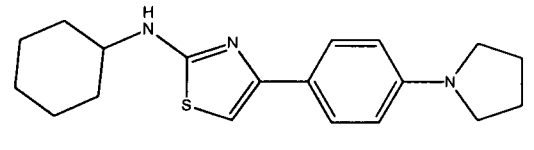 | **ATZ-F4** | $C_{19}H_{25}N_3S$ | 327.4866 | 98 | 87 |
| 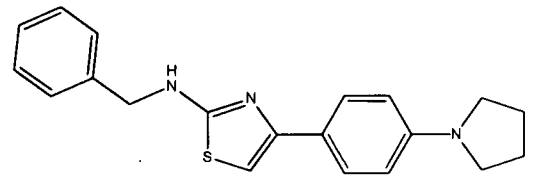 | **ATZ-F5** | $C_{20}H_{21}N_3S$ | 335.466 | 100 | 53 (85+) |
| 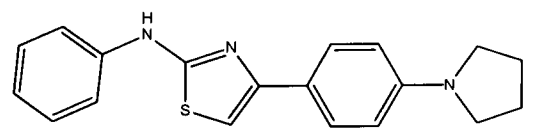 | **ATZ-F6** | $C_{19}H_{19}N_3S$ | 321.4392 | 100 | 55 (90+) |
| 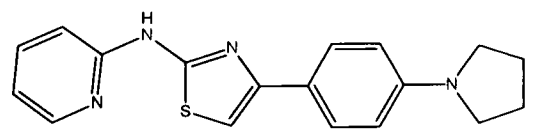 | **ATZ-F7** | $C_{18}H_{18}N_4S$ | 322.427 | 95 | 98 |
| 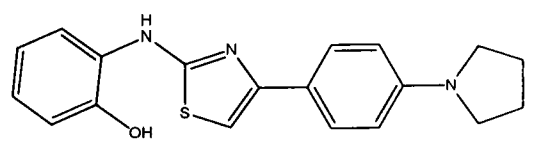 | **ATZ-F8** | $C_{19}H_{19}N_3SO$ | 337.4386 | 81 | 59 |
| 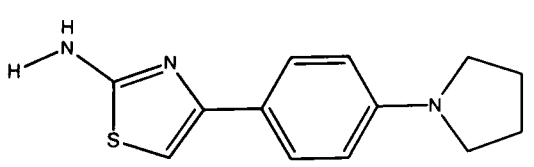 | **ATZ-F9** | $C_{13}H_{15}N_3S$ | 245.3416 | 92 | 85 |
| 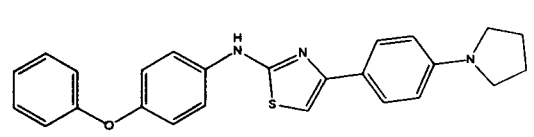 | **ATZ-F10** | $C_{25}H_{23}N_3SO$ | 413.5362 | 100 | 82 |

| | compound | formula | M.W. | yield (%) | purity (%) |
|---|---|---|---|---|---|
| 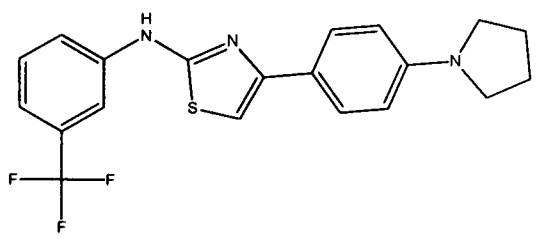 | **ATZ-F11** | $C_{20}H_{18}N_3SF_3$ | 389.4375 | 99 | 97 |
| 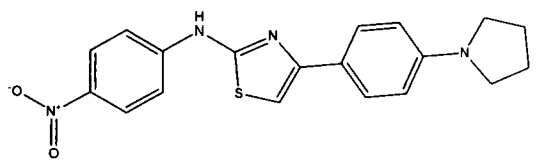 | **ATZ-F12** | $C_{19}H_{18}N_4SO_2$ | 366.4368 | 100 | 100 (85+) |
| 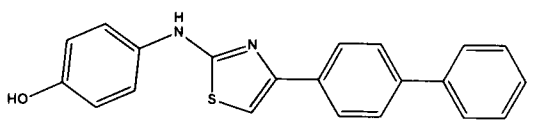 | **ATZ-G1** | $C_{21}H_{16}N_2SO$ | 344.4302 | 76 | 87 |
| 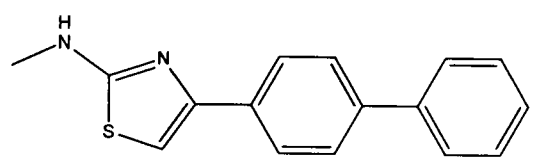 | **ATZ-G2** | $C_{16}H_{14}N_2S$ | 266.36 | 100 | 75 |
| 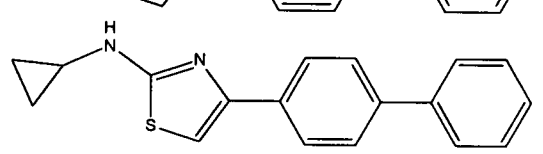 | **ATZ-G3** | $C_{18}H_{16}N_2S$ | 292.3978 | 88 | 48 (70+) |
| 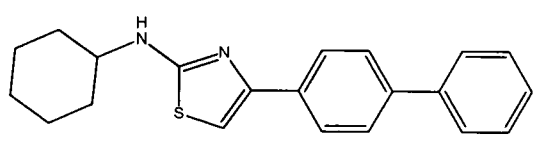 | **ATZ-G4** | $C_{21}H_{22}N_2S$ | 334.4782 | 95 | 84 |
| 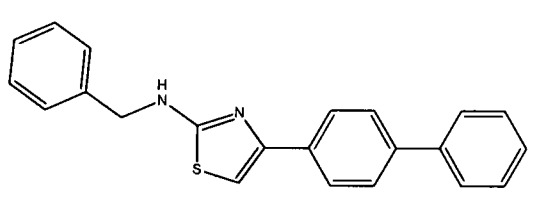 | **ATZ-G5** | $C_{22}H_{18}N_2S$ | 342.4576 | 92 | 68 |
| 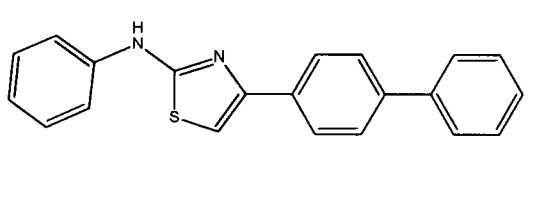 | **ATZ-G6** | $C_{21}H_{16}N_2S$ | 328.4308 | 95 | 97 |
| 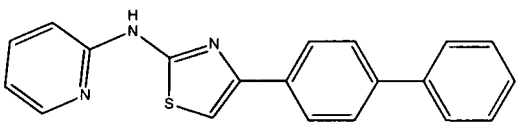 | **ATZ-G7** | $C_{20}H_{15}N_3S$ | 329.4186 | 100 | 93 |
| 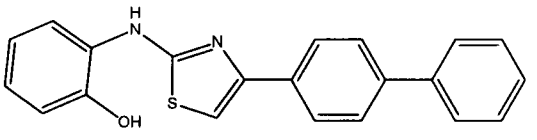 | **ATZ-G8** | $C_{21}H_{16}N_2SO$ | 344.4302 | 100 | 83 |
| 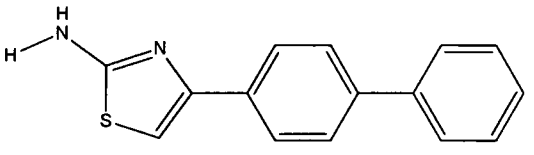 | **ATZ-G9** | $C_{15}H_{12}N_2S$ | 252.3332 | 100 | 92 |
| 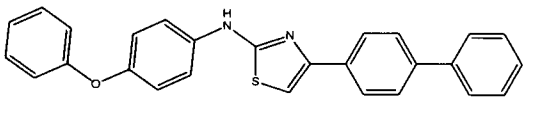 | **ATZ-G10** | $C_{27}H_{20}N_2SO$ | 420.5278 | 66 | 100 |
| 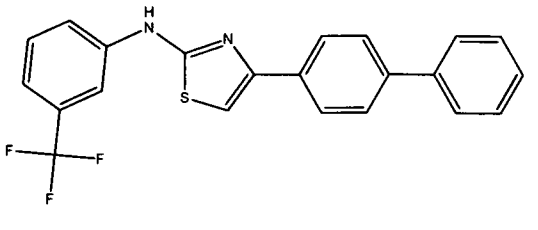 | **ATZ-G11** | $C_{22}H_{15}N_2SF_3$ | 396.4291 | 100 | 97 |

| | compound | formula | M.W. | yield (%) | purity (%) |
|---|---|---|---|---|---|
| 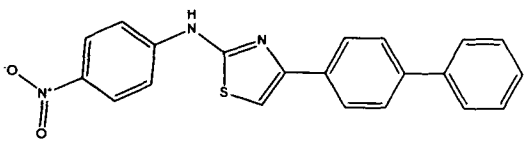 | **ATZ-G12** | $C_{21}H_{15}N_3SO_2$ | 373.4284 | 100 | 96 (80) |
| 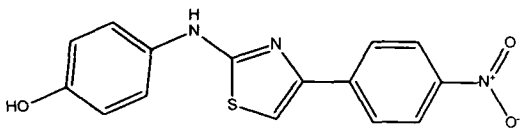 | **ATZ-H1** | $C_{15}H_{11}N_3SO_3$ | 313.3302 | 100 | 100 |
| 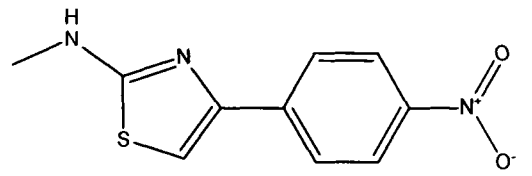 | **ATZ-H2** | $C_{10}H_9N_3SO_2$ | 235.26 | 100 | 63 |
| 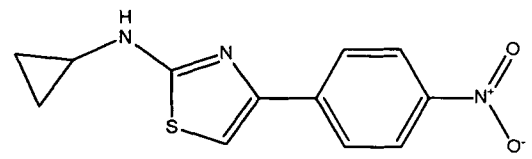 | **ATZ-H3** | $C_{12}H_{11}N_3SO_2$ | 261.2978 | 67 | 83 |
| 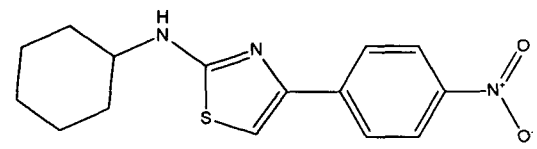 | **ATZ-H4** | $C_{15}H_{17}N_3SO_2$ | 303.3782 | 100 | 93 |
| 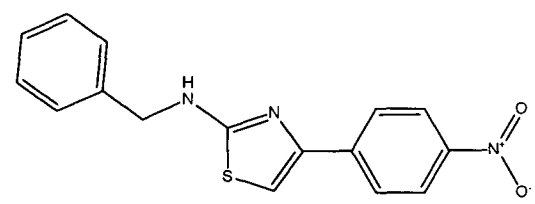 | **ATZ-H5** | $C_{16}H_{13}N_3SO_2$ | 311.3576 | 100 | 80 (90+) |
| 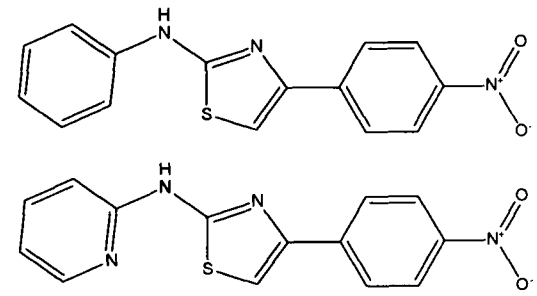 | **ATZ-H6** | $C_{15}H_{11}N_3SO_2$ | 297.3308 | 100 | 78 |
| 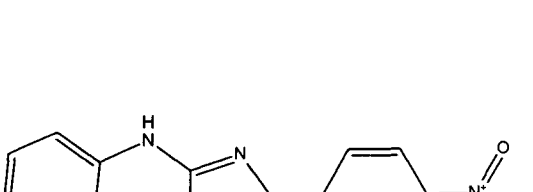 | **ATZ-H7** | $C_{14}H_{10}N_4SO_2$ | 298.3186 | 83 | 63 |
|  | **ATZ-H8** | $C_{15}H_{11}N_3SO_3$ | 313.3302 | 100 | 76 (90+) |
| 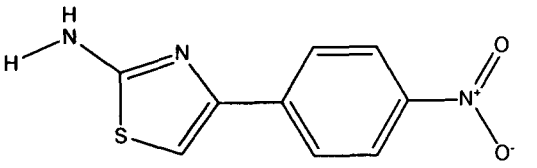 | **ATZ-H9** | $C_9H_7N_3SO_2$ | 221.2332 | Reaction failed twice | |
| 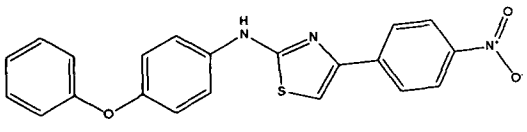 | **ATZ-H10** | $C_{21}H_{15}N_3SO_3$ | 389.4278 | 100 | 92 |
| 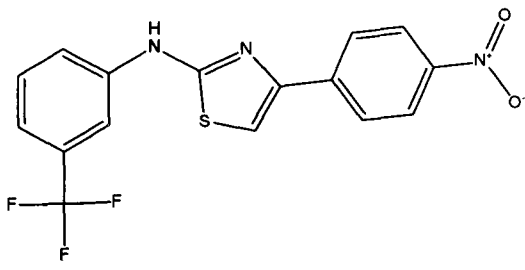 | **ATZ-H11** | $C_{16}H_0N_3SO_2F_3$ | 365.3291 | 100 | 89 |

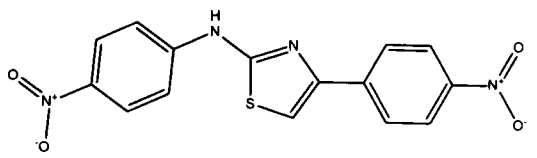

| compound | formula | M.W. | yield (%) | purity (%) |
|---|---|---|---|---|
| **ATZ-H12** | $C_{15}H_{10}N_4SO_4$ | 342.3284 | 99 | 62 |